Mechanical behaviour of a new automotive high manganese TWIP steel in the presence of liquid zinc

Coline Béal

Année 2011

Thèse

Mechanical behaviour of a new automotive high manganese TWIP steel in the presence of liquid zinc

Présentée devant
L'Institut National des Sciences Appliquées de Lyon

Pour obtenir
Le grade de docteur

École doctorale : Matériaux de Lyon
Formation doctorale : Matériaux

Par
Coline BÉAL
(Ingénieur)

Jury

	M. BOUZEKRI	Ingénieur de recherche (ArcelorMittal)
	D. FABREGUE	Maître de Conférences (INSA de Lyon)
Rapporteur	P. JACQUES	Directeur de recherche FNRS (Université Catholique de Louvain)
	X. KLEBER	Professeur (INSA de Lyon)
Rapporteur	P. PAILLARD	Maître de Conférences (Polytech Nantes)
	C. SCOTT	Expert (Areva)
	M. SUERY	Directeur de recherche CNRS (Grenoble INP)

Laboratoire de recherche : MATEIS – UMR 5510

Abstract:

High manganese TWIP (TWinning Induced Plasticity) steels are particularly attractive for automotive applications because of their exceptional properties of strength combined with an excellent ductility. However, as austenitic steels, they appear to be sensitive to liquid zinc embrittlement during welding, the liquid zinc arising from the melted coating due to the high temperatures reached during the welding process. In this framework, the cracking behaviour of a high manganese austenitic steel has been investigated in relation to the liquid metal embrittlement (LME) phenomenon by hot tensile tests carried out on electro-galvanized specimens using a Gleeble 3500 thermomechanical simulator. The influence of different parameters such as temperature and strain rate on cracking behaviour has been studied. Embrittlement appears within a limited range of temperature depending on experimental conditions. Conditions for which cracking occurs could be experienced during welding processes. The existence of a critical stress above which cracking appears has been evidenced and this critical stress can be used as a cracking criterion. Finally, the study of the influence of different parameters such as time of contact between steel and liquid zinc before stress application, coating and steel on LME occurrence provides understanding elements of LME mechanism and permits to suggest solutions for preventing cracking during spot welding of such steels.

Keywords: TWIP steels - High manganese austenitic steels - Liquid Metal Embrittlement - Cracking - Hot tensile tests - Gleeble - Zinc - Resistance Spot welding

Résumé :

Les aciers TWIP (TWinning Induced Plasticity) à haute teneur en manganèse sont particulièrement prometteurs pour les applications automobiles de par leur excellent compromis entre résistance mécanique et ductilité. Cependant, la microstructure austénitique leur confère une sensibilité à la fragilisation par le zinc liquide durant les procédés de soudage ; le zinc liquide provenant de la fusion du revêtement résultant de l'élévation de température à la surface de l'acier. Dans cette étude, la fissuration d'un acier austénitique à haute teneur en manganèse a été étudiée en rapport avec le phénomène de fragilisation par les métaux liquides par des essais de traction à chaud réalisés sur des éprouvettes électrozinguées au moyen d'un simulateur thermomécanique Gleeble 3500. L'influence de nombreux paramètres tels que la température et la vitesse de déformation sur la fissuration a été étudiée. La fragilisation apparaît dans un domaine de température limité qui dépend des conditions expérimentales. Les conditions pour lesquelles la fissuration apparaît peuvent être rencontrées durant les procédés de soudage. L'existence d'une contrainte critique pour laquelle la fissuration apparait a été mise en évidence et celle-ci peut être utilisée comme critère de fissuration. Enfin, l'étude de l'influence de différents paramètres tels que le temps de contact entre l'acier et le zinc liquide avant l'application des contraintes, le revêtement et l'acier sur l'apparition de la fragilisation apporte des éléments de compréhension du mécanisme de fissuration et permet de proposer des solutions pour éviter la fissuration durant le soudage par point de l'acier étudié.

Mots clés : Aciers TWIP - Aciers austénitiques à haute teneur en manganèse - Fragilisation par les Métaux Liquides - Fissuration - Traction à chaud - Gleeble - Zinc - Soudage par point

Contents

Introduction **1**

Chapter I. Literature review **5**

I. TWIP steels **5**

I.1. Metallurgy of the Fe-Mn-C TWIP steels *5*

I.2. Deformation mode *7*

I.3. Mechanical properties *9*

Conclusions *13*

II. Spot Welding **14**

II.1. Principle *14*

II.2. The spot weld *17*

II.3. Welding defects *20*

II.4. Spot weld inspection *23*

Conclusions *23*

III. Liquid Metal Embrittlement **24**

III.1. Description of the occurrence of LME *25*

III.2. Fracture mode *26*

III.3. Factors influencing LME *28*

III.3.1. Contact between solid metal and liquid metal 28

III.3.2. Temperature 31

III.3.3. Composition of solid and liquid metals 32

III.3.4. Solid metal microstructure 33

III.3.5. Stress 35

III.3.6. Strain rate 36

III.3.7. Time of exposure 36

III.4. Embrittlement of steels by liquid zinc *37*

III.5. Models *39*

III.5.1. Dissolution-diffusion: Robertson and Glickman [JOS 99a] 40

III.5.2. Brittle fracture: Stoloff, Johnson, Westwood and Kamdar [KAM 87], [JOS 99a] 40

III.5.3. Ductile failure: Lynch [JOS 99a] 40
III.5.4. Liquid metal atoms penetration: Gordon [JOS 99a] 41
Conclusions *42*
IV. Zinc coating process **43**
IV.1. Hot-dip galvanizing *43*
IV.1.1. Principle 43
IV.1.2. Coating characteristics 45
IV.1.3. Growth kinetics of the intermetallic layers 47
IV.1.4. Fe-Mn-Zn system 47
IV.2. Electrogalvanizing *50*
Conclusions *50*
Summary **51**

Chapter II. Experimental procedures **53**
I. Studied steel **53**
II. Cups immersed in liquid zinc **54**
II.1. Cups characteristics *54*
II.2. Cups preparation *56*
II.3. Molten zinc bath *57*
III. Tensile tests **58**
III.1. Gleeble tests *58*
III.1.1. Principle 58
III.1.2. Specimen 59
III.1.3. Thermo-mechanical cycles 60
III.1.4. Description of embrittlement 62
III.2. Room temperature tests *63*
IV. Observations **63**
Conclusions **65**

Chapter III. Embrittlement of the Fe22Mn0.6C steel by liquid zinc **67**
I. Tensile behaviour of the Fe22Mn0.6C steel **67**
I.1. Room temperature behaviour *67*
I.2. High temperature behaviour *69*
I.3. Conclusions *75*

II. Sensitivity of the Fe22Mn0.6C steel to the liquid zinc embrittlement 76
III. Influence of temperature 80
IV. Influence of strain rate 83
V. Criterion of occurrence of LME 85
VI. Influence of the microstructure 90
VI.1. TD specimens 90
VI.2. Comparison between TD and LD specimens 92
VI.3. Conclusions 94
VII. Residual stresses 95
VII.1. Description of cracking 95
VII.2. Determination of critical stress 96
VII.3. Cracks observations 102
Conclusions 107

Chapter IV. Towards an explanation of cracking mechanisms 109
I. Influence of coating and steel 109
I.1. Influence of coating 109
I.1.1. Galvanized specimens 109
I.1.2. Annealed EG specimens 110
I.2. Influence of steel 111
I.2.1. TWIP steel having different chemical composition 111
I.2.2. AHSS steels 114
II. Influence of time of contact between the substrate and the liquid metal: isothermal holding 118
II.1. Holding and tensile testing at the same temperature (Holding A) 119
II.2. Holding at T and tensile testing at 800°C (Holding B) 125
II.2.1. Influence of holding time 125
II.2.2. Influence of holding temperature 126
II.3. Observations 128
II.4. DP1180 and TRIP800 steels 135
II.5. Conclusions 137
III. Cracking mechanisms 139
Conclusions 145

Chapter V. Links with spot weld cracking 147
I. Simulations 147
II. Influence of heating rate 152
III. Welding experiments 154
III.1 Welding with spacers 154
III.2 Welding of scratched sheets 157
III.3 Influence of expulsion on cracking 158
IV. Solutions to avoid cracking during spot welding 159
Conclusions 161

Conclusions 163
Outlooks 166

References 169

Introduction

With increasing environmental requirements, cars fuel consumption has to be decreased by, among other things, reducing the vehicles weight without decreasing the safety of passengers and pedestrians. The reduction of sheets thickness permitting a car structure lightening is conceivable provided sheets exhibit higher mechanical properties in order to not degrade the mechanical behaviour of the structure. In this framework, new steels meeting both environmental and safety requirements have recently been developed. Among them, high manganese austenitic steels combining exceptional properties of strength and ductility are particularly promising. Better strength to weight ratios can be achieved whereas their high ductility gives high potential to form parts of complex geometry. These steels are particularly suitable for structural parts. These attractive properties stem from a fully austenitic structure and a principal deformation twinning mode in addition to the classical mechanism of dislocation gliding, known as the TWinning Induced Plasticity (TWIP) effect.

Resistance spot welding is an assembly process widely used in the automotive industry for joining steel sheet components. This process is inexpensive, fast and well suited to mass production. A typical vehicle contains thousands spot welds. Hence, to ensure the integrity of the whole structure during vehicle lifetime, welded joints must provide sufficient quality and safety strength.
Steel sheets are generally (zinc) coated to protect them from corrosion. To use the coated metal with confidence, it must be checked that the presence of zinc does not affect the spot weld quality and performance.

However, cracks have been noticed in the heat affected zone (HAZ) of the studied TWIP steel spot welds as illustrated in figure 0.1 [BOU 07]. The main crack passes through the whole sheet thickness. The detrimental effect of such crack is obvious and the understanding of responsible phenomenon is essential. The microprobe analysis of the previous spot weld reveals the presence of zinc all along crack [PET 08]. Moreover, zinc seems to be responsible for such cracking since zinc coated steel is more likely to crack than uncoated steel [BOU 09]. During high temperature processes, the zinc present at the surface of the steel is likely to melt (due to its low melting point 420°C), leading to the Liquid Metal Embrittlement (LME) phenomenon.

Figure 0.1. Cracks observed on dissimilar spot weld TWIP 1,2mm/Usibor 2,5mm/Usibor 1,75mm [BOU 07]

LME results from the simultaneous action of stresses and the presence of a liquid metal and leads to severe deterioration of the material's mechanical properties (instantaneous loss of ductility). It occurs within a limited temperature range called “ductility trough” [JOS 99, FER 96, FER 97] and although known since 1874 and subject to numerous investigations, the mechanisms involved are still poorly understood. More recently, Fernandes and Jones [FER 96, FER 97] suggested that the occurrence of LME strongly depends on the test conditions and procedures employed. The LME phenomenon has mainly been studied from the angle of mechanical testing while specimens are in contact with liquid metal [LEG 00, NIC 01, BOS 07, CLE 03]. Embrittlement of austenitic stainless steels by zinc has often been reported [DIL 90]. However, to our knowledge, the literature includes no reports dealing with the embrittlement of austenitic TWIP steels by liquid zinc. All these results lead to the need to carry out detailed investigations on electro-galvanized high manganese austenitic steels to use the full potential of this material.

The first objective of the PhD is to characterize the behaviour of the TWIP steel in presence of liquid zinc and determine conditions leading to liquid zinc embrittlement of the steel. For this purpose, a test permitting to measure the cracking sensitivity has been developed: it consists in performing hot tensile tests on bare and electro-galvanized specimens using Gleeble simulator.
The second objective was to provide some elements for understanding cracking mechanisms occurring during spot welding and proposing solutions for inhibiting this phenomenon.

The first chapter is a literature review aiming at providing necessary elements for understanding the problematics of the present study. The first part presents the high manganese TWIP steels. Then, the spot welding process is described. The different aspects of the Liquid Metal Embrittlement phenomenon are exposed in the third part, and the last part deals with the galvanizing of high manganese steel.

The second chapter exposes, after a brief presentation of the studied steel, the different experimental techniques used in the study. Two main tests have been carried out: immersion of cups containing high residual stresses in a liquid zinc bath and hot tensile tests using a Gleeble simulator.

The third chapter presents the tensile behaviour of the studied steel before describing its behaviour in presence of liquid zinc through hot tensile tests and immersion of cups in liquid zinc. Hot tensile tests permits to investigate the influence of different experimental parameters such as temperature and strain rate.

In the fourth chapter, the influence of additional parameters such as time of contact between steel and liquid zinc is investigated with the aim of understanding cracking mechanisms.

The last chapter aims at correlating results obtained from Gleeble tests with the particular case of spot welding by numerical simulations and different welding experiments. Finally, different solutions that would permit to inhibit cracking during spot welding are proposed.

Chapter I. Literature review

This chapter is constituted by four main parts. The first one presents the high manganese TWIP steels, whereas the second exposes the spot welding process. The welding cycle is described as well as the metallurgy of the resulting spot weld and potential defects that can appear during welding process. Then, a literature survey concerning the Liquid Metal Embrittlement is proposed. A description of the phenomenon, the influence of key parameters and the different models are exposed. Finally, the galvanizing process is detailed. The particular case of galvanizing of high manganese steel is outlined.

I. TWIP steels

Twinning Induced Plasticity (TWIP) steels combine high strength with high ductility making them very attractive for the automotive industry. TWIP steels possess a fully austenitic structure at room temperature mainly due to the high content of manganese. Disclosed by Robert Hadfield in 1882, they have been rapidly used in industrial applications and particularly for railroad crossings. The original composition, Fe–1.2% C–13% Mn, has been recently modified in order to improve properties, particularly the weldability. During the last decade, many studies have been conducted on the austenitic Fe-Mn-C alloys in the prospect of automotive applications. This part focuses on the main characteristics of the Fe-Mn-C TWIP steels.

I.1. Metallurgy of the Fe-Mn-C TWIP steels

Low alloyed steels are generally ferritic (bcc structure) or contain different phases as a result of heat treatments. Adding adequate alloying elements permits to stabilize the austenite and to obtain fully austenitic (fcc) structures at room temperature. Nickel and chromium are used in the case of austenitic stainless steels and manganese is employed in the case of TWIP steels. Other alloying elements such as C (<1 wt.%), Al (<3 wt.%) or Si (<3 wt.%) are added in austenitic TWIP steels in order to strengthen the matrix by solid solution hardening.

These austenitic steels could be more or less stable. In effect, martensitic transformation can occur under internal or external stresses resulting in the apparition of two martensitic phases: α' martensite (bct almost bcc structure with a lattice parameter varying with the carbon

content from 0.287nm to 0.300 nm) and ε martensite (hcp structure with lattice parameters a = 0,2538 nm and c = 0,4080 nm) [ALL 04]. Two transformation mechanisms can occur: the direct transformation from austenite into α' martensite or the two-steps transformation in which the α' phase is formed from the ε martensite [BRA 07]. The phase diagram proposed by Schumann [SCH 72] for the Fe-Mn-C system is shown in figure I.1. The different phases obtained at room temperature after quenching as a function of carbon and manganese content are shown. It clearly shows the possibility for this system to obtain a single-phase austenitic steel at room temperature for high amount of Mn and a certain amount of C. The studied steel (22 wt. % Mn 0.6 wt.% C) lies in this austenitic domain. In the obtained solid solution, carbon is in insertion and manganese in substitution. Both elements stabilize the austenite.

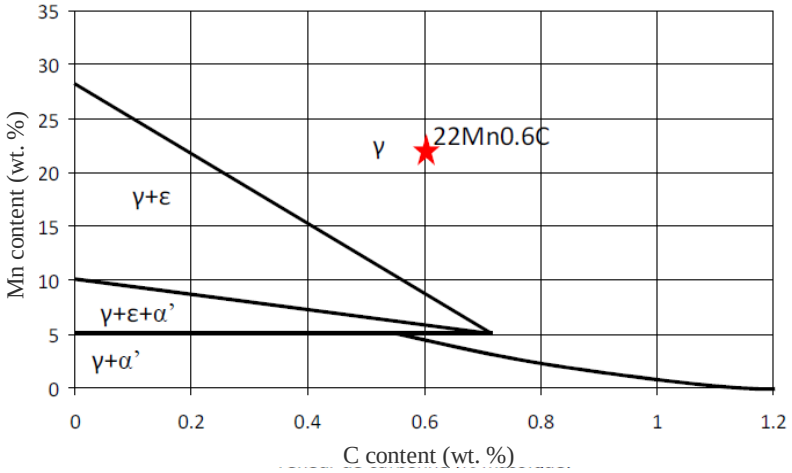

Figure I.1. Phase diagram of Fe-Mn-C system [BAR 09] from [SCH 72]

The typical microstructure of the studied steel is presented in figure I.2. It is worth noticing the small grain size (about 2.6μm). This feature contributes to the excellent mechanical properties of this steel with the strengthening by twinning.

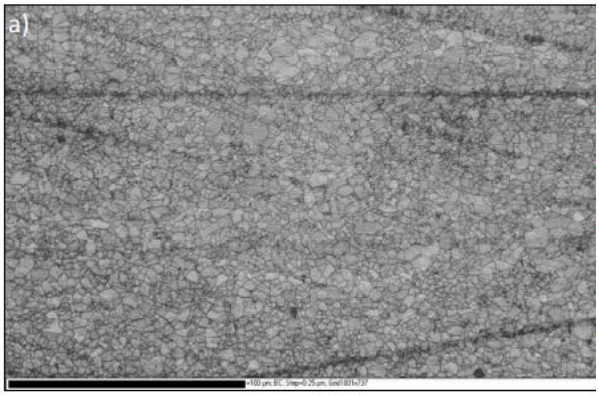

Figure I.2. EBSD map (band contrast) of the studied steel in the initial state [BAR 09]

I.2. Deformation mode

Different deformation mechanisms controlled by the stacking fault energy (SFE) of the austenitic phase can be activated in high-Mn TWIP steels [VER 04]. According to [ALL 04b] and [DUM 07], the formation of α'-martensite, resulting in a reduction of ductility, occurs for SFE<12mJ/m^2. The austenite to ε martensite transformation occurs for SFE<18 mJ/m^2 while mechanical twinning requires values between 12 and 35 mJ/m^2. For higher SFE, only dislocation gliding mechanism is activated.

Most austenitic steels have low-to-moderate SFE. The SFE varies with the temperature and the steel composition. In figure I.3, it can be seen that increasing temperature tends to increase SFE. Allain *et al.* [ALL 04b] study the evolution of the SFE with temperature in the Fe22Mn0.6C austenitic steel. They show that decreasing temperature leads to a reduction of the SFE so that at 400°C, only dislocation gliding occurs, at 20°C, dislocation gliding is in competition with mechanical twinning and at -196°C, ε martensitic transformation is activated.

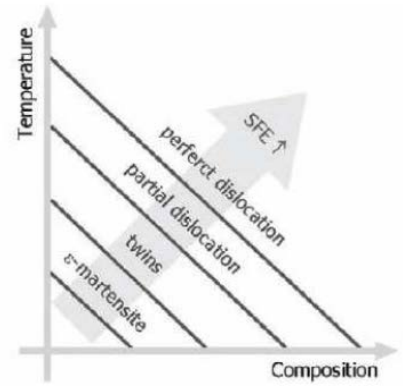

Figure I.3. Schematic representation of the influence of the SFE on the deformation mode [HAM 07a]

The stability of austenite and its ability to deform by twinning or by martensitic transformation strongly depend on alloying elements. The evolution of the calculated SFE with manganese and carbon content is shown in figure I.4. It can be seen that increasing carbon and manganese contents increases the SFE. In addition, the straight lines proposed by Schuman [SCH 72] to describe the occurrence of thermal and mechanical martensitic transformations are also plotted. The dashed line represents the carbide precipitation limit at 700°C. For instance, a steel containing 0.6wt.%C and 22wt.%Mn will have a SFE about 20mJ/m^2 and consequently, will mainly deform by mechanical twinning.

Also, Al generally increases the SFE while Si tends to decrease it [BOU 01], [HAM 07b], [PAR 10].

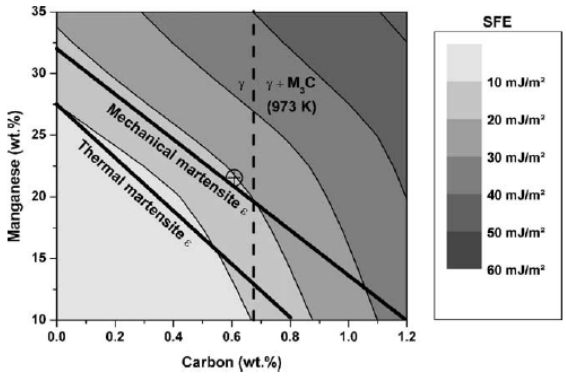

Figure I.4. The calculated room temperature iso-SFE lines in the carbon/manganese (wt.%) map [ALL 04b]

Twin boundaries act as obstacles to dislocation glide providing work hardening. While straining, the volume fraction of twins increases as illustrated in figure I.5, providing a continuous refinement of the structure, hence the mean free path of dislocation decreases delaying necking to higher strain (dynamical Hall-Petch effect) [ALL 04].

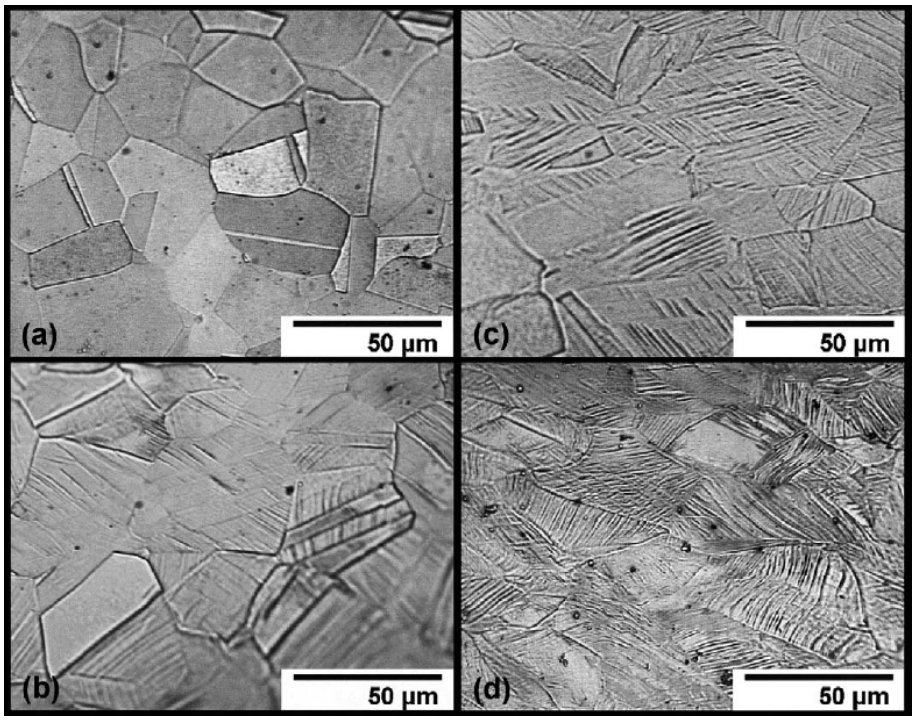

Figure I.5. Evolution of the microstructure of a Fe–22Mn–0.6C steel with strain: (a) unstrained (b) 18% strain (c) 26% strain (d) 34% strain [ALL 04c]

I.3. Mechanical properties

Austenitic Fe-Mn-C steels exhibit outstanding properties of strength (>1000MPa) and ductility (>50%) based on a high work-hardening capacity as compared to the other steel grades used in car manufacturing (figure I.6).

The exceptional properties of TWIP steels arise from the fully austenitic structure and the twinning deformation mode in competition with the classical dislocation gliding.

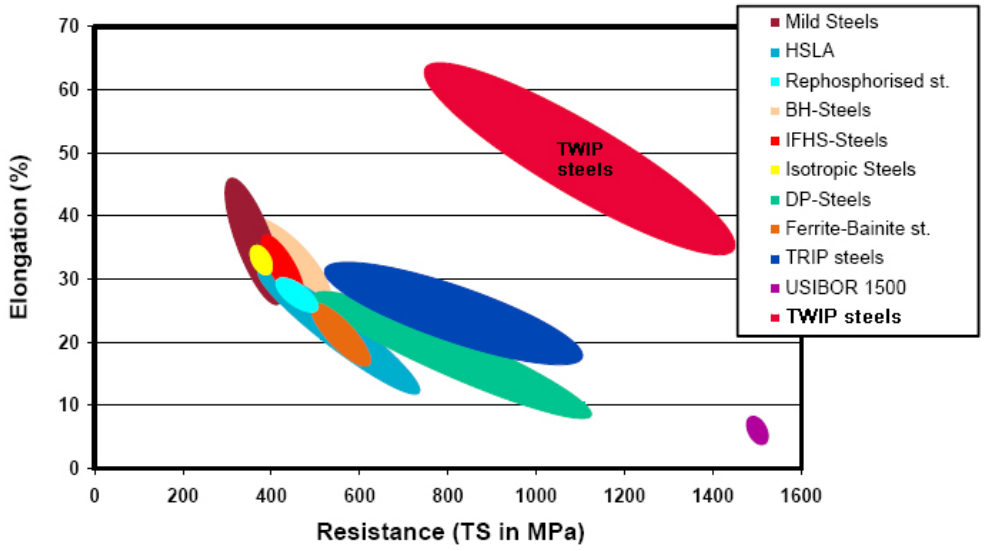

Figure I.6. Ductility/strength in tension diagram for different automotive steels [CUG 05]

Mechanical behaviour of the Fe-22Mn-0.6C steel used in this work has been studied by Allain [ALL 04]. Tensile curves obtained at different temperatures at a strain rate of 7.10^{-4} s^{-1} are presented in figure I.7.

Corresponding mechanical properties are characterized by:

- A rather low yield strength (about 400MPa at room temperature)
- A very high ultimate tensile strength (>1000MPa at room temperature), decreasing with increasing temperature
- A very ductile behaviour and particularly a high uniform elongation
- A remarkably high strain hardening rate

It can be observed that the steel reaches high strength when it is highly deformed. This is of great interest for designing parts with complex shapes obtained by deep drawing.

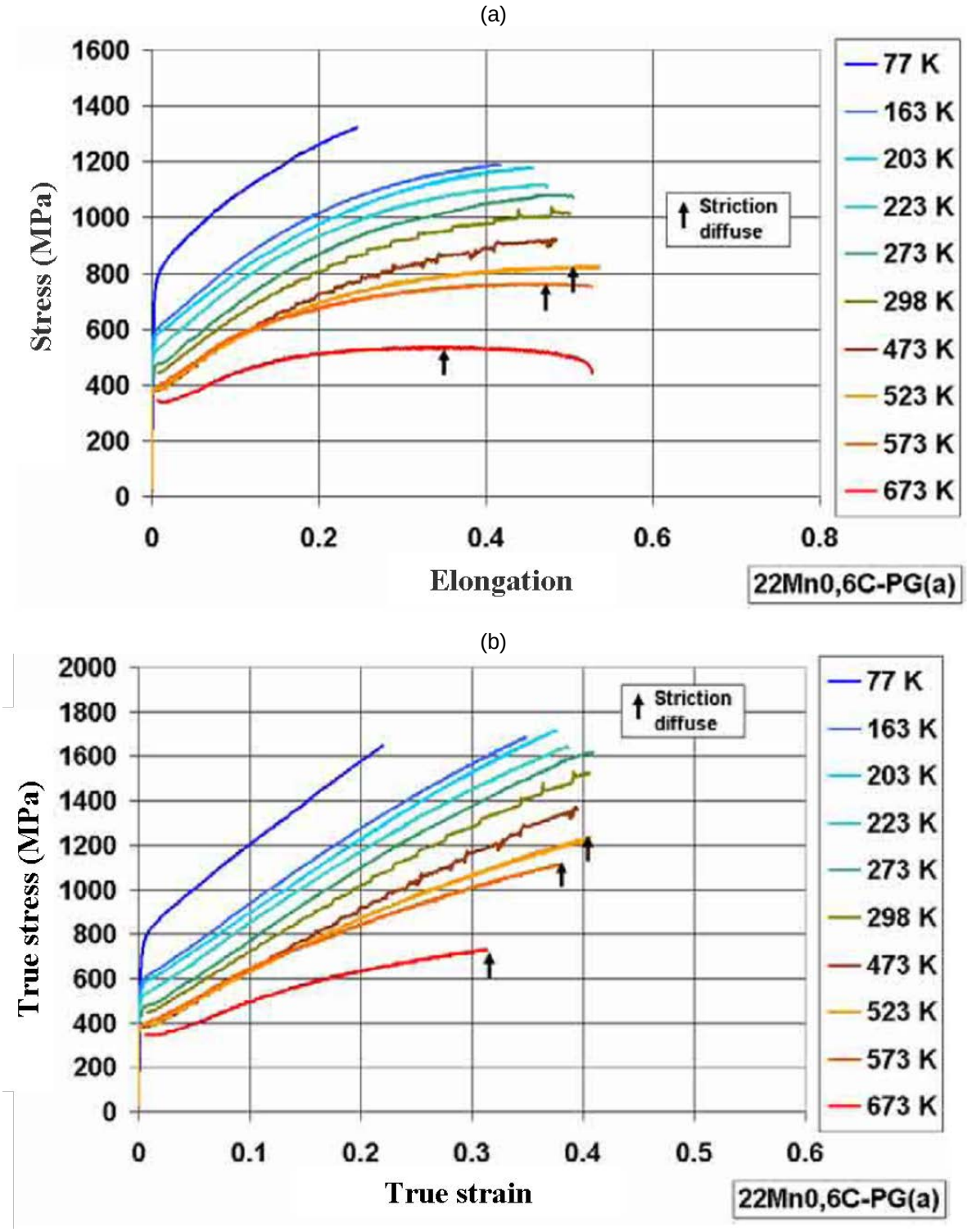

Figure I.7. (a) Engineering and (b) true tensile curves at different temperatures of a Fe-22Mn-0.6C fine-grained TWIP steel [ALL 04]

The decrease of yield strength and ultimate tensile strength with increasing temperature of the Fe-25Mn-3Si-3Al TWIP steel is clearly shown in figure I.8. The elongation values achieve a maximum at room temperature. These particular variations are commonly observed in TWIP steels and are generally attributed to the increasing amount of deformation twins with

decreasing temperature: at the temperature of maximum elongation, the gradual formation of deformation twins during the entire deformation process leads to enhanced elongation. However, for lower temperatures, reduced elongation is due to the premature twinning: the twin formation is completed in the early stages of deformation [ALL 04], [CUR 10].

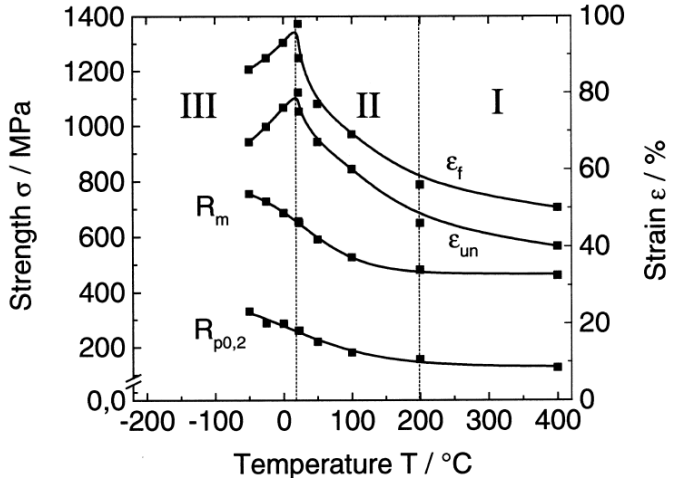

Figure I.8. Evolution of mechanical properties with temperature at quasistatic loading of Fe-25Mn-3Si-3Al TWIP steel [GRÄ 00]

The fracture surface analysis of the Fe-22Mn-0.6C steel shows a ductile intragranular rupture for every testing temperature as illustrated in figure I.9 [ALL 04].

Besides, Charpy-impact-tests performed on Fe-25Mn-3Si-3Al TWIP steel by [GRÄ 00] do not reveal any brittle-to-ductile transition even at very low temperature (-196°C), the steel being ductile in the whole temperature range.

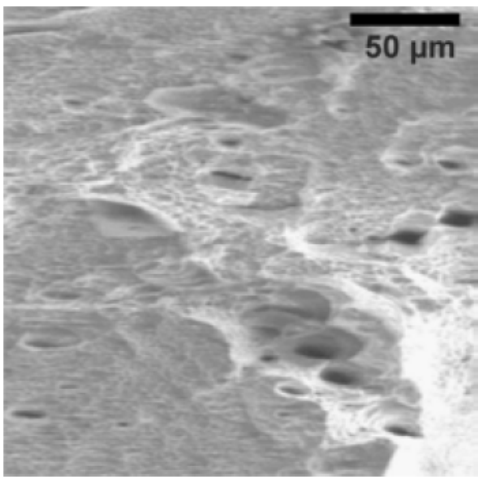

Figure I.9. Fracture surface of a Fe-22Mn-0.6C fine-grained TWIP steel deformed at room temperature [ALL 04]

The tensile behaviour of austenitic TWIP steels at high strain rate has been studied for different steels having different chemical compositions [GRÄ 00], [XIO 09], [CUR 10]. Results illustrated in figure I.10 show a relatively weak strain rate sensitivity regarding strength for low strain rates. A clear increase is observed for strain rate upper than 100 s^{-1}. However, elongation is significantly reduced when strain rate is increased up to 10^{-1} s^{-1} and slightly increases beyond. This can be attributed to the increase of the stacking fault energy caused by temperature rise brought about by the adiabatic deformation heating.

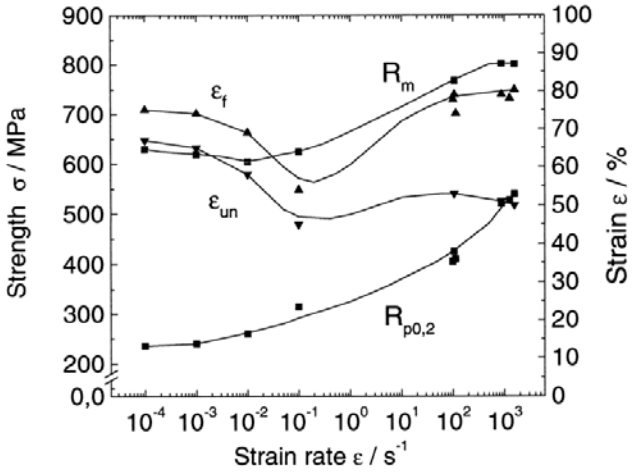

Figure I.10. Evolution of mechanical properties with strain rate at room temperature of Fe-25Mn-3Si-3Al TWIP steel [GRÄ 00]

Negative strain rate sensitivity in a limited temperature range has also been observed for low strain rates (<1s^{-1}) [ALL 04], [BAY 04], [LEB 09]. Figure I.11 shows a decrease in true stress with increasing strain rate. This is generally attributed to dynamical ageing due to carbon atoms. However, results must be analysed with care in so far as the adiabatic heating increase with increasing strain rate may affect the mechanical behaviour of the steel.

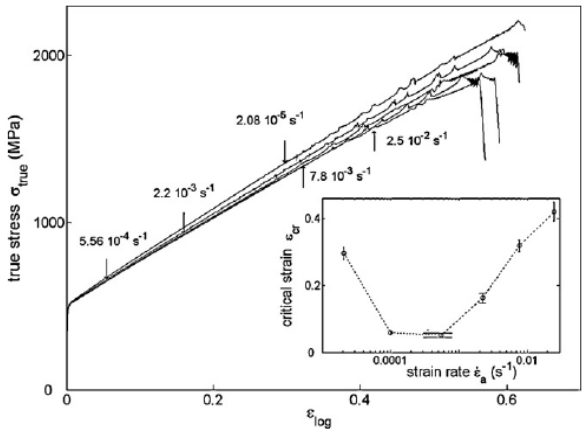

Figure I.11. Negative strain rate sensitivity of Fe22Mn0.6C TWIP steel [LEB 09]

Conclusions

High manganese TWIP steels combining exceptional properties of strength and ductility are particularly promising. Deformation behaviour of such steels have been widely studied in relation to microstructure and texture evolution by microscopy analysis (SEM and TEM), XRD measurements, EBSD technique [CHO 99], [DAI 99], [VER 04], [YAN 06], [UEJ 08], [BAR 09], [BRA 09], [IDR 09], [DAI 10], [IDR 10], [GUT 10] and several models have been proposed for predicting the SFE and mechanical properties as a function of the chemical composition or describing the microstructure-mechanical behaviour relationships [KAR 00a], [KAR 00b], [BOU 01], [KAR 01], [ALL 04a], [ALL 04c], [DUM 07], [BOU 08], [SHI 08], [DIN 09].

However, welding of such steels has been poorly investigated.

II. Spot Welding

Resistance spot welding is an assembly process used in many industrial fields such as automotive manufacturing industry, aerospace and nuclear sector. The invention of the resistance welding is attributed to Elihu Thomson who would have discovered in 1877 the possibility of welding by using an electrical current. However, this technology was significantly developed few years later, during the inter-war years, when wood was replaced by metals in body cars [DRO 93]. Nowadays, it still constitutes the main assembly process used in the automotive industry. For instance, a body in white structure contains between 3000 and 5000 spot welds as shown in figure I.12.

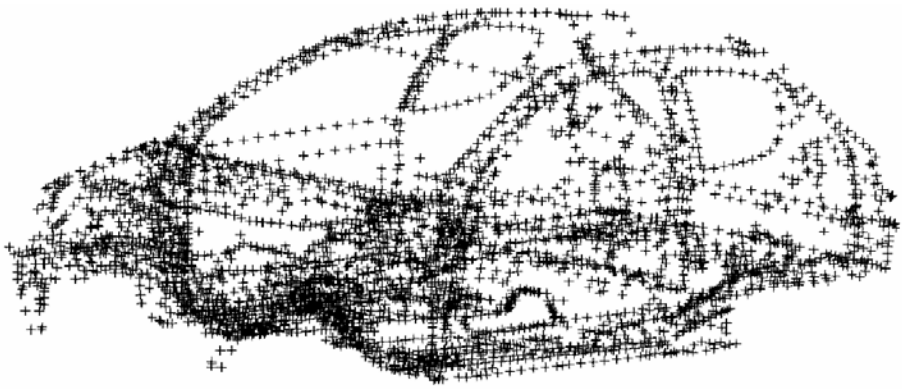

Figure I.12. Spot welds in a body in white structure [ROS 07]

Resistance welding lies on the Joule effect: the heat needed to create the joint is generated by the resistance of the interface of the materials to be welded to a high intensity current flow between electrodes.
Reduced costs, fastness, high possibility of automation are some of the major advantages of the resistance welding process.

II.1. Principle

Spot welding is a resistance welding process used for sheets of thicknesses ranging from 0,5 to 10 mm. The sheets to be welded can have different characteristics (composition, thickness). Widely used in the automotive industry, it associates the Joule effect with a mechanical pressure applied perpendicularly to the assembly as seen in figure I.13. Mechanical pressure as well as electrical current is applied via two electrodes made of copper alloy.

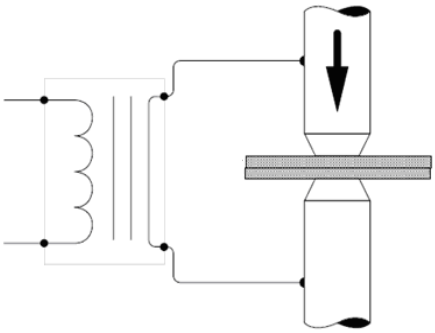

Figure I.13. Schematic principle of spot welding from [BLO 01]

The welded joint results from the succession of different mechanical, electrical and metallurgical stages constituting the welding cycle as illustrated in figure I.14. The different stages of the welding cycle are the following:

1. **Squeezing**. It is an essentially mechanical step. Electrodes are brought in contact with the surface of the sheets and a pressure is applied on pieces to assembly. This step permits to clamp sheets together and to assure a good electrical contact. The squeezing time must be sufficient to reach the applied pressure ranging from 200 to 600 daN according to thickness and nature of material.
2. **Welding**. The current flow through the stack-up of sheets produces sufficient energy to melt a zone at the interface of sheets. The heat generated by Joule effect in an electrical circuit can be expressed as

$$Q = \int_0^T RI^2 dt \qquad \text{(eq. I.1)}$$

where R is electrical resistance in the circuit, I current, T duration of the phenomenon, t time. The current (5-20 kA) is applied between the electrodes during a finite time, the as called “welding time”. It is worth noting that the welding current can be applied in different ways: progressive rise or extinction (respectively “up slope” and “down slope”), by pulses… Moreover, different heat treatments such as pre-heating or post weld heat treatments can be performed in order to modify the weld microstructure and the mechanical properties.

3. **Holding**. The current is removed while pressure is maintained to permit the solidification of the melted zone. The assembly is rapidly cooled by thermal conduction through the water-cooled electrodes and the sheets volume. Applying pressure during cooling permits to form a homogeneous nugget and to avoid the formation of porosity. The holding time is generally identical to the welding time.

4. **Separation of the electrodes**. At the end of the cycle, the electrodes are removed and the workpieces move for next spot.

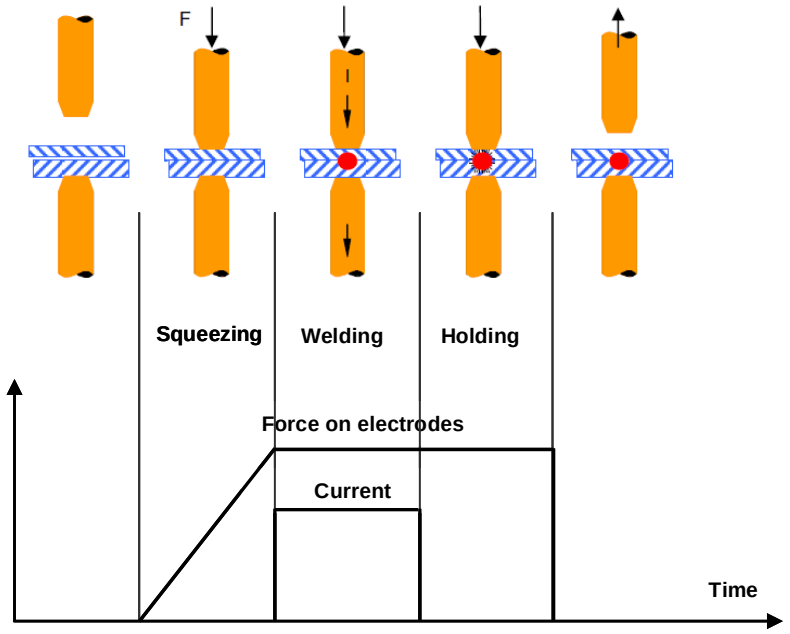

Figure I.14. Representation of spot-welding cycle from [DAN 09]

According to the equation (I.1), the heat generated by applying current trough the stack-up of sheets depends on the amplitude and duration of the current and on the electrical resistance of the sheet stack-up between the electrodes; the latter being the sum of the contributions of the contact resistance at the electrode-sheet interfaces (R1, R5), the one at the sheets interface (R3) and the bulk resistance (R2, R4) as illustrated in figure I.15. R1, R3 and R5 are contact resistance, hence, are very sensitive to pressure distribution and surface conditions at the contact interfaces. R2 and R4 depend on electrical resistivity of material to be welded which varies with temperature.

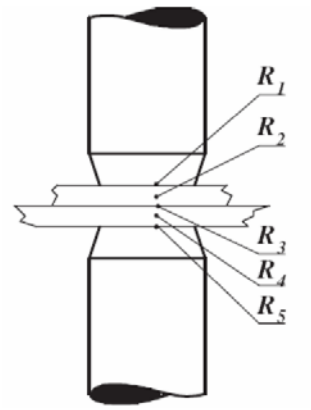

Figure I.15. Localization of individual resistances [DRO 93]

During the welding of coated sheets, the coating may significantly affects the contact resistance. Therefore, the coating must be taken into account in the choice of welding parameters. For instance, zinc resistivity is lower than that of steel. Consequently, zinc coated steel sheets require higher welding current than uncoated sheets.

II.2. The spot weld

When the current is applied between the electrodes, temperature increases by Joule effect first at the interface, then, to a lesser extent, in the bulk material. The temperature rise implies an important expansion, proportional to the coefficient of thermal expansion of the welded materials. This expansion is limited in the axis of electrodes due to the pressure exerted by the electrodes. When the melting temperature of the metals to be welded is reached, a liquid nugget develops on both sides of the interface. An amount of the heat is dissipated in the neighbouring base metal, the as called Heat Affected Zone (HAZ). When the current is removed, the pressure is maintained and the solid nugget solidifies implying contractions. These thermal contractions/expansions lead to the generation of stresses/strains in the assembly.

The geometry of a spot weld presents three particularities: the discontinuity of the assembly, the presence of a notch likely to act as a stress concentrator in case of mechanical loading and indentation of external surfaces corresponding to the penetration of the electrodes (figure I.16).

A spot weld contains three main zones as a consequence of the different treatments experienced during the welding cycle:
- the molten zone corresponds to the zone where the metal has fully melted and then solidified very quickly,
- the heat affected zone where the microstructure of the base metal has been modified by the thermal cycle,
- the base metal does not experience any microstructural modifications.

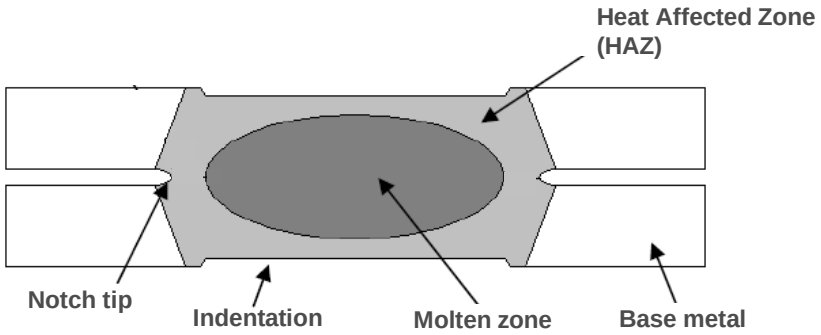

Figure I.16. Schematic representation of a spot weld from [DAN 09]

In the molten zone as well as in the HAZ, the microstructure is determined by the experienced heating and cooling cycles. Figure I.17 shows an example of the welding cycle calculated by Sorpas software in the case of a homogeneous assembly of 1,5mm DP580 sheets [DAN 09]. The heating and cooling rates are extremely high, in the range of 1000°C/s, the complete welding cycle being realized in less than one second. Consequently, transformations occurring during welding are far from equilibrium and phase diagrams are inadequate. Nevertheless, they can be useful for determining transformations likely to occur during welding and subsequent microstructures.

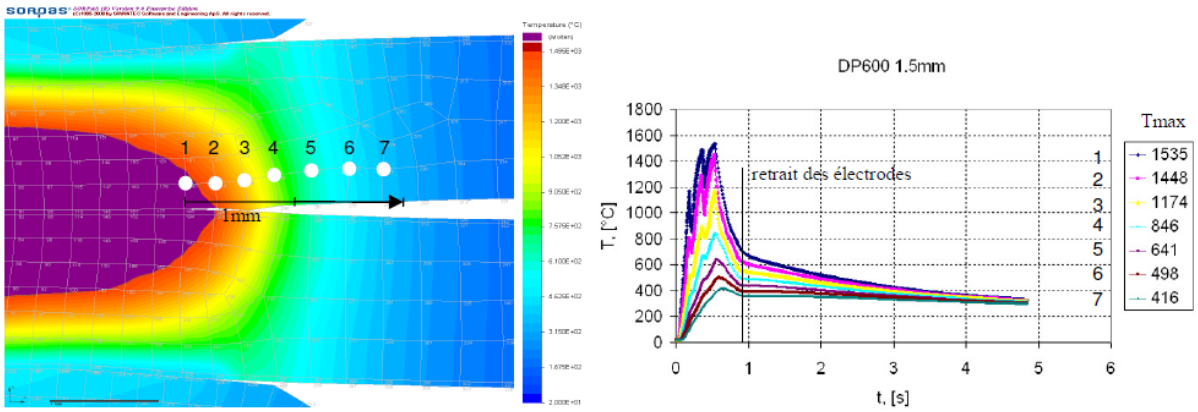

Figure I.17. Results of simulations of thermal cycles near the interface from the molten zone to the base metal (DP590): (a) position of selected nodes, b) corresponding thermal cycles [DAN 09]

The different microstructures appearing upon heating and cooling in the case of a low alloyed steel (0,15%C) are as follows (figure I.18):

1 The **base metal**: in this zone, the temperature does not exceed 600°C so that the metal does not experience any major microstructural modifications.

2 In the **subcritical zone**, the maximal temperature ranges from ~ 600 °C and A_{C1}. This zone does not undergo any observable microstructural changes; however, some metallurgical modifications, such as nucleation of fine precipitates can occur. Grain size is not changed.

3 The **intercritical zone** experiences temperatures between A_{C1} and A_{C3}. This zone is partially transformed with coexistence of ferrite α and newly formed austenite γ.

4 The **grain refined zone** for temperatures between A_{C3} and a grain-coarsening temperature depending on steel. A fine but non homogeneous austenitic structure replaces the initial microstructure. Grain size increases with increasing temperature. The rapid cooling leads to a fine bainite-martensitic microstructure.

5 The **grain growth zone** for temperatures between grain-coarsening temperature and the melting temperature. The enhanced austenitic grain growth promotes a high quench ability. The microstructure obtained after rapid cooling is generally martensitic.

6 The **molten zone** for temperatures above the melting temperature. After rapid cooling, the microstructure is made of dendrites. Interdendritic segregations can be observed.

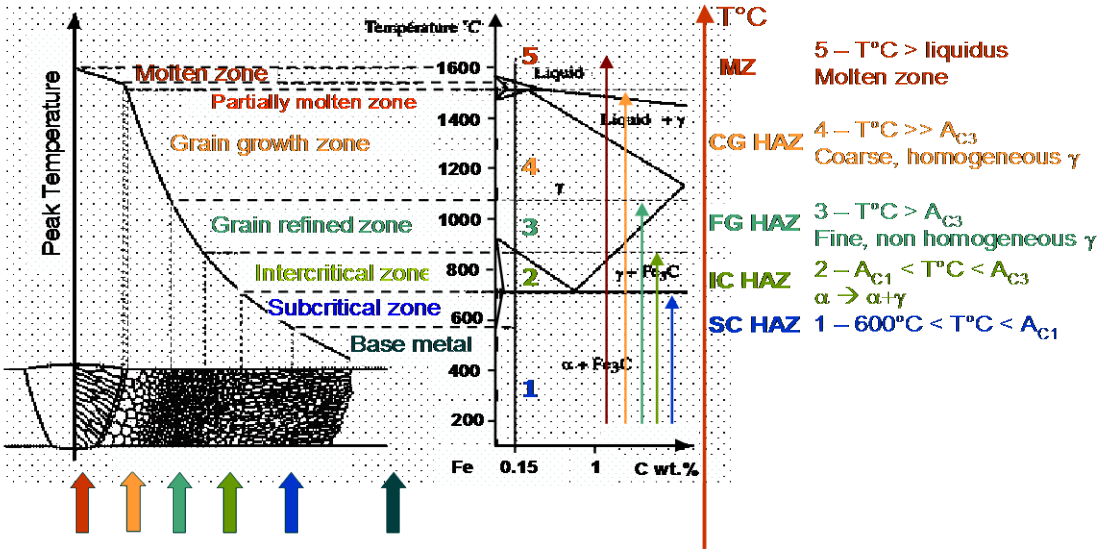

Figure I.18. Microstructures generated during heating from [BLO 01]

For high alloyed steels such as high manganese TWIP steels, phase diagrams are different from the previous one, and consequently, the expected microstructures are also modified. For instance, the steel under study contains high contents of manganese and carbon and does not exhibit any phase transformation. Thus, the microstructure resulting from spot welding will be very different from the previous one. It should exhibit only more or less coarsened γ phase.

II.3. Welding defects

Different types of defects may be created during welding process such as porosity (due to the shrinkage of the nugget and the subsequent volume deficit) and cracks. If some of them do not have any detrimental effect on weld quality, others can be really hazardous for the structural integrity of welds since they may decrease mechanical properties and corrosion resistance of welded structures [KOU 03] [ZHA 06].

During cooling, and particularly during solidification, material must withstand different strains and/or stresses:

- Solidification shrinkage (higher density in the solid state as compared to the liquid state)
- Thermal contraction (with decreasing temperature according to the thermal expansion coefficient)
- External strains/stresses depending on process used (clamping,…).

The combination of a tensile stress field and a weakened structure is required for cracking to occur.

Hot cracking (solidification and liquation cracking) occurs at elevated temperatures, close to the melting point of the material, while cold cracks (hydrogen related cracks) form after the weld metal has cooled down to room temperature. Cracking may appear at all locations of a weldment: in the nugget, in the HAZ, and in the base metal. Some structures such as austenitic stainless steels, aluminum alloys or nickel-based-alloys are particularly sensitive to this kind of defects.

Solidification cracking occurs during the final stages of solidification of the weld metal at elevated temperatures [LIP 05]. The formation of impurity-enriched liquid films having very low mechanical properties and low melting point along grain boundaries during the final stage of solidification weakens the structure. When localized tensile stresses/strains in the material exceed a threshold level, cracks appear. Cracking occurs when the permeability of the solid skeleton is too high to enable liquid flow and when there is not

enough liquid to feed up formed cracks. The microstructure and the mechanical properties of the solid squeleton strongly influence the solidification cracking susceptibility. Tensile tests of solidifying metal can be carried out to determine the ductility evolution as a function of temperature. An example of ductility curve is shown in figure I.19. Ductility progressively decreases below the coherency temperature, which corresponds to the instant when dendrites start to be in contact to form a solid network, and is sharply recovered near solidus.

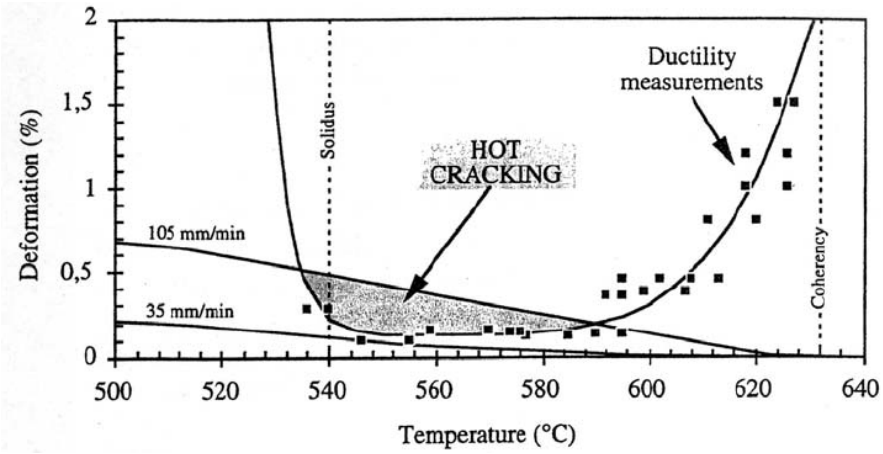

Figure I.19. Evolution of ductility with temperature [MAG 96]

Cracking occurs when the solidifying metal suffers a reduction of ductility and is unable to support strain in a certain temperature range between the solidus and liquidus temperature known as the Brittle Temperature Range (BTR). Besides, strain rate also significantly affect the cracking behaviour [SHA 03]. [LIU 06] show that increasing strain rate tends to increase the solidification cracking susceptibility in aluminum alloy. Fracture surfaces often reveal the well-developed dendritic morphology and the intergranular, without plasticity, characteristics of cracks.

Ductility-dip cracking refers to the solid state cracking resulting from a sharp drop in ductility at elevated temperatures (below the effective solidus temperature). Such cracking typically occurs in the HAZ or in reheated weld metal [YOU 08]. It is generally associated with single phase austenitic alloy with large grain size [LIP 05]. Like previous cracking mechanism, ductility-dip cracking leads to intergranular cracks. Figure I.20 presents the strain-temperature curves obtained using the Gleeble thermomechanical simulator for different alloy spot welds. The test consists in performing a gas tungsten arc spot weld in the centre of the gage section. Specimens are then heated to the testing temperature, held 10 seconds at this temperature. Then, a finite strain is applied at a given strain rate. After cooling

at room temperature, specimen is examined using a binocular microscope to determine if cracking has occurred [NIS 03]. Curves represent the cracking susceptibility. A domain of reduced ductility (and thus, cracking resistance) is clearly seen.

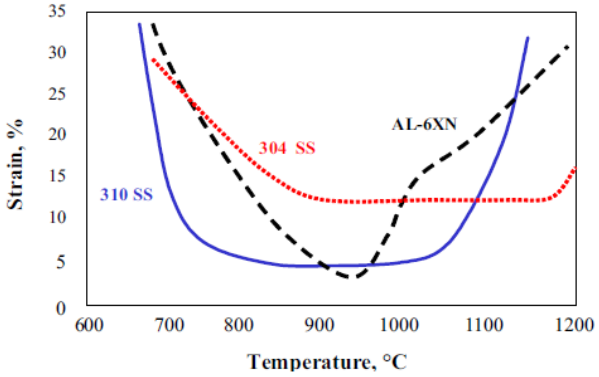

Figure I.20. Dependence of ductility on temperature for three austenitic stainless steels [LIP 05]

Liquation cracking occurs in the HAZ at temperatures below the solidus of the bulk material. Cracking is caused by liquation of low-melting-point components or eutectic phases along grain boundaries. Liquation results from the high temperatures reached in the HAZ material during welding operations. These intergranular liquid films obviously weaken the structure since they have no strength to resist thermal and mechanical stresses. Opening of this liquid film, due to thermal and/or mechanical stresses developed during cooling leads to cracking. Liquation cracking is intergranular. It is worth noting that even if the liquation cracking is avoided during welding, liquated grain boundaries make the HAZ highly susceptible to ductility loss after welding. In order to forecast the possibility of liquation cracking, a good knowledge of the nature, amount and solubility of elements present in the base metal, as well as the melting temperature of their eutectics is essential [SEN 00], [YAN 01], [ZHA 06].

In both solidification and liquation cracking, an analogy can be done with the liquid metal embrittlement phenomenon, in that cracking occurs while the solid metal is wetted by a liquid under tensile stresses and results in intergranular cracking (see §III).

II.4. Spot weld inspection

The quality and the structural integrity of spot welds can be determined by visual inspection (permit to detect surface defects), non destructive techniques such as ultrasonic, X-ray imaging or liquid penetrant inspection and destructive techniques (metallographic cross section observations or mechanical testing). This permits to study the influence of welding parameters on the quality of the weld.

Conclusions

Spot welding process has been used for many years particularly in the automotive industry. However, phenomena involved in welding cycle are very complex in that many electrical, mechanical, thermal and metallurgical interactions exist. Moreover, due to high temperatures, high heating and cooling rates experienced during welding cycle impeding direct measures, determination of relevant parameters such as temperature, stress, strain… in a weldment is difficult. Numerical simulations such as finite element can provide good approximations. Besides, thermomechanical simulators like Gleeble permit to reproduce welding cycle and study the resulting microstructure.

Different mechanisms are involved in weld cracking such as solidification and liquation cracking. Another origin of weld cracking can arise from the melting of coating during welding process and the subsequent liquid metal embrittlement phenomenon.

III. Liquid Metal Embrittlement

Liquid Metal Embrittlement (LME) is one case of environmentally assisted cracking (as hydrogen embrittlement or stress corrosion cracking) resulting from a synergetic action of aggressive environment and stresses. LME refers to the brittle fracture of a usually ductile metal stressed while in contact with a liquid metal. LME can occur for instance, during high temperature processes or in nuclear power industry where structural materials are in contact with molten metals.

Although known since 1874 [JOH 74] and much investigated, mechanisms involved in LME phenomenon are still poorly understood. Empirical predictions of LME susceptibility have been proposed: embrittled systems usually have a low mutual solubility and a lack of intermetallic compounds [KAM 87], [JOS 99a]. A high mutual solubility may result in the dissolution of the solid metal by the liquid one and may lead to blunt the crack tip and stop further crack growth. But exceptions to both predictions are known.

Only some particular liquid metal/solid metal systems are prone to embrittlement, while others seem to be immune. For example, the LME is well known for Al_{solid}/Ga_{liquid}, Ni_{solid}/Bi_{liquid}, Cu_{solid}/Bi_{liquid} systems. It is referred to as the *LME specificity*. More recently, Fernandes and Jones [FER 96a], [FER 97] questioned this specificity and suggested that the occurrence of LME strongly depends on the testing conditions and procedures employed. A given couple can appear to be immune under a particular set of conditions, which does not preclude embrittlement under different testing conditions. The occurrence of embrittlement of a martensitic steel by liquid lead or Pb-17Li depending on experimental conditions has often been reported [GLA 04]. For instance, Legris *et al.* [LEG 00] show that a martensitic 9% Cr 1% Mo steel can be prone to embrittlement by liquid lead provided particular metallurgical and mechanical conditions are fulfilled: the steel was hardened using an adapted heat treatment and triaxiality was introduced by machining a notch. Under usual conditions, liquid lead has no apparent detrimental effect, a fact that would have led to the wrong conclusion that the steel is not sensitive to the liquid lead embrittlement.

The LME phenomenon is commonly studied by mechanical testing while specimens are in contact with liquid metal (immersed in the liquid metal or coated with a liquid film) and subsequent fracture surface analysis is carried out [FER 96a], [FER 97], [JOS 99b], [LEG 00], [SAM 00], [NIC 01b], [LEG 02], [CLE 03], [GLA 04], [BOS 07]…

Some less common techniques, such as acoustic emission [KOD 94], in situ transmission electron microscopy observations [HUG 98], X-Ray microradiography [PER 03], [PER 04] or X-Ray microtomography [LUD 00] have also been used.

III.1. Description of the occurrence of LME

LME results from the simultaneous action of stresses and the presence of a liquid metal, and leads to severe deterioration of the mechanical properties (instantaneous loss of ductility) of the usually ductile material. LME is characterized by a significant reduction of elongation to rupture and fracture strength observed during a tensile test in the embrittling environment compared to what observed in inert environments [KAM 87], [JOS 99b], [VER 05]. Figure I.21 presents the tensile curves of copper tested under Ar and in liquid Bi at 300°C for a strain rate of 10^{-4} s^{-1} [JOS 99b]. The drastic reduction of elongation to fracture is characteristic of LME.

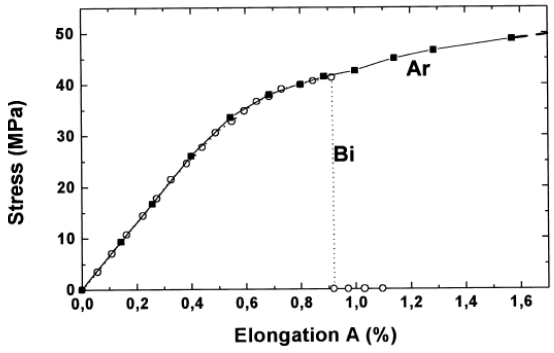

Figure I.21. Tensile curves of copper tested under Ar and in liquid Bi at 300°C at 10^{-4} s^{-1} [JOS 99b]

The analogy of the two tensile curves obtained in the embrittling environment and under Ar until the premature fracture seems to indicate that mechanical properties, such as yield strength, Young's modulus and work hardening, keep unchanged by the presence of the liquid metal. This result has often been reported [KAM 87], [HIL 95].

However, elongation to rupture and fracture strength are drastically reduced. Solid metal can even break well before yield strength is achieved [KAM 87], [NIC 01b]. Nevertheless, if general plasticity is not required, localized plasticity seems to be necessary in the embrittlement process [FER 96b], [JOS 99a].

III.2. Fracture mode

LME is characterized by a very high crack propagation rate (one centimetre to several meters per second) as compared to the rate in the air or vacuum [KAM 87], [JOS 99a].

LME is often associated to intergranular fracture since grain boundaries mechanisms are involved in LME mechanisms (see §III.3.1). However, several types of failure have been observed depending on studied solid metal / liquid metal couple and experimental conditions. Ductile failure has even been observed [KAM 87].

Brittle transgranular fracture has been observed for the martensitic steel T91 tested in liquid Pb-Bi eutectic couple [LEG 02] and in liquid lead [LEG 00], [NIC 01b] as illustrated in figure I.22.

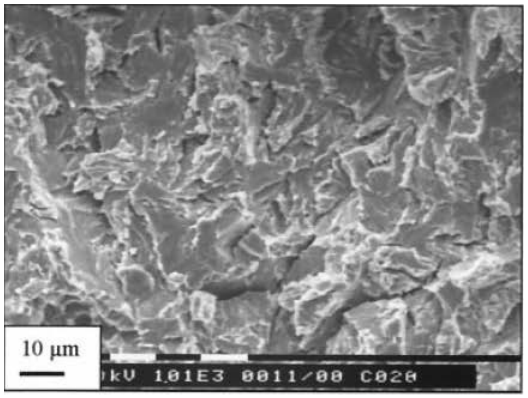

Figure I.22. Brittle transgranular fracture of martensitic steel tested in liquid lead [NIC 01b]

Intergranular cracking (figure I.23) was observed for Cu tested in liquid Bi [JOS 99b], brass in liquid gallium [FER 96a] and Ni tested after contact with liquid Bi [MAR 00a], [MAR 01].

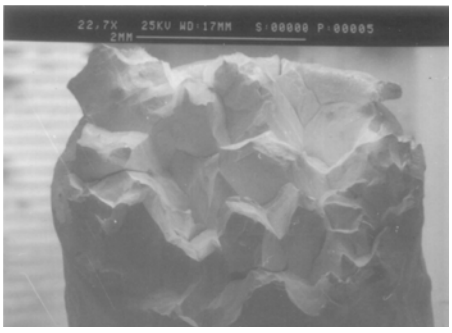

Figure I.23. Brittle intergranular fracture of brass tested in liquid gallium [FER96a]

Mixed fracture mode with both brittle and ductile zones has been observed for F82H-mod. HAZ specimens tested in Pb-17Li at 250°C [SAM 00], MANET II steel in liquid Pb-Bi eutectic [GLA 03], brass / liquid gallium [FER 97], A508 III steel/liquid Na [HIL 95]. Auger

and Lorang [AUG 05] explain the mixed brittle/ductile fracture surface of T91 steel tested in liquid Pb-Bi by the quantity of embrittling liquid available. Indeed, the fracture surface analysis reveals brittle fracture localized in the outer surface whereas the centre of specimen fails by ductile linking up of brittle cracks. The propagation of brittle cracks is controlled by the supply of liquid metal at the crack tip. Brittle crack propagates as long as liquid metal is pulled at the crack tip by capillarity. Because of experimental procedure (evaporation and condensation of Pb-Bi on the surface of steel), only small quantity of liquid metal is available to fill in the crack and when no more liquid remains, the brittle crack stops and ductile fracture occurs by shear void coalescence normally expected for this material as shown in figure I.24 where the transition from liquid Pb-Bi-induced brittle fracture to ductile fracture is clearly evidenced. Also, Glasbrenner *et al.* [GLA 03] claim that embrittlement in MANET II steel occurs only when the crack tip is wetted by liquid Pb-Bi eutectic. These results suggest that the presence of the embrittling liquid metal at the crack tip is a necessary condition for the brittle crack propagation.

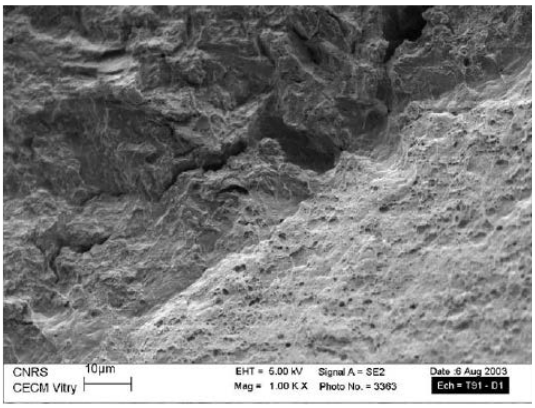

Figure I.24. Transition from brittle to ductile fracture of T91 steel by lack of supply of liquid Pb-Bi [AUG 05]

For a given solid metal/liquid metal couple, different cracking modes can be observed depending on experimental conditions. Thus, Clegg and Jones [CLE 03] identify four cracking types for the EN19 steel tested in liquid tin depending on testing temperature and the initial steel's strength (figure I.25). Type A classifies unembrittled specimens which failed after plastic deformation by necking and ductile cup and cone failure. This fracture type predominates for temperature upper than the ductility recovery temperature where LME does not occur anymore.

Type D is typical of LME-induced brittle fractures. No or very little plastic deformation occurs before fracture. This fracture type predominates at low temperatures and for high strength specimens.

Types B and C occur for intermediate temperatures and strengths.

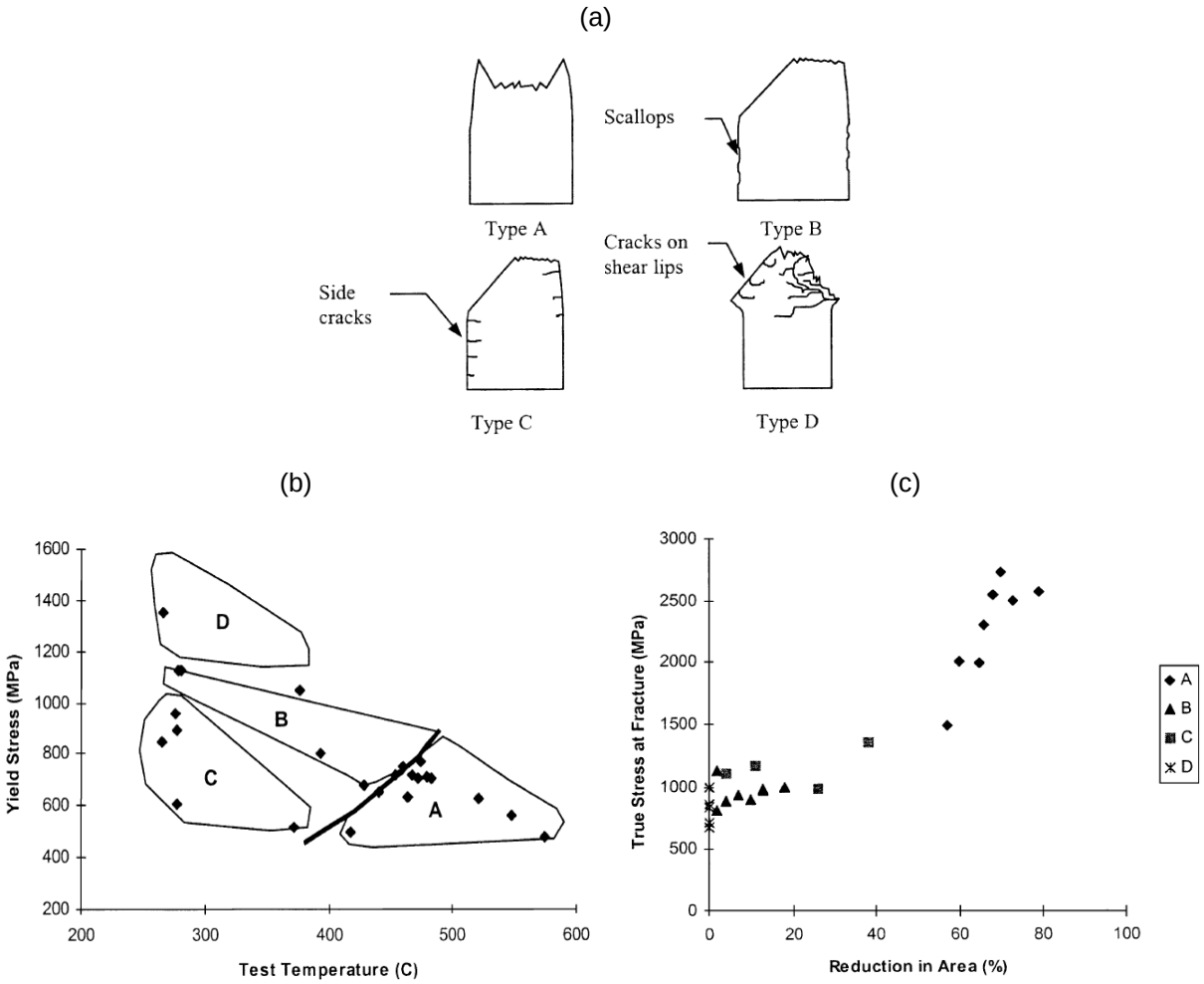

Figure I.25. (a) Schematic representation of the different cracking modes. (b) Grouping of the different cracking modes according to testing temperature and yield strength. (c) Mechanical properties corresponding to each cracking type [CLE 03]

III.3. Factors influencing LME

The influence of different parameters on the occurrence of LME is detailed below.

III.3.1. Contact between solid metal and liquid metal

LME can occur only if there is an intimate contact between the solid material and the embrittling liquid metal. The contact between a solid metal and a liquid metal is governed by the equilibrium of interfacial tensions γ_{GB} (grain boundary energy) and γ_{SL} (solid-liquid

interface energy). Under certain conditions, the contact between the polycrystalline solid metal (or alloy) and the liquid metal may result in a rapid penetration of the liquid phase along grain boundaries. In the absence of external stress, the phenomenon is known as grain boundary penetration, and the associated thermodynamic driving force is the reduction of interfacial energy. Grain boundary penetration is observed if the condition (I.2) is satisfied:

$$\gamma_{GB} \geq 2\gamma_{SL} \qquad \text{(eq. I.2)}$$

Both energies depend on each considered grain boundary. Moreover, they are also dependent on temperature. As a consequence, a wetting transition temperature T_w can be defined (figure I.26) above which the grain boundary is replaced by an intergranular film of liquid metal as illustrated in figure I.27 where an intergranular Bi-rich film overruns the grain boundary of a polycrystalline Ni specimen. Wolski *et al.* [WOL 02] pointed out the existence of a very long nanometric film of bismuth ahead of the micrometric film in pure nickel polycrystals after 8h exposure at 700°C resulting in a strong brittleness when subsequent stresses are applied at room temperature.

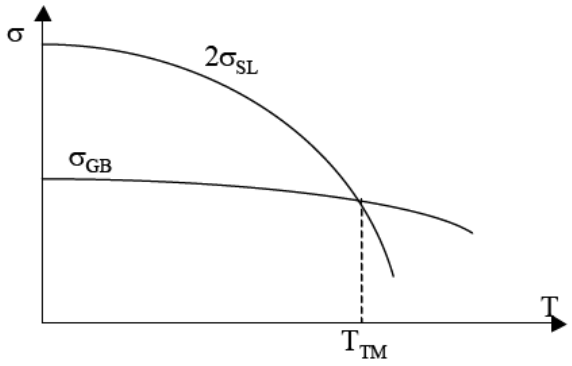

Figure I.26. Evolution of interfacial energies as a function of temperature [LAP 05]

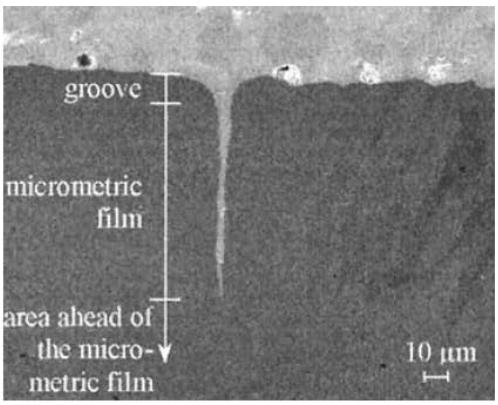

Figure I.27. Complete wetting of polycrystalline Ni by liquid Bi [MAR 00a]

Grain boundary wetting depends on several parameters, such as temperature, stress, grain boundary structure and energy.

Grain boundary penetration can lead to embrittlement when the material is tested at temperatures where the penetrated liquid is solidified [MAR 00a], [WOL 02] or can lead to embrittlement if the solid metal is stressed while still in contact with the liquid one.

The contact between solid metal and liquid metal can be realized by various experimental techniques. The most commonly used techniques consist in immersing specimen directly in the liquid metal or deposit a droplet of liquid metal on the solid metal surface. An alternative technique for ensuring contact between solid metal and liquid metal is vapour condensation of the embrittling element on solid substrate to form a liquid layer on solid metal surface [MAR 01].
Liquid metal may also arises from alloying elements segregated at grain boundaries. For temperatures above melting temperature of these elements, LME can occur. Such embrittlement has been observed in the aluminum alloy AA6262 by lead segregated at grain boundaries [WOU 03]. Also, Lv *et al.* [LV 10] show a decrease in mechanical properties of a high-Mn austenitic steel at high temperature due to formation of low melting point eutectic $(FeMn_3)P$ at grain boundaries in steels having higher phosphorous content.

Grain boundary wetting is generally considered as a necessary condition for LME to occur. If the contact between the solid metal and the liquid metal is interrupted, no embrittlement is possible. For instance, an oxide layer can be very effective to protect the solid metal from an embrittling liquid metal by preventing interactions between the solid material and the liquid metal. Thus, the martensitic T91 steel is prone to embrittlement by liquid Pb–Bi or liquid Pb provided the passivation layer is removed or has cracked to permit an intimate contact with liquid metal [LEG 00], [GLA 04], [AUG 05]. Deloffre *et al.* [DEL 04] show that different aluminized coatings applied on 316L austenitic steel and T91 martensitic steel offer satisfying protection against corrosion by liquid Pb-Bi in certain conditions.
Ina and Koizumi [INA 04] claim that LME can also occur in the absence of liquid metal on the solid metal surface. Indeed, they perform tensile test after liquid Ga metal was removed from the solid Al metal surface after various times of exposure. Liquid metal penetrates the solid metal grain boundaries during exposure and this penetration induces embrittlement even if the liquid metal is removed from the solid metal surface before testing.

From a practical point of view, a method commonly used to force contact between the solid metal and the liquid one consists in applying soft soldering fluxes such as a mixture of zinc chloride with additions of chloride ammonium or hydrochloric aniline in the surface of the solid metal. Auger and Lorang [AUG 05] used an ion etching cleaning process to remove the oxide superficial layer of the T91 steel and a physical vapor deposition (PVD) under ultra-high vacuum (UHV) to deposit Pb-Bi at the surface of the steel before tensile testing.

III.3.2. Temperature

LME occurs in a limited temperature range called “ductility trough”. This domain depends on several parameters such as the compositions of both solid and liquid metals, the microstructure of the solid metal and the strain rate. Generally, LME appears at the melting point of the embrittling metal and disappears above a ductility recovery temperature. An example of ductility recovery is shown in figure I.28 where areas under the stress-strain curves obtained with notched T91 steel specimens tested in liquid lead are plotted for different testing temperatures. Ductility is progressively restored until 723K where the behaviour in liquid lead is identical to the behaviour in air.

Analogies have been made with the brittle to ductile transition phenomenon observed for bcc and hcp metals. However, contrary to the brittle to ductile transition, LME appears at a given temperature (the lower limit of the ductility trough); the solid metal exhibiting a ductile behaviour below this temperature. This lower temperature corresponds, in many systems, to the melting point of the embrittling metal. But, for some couples, LME occurs only for temperature higher than the melting point of the liquid metal. Glasbrenner *et al.* [GLA 03] do not observe embrittlement of MANET II steel by liquid Pb-Bi for temperature lower than 250°C while the melting point of Pb-Bi is 125°C.

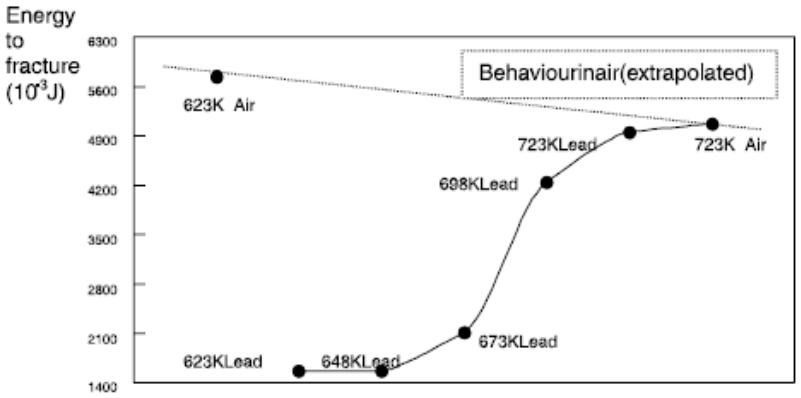

Figure I.28. Ductility recovery for temperatures upper than 723K for T91 steel tested in liquid lead [NIC 01b]

The ductility recovery with increasing temperature can be explained by the ductility increase with temperature counteracting the inherent propensity for fracture in the embrittling liquid metal environment [KAM 87], [NIC 01b]. Fernandes and Jones [FER 97] suggest that the upper limit of the ductility trough corresponds to the cross-slip-crack initiation transition temperature in that below this temperature, stresses generated at the dislocation pile-ups can increase so that crack initiation can occur and above this temperature, stress are sufficiently relieved by cross-slip so that crack nucleation is prevented.
Clegg and Jones [CLE 03] explain the ductility recovery of the En19 steel by an increased dissolution of the surface of the steel by the liquid tin with increasing temperature resulting in a more difficult crack initiation and propagation. Moreover, they show that the ductility recovery temperature decreases with decreasing specimen strength.

It is worth noting that such loss of ductility in a limited temperature range can be observed in other phenomenon such as hydrogen embrittlement or hot cracking (see §II.3).

III.3.3. Composition of solid and liquid metals

Compositions of solid and liquid metals significantly affect the LME occurrence as they modify several physico-chemical parameters of the solid metal-liquid metal system, such as interfacial energy, mutual solubilities, wettability, intermetallics. A fine modification of one of the two compositions can either increase or prevent LME. For instance, figure I.29 presents the influence of the embrittling environment on mechanical behaviour of aluminum [WES 79]. Adding alloying elements (even few %) in liquid Hg can lead to important embrittlement. Some alloying elements have a significant effect on the severity of embrittlement. Some improve the adsorption of liquid metal atoms, thus, enhance LME. For instance, manganese is known to increase the width of the ductility trough of beta-brass in gallium solutions by changing the slip behaviour from wavy glide to planar slip [FER 97]. Others improve the grain boundary stability and decrease the LME susceptibility. At last, some have no influence on cracking behaviour. Hilditch *et al.* [HIL 95] show that the presence of chromium in steel does not modify LME behaviour of steels in liquid sodium.

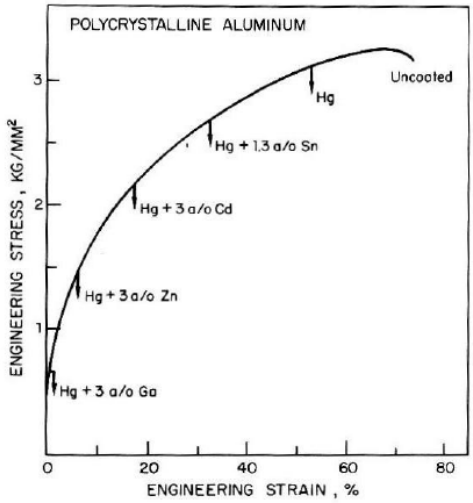

Figure I.29. Embrittlement of polycrystalline aluminum: influence of liquid metal composition [WES 79]

III.3.4. Solid metal microstructure

Crystallographic structures favouring stress concentration are generally more sensitive to LME (bcc structures are more sensitive than fcc structures). However, in a fcc structure, embrittlement can occur if the dislocation movement is restricted by obstacles. Obstacles, such as grain boundaries or twins, serve as a stress concentrator. The more obstacles are easy to overcome, weaker is the probability to observe LME.

Fernandes and Jones [FER 97] study the behaviour of two brass alloys having different microstructures in molten gallium. The alpha alloy (fcc) does not exhibit any embrittlement by liquid gallium, contrary to the alpha-beta alloy (bcc). The authors explain the different results by the dependence of stresses generated at dislocations pile-ups on the type of slip behaviour. In the alpha brass, the wavy glide leads to stress relieving by dislocation climb and plastic deformation is favoured. However, in the alpha-beta brass, the planar glide induces a local stress concentration promoting brittle crack initiation. The influence of experimental conditions such as temperature and strain rate on the dislocation mobility can explain the occurrence of LME or not.

Moreover, the hardness and the deformation behaviour of the solid material have a significant effect on its LME susceptibility, the hardest materials being generally more severely embrittled [HIL 95], [JOS 99], [LEG 00], [LEG 02], [VER 05]. Very high yield strengths lead to important local stress concentrations.

Microstructure of solid metal is significantly modified during heat treatments or welding processes. A solid metal initially not sensitive to LME can appear sensitive after welding.

Sample and Kolbe [SAM 00] show that neither F82Hmod. steel nor OPTIFER IVb steel exhibit a LME susceptibility in the tempered fully martensitic state when tested in Pb-17Li at 250°C and 400°C. However, LME is evidenced in the simulated HAZ specimens (1300°C/3 min, water quenched) stressed in Pb-17Li at 250°C whereas a ductility recovery is observed at 400°C. Moreover, it is shown that an appropriate post weld heat treatment modifying properties of HAZ specimens to those exhibited by the normal heat treated specimens (750°C/1 h for F82H-mod. and 730°C/3 h for OPTIFER IVb) is very effective in preventing the LME.

Embrittlement is generally increased with increasing grain size. Actually, increasing grain size has two distinct effects on LME: elongation to rupture as well as fracture stress is significantly reduced (LME follows the Cottrell-Petch relationship of grain size dependence on fracture stress [KAM 87]) and temperature of ductility recovery is significantly increased [FER 97], [JOS 99]. The figure I.30 presents the influence of grain size on the embrittlement (reduction of cross-sectional area) of brass CZ109 by liquid Ga.

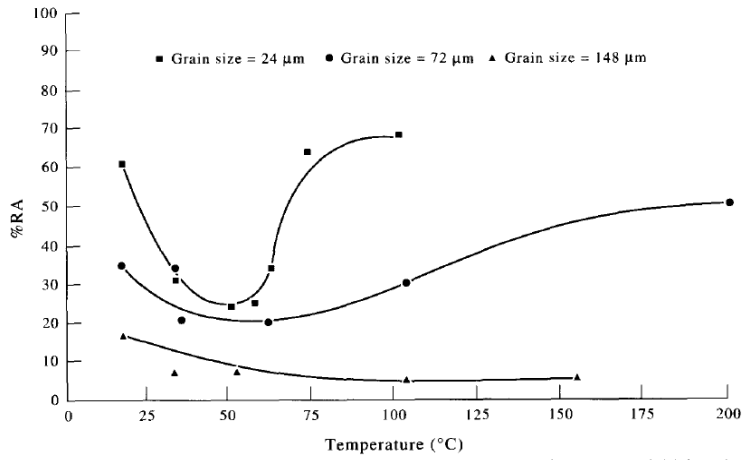

Figure I.30. Influence of grain size on the ductility trough [FER 97]

The misorientation between grains has also an influence on LME occurrence. According to Nichols and Rostoker [NIC 61], when the misorientation between neighbouring grains is small, grain boundaries are easily overcome by dislocations and plastic deformation is promoted.

Moreover, as mentioned above, grain boundary penetration depends upon the grain boundary structure and energy. Liquid metal penetration is harder in grain boundaries having lower energy according to the equation I.2 $\gamma_{GB} \geq 2\gamma_{SL}$ [HUG 99], [PEN 00], [KOB 06]. However,

applying external loads modifies the penetration behaviour. Low energy Al grain boundaries not penetrated by liquid Ga in absence of stress, undergo rapid liquid Ga penetration when tensile stresses are applied. Lower energy grain boundaries require higher tensile stresses to be penetrated [LUD 05].

III.3.5. Stress

LME definitions specify that stress (applied or residual) is a prerequisite. A threshold stress would be necessary for LME to occur. However, this threshold stress can be very low. Actually, the question is to know whether the studied metal is free of stress or is containing high stress concentrations in so far as grain-boundaries and other obstacles may act as stress concentrators.

The presence of a notch in the tested specimen can locally increase the stress level and thus, can have a significant effect on LME occurrence. Fernandes and Jones [FER 96a] and Nicaise *et al.* [NIC 01b] observe embrittlement of CZ106 brass by liquid gallium and martensitic steel by liquid lead, respectively, provided a notch was machined in the specimens leading to a stress concentration at the notch tip. The ductility recovery temperature is generally increased for notched specimens compared to smooth ones [KAM 87].

Hancock and Ives [HAN 71] (cited in [KIN 04]) demonstrate that prestraining copper-aluminum specimens before testing in liquid mercury increases the degree of embrittlement in that both elongation to rupture and fracture stress drastically decreases with increasing prestrain (figure I.31).

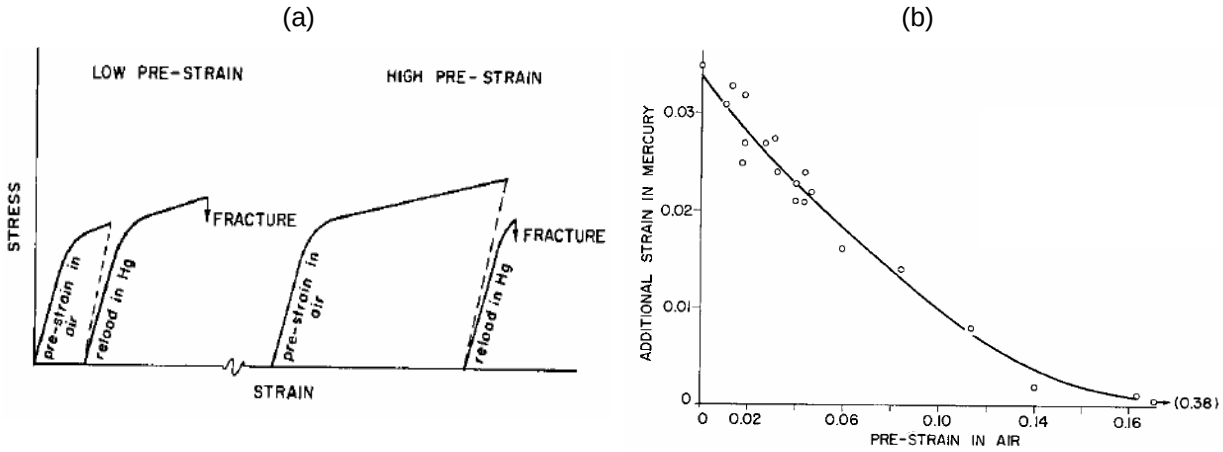

Figure I.31. (a) Prestrain procedures, (b) decrease of additional strain to fracture in mercury after prestrain in air [HAN 71]

III.3.6. Strain rate

The severity of embrittlement (depth of the ductility trough) as well as the domain of embrittlement (width of the ductility trough) is strongly dependent on strain rate: as illustrated in the figure I.32, they increase with increasing strain rate. Strain rate must be changed by orders of magnitude to observe modifications of the ductility recovery temperature.

Decreasing strain rate tends to decrease the upper temperature of the ductility trough and thus, narrow the domain of brittleness until its disappearance. This is generally explained by an easier plastic flow at low strain rate.

However, the opposite effect (a more important embrittlement for lower strain rates) has also been reported [PRI 86], [ROS 60] (cited in [HAM 08]).

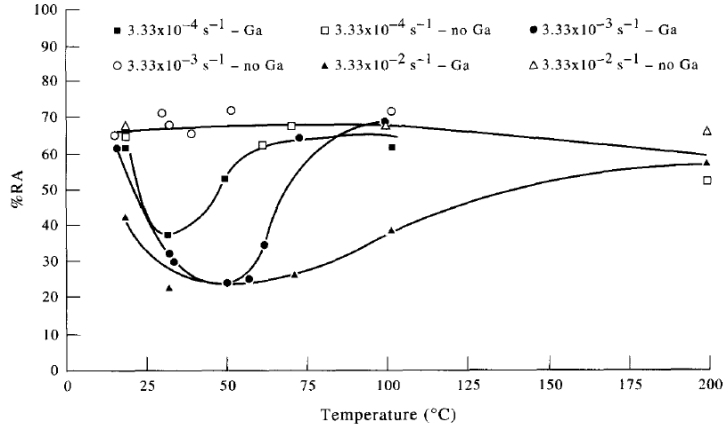

Figure I.32. Effect of strain rate on embrittlement of CZ109 brass by liquid Ga [FER 97]

III.3.7. Time of exposure

For certain authors [KAM 87], [JOS 98], the time of contact of the solid metal with the liquid one before testing does not seem to have an influence on the LME occurrence. Nevertheless, for others, [SAM 96], [SAM 00], [GLA 03], [BOS 07] pre-exposure is necessary for enhancing wetting.

Ina and Koizumi [INA 04] study the effect of pre-exposure time on Al–Ga, Ag–Hg and Cu–Hg couples. Before tensile testing at 35°C and 0,02 s^{-1}, the embrittling metal was removed from the solid metal surface. Results show that LME occurs even after the liquid metal is removed from the solid surface if the exposure time is long enough for storing sufficient liquid metal in grain boundaries to induce LME during subsequent tensile test. Hence, embrittlement increases with increasing exposure time.

III.4. Embrittlement of steels by liquid zinc

Steels can be considered as materials having a poor resistance to LME in so far as many steels can be embrittled by various liquid metals. LME of steels is often reported in the case of nuclear or chemical applications. Many studies dealing with the embrittlement of steels chosen as structural steel in nuclear applications by liquid Pb, Bi, Pb-Bi eutectic or Pb-17Li are available in the literature [LEG 00], [SAM 00], [NIC 01b], [GLA 03], [GLA 04], [AUG 05], [BOS 07], [HAM 08].

Here, a focus on the embrittlement of steels by liquid zinc is made. Embrittlement of steel by liquid zinc is an exception to the empirical rule of LME since iron and zinc can form various intermetallic compounds (see §IV.1.2). Liquid zinc embrittlement of steels can occur during galvanizing or during high temperature processes such as welding of zinc-coated steels. Embrittlement of austenitic stainless steels by liquid zinc mainly due to interactions with galvanized steel or zing-pigmented paints resulting from welding or fire damage has often been reported [DIL 90].

An example of embrittlement by liquid zinc is shown in the figure I.33 where strain to elongation is significantly reduced in presence of zinc.

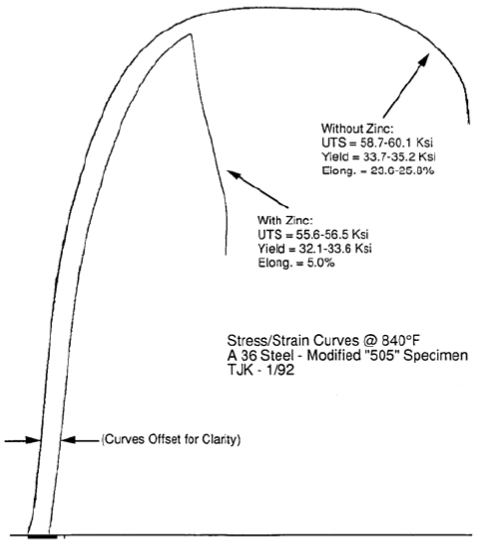

Figure I.33. Stress-strain curves of A36 steel tested with and without zinc at 449°C [KIN 04]

Different conditions are prerequisite to observe liquid zinc embrittlement of steels:

- presence of a susceptible steel (composition, microstructure, thermal and mechanical history)
- presence of high stresses or local strain/stress concentration
- presence of molten zinc

and numerous parameters have a significant influence on LME occurrence such as the liquid composition (which influences the potential intermetallic layers formed at the interface of steel and liquid zinc) and potential pre-existing cracks in the steel (hydrogen or HAZ cracks) [KIN 04], [JAM 09], [CAR 10].

Typical observations of cracks obtained during galvanizing are presented in figure I.34. Observations of cross section reveal the intergranular propagation and the formation of intermetallic phases along crack. The fracture surface exhibits a brittle intergranular surface resulting from the structure decohesion induced by liquid zinc grain boundary penetration.

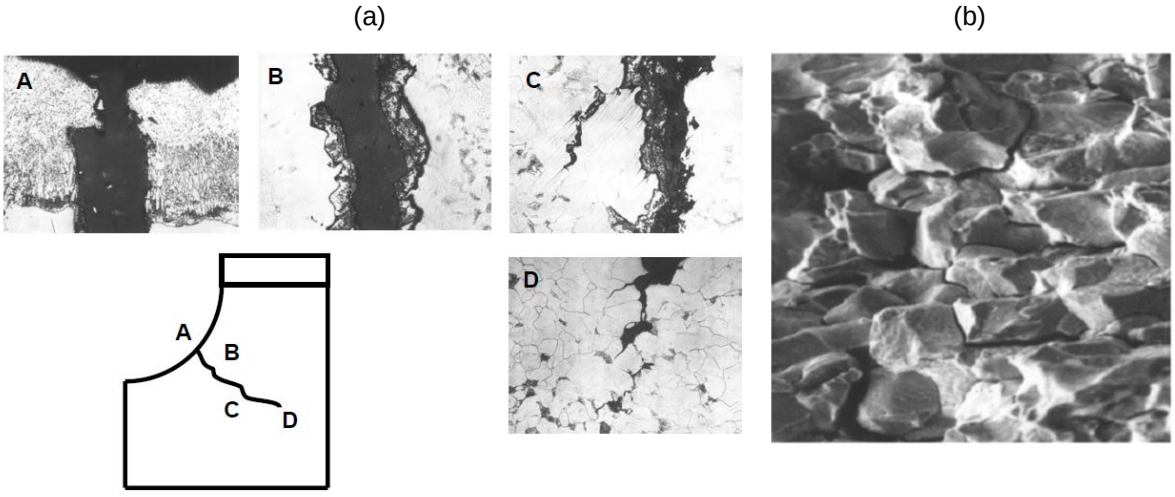

Figure I.34. Cross section (a) and fracture surface (b) observations of crack formed during galvanizing [KIN 04]

All of the necessary conditions previously mentioned can be experienced during welding of zinc-coated steels:

- zinc is likely to melt on the steel surface when temperatures upper than its melting point are achieved
- certain zones of weldment are partially or fully transformed to austenite during welding process
- high stresses are achieved in the weld due to the thermo-mechanical cycle.

Sigler *et al.* [SIG 08] studied the LME occurring during resistance spot welding of Zn coated TRIP 590 and DP 600 steels (figure I.35). They pointed out different parameters influencing the occurrence of LME. Firstly, the presence of tensile stresses (thermal stresses, mechanical strains or stresses induced by phase transformations) is needed. Secondly, the presence of zinc on the steel surface (liquid zinc penetrates the prior austenite grain boundaries resulting in local grain boundary decohesion) is essential. At last, a microstructure fully transformed to austenite is also a key parameter for the occurrence of LME. Indeed, areas that have not undergone austenite phase transformation appear much less sensitive to cracking. In addition, the formation of brittle Zn-Cu phases, Cu coming from the electrodes, within the cracks previously initiated by the zinc coating emphasizes the crack growth and propagation during cooling.

One successful method in decreasing the cracking susceptibility was the use of extended holding times.

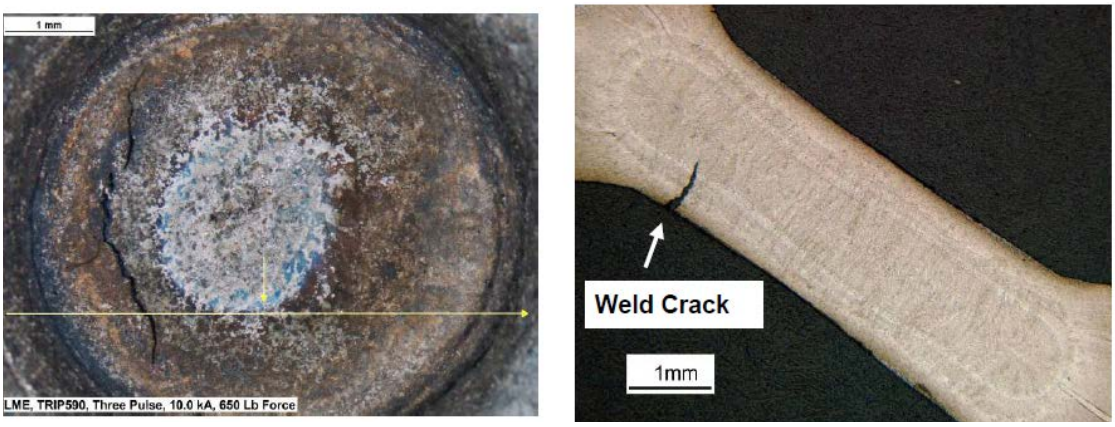

Figure I.35. Weld crack in Zn coated TRIP590 steel [SIG 08]

III.5. Models

Several models have been proposed to describe the LME mechanisms. Most of them are based on the Rebinder effect: the reduction of the surface energy of the solid metal induced by the adsorption of liquid metal atoms. The most commonly accepted are the adsorption-induced reduction in cohesion model and the enhanced dislocation emission model. However, none of them can fully explain or predict the embrittlement of a particular metal by another one.

A brief summary presents the most commonly accepted models.

III.5.1. Dissolution-diffusion: Robertson and Glickman [JOS 99a]

These models are based on the dissolution of the solid metal at the crack tip enhanced by stress and capillarity effects. The dissolved solid metal atoms rapidly diffuse through the liquid metal and crack propagates. This mechanism being thermally activated, the degree of embrittlement should increase with increasing temperature since solubility increases, which is in contradiction with practical observations. In addition, this model is totally discrepant with the empirical rule according to which LME occurs for metals couples having a low the mutual solubility.

III.5.2. Brittle fracture: Stoloff, Johnson, Westwood and Kamdar [KAM 87], [JOS 99a]

This model is based on the weakening of interatomic bond. The adsorption of a liquid metal atom B (figure I.36) at the crack tip A-A_0 leads to an electronic rearrangement causing the decrease of the strength of interatomic bonds because of the decrease of the surface energy. When the applied stress exceeds the now reduced breaking stress of the interatomic bond, the bond breaks and the crack can propagate to the next solid atom A_1. The liquid metal atom B becomes stably chemisorbed on the freshly created surface. The mechanism continues as long as metal atoms reach the crack tip and until the specimen breaks.

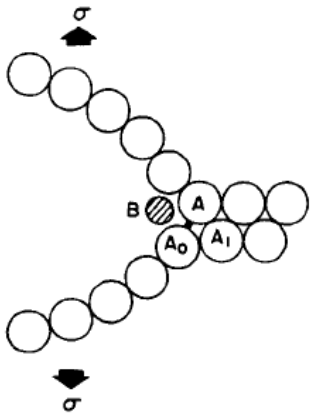

Figure I.36. Schematic illustration of displacement of atoms at the crack tip caused by the adsorption of a liquid metal atom B [JOS 99a]

III.5.3. Ductile failure: Lynch [JOS 99a]

Lynch's model is also based on the weakening of interatomic bond due to adsorption of liquid metal atoms at the crack tip but assumes that cracks do not propagate by interatomic bond breaking but by coalescence due to enhanced nucleation and intensive slip of dislocations at crack tip (figure I.37).

In inert environments, many dislocations nucleate from sources in the area ahead of crack tips. Most of them either egress behind crack tips contributing to crack blunting or do not intersect crack tips. Only a small number of them emerges exactly at crack tip and contributes to crack propagation. In the embrittling environment, the weakening of interatomic bond due to adsorption of liquid metal atoms at the crack tip promotes localized nucleation of dislocations. Injection of these dislocations from crack tips to suitably inclined slip planes permits the crack advance. Moreover, dislocations activity in front of crack tips permits the formation of voids at small particles in a plastic zone ahead of cracks. Coalescence of them with the propagation crack permits crack advance as well as opening.

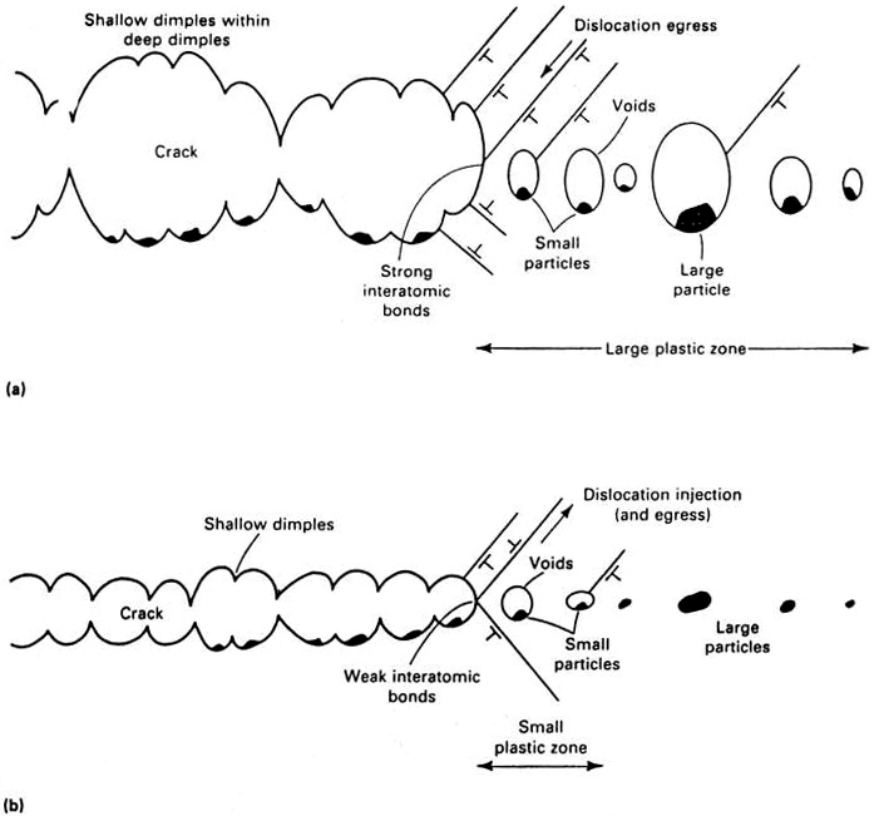

Figure I.37. Schematic illustration of crack growth by microvoid coalescence (a) in inert environment and (b) in embrittling liquid metal environment [KAM 87]

III.5.4. Liquid metal atoms penetration: Gordon [JOS 99a]

This model is based on the penetration of liquid metal atoms along grain boundaries. It involves two phases: an initiation stage controlling the mechanism and the propagation stage. The initiation stage consists in the adsorption of the liquid metal atom on the surface, dissolution and subsequent stress-aided diffusion and penetration along grain boundaries. The presence of the embrittler atoms at grain boundaries decreases the crack resistance and

increases the difficulty of slip. Crack nucleates probably at the head of already existing dislocation pile-ups once sufficient embrittler atoms have penetrated and stress exceeds the lowered crack resistance, and then the crack propagates.

Conclusions

Although widely investigated, LME mechanisms are still poorly understood. Nevertheless, different conditions seem to be mandatory for cracking to occur:

- Intimate contact or wetting of the solid metal by the liquid metal
- Local stress concentration (depending on testing temperature, strain rate, solid metal microstructure, presence of a notch…)

It is important to notice that LME occurrence strongly depends on testing conditions and mechanical properties and microstructure of the solid metal. A tiny modification of one of those conditions can significantly modify the cracking behaviour of the solid metal.

The reduction of the cohesion of the solid metal induced by the adsorption of liquid metal atoms seems to be the mechanism responsible for LME. Different solutions to prevent, or at least reduce, embrittlement by liquid metals can be proposed:

The most obvious solution is replacing embrittling metal by non embrittling metal or modifying the solid metal composition. But in many industrial applications, this possibility is not feasible.

Another possibility consists in depositing a metal layer at the solid surface which will act as a barrier between the embrittling liquid metal and the solid metal [KAM 87].

IV. Zinc coating process

We previously show that Zn constitutes an embrittling element for steels. However, most of steels are coated with Zn. Indeed, high corrosion resistance of automotive steels is mandatory for car manufacturers. Two approaches can be adopted to enhance the corrosion resistance of high-Mn austenitic steels:

- improving the intrinsic corrosion resistance of the steel by adding adequate alloying elements (Cr or Al). However, these elements may decrease mechanical properties.
- modifying the steel surface by depositing a protective layer.

Because of its sacrificial properties, zinc is the most widely metal used for protecting steels against corrosion. Indeed, zinc offers a double protection. On one hand, zinc layer acts as a barrier isolating steel from environment. On an other hand, zinc has the ability to cathodically protect steel (because it is more electronegative than steel) and consequently, sacrificially corrodes if coating is damaged. Different processes can be used to apply zinc-based coatings on steel: hot-dip galvanizing, electrogalvanizing, metallizing, painting...

IV.1. Hot-dip galvanizing

IV.1.1. Principle

Hot-dip galvanizing is the most commonly used method. It consists in immersing the steel in a molten zinc bath to create a metallurgical bond between zinc and steel. Batch process is used for galvanizing finished parts while continuous treatment is used for coiled products. Different steps are necessary for preparing the surface steel before immersion in liquid zinc (figure I.38):

1. **cleaning** in order to remove oils, grease and all that could inhibit the subsequent oxide dissolution; followed by rinsing in water
2. **pickling** in a dilute solution of either hydrochloric or sulfuric acid permits to remove surface oxides and provide a chemically clean metallic surface; followed by rinsing in water
3. **fluxing** aims at inhibiting oxidation prior to contact with liquid zinc and ensuring a good wettability of the steel surface by liquid zinc. In the dry process, workpieces are immersed in an aqueous solution of zinc ammonium chloride at about 60°C and then, dried at about 120°C to prevent zinc splattering when immersed in liquid zinc. In the

wet process, products pass through a molten flux blanket floating on top of the liquid zinc bath immediately before galvanizing. After fluxing, workpieces are covered by a thin layer of salts. During immersion in the liquid zinc bath, flux decomposition permits to start the metallurgical reactions between iron and zinc.

Once the surface prepared, pieces are immersed in the liquid zinc bath maintained at temperatures typically ranging from 430 to 460°C (Zn melting point being 419°C). Immersion times can be varied from 3 up to 15 minutes depending upon pieces shape and dimensions. Different elements can be added in the bath such as lead, nickel, tin or aluminum. For instance, aluminum is added in order to prevent excessive oxidation of the surface of the bath by formation of an alumina layer and to obtain a ductile coating by inhibiting the formation of brittle Fe-Zn phases by the formation of a very thin Fe_2Al_5 layer containing 10 to 15% Zn in solid solution at the surface of the steel. The inhibition time of this barrier depends on the bath temperature as well as its aluminum content.

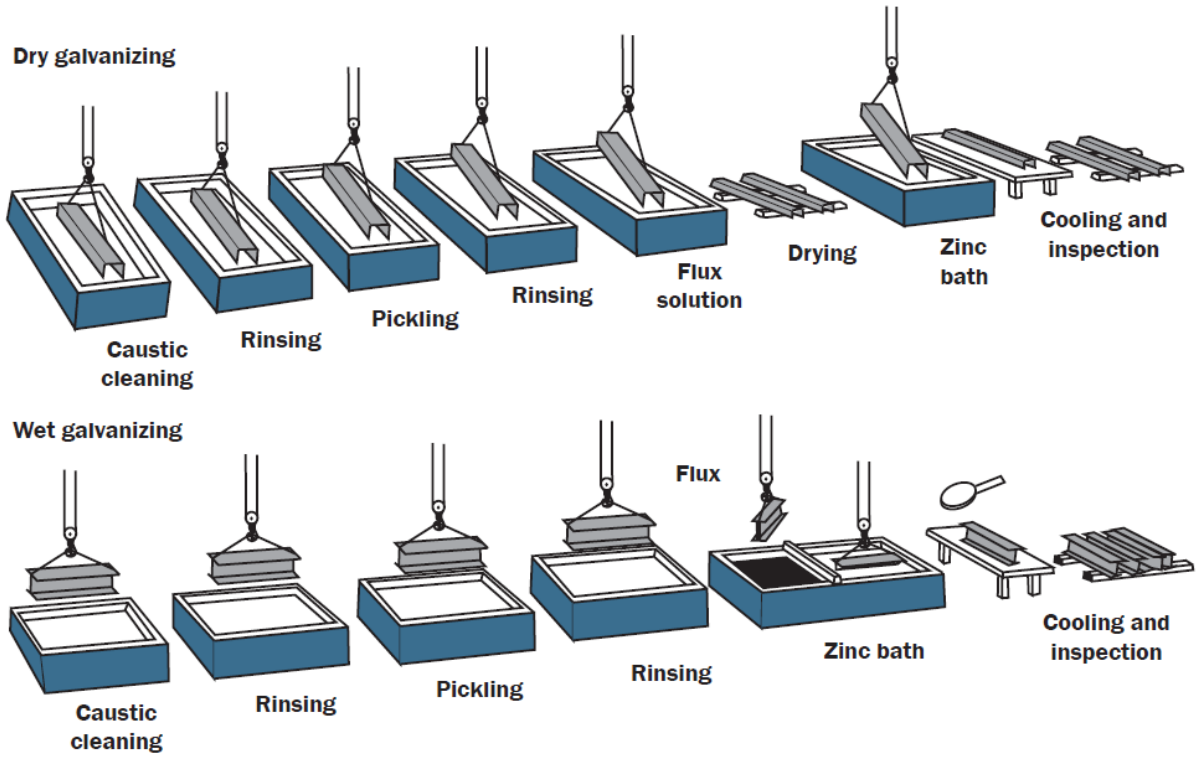

Figure I.38. Hot-dip galvanizing process: dry and wet fluxing [ZIN 10]

IV.1.2. Coating characteristics

Different phenomena take place at the interface between steel and zinc when a steel workpiece is immersed in the molten zinc bath, particularly, wetting of steel by liquid zinc, iron dissolution and reactions between iron and zinc [GIO 04b]. Consequently, the obtained coating does not only consist of a zinc layer on the substrate but results from the formation of different intermetallic phases. Coating structure mainly depends on both steel and bath compositions, and experimental procedure particularly immersion time and bath temperature. The reactions, and subsequent phases, between iron and zinc are governed by the Fe-Zn phase diagram figure I.39 (a). Figure I.39 (b) represents the zinc rich corner of this diagram. The different phases, with increasing iron concentration are: eta (η), zeta (ζ), delta (δ), gamma1 (Γ1) and gamma (Γ). Characteristics of such phases are listed in table I.1. They are generally harder than the substrate.

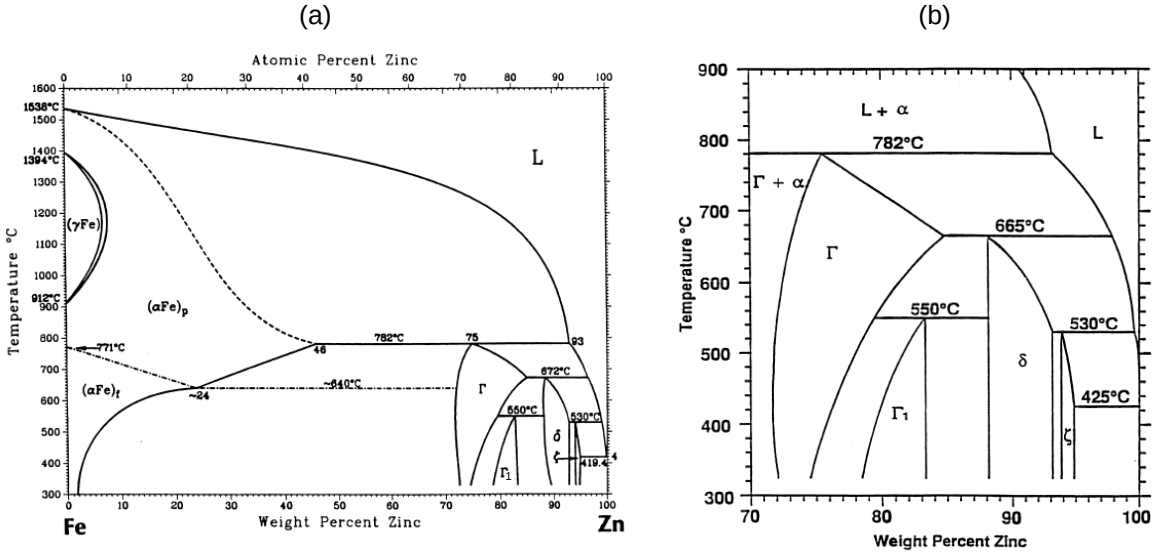

Figure I.39. Fe-Zn phase diagram (a) and the zinc rich corner (b) from [MAR 00b]

Phase	Formula	Fe (wt.%)	Crystal structure (nm)
eta (η)	Zn	< 0,03%	Hexagonal (a=0.266, c=0.495)
zeta (ζ)	$FeZn_{13}$	5 to 6	Monoclinic (a=1.3424, b=0.7608, c=0.5061)
delta (δ)	$FeZn_{10}$ $FeZn_7$	7 to 12	Hexagonal (a=1.283, c=5.77)
gamma$_1$ (Γ_1)	Fe_5Zn_{21} $FeZn_4$	17 to 19,5	FCC (a=1.798)
gamma (Γ)	Fe_3Zn_{10} $FeZn_3$	23,5 to 28	BCC (a=0.89741)

Table I.1. Fe-Zn phases characteristics from [MAR 00b], [QUA 04], [BHA 91], [HON 03]

The chronological sequence of Fe-Zn phase formation is as follows (figure I.40): nucleation of zeta (ζ) phase, nucleation of delta (δ) phase at the steel/ζ interface and finally nucleation of Γ/Γ1 phases at the steel/δ interface. It was found that, for an iron substrate (0.003 wt% C, 0.258 wt% Mn), δ and ζ form quasi instantaneously while Γ and Γ1 phases form after an incubation time of 30 seconds [MAR 00b].

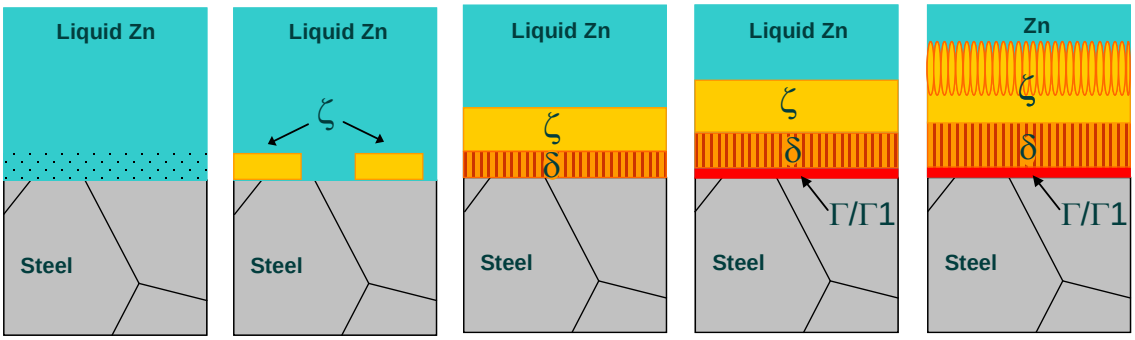

Figure I.40. Chronological sequence of Fe-Zn phases formation in a pure Zn bath from [MAR 00b]

For an ULC steel specimen immersed in pure zinc, the different phases can be identified by optical microscopy: gamma (Γ) phase, delta (δ) phase and zeta (ζ) phase as shown in figure I.41. Gamma (Γ+Γ1) phases appear as a very thin layer between the substrate and the δ phase. The δ and ζ phases possess a columnar structure resulting from the preferential growth perpendicular to the substrate. The ζ phase can represent 50% of the coating. If the bath is supersaturated with iron, many small ζ crystals can form. They are separated from each other by the zinc η phase. During cooling, internal stresses may develop in the different layers due to the differences in the thermal expansion coefficient of the substrate and the different phases and may lead to cracking in the hard (and brittle) ζ, δ and γ phases [TZI 01].

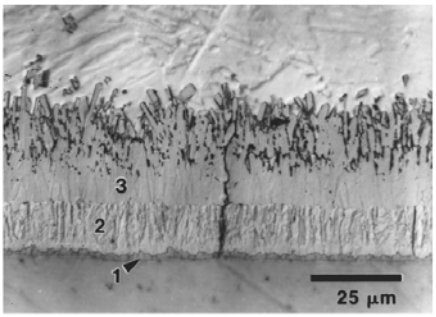

Figure I.41. Different Fe-Zn phases obtained after immersion of a ULC steel in a pure Zn bath at 450°C during 5 minutes: (1) Γ phase, (2) δ phase (3) ζ phase [MAR 00b]

IV.1.3. Growth kinetics of the intermetallic layers

Galvanizing kinetics is governed by chemical reactions occurring at the solid-liquid and solid-solid interfaces and by the double diffusion of Zn and Fe. The different phases exhibit different growth kinetics affecting the total coating kinetics. For immersion times up to 300s at 450°C, the ζ phase grows very quickly then slows down whereas the δ phase grows slowly firstly and then faster after some time. The Γ phase appears after an incubation time and seems to achieve a maximal thickness of about 1 μm. While the Γ phase grows on the substrate, it is, at the same time, consumed by the growing δ phase. In the same way, the δ phase grows in the ζ phase which advances in the liquid zinc.

The kinetics of the coating formation is influenced by the bath temperature and can be evaluated using the following equation:

$$Y=Kt^n \qquad \text{(eq. I.3)}$$

where Y is the layer thickness, K is the growth rate constant, t is reaction time and n is the growth-rate time constant. Two types of layer growth kinetics have been evidenced, characterized by the value of the n constant: a parabolic mode with n=1/2 for temperatures below 495°C and above 520°C and a linear mode with n=1 between these temperatures [GEL 74], [QUA 04], [MAR 00b].

Nevertheless, the kinetics of coating growth is strongly affected by the steel's composition. Phosphorous and silicon particularly affect the morphology of coating and phase growth kinetics [ARA 97], [QUA 04].

IV.1.4. Fe-Mn-Zn system

The coating layers previously described are observed in the presence of pure iron or low alloyed steel. However, the steel composition significantly affects the coating morphology. A focus on the high Mn content steel is made here.

When high Mn content steel is galvanized, manganese must be taken into account in intermetallic phases formed during immersion in the galvanizing bath. The Fe-Mn-Zn system has been poorly investigated. The three binary Fe-Mn, Mn-Zn and Mn-Zn phase diagrams are known but limited data on the ternary system is available in literature.

Reumont *et al.* [REU 95] established the isothermal section at 450°C of the Fe-Mn-Zn system. Diagram shows that numerous phases can be formed (figure I.42). ζ-$MnZn_{13}$ and δ-$MnZn_9$ intermetallic compounds are respectively isomorphic with ζ-$FeZn_{13}$ and δ-$FeZn_{10}$.

Thus, Mn can replace 75% of the Fe atoms in the ζ-$FeZn_{13}$ phase and can substitute over 90% Fe in the δ-$FeZn_{10}$ phase. Moreover, the solubility of Mn in Γ and Γ_1 is appreciable.

Isothermal sections at 625°C, 720°C and 1000°C are presented in figures I.43, I.44 and I.45 respectively [BHA 91].

Reumont *et al.* [REU 95] show that when a steel containing 20-25% at. Mn is immersed in a pure zinc bath, the intermetallic compounds present in the coating are δ, ζ and η. Γ and Γ_1 intermetallic phases do not appear. However, diffusion thermal treatment of galvanized steel or zinc vapour phase deposition on the same substrates lead to the formation of Zn-poorer phases such as Γ, Γ_1 and δ phases.

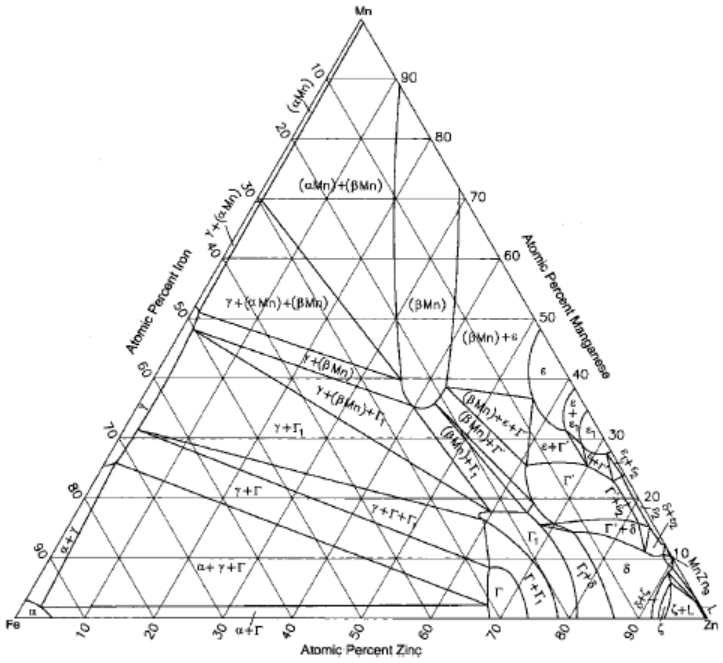

Figure I.42. Isothermal section at 450°C for the Fe-Mn-Zn system [RAG 03]

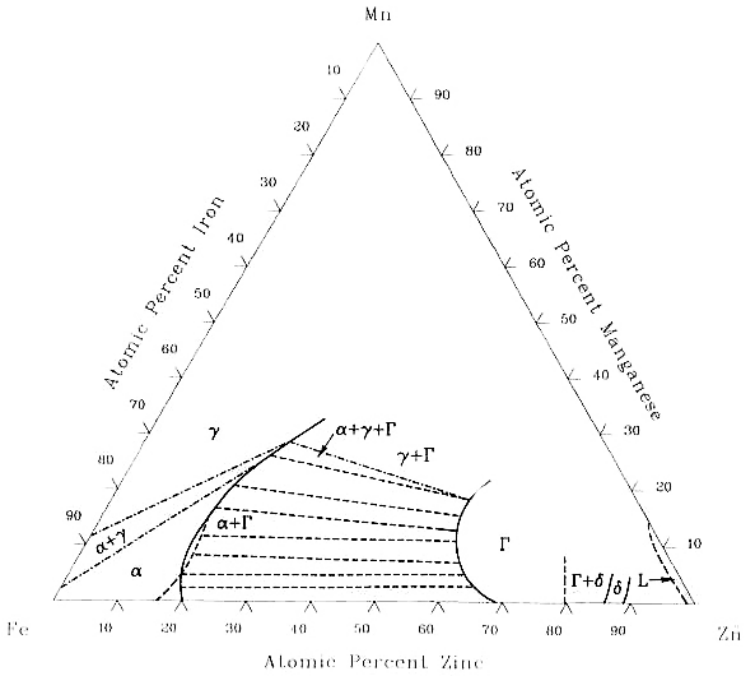

Figure I.43. The Fe-Mn-Zn system at 625°C [BHA 91]

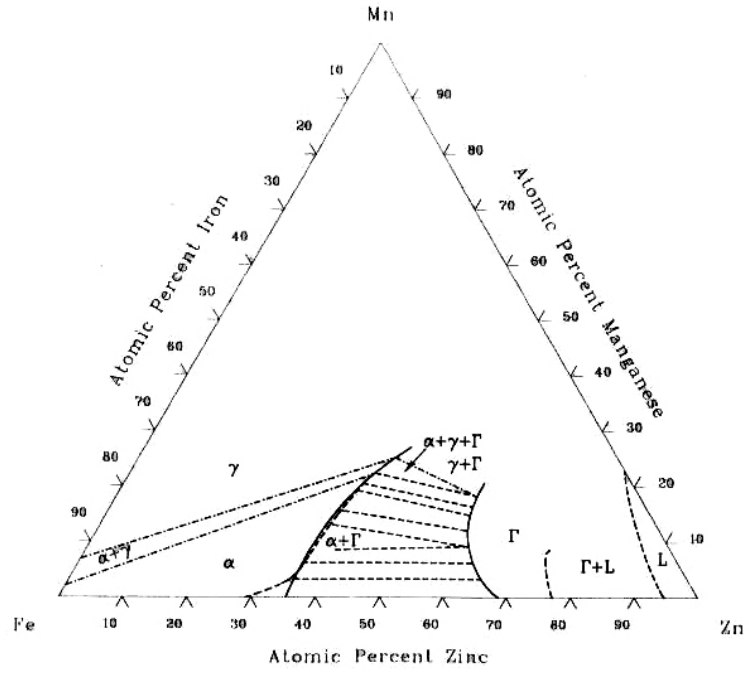

Figure I.44. The Fe-Mn-Zn system at 720°C [BHA 91]

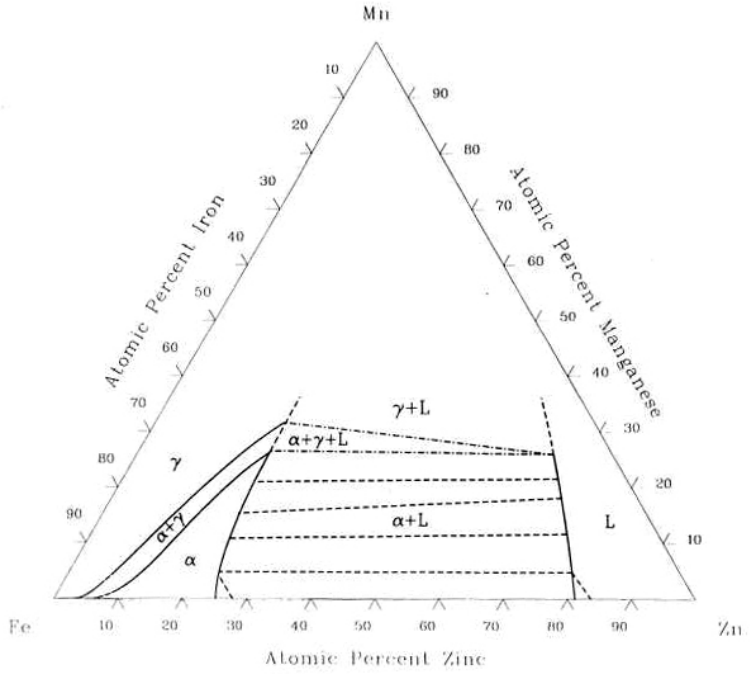

Figure I.45. The Fe-Mn-Zn system at 1000°C [BHA 91]

IV.2. Electrogalvanizing

Electrogalvanized coatings are applied to the steel surface from an aqueous electrolyte of zinc ions by electrodeposition. The zinc coating is formed by reduction of zinc ions on the steel surface which is the cathode [ZIN 10]. As for hop-dip galvanizing process, a surface preparation step is necessary to clean the steel surface before the electrogalvanizing step [DEP 07]. The resulting coating consists of a pure zinc ductile and thin (<10μm) layer, tightly adherent to the steel.

Conclusions

Zinc is commonly used for protecting steel from corrosion. It can be applied at the surface of the steel by different techniques. Galvanizing consists in immersing the workpiece in the liquid zinc bath. The resulting coating consists of different intermetallic phases function of steel and bath composition, immersion time... In the electrogalvanizing process, zinc is applied by electrodeposition and the resulting coating consists of a pure zinc layer.

Hot-dip galvanizing of the studied steel produces unsatisfactory coating because of oxidation of manganese impeding a good wetting. As a consequence, the steel under study is electrogalvanized.

Summary

The studied steel, a high Mn TWIP steel, offers an exceptional combination of strength and ductility thanks to the twinning mechanism. However, investigations on welding and particularly on weld cracking of this steel have never been reported.

Coating seems to have an influence on cracking mechanism since EG steel is more likely to crack than uncoated steel [BOU 09]. Hence, weld cracking is probably related to the liquid metal embrittlement phenomenon, liquid metal arising from the coating.

Different conditions are necessary to embrittlement of steels by liquid zinc:

- an intimate contact between the steel and the liquid zinc
- a sensitive structure
- the presence of high stresses

LME is generally studied by tensile testing while specimens are in contact with liquid metal (immersed in the liquid metal or covered by a liquid metal film). In this work, original tests have been developed in which all necessary conditions are gathered. Furthermore, testing temperature and strain rate, known as very influencing parameters can be easily modified. Experimental procedures are detailed in the next part.

Chapter II. Experimental procedures

It appears that the Liquid Metal Embrittlement phenomenon is responsible for cracking occurring during spot welding of Fe22Mn0.6C steels. Literature review reveals that the following conditions are required to observe cracks in steels:

- the presence of liquid zinc,
- the presence of high stresses and
- an austenitic microstructure.

Different tests gathering the latter conditions have been developed with the aim of firstly precisely defining the necessary conditions for cracking to occur and secondly understanding cracking mechanisms. Two main tests were carried out: immersion of cups containing high residual stresses in a liquid zinc bath and hot tensile tests performed on zinc coated specimens. Experimental details concerning the studied steel, the tests in liquid zinc bath, the hot tensile tests and subsequent observations are given in this chapter.

I. Studied steel

The steel used in the following contains as main alloying element 22 wt. % Mn and 0.6 wt. % C (balance Fe). The high manganese content stabilizes the austenitic phase so that the steel is fully austenitic at room temperature and exhibits no phase transformation in the studied temperature range ($T \geq RT$).

Slabs resulting from the continuous casting are first hot rolled to a thickness of 3mm, and then, cold rolled to obtain a final thickness of 1.5mm. Heat treatment of 2min at 800°C is then carried out to obtain fully recrystallized sheets with an average grain size of about 2μm. The initial texture was investigated by Barbier [BAR 09]. Results reveal a rather weak texture. Microstructure of steel is illustrated in figure II.1 where EBSD maps are presented.

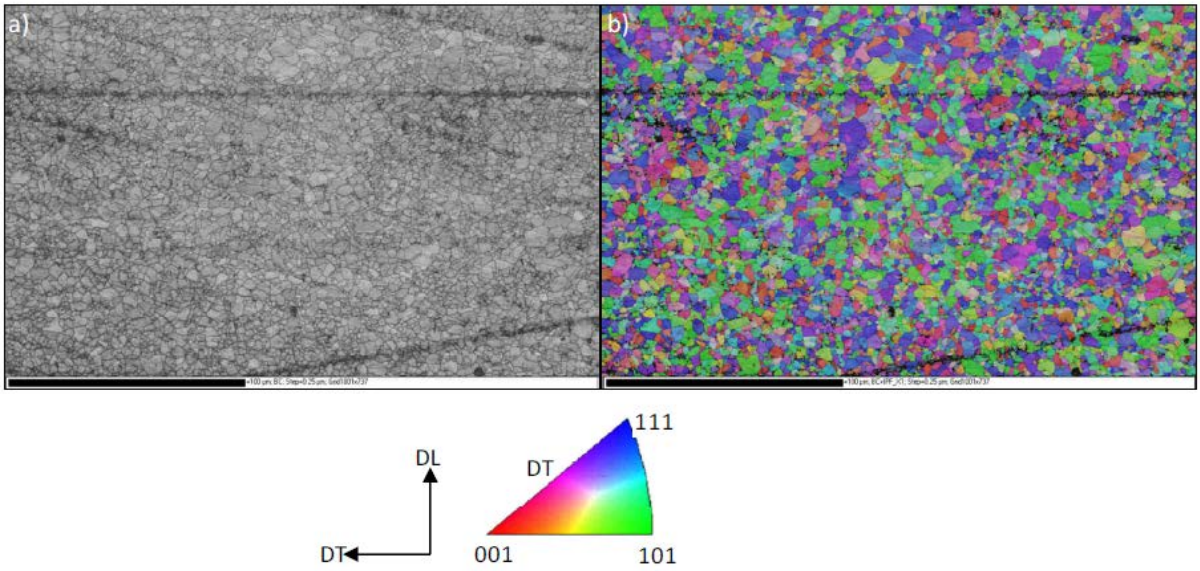

Figure II.1. EBSD maps of steel in the initial state. (a) Band contrast, (b) Orientation map given by the standard triangle of the inverse pole figure [BAR 09]

The main mechanical characteristics of the studied steel obtained at room temperature are summarized in the table II.1.

σ_y (MPa)	UTS (MPa)	U. El (%)	Total El (%)
600	1776	52.8	52.8

Table II.1. Main characteristics (transverse direction) of the Fe2Mn0.6C steel at room temperature [CUG 05]

II. Cups immersed in liquid zinc

A simple test permitting to determine the overall cracking conditions consists in immersing cups containing high residual stresses in a liquid zinc bath.

II.1. Cups characteristics

Tests in liquid zinc bath were carried out on cups having different geometry (see figure II.2) realized by deep drawing. Diameter (75 and 33mm), thickness (1.2, 1.6 and 3 mm) and drawing ratio β (1.6 and 1.8) were varied to obtain different stress profiles inside cups.

Figure II.2. Different cups geometry

Residual stresses have been evaluated by ArcelorMittal based on FE simulations [SCO 09]. Residual stresses obtained in the outer surface of a 75mm diameter, β 1.8 cup are shown in figure II.3. The zero point corresponds to the centre of the base of the cup. Maximum stresses are 1500MPa and 1150MPa for axial and circumferential components respectively. One can notice that at the cup rim, the stress state is uniaxial with circumferential stresses only. However, at approximately 20mm from the rim, the stress state is biaxial with very high (upper than 1GPa) axial and circumferential stresses.

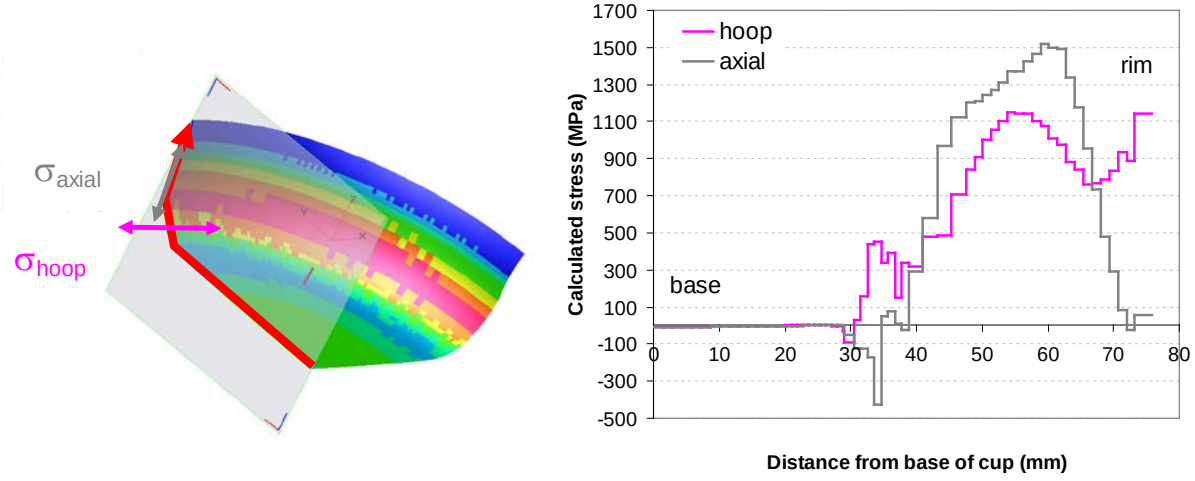

Figure II.3. FEM calculation of residual axial and hoop stresses on the outer surface of a 75mm diameter, β 1,8 cup [DIE 09]

Figure II.4 shows the evolution of calculated hoop stress along the cup wall on the external, neutral and inner fibres. Stresses have been calculated along four line profiles (RD, 30°, 45°, TD). It can be seen that stresses vary through the thickness from tensile stress on the outer

surface to compression stress on the inner surface (except near the rim where stresses are only tensile) while the neutral fibre is alternately in tension and in compression. Results are very similar for the four directions revealing the absence of anisotropy.

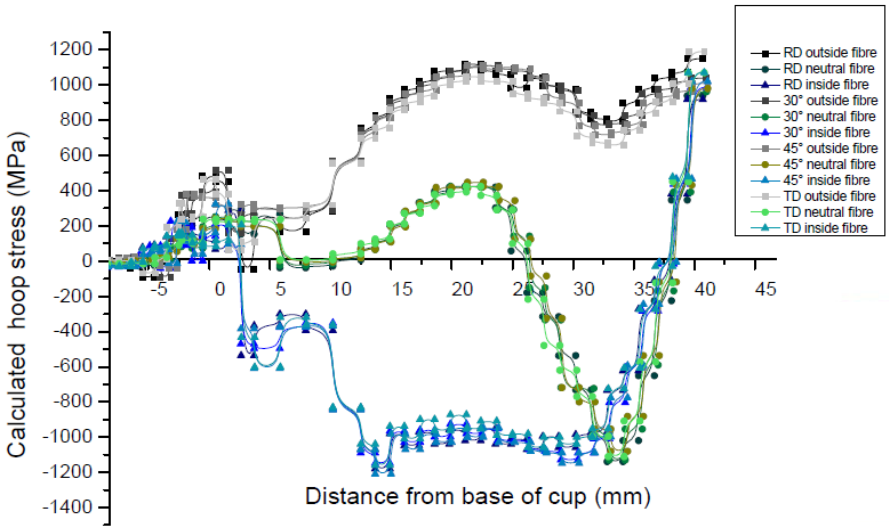

Figure II.4. FEM calculation of residual hoop stresses on the outer fibre, on the neutral fibre and on the inner fibre along four line profiles [SCO 09]

II.2. Cups preparation

Before the immersion in the molten zinc bath, a surface treatment is required [MAR 00b]. Indeed, if a bare steel specimen without treatment is immersed in the zinc bath, it remains uncoated as illustrated in figure II.5. This is due to the oxide layer present at the surface of the steel which prevents the wettability of steel's surface by liquid zinc.

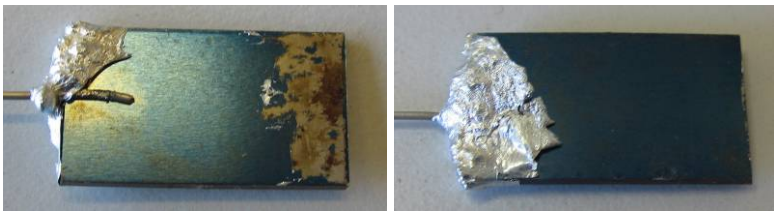

Figure II.5. Uncoated steel after immersion in a liquid zinc bath

The treatment consists in removing the oxide layer from the steel's surface and to protect it from subsequent oxidation until the contact with liquid zinc [VEB 08].

The specimen is successively
- degreased with acetone,
- pickled in a hydrochloric solution (50% HCl 37% and 50% H_2O) at 40°C during 5 minutes,

- rinsed in water during few seconds and, finally,
- fluxed in an aqueous solution of $ZnCl_2$ (107g/L) and NH_4Cl (136g/L) at 50°C during 10 minutes.

The specimen is then dried in a furnace at 120°C during 10 minutes to avoid splashing during subsequent immersion in the liquid zinc bath.

After the fluxing treatment, the specimen is covered by a fine layer of $ZnCl_2$, $2NH_4Cl$ crystals protecting steel surface from oxidation. Moreover, during immersion of fluxed specimen in the zinc bath, flux decomposition permits to start the metallurgical reactions between iron and zinc; two principal reactions occur: dissolution of the steel by the zinc and nucleation and growth of intermetallic compounds.

After this surface preparation, the specimen is immersed in the molten zinc bath.

II.3. Molten zinc bath

The galvanizing furnace used for this study is shown in figure II.6. The crucible is 130mm height and 90mm diameter. About 4 kg zinc can be melted in the crucible.

Two different baths were used: one of pure zinc and one containing 0.2 wt% Al and 0.02 wt% Fe. Adding aluminum in the zinc bath prevents an excessive oxidation of the zinc bath surface.

The temperature of the galvanizing bath was varied from 420°C to 840°C and the immersion times range from few seconds to 20 minutes. Bath temperature is measured with a thermocouple directly immersed in the molten zinc bath.

Figure II.6. Furnace used for galvanizing

III. Tensile tests

III.1. Gleeble tests

III.1.1. Principle

3500 Gleeble simulator permits to carry out thermo-mechanical testing of conductive materials and thus, to simulate high temperature processes such as welding processes.

As illustrated in figure II.7, high thermal conductivity grips (in copper in this study) hold the specimen. An electrical current is applied between the grips, through the specimen, the latter being heated by Joule effect. The thermal cycle is controlled by a type K thermocouple welded in the central part of specimen. The specimen is then cooled by heat dissipation trough cooled grips or by water or gas quenching, depending on the desired cooling rate.

The specimen can be strained via the displacement of grips. A longitudinal extensometer is used to measure the corresponding strain with a gauge length of 15mm (figure II.7 (d)).

All testing data such as temperature, force or stroke are collected during the test.

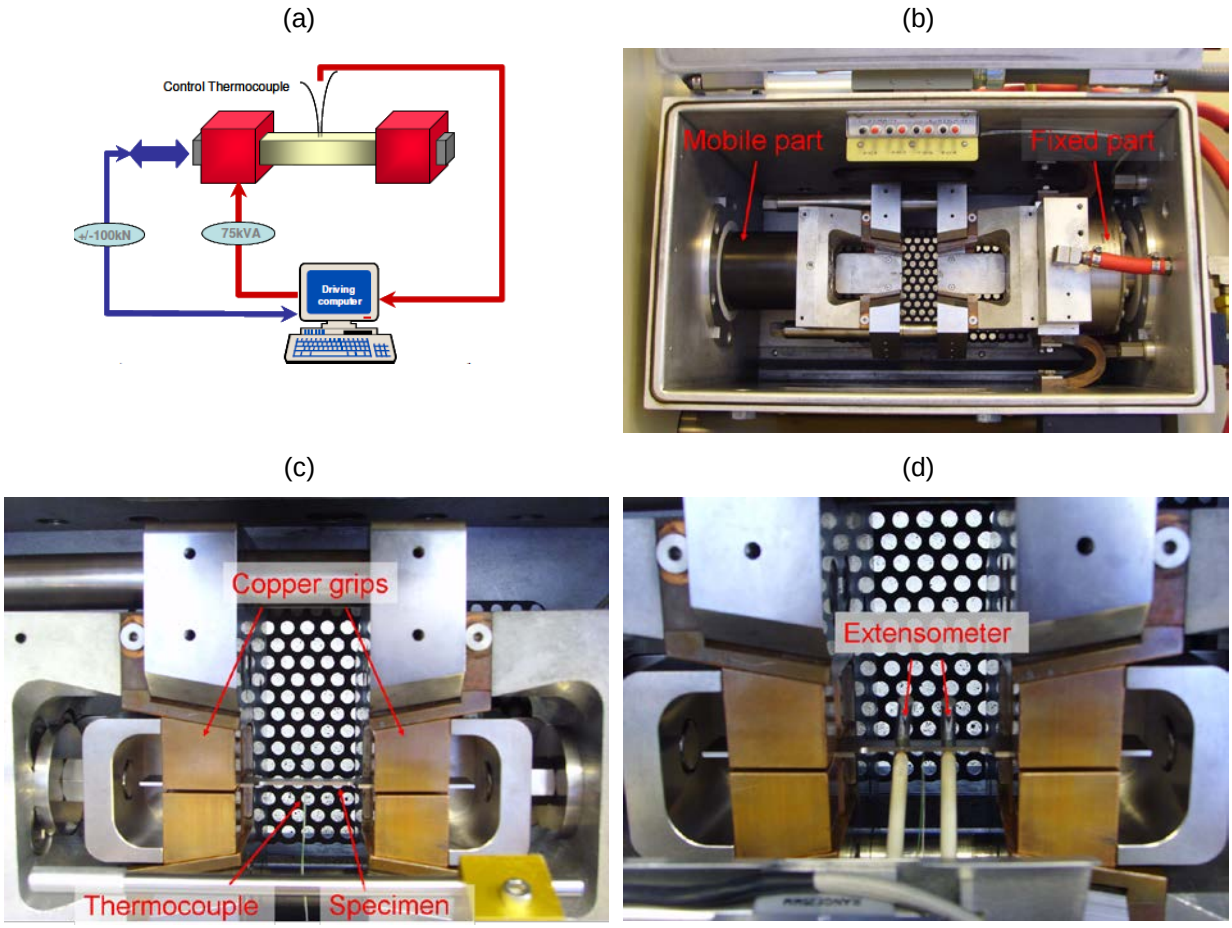

Figure II.7. 3500 Gleeble simulator: (a) Principle [DAN 09], (b) testing chamber, (c) and (d) specimen set up

The major advantage of this set up is that thermal and mechanical cycles are controlled dynamically and quasi independently of each other. Control mode (including stroke, force, stress or strain) can be changed from one to another during the test. Furthermore, tests can be performed under inert atmosphere.

III.1.2. Specimen

Tensile specimens, illustrated in figure II.8 (a), were machined from 1.5mm thick sheets. The tensile direction is perpendicular to the rolling direction. Two sets of specimens have been used: bare specimens as reference specimens and electrogalvanized (EG) specimens (pure zinc layer of 7,5µm thickness on each face) to study the effect of liquid zinc. Furthermore, in order to investigate the influence of coating process on liquid zinc embrittlement, some galvanized specimens (immersed in a molten zinc bath) were also used.

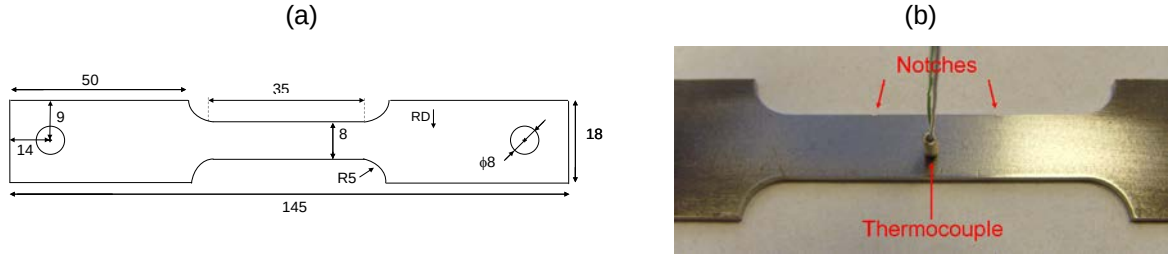

Figure II.8. Tensile specimen: (a) geometry, (b) notches and thermocouple localization

In order to avoid “loosening” of the extensometer, two fine notches (distant 15mm one from the other) are manually machined on one side of the gauge length (figure II.8 (b)).
One face of specimens is ground to remove the oxide layer in the case of bare specimen or the zinc layer in the case of EG specimens and cleaned with acetone to provide a good surface state for welding the controlling thermocouple T1. The latter is welded in the central part of the lower face of specimens (figures II.7 (c) and II.8 (b)).

In order to determine the temperature field in the strain gage, two supplementary thermocouples T2 and T3 were welded at a varying distance from T1. The temperature field was determined for each testing temperature. It was found that the homogeneous zone is logically narrowing with increasing temperature as shown in figure II.9 where the temperature evolution along the middle line (a) is plotted for testing temperature of 500°C (b) and 900°C (c). The symmetry of the temperature field has been established for all testing temperatures.

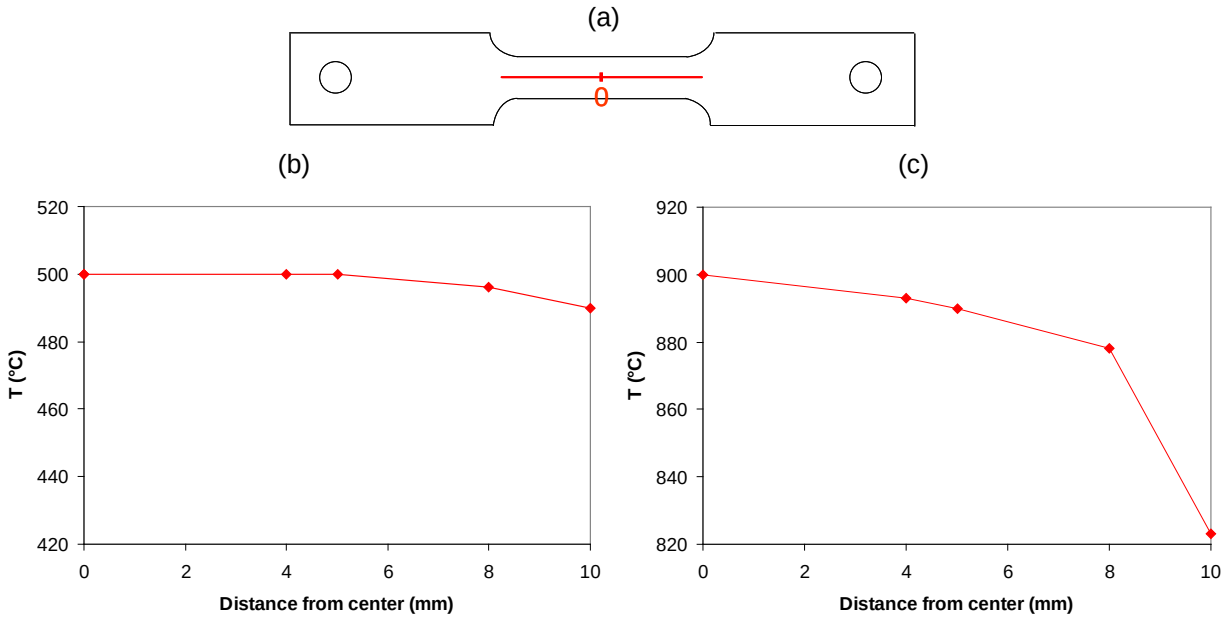

Figure II.9. Evolution of temperature along the middle line (a) at 500°C (b) and 900°C (c)

Up to 950°C, the temperature is homogeneous (maximal difference of 10°C) within an area of around 10mm centered in the strain gage as illustrated in figure II.10.

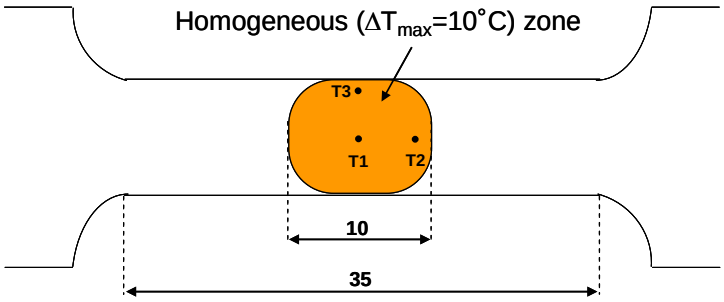

Figure II.10. Homogeneous zone in tensile specimens

III.1.3. Thermo-mechanical cycles

In order to investigate the cracking behaviour, hot tensile tests were performed. As seen in figure II.11, the specimen is heated to the target temperature (upper than the zinc melting point of 419°C to permit a contact between steel and liquid zinc) with a heating rate of 80°C/s while the force is kept null (force control). During heating, stroke slightly increases to maintain the force null because of thermal expansion. This permits to avoid bending of the sample. When the testing temperature is reached, tensile test is performed at a constant displacement speed (stroke control) until failure occurs. Before beginning mechanical loading, stroke value is put back to zero in order to not take into account the expansion

compensation during heating in subsequent data analysis. Once specimen broken, it is air cooled.

The heating and tensile testing of the specimens were carried out in air environment.

The influence of different parameters such as temperature and strain rate on cracking resistance was investigated. Testing temperatures range from 460° to 1000°C. Displacement speeds used in this study range from 0.02mm/s to 20mm/s corresponding to strain rates of $1.3.10^{-3}$ s^{-1} and 1.3 s^{-1} respectively, assuming homogeneous strain within the strain gauge.

In general, several experiments were conducted for each testing conditions in order to check the repeatability of the results.

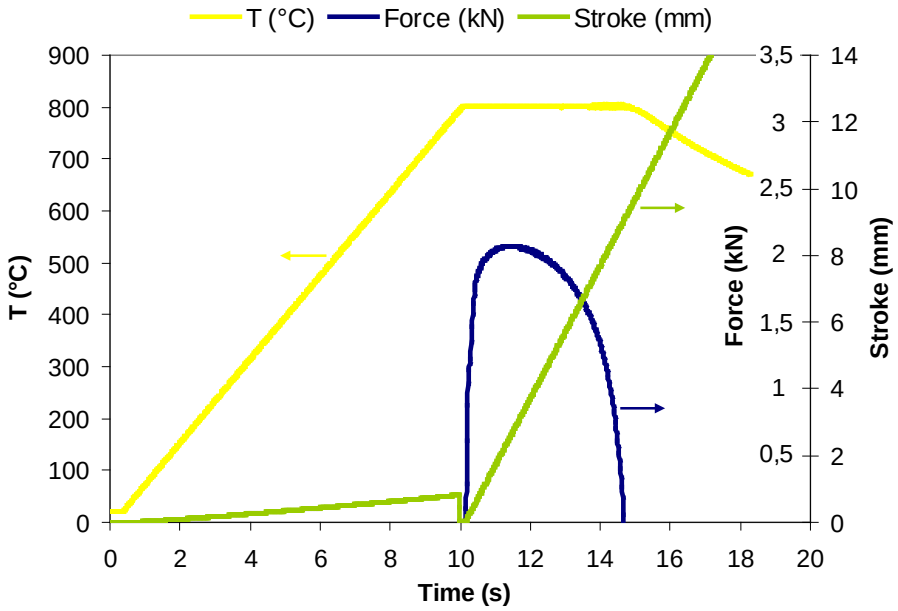

Figure II.11. Thermo-mechanical cycle

The influence of time of contact between the solid steel and the liquid zinc was investigated by holding the specimen at temperature (upper than zinc melting point) before tensile test. Two different tests were performed. The first one (Holding A) consists in holding the specimen at the same temperature as the tensile test one (figure II.12 (a)). During the second type of cycle (Holding B), the specimen is held at a temperature lower than 800°C, temperature of the subsequent tensile test (figure II.7 (b)). Holding times were varied from 10 seconds to 5minutes and holding temperatures range from 500°C to 800°C.

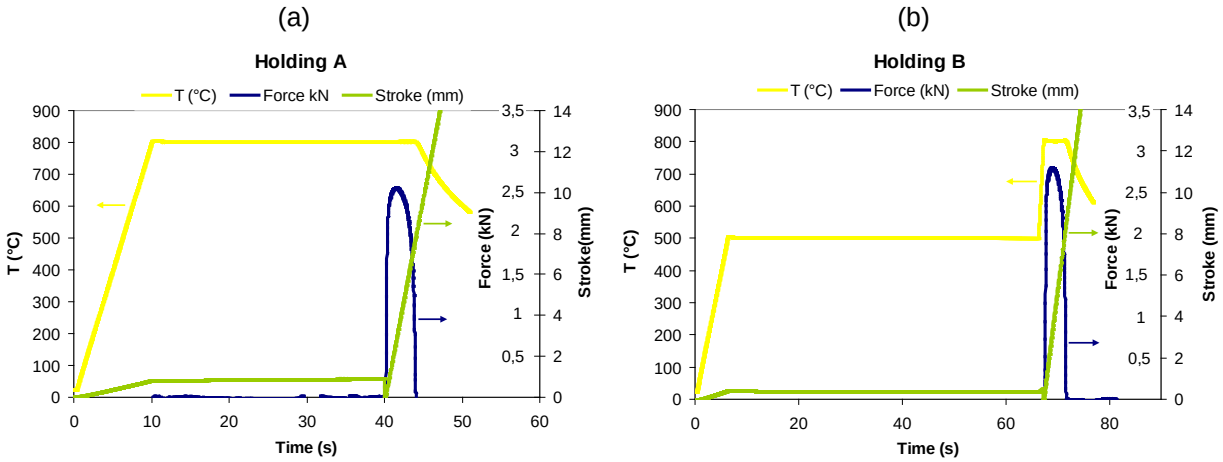

Figure II.12. Thermo-mechanical cycles: (a) Holding and tensile test at same temperature (b) Holding and tensile test at different temperature

III.1.4. Description of embrittlement

Mechanical behaviour is determined by analysing the obtained tensile curves. Engineering values are directly deduced from force and extensometer recorded values according to the relations (II.1 and II.2)

$$\sigma_E = \frac{F}{S_0} \qquad \text{(eq. II.1)}$$

$$\varepsilon_E = \frac{l - l_0}{l_0} = \frac{\Delta l}{l_0} \qquad \text{(eq. II.2)}$$

where F is the force applied to the specimen, S_0 is the initial section of the specimen, Δl is elongation and l_0 is the initial gauge length.

The true stress and strain take into account the variation of the specimen section during the test and are given by the relations (II.3 and II.4)

$$\sigma = \frac{F}{S} = \frac{F.l}{S_0.l_0} = \sigma_E.(1+\varepsilon_E) \qquad \text{(eq. II.3)}$$

$$\varepsilon = \int_{l_0}^{l} \frac{\delta l}{l} = \ln\left(\frac{l}{l_0}\right) = \ln(1+\varepsilon_E) \qquad \text{(eq. II.4)}$$

Yield strength, ultimate tensile strength (UTS) and flow stress at different strain levels (1%, 5%, 10%) were determined from true tensile curves obtained with bare specimens as illustrated in figure II.13 (a).

The severity of embrittlement was characterized by the critical stress corresponding to the maximal true stress achieved by EG specimens as shown in figure II.13 (b).

To take into account both the reduction of strength and ductility observed in case of liquid zinc embrittlement, the energy to fracture calculated as $\int \sigma d\varepsilon$ in tension is a relevant parameter and thus has been calculated for each test.

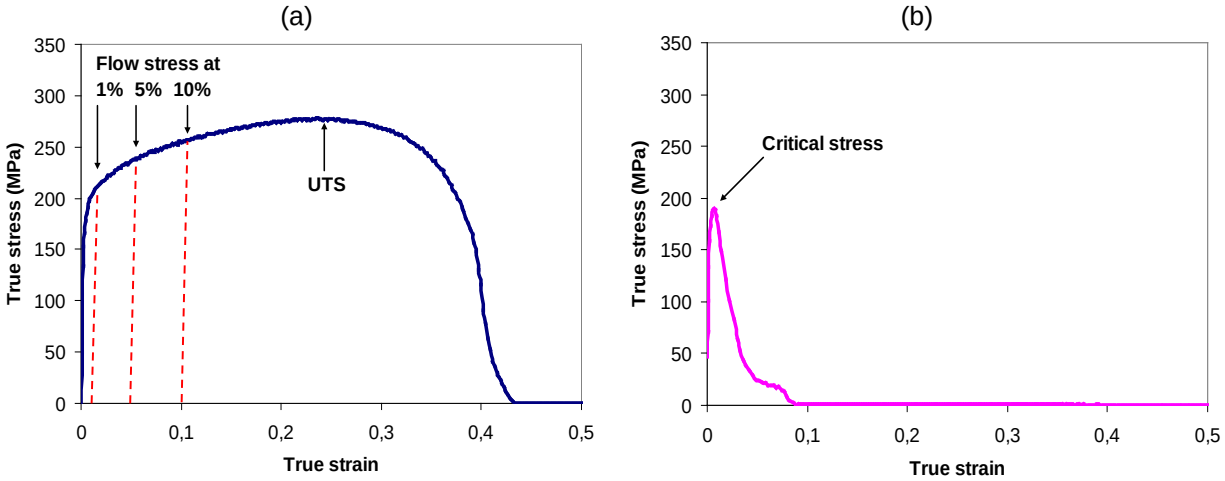

Figure II.13. Determination of relevant stress values: (a) UTS and flow stress at different strain levels for bare specimens and (b) critical stress reached by EG specimens

III.2. Room temperature tests

Tensile tests at room temperature were performed on MTS Adamel DY35 with an extensometer. Specimens used for such tests are shown in figure II.14. The strain rate is 4.2 $.10^{-3}$ s^{-1}.

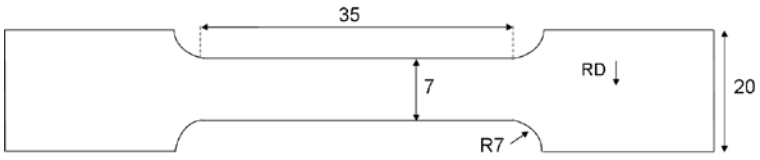

Figure II.14. Tensile specimens for room temperature tests

IV. Observations

Different types of observation have been carried out:

- fracture surface analysis of broken Gleeble specimens and cracked cups (figure II.15 (a) and (b) respectively)
- cracks and coating observations of Gleeble specimens along longitudinal section (figure II.15 (c))
- observations of the surface of the cracked cup (figure II.15 (d))

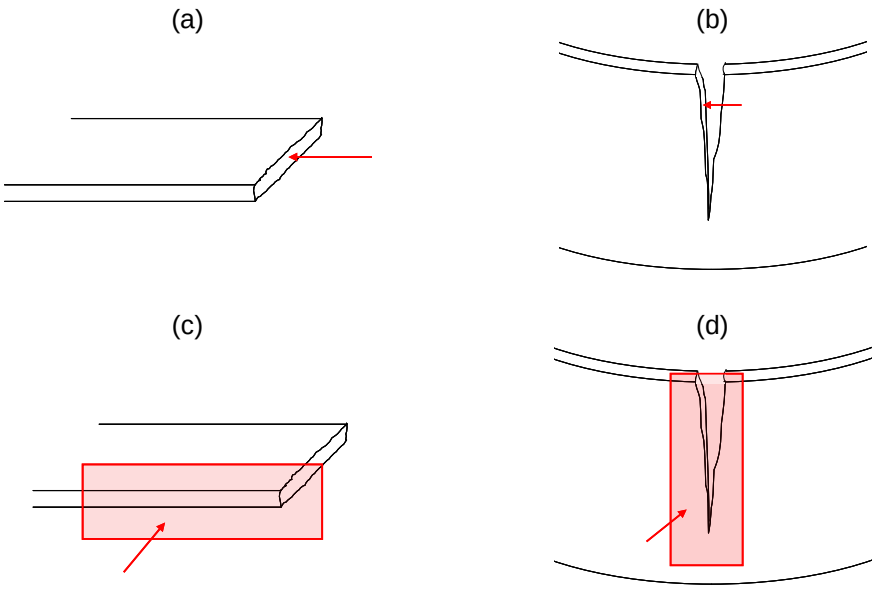

Figure II.15. Different observations: fracture surface of Gleeble specimen (a) and cracked cup (b), longitudinal section of Gleeble specimen (c) and surface of cracked cup

The fracture surface observation does not require any specific preparation. Specimens are cut and then, observed.

For observations of longitudinal section of Gleeble specimen and surface of cracked cup, specimens are cut, mounted, mechanically ground (SiC paper 180/400/1200) and polished with the 3μm diamond paste.

For revealing grain boundaries, some Gleeble specimens have been polished with OPS (colloidal silica) solution during 10 minutes.

For observing the different phases formed during galvanizing, specimens have been etched with 2% Nital during approximately 10 seconds.

Microstructural investigations have been performed by optical microscopy and scanning electron microscopy operating with an acceleration voltage of 20kV.

Different scanning electron microscopes (SEM) have been used:

- Philips XL20 equipped with a tungsten-filament
- JEOL840 equipped with a tungsten-filament
- FEG-SEM Zeiss Supra55VP equipped with Oxford 80mm^2 EDX detector

EDX system permits to perform chemical analysis of the unetched surfaces.

Intermetallic phases formed at the interface between the steel and zinc have been identified by X-Ray diffraction (XRD) using Cu Kα radiation (1.5405Å) in a Bruker D500 diffractometer.

Conclusions

The Gleeble test developed in this study is very relevant since it is very fast and flexible. Indeed, testing parameters such as temperature or strain rate can easily be changed in a large range so that factors affecting embrittlement can be identified. It provides, thanks to the extensometer, quantitative results on the influence of these parameters on the occurrence of LME. It is important to emphasize that very high heating rate and intermediate strain rate can be applied, permitting to simulate welding conditions. Moreover, this test can be applied to other solid metal/liquid metal couples to investigate the LME phenomenon.

Tests performed on cups in liquid zinc bath bring complementary information on necessary conditions of embrittlement, particularly on the influence of stress.

Microscopy observations will permit a better understanding of cracking mechanisms.

In the next chapters are presented the experimental results of embrittlement of our material by liquid zinc.

Chapter III. Embrittlement of the Fe22Mn0.6C steel by liquid zinc

The literature review presented in the first chapter reveals that embrittlement by liquid zinc occurs under particular experimental conditions. If these conditions are not fulfilled, no detrimental effect of the presence of liquid metal is observed. This chapter aims at highlighting the liquid zinc embrittlement of the studied steel and precisely determining conditions leading to embrittlement.
The behaviour of the Fe22Mn0.6C TWIP steel has been mainly studied using a simple uniaxial tensile load.

Firstly, the tensile behaviour of the steel is studied in the absence of liquid zinc. Then, the embrittlement by liquid zinc is investigated. The influence of external (temperature, strain rate or stress) and internal (microstructure of the steel) parameters is detailed with the aim of defining the most critical conditions.

I. Tensile behaviour of the Fe22Mn0.6C steel

I.1. Room temperature behaviour

Room temperature tensile tests have been performed at a strain rate of $4.2.10^{-3}$ s^{-1}. Engineering and true stress/true strain curves have been plotted using expressions II.1-4. These curves are presented in figure III.1.
It can be seen that the Fe22Mn0.6C steel combines very high strength (UTS above 1800MPa) with high elongation (upper than 60%). The yield strength is quite high (upper than 600 MPa).
At room temperature, the fracture occurs without macroscopic necking: the engineering curve does not decrease at high strains and specimens do not exhibit localized section reduction.

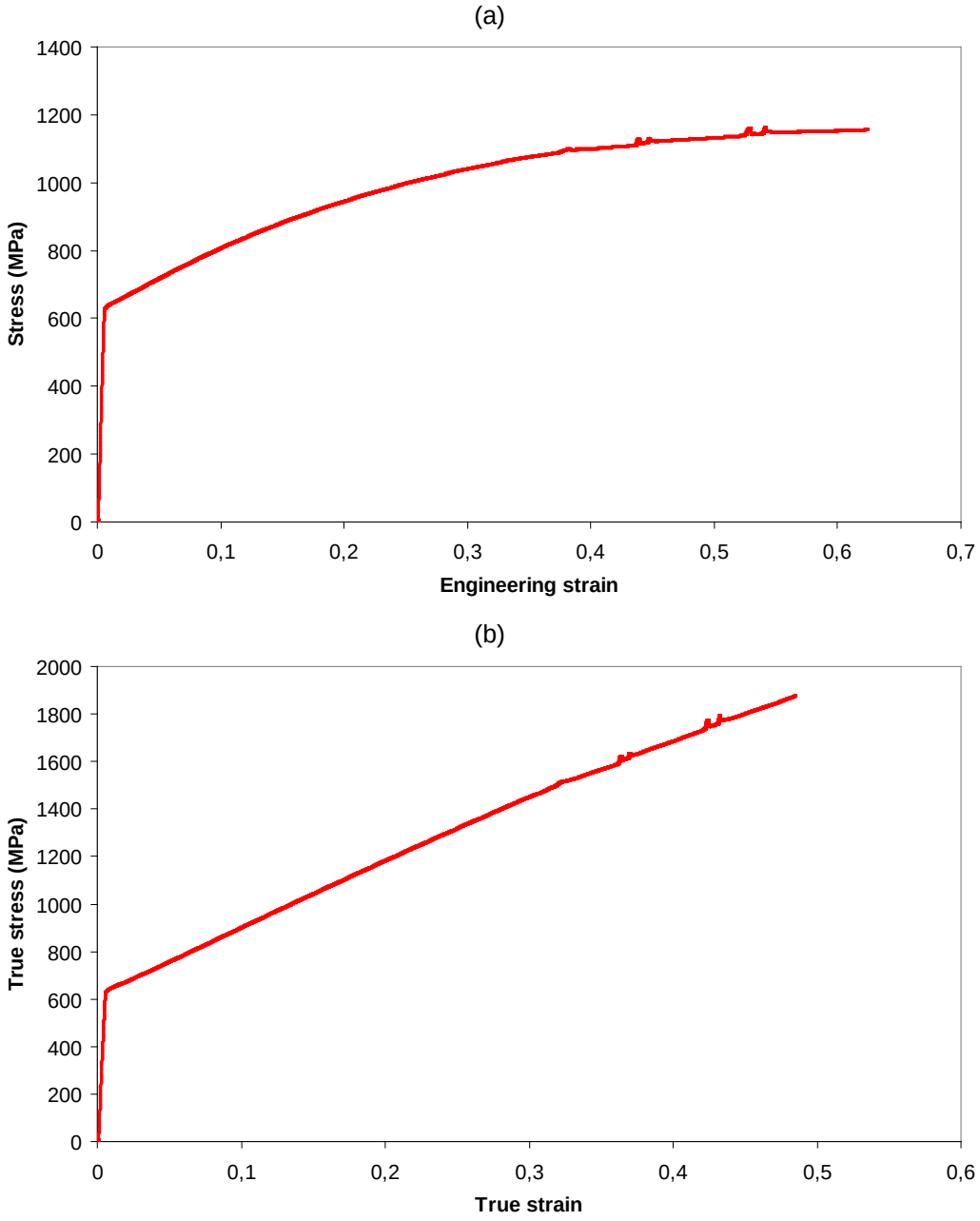

Figure III.1. Engineering (a) and true (b) tensile curves obtained at room temperature

SEM micrograph of the fracture surfaces of specimens tested at room temperature is shown in figure III.2. They are typical ductile fracture surfaces characterized by the presence of dimples of about 1μm.

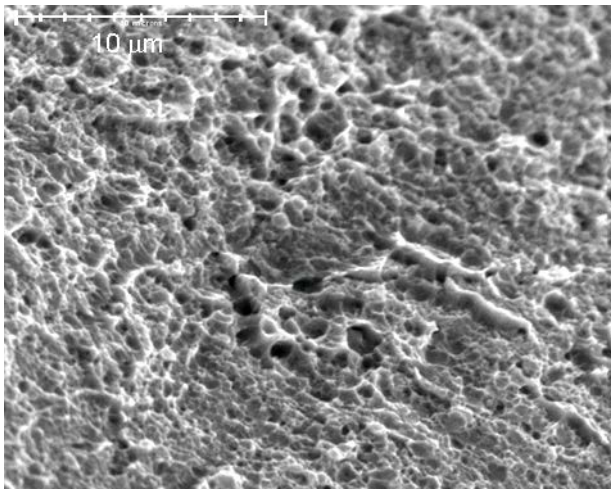

Figure III.2. SEM micrograph of the fracture surface after room temperature tensile test

The observed mechanical properties easily explain the important interest of the Fe22Mn0.6C steel for energy absorption applications.

I.2. High temperature behaviour

Hot tensile tests have been performed on bare specimens in order to determine the reference behaviour of the steel. Testing temperature ranges from 400°C to 1000°C and four displacement speeds were used: 0.02mm/s, 0.2mm/s, 2mm/s and 20mm/s corresponding to strain rates of $1.3.10^{-3}$ s^{-1}, $1.3.10^{-2}$ s^{-1}, $1.3.10^{-1}$ s^{-1} and 1.3 s^{-1} respectively.

Figures III.3 presents the engineering and true tensile curves obtained at different temperatures and for a strain rate of $1.3.10^{-1}$ s^{-1}.

It can be seen that the ultimate tensile strength (UTS) as well as yield strength decreases with increasing temperature. The decrease of the ultimate tensile strength is to a large extent due to the collapse of strain hardening above 700°C.

Tensile curves indicate that localized deformation occurs during testing. It is clearly seen a difference between the uniform elongation and the elongation to fracture. For all testing temperatures, the latter ranges from 45% to 55%.

The localized deformation is clearly visible on specimens after tensile test as illustrated in figure III.4.

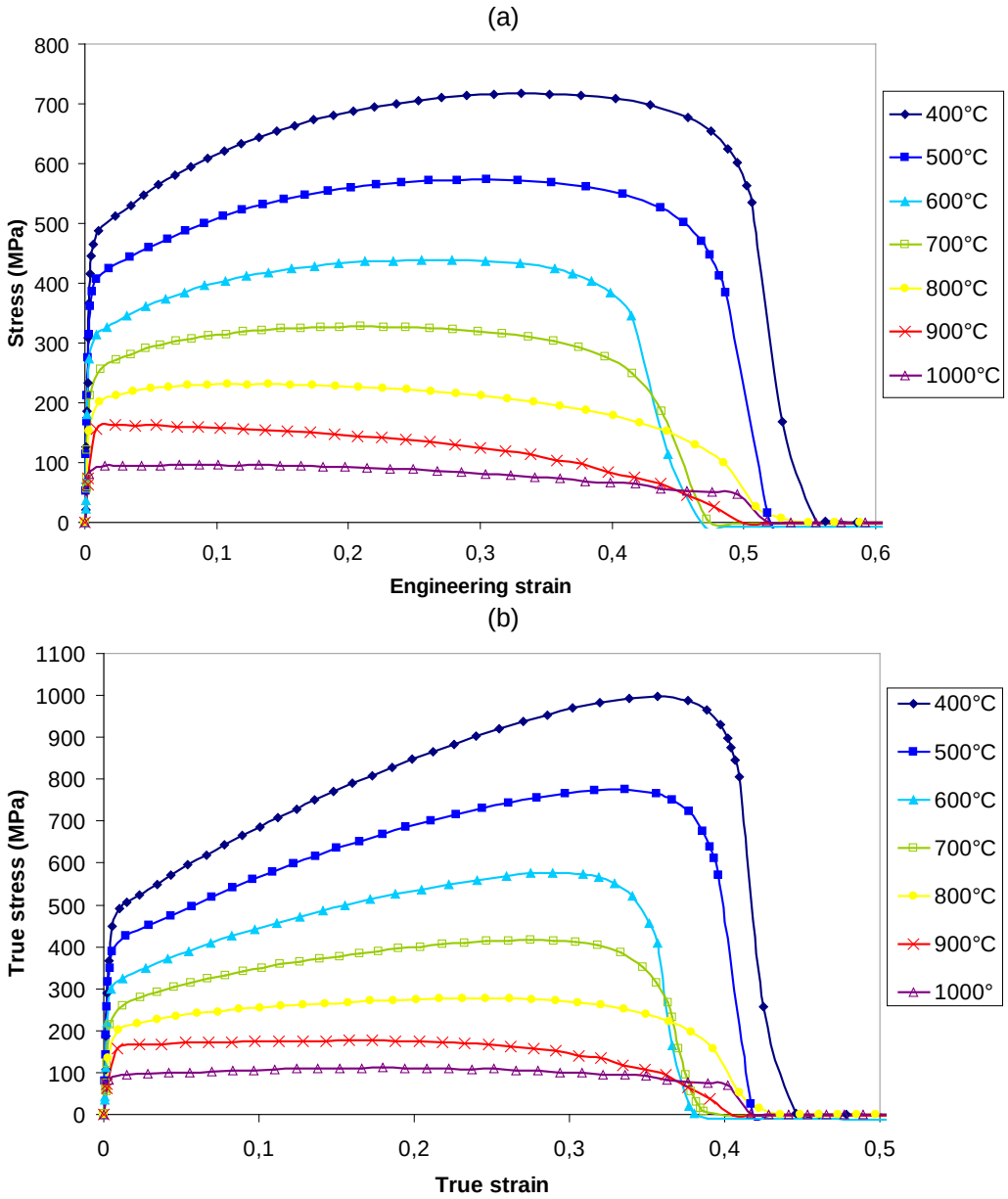

Figure III.3. Engineering (a) and true (b) tensile curves obtained at different temperatures for a strain rate of $1.3.10^{-1}$ s^{-1}

Figure III.4. Specimen after tensile test at 900°C, $1.3.10^{-1}$ s^{-1}

Until 500°C, the fracture surface is clearly ductile similar to the one obtained after tensile testing at room temperature. However, the fracture surface of bare specimens submitted to tensile test at higher temperature is quite different as shown in figure III.5. The small dimples

of 1µm observed on room temperature specimen are not visible on specimen tested at 800°C. On the latter, larger dimples are present (figure III.5 (a)) and typical morphology of oxidized surface is observed (figure III.5 (b)). It is worth noticing that all tensile tests are carried out in air in order to keep the same experimental conditions that during spot welding. The oxidation layer of approximately 2µm thickness is clearly visible on longitudinal section (figure III.5 (c)). Corresponding EDX measurements are shown in figure III.5 (d).

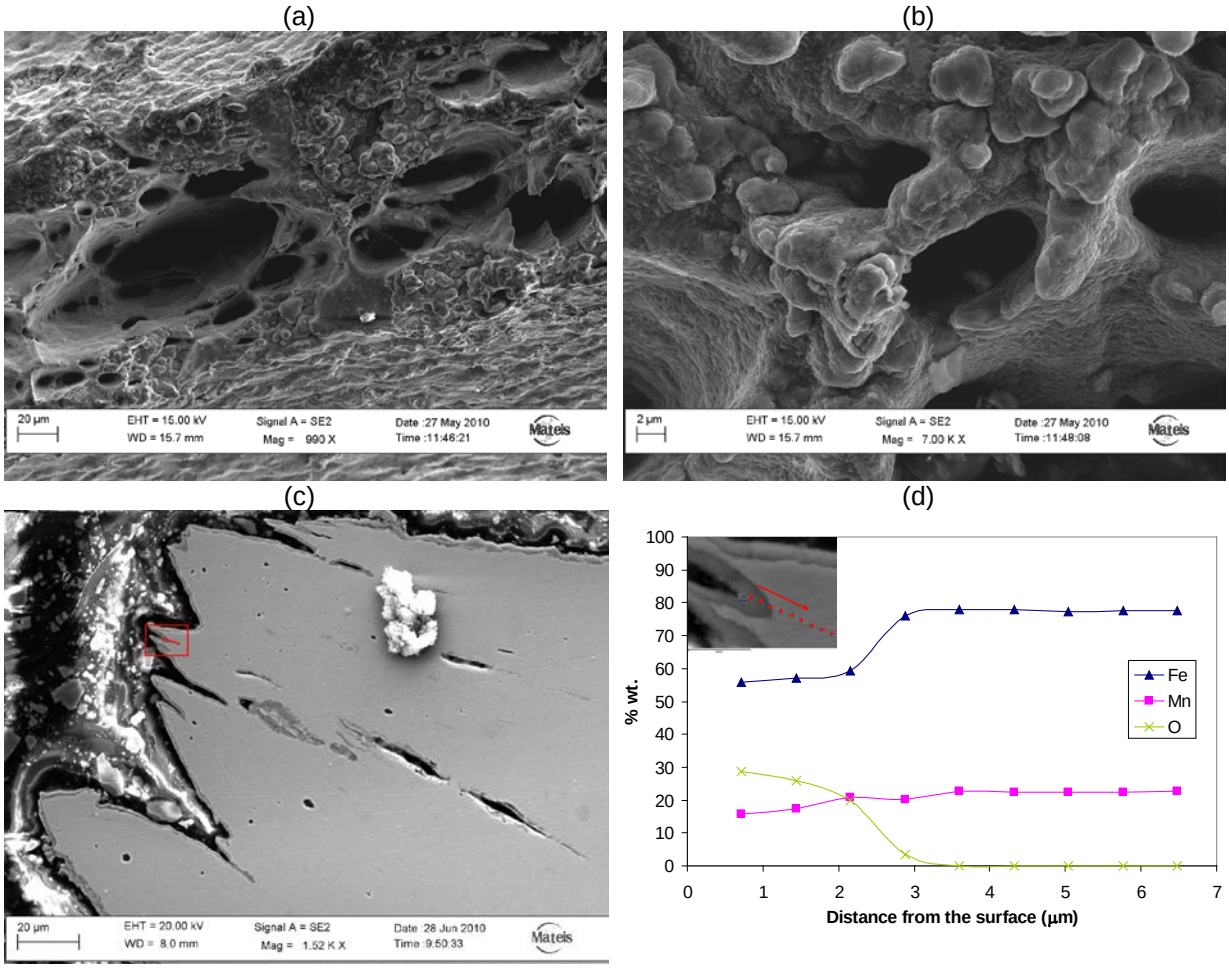

Figure III.5. SEM micrographs of (a) and (b) the fracture surfaces, (c) longitudinal section of bare specimens after tensile test at 800°C, (d) EDX profile along the line shown in (c)

The evolution of flow stresses at 1% and 5% strain levels and the UTS with temperature for strain rates of $1.3.10^{-3}$ s^{-1} and 1.3 s^{-1} is presented in figure III.6; each point being an average of several measurements. Same scales have been voluntarily used for the two strain rates in order to make comparison easier.

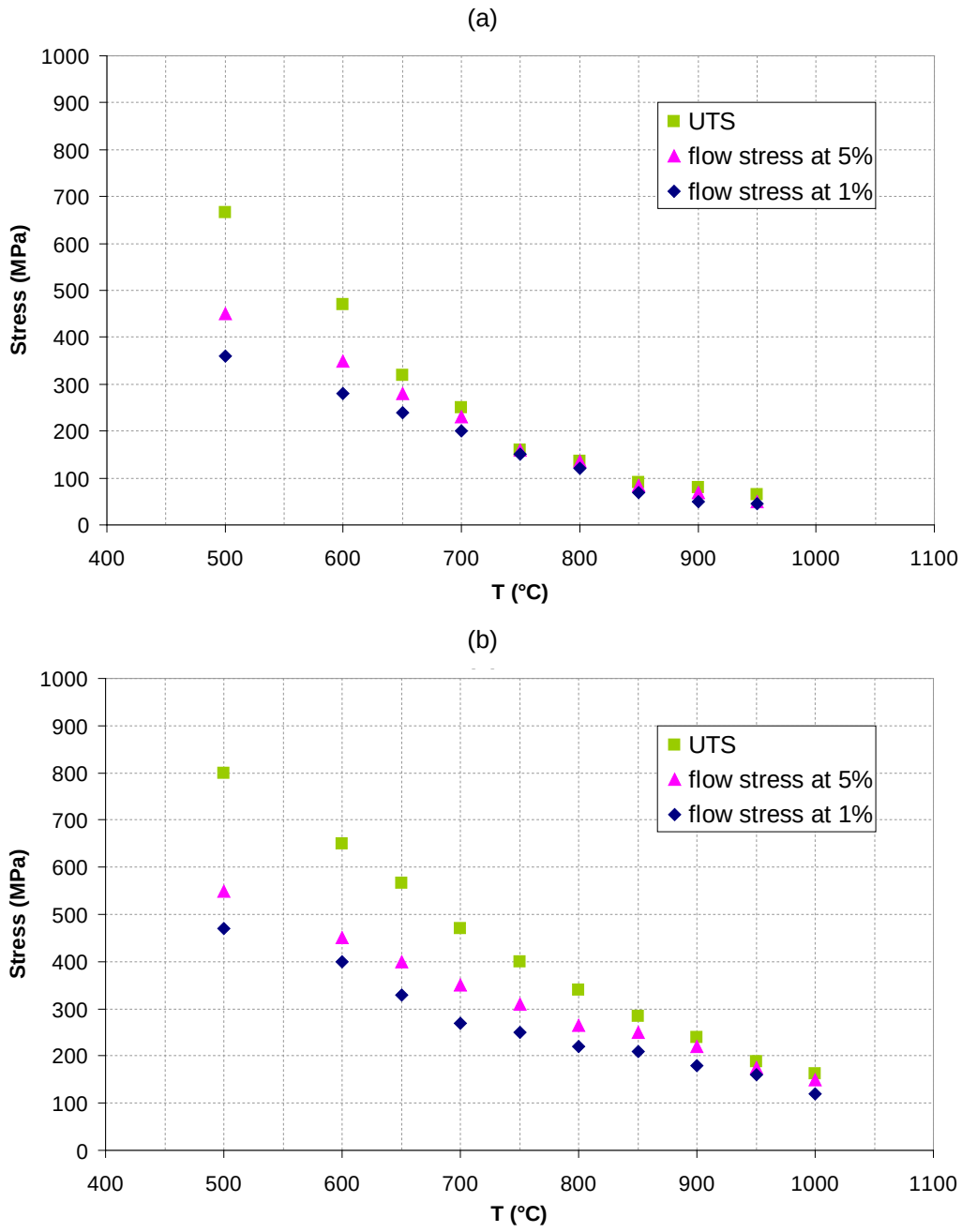

Figure III.6. Evolution of mechanical strength with temperature at (a) $1.3.10^{-3}$ s^{-1} and (b) 1.3 s^{-1}

The progressive decrease of mechanical strength with increasing temperature is clearly seen whatever the strain rate. The drop in strain hardening is also clearly observed since for higher temperatures, no more difference can be noticed between the different stress values.

Besides, increasing strain rate tends to increase mechanical strength. For instance, at 600°C, the flow stress at 1% is about 280 MPa for a strain rate of $1.3.10^{-3}$ s^{-1} whereas it is about 400 MPa for a strain rate of 1.3 s^{-1}. Moreover, strain hardening is maintained at higher temperatures with increased strain rate. Indeed, for a strain rate of $1.3.10^{-3}$ s^{-1}, no more

difference between stress values can be noticed at 750°C while at 1.3 s^{-1}, there is still a difference of about 150MPa between $\sigma_{1\%}$ and UTS.

The evolution of mechanical strength with strain rate at 800°C is shown in figure III.7. As expected, stress considerably increases with increasing strain rate.

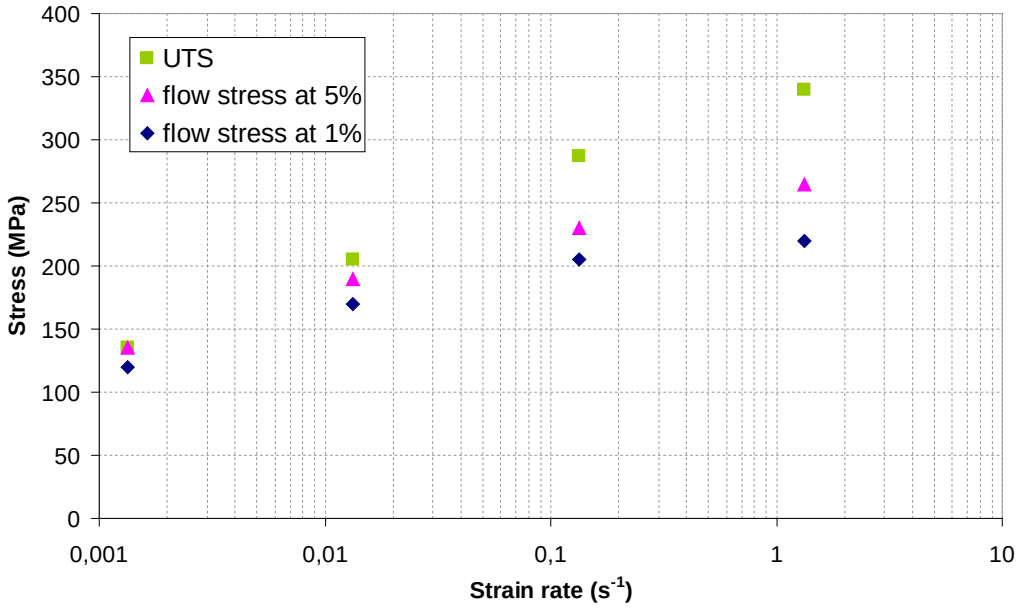

Figure III.7. Evolution of mechanical properties with strain rate at 800°C

Cold rolled specimens have also been investigated. The microstructural differences in terms of defects (dislocation and twin) density as well as grains shape between such specimens and the recrystallized ones are clearly evidenced by their mechanical behaviour. Tensile curves obtained in the transverse direction at different temperatures for a strain rate of $1.3.10^{-1}$ s^{-1} are presented in figure III.8. No more work hardening is observed in the cold rolled specimens meaning that the dynamic Hall and Petch hardening is suppressed due to the high initial concentrations of twins.

It is important to point out that cold rolled specimens do not break perpendicularly to tensile load but slantwise as illustrated in figure III.9.

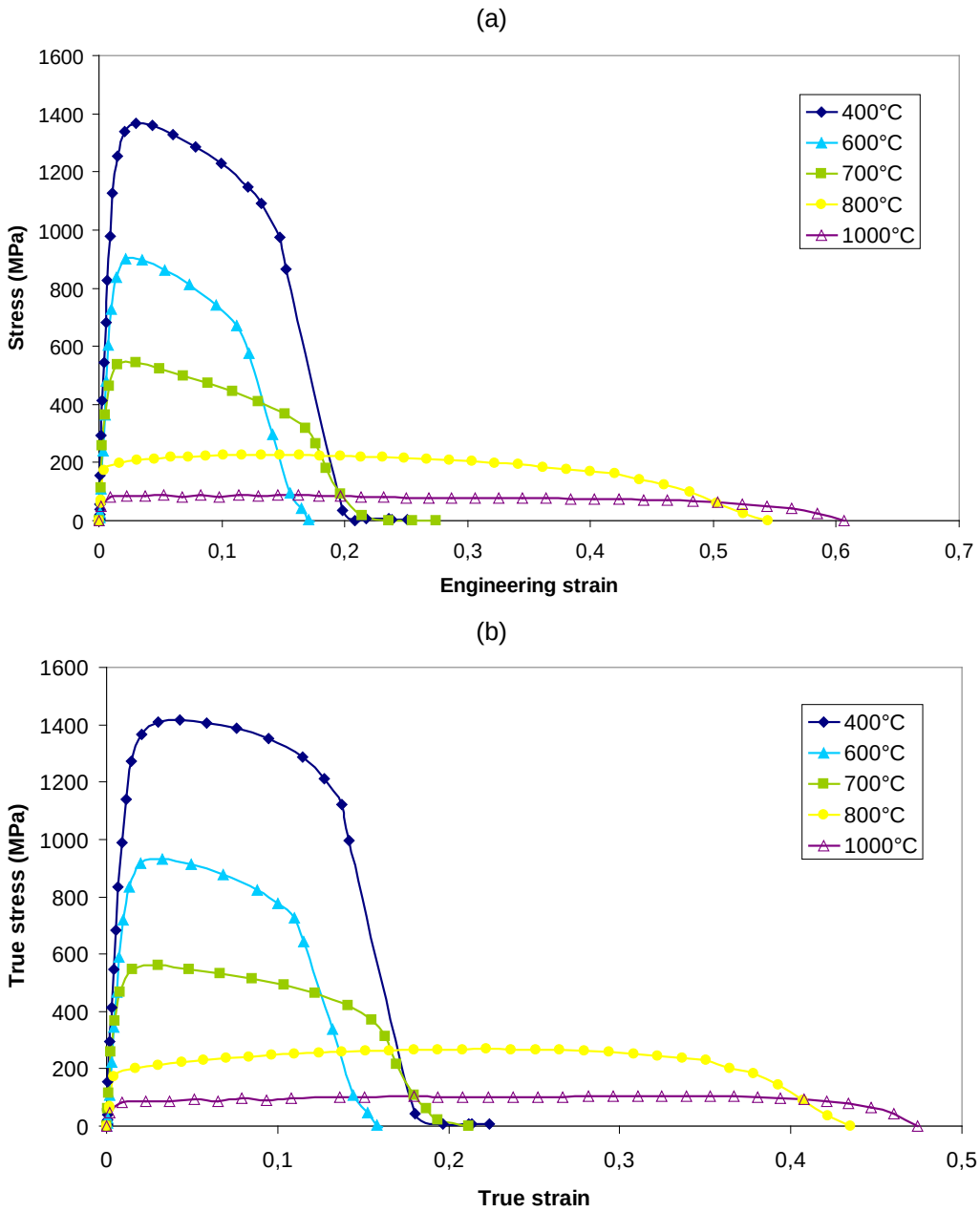

Figure III.8. Engineering (a) and true (b) tensile curves obtained on cold rolled specimens at different temperatures for a strain rate of $1.3.10^{-1}$ s^{-1}

Figure III.9. Cold rolled specimen after tensile test at 600°C, $1.3.10^{-1}$ s^{-1}

From figure III.10, it is clear that cold rolled specimens exhibit higher levels of stress than recrystallized ones for temperatures below 700°C. However, elongation is significantly

reduced (~20% for as rolled specimens versus ~40% for recrystallized specimens). For T≥800°C, cold rolled specimens exhibit the same behaviour as standard specimens, which can be explained by a quasi instantaneous recrystallization at those temperatures [BEU 06].

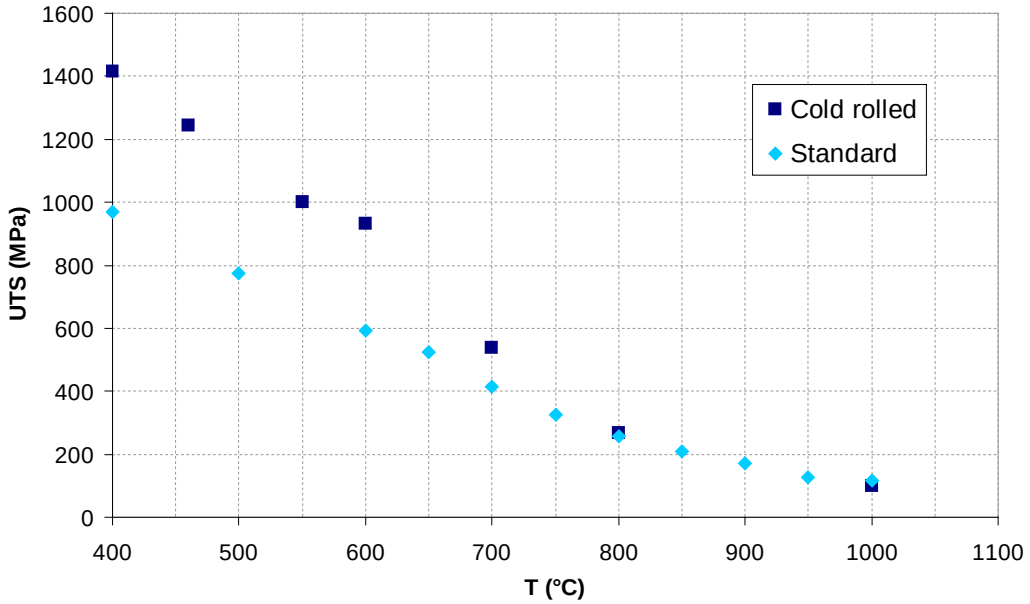

Figure III.10. Evolution of UTS with temperature for cold rolled and standard specimens at $1.3.10^{-1}$ s^{-1}

I.3. Conclusions

Tensile tests performed on bare specimens confirm that the Fe22Mn0.6C steel offers a combination of very high strength with high elongation. The best combination strength/ductility is obtained at room temperature where the UTS is greater than 1800MPa and the total elongation is around 60%.

Increasing temperature tends to decrease mechanical properties because of thermal softening and transition from twinning (inducing dynamic Hall and Petch effect) to dislocation glide.

It is important to point out that for a given temperature, the level of tensile stress can be increased by increasing strain rate or modifying microstructure by the use of cold rolled specimens for example.

II. Sensitivity of the Fe22Mn0.6C steel to the liquid zinc embrittlement

Tensile curve obtained at 800°C and $1.3.10^{-1}$ s^{-1} with EG specimens is presented in figure III.11 (a). For a better comparison, the curve obtained with bare specimen has been reported on the same figure. The embrittling effect of liquid zinc is clearly evidenced since elongation to fracture as well as fracture strength is drastically reduced. In the following, the so called critical stress for cracking will be defined as the maximal stress observed on tensile curve in embrittlement conditions.

In the case considered in figure III.11 (a), cracking occurs at a very small strain and thus, the EG specimen exhibits very few macroscopic deformation when observed after testing as compared to the bare specimen (figure III.11 (b)).

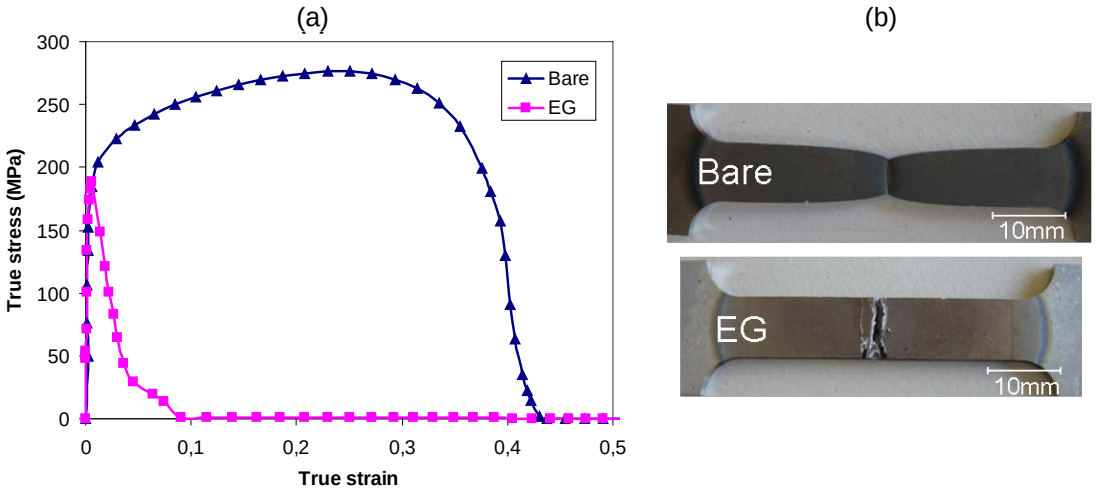

Figure III.11. (a) True tensile curve at 800°C for a strain rate of $1.3.10^{-1}$ s^{-1}: bare and EG specimens, (b) specimens after tensile test

This change in the mechanical behaviour is also reflected in the fracture surfaces. While the fracture surfaces obtained in the same experimental conditions with bare specimens are characteristic of ductile failure, the fracture surfaces of the EG specimens are characteristic of failure in presence of liquid as shown in figure III.12.

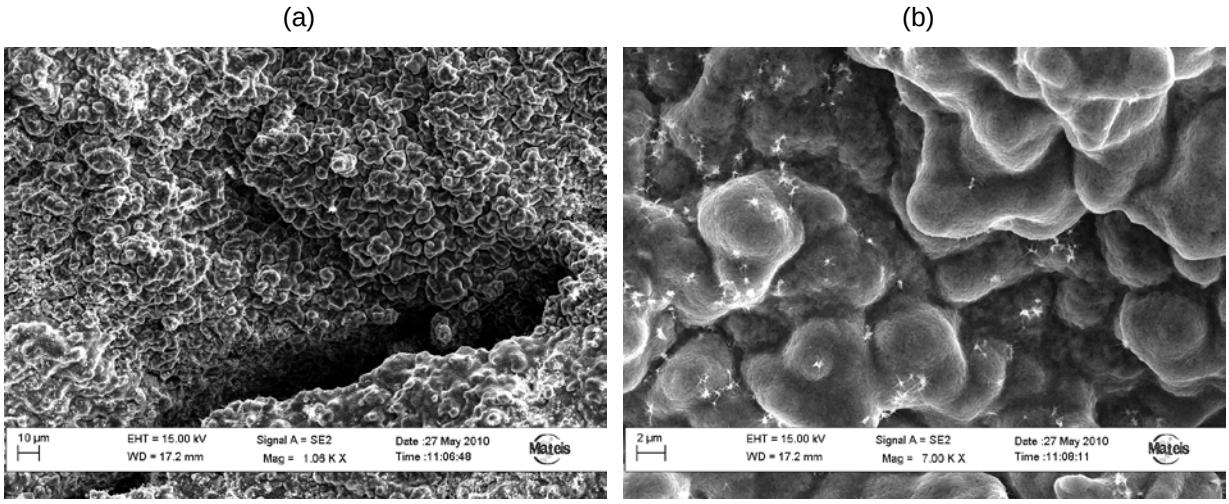

Figure III.12. SEM micrographs of the fracture surfaces of EG specimens after tensile test at 800°C

EDX analyses reveal the presence of zinc on the whole fracture surfaces of EG specimen (figure III.13). The major quantity of zinc probably settled once specimen has broken. Moreover, oxidation certainly occurs, modifying the newly formed fracture surface. A dissolution treatment must be performed to clean the original fracture surface off from deposited layers without altering it. Unfortunately, such treatment could not have been performed successfully and the original fracture surfaces have not been observed. But results of tensile tests clearly indicate the embrittlement of steel by liquid zinc.

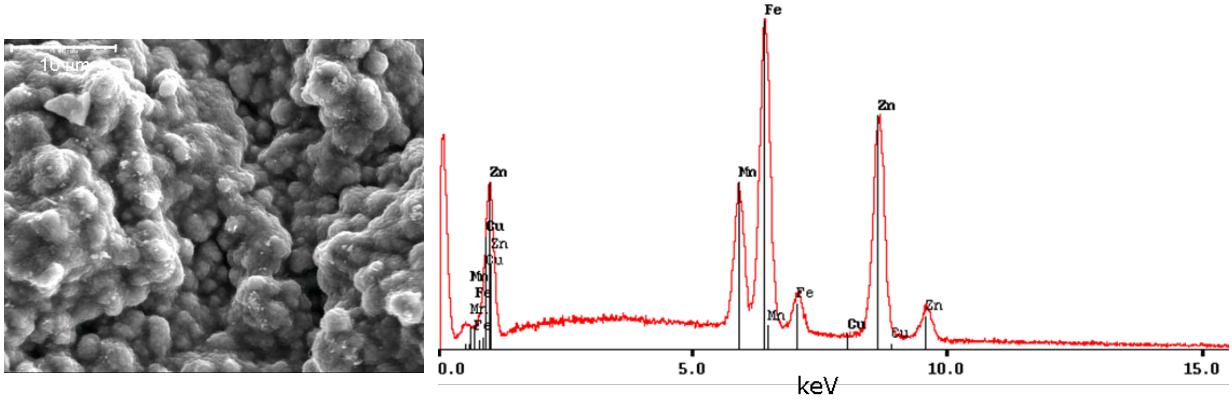

Figure III.13. EDX analyses of the fracture surface of EG specimen

Different compounds can be observed on fracture surfaces of EG specimens. Figure III.14 displays some examples. These phases have not been identified due to their small size and their repartition on the fracture surface. One can reasonably think that they are not involved in the cracking mechanisms and they appear only after cracking has occurred. It can be supposed from [ALA 10] that these phases result from zinc oxidation.

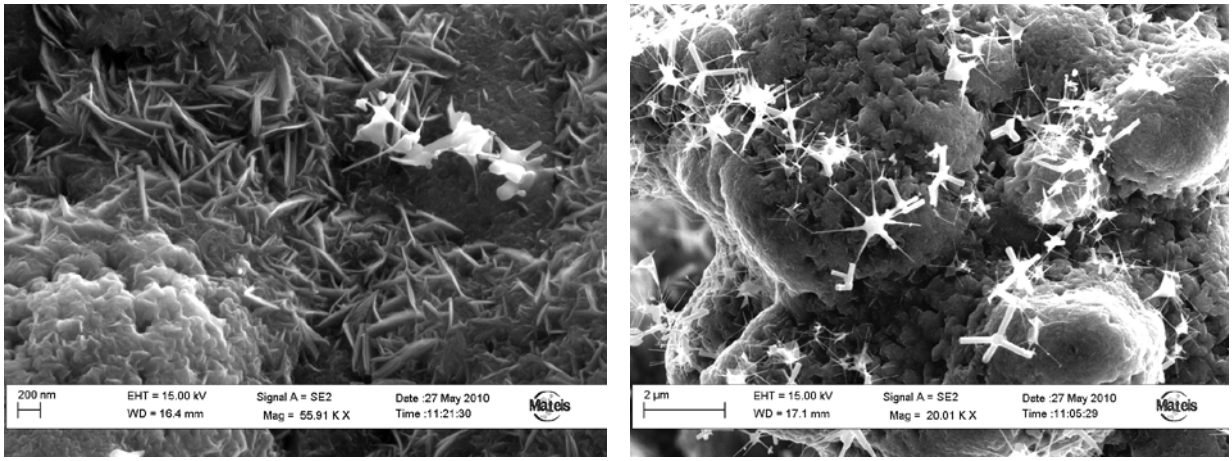

Figure III.14. Different compounds in the fracture surface of embrittled specimen

If displacement is stopped before specimen completely breaks but once critical stress has been reached, cracks are observed on surface specimen as illustrated in figure III.15. Cracks initiate but does not propagate through the whole specimen's thickness.

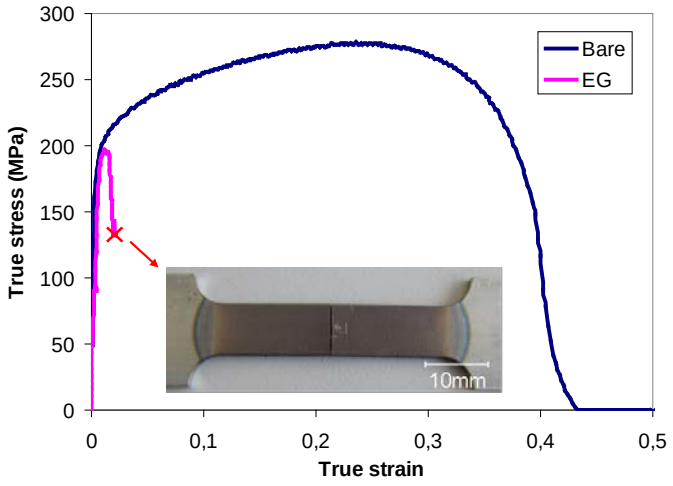

Figure III.15. Interrupted tensile test on EG specimen

In order to observe the fracture surface, this specimen partly broken at high temperature, has been tensile strained at room temperature until fracture. The two different zones can be distinguished:

- the fracture surface produced in contact with liquid zinc at 800°C presents a surface similar to the EG specimen broken at 800°C (figure III.16 (c))
- the fracture surface produced during the room temperature deformation is a dimpled surface typical of ductile failure (figure III.16 (b))

The EDX analyses reveal the presence of zinc on the whole surface produced in contact with liquid zinc. However, zinc has not been detected in the surface produced at room temperature. If zinc had penetrated beyond the cracked zone, it could probably not be detected using the experimental techniques employed in this work. But the ductile surface observed tends to indicate that zinc has not penetrated further than the cracked zone.

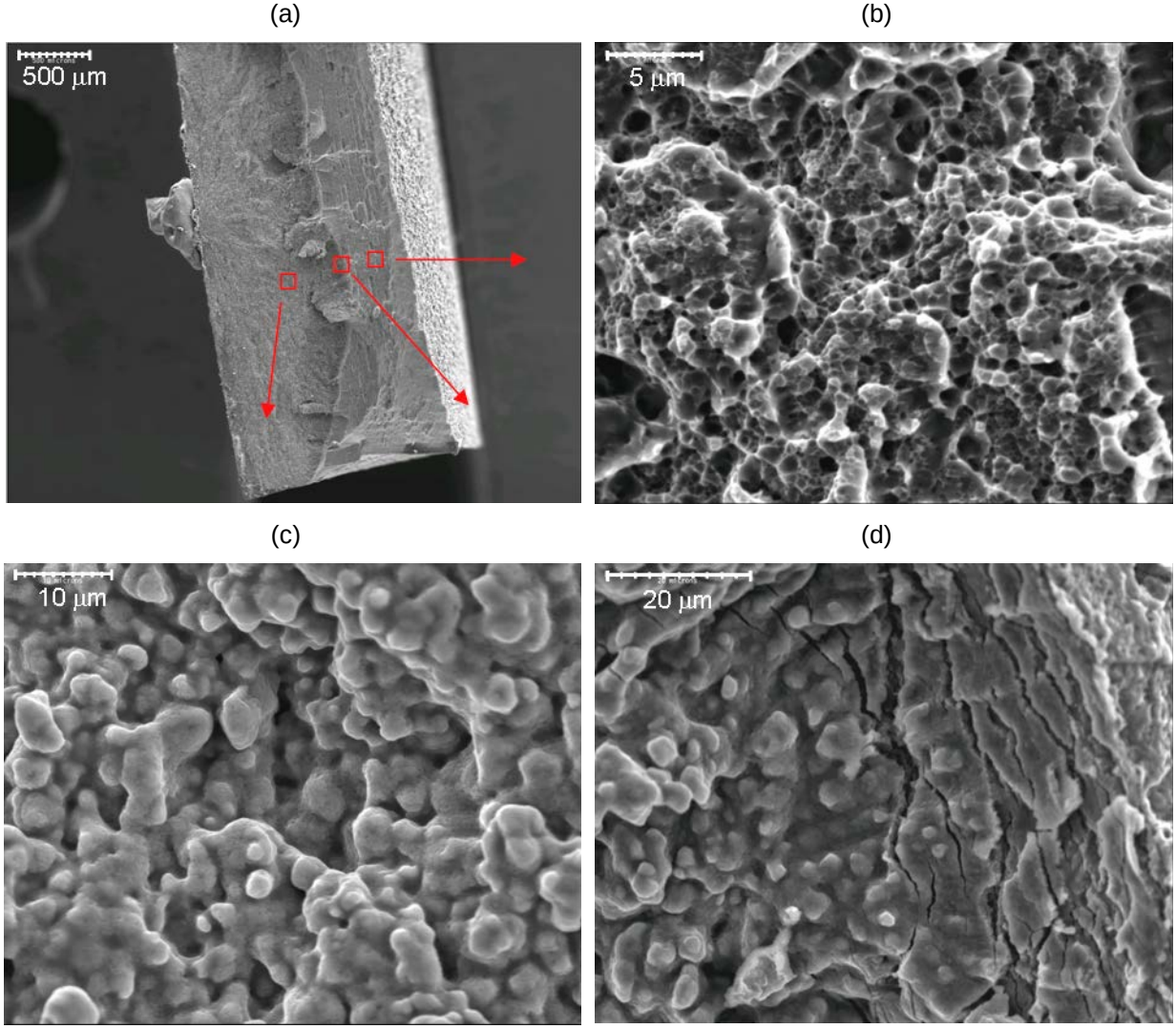

Figure III.16. SEM micrographs of the different zones of the fracture surface (a): (b) dimpled surface after room temperature deformation, (c) surface in contact with liquid zinc and (d) interface between the two previous zones

The embrittling effect of liquid zinc on the Fe22Mn0.6C steel is clearly during tensile test performed at 800°C with a strain rate of $1.3.10^{-1}$ s^{-1}. In the presence of liquid zinc, the fracture elongation as well as the fracture strength is drastically reduced. The original fracture surface is not easily observable since it has been covered by zinc.

III. Influence of temperature

Figure III.17 reports the true tensile curves obtained for bare and EG specimens at different temperatures with a constant strain rate of $1.3.10^{-1}$ s^{-1}.

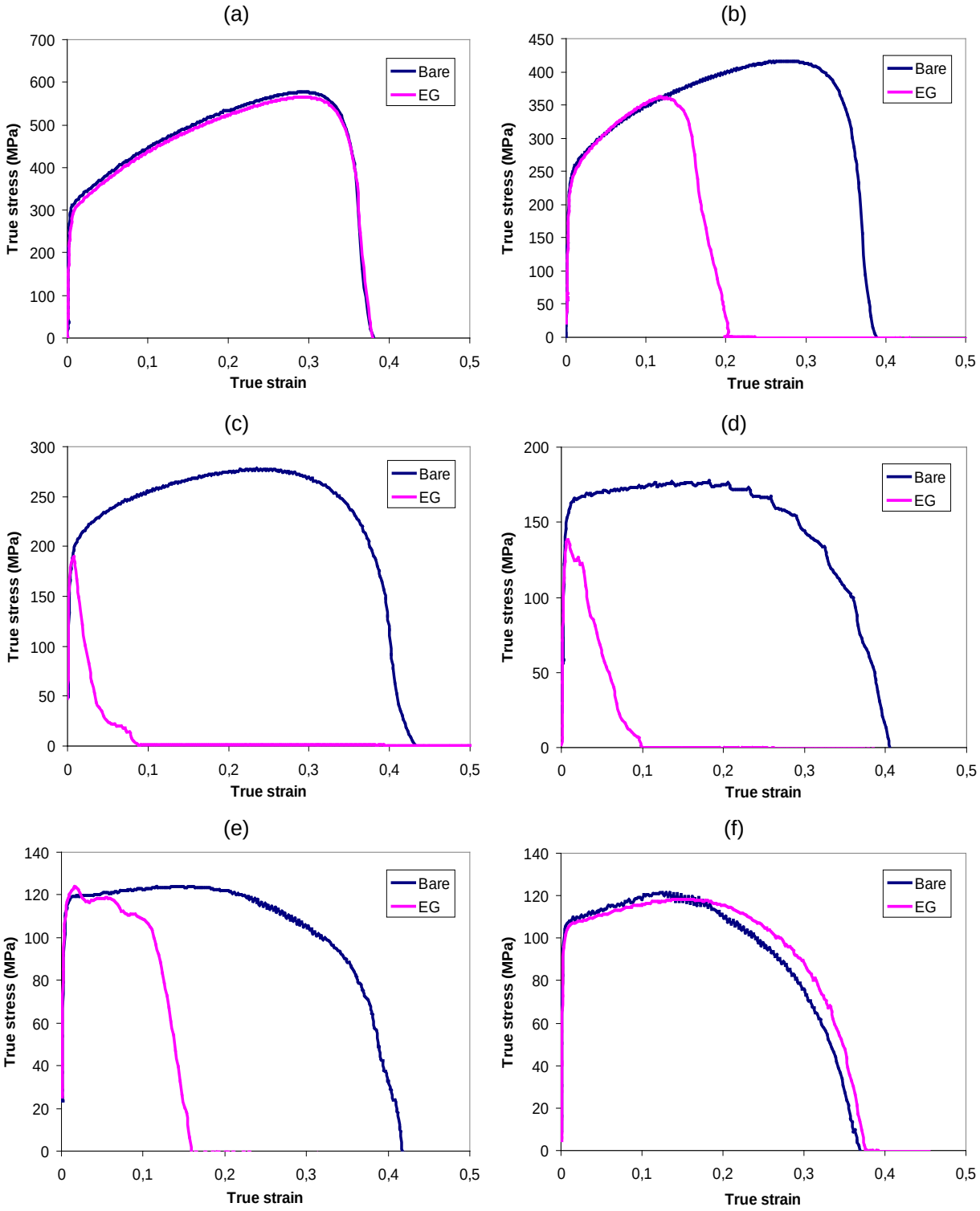

Figure III.17. Influence of temperature on LME for a strain rate of $1.3.10^{-1}$ s^{-1}: (a) 600°C, (b) 700°C, (c) 800°C, (d) 900°C, (e) 950°C and (f) 1000°C

It is clear that no LME occurs up to 600°C since there is no noticeable difference in the mechanical behaviour of bare and EG specimens (figure III.17 (a)).
However, the embrittling effect of liquid zinc is clearly evidenced between 700°C and 950°C (figures III.17 (b)-(e)). Within this limited temperature range, elongation to fracture and fracture strength are drastically reduced by the presence of liquid zinc at the specimen surface. Ductility is progressively recovered with increasing testing temperature up to 1000°C where no difference between bare and EG results can be noticed anymore (figure III.17 (f)).

It is important to point out that the presence of liquid zinc does not modify the elastic and plastic behaviour of the steel until the premature fracture which is characteristic of LME phenomenon (see Chapter I §III.1.1).

The severity of the embrittlement is clearly observed by plotting the fracture energy ($=\int\sigma d\varepsilon$) in tension as a function of testing temperature as shown in figure III.18 (a), each point being an average of several measurements. The error bars indicate the measurement scattering between individual specimens estimated to be about 10%.

It is clear that bare specimens exhibit a gradual decrease of energy to fracture with increasing testing temperature because of the strong decrease of the strength and the non evolution of the ductility of the material.
EG specimens undergo an important embrittlement between 700 and 950°C whereas for lower temperatures the results obtained with EG and bare specimens almost coincide. The energy obtained for EG specimens over this finite temperature range is considerably decreased compared to bare specimens. This is the result of the drastic reduction of elongation to fracture and fracture strength during the tensile test as observed in figure III.17 (c) and (d). At 850°C, embrittlement is so severe that fracture of EG specimens occurs within macroscopic elastic behaviour which indicates that no macroscopic plastic deformation is necessary to initiate embrittlement. Ductility recovery at 1000°C is clearly shown.
This “ductility trough” representation is commonly observed in LME studies and has previously been reported for many systems (see chapter I §III.3.2). It is worth noticing that the lower temperature of the “ductility trough”, 700°C in this case, is well higher than the zinc melting point (419°C) while, in many systems, this lower temperature corresponds to the melting point of the embrittling metal. This could be linked to the experimental procedure: the

specimen is not immersed in liquid zinc and its contact with the latter is due to the melting of the zinc coating during heating.

Also, the ductility recovery temperature is higher than 907°C, the zinc boiling point. Hence, this recovery of mechanical properties could be attributed to the vaporization of liquid Zn leading to a decrease of available liquid Zn to promote embrittlement.

The "ductility trough" is clearly evidenced in the figure III.18 (b) where the relative reduction of fracture energies ($(E_{bare}-E_{EG})/E_{bare}x100$) is plotted as a function of testing temperature. If the reduction of energy is upper than 10%, one can consider that LME occurs. The influence of different parameters can be described by the severity of embrittlement (depth of the ductility trough) or the domain of embrittlement (width of the ductility trough) and particularly the lower limit of the ductility trough.

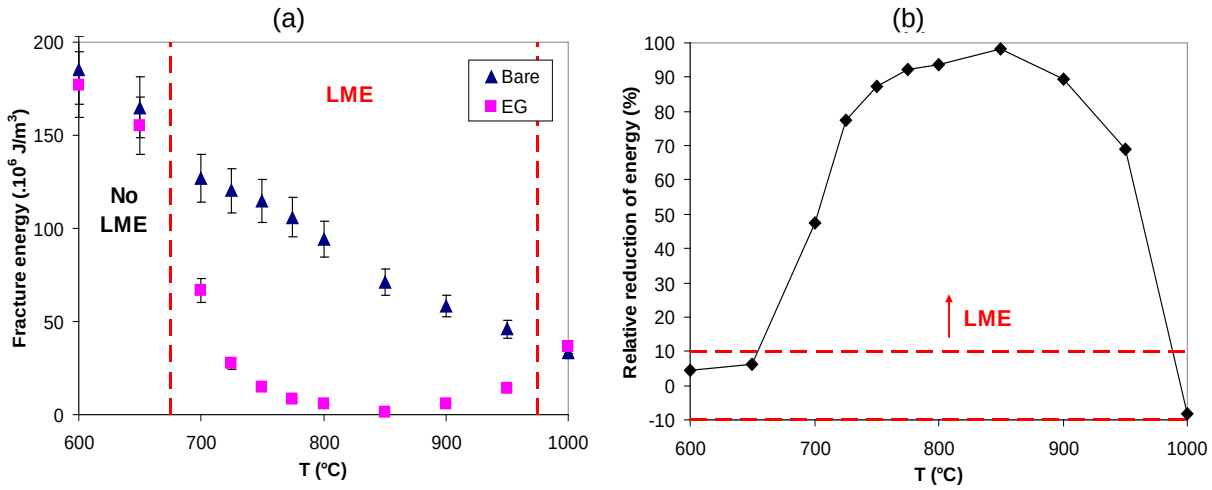

Figure III.18. Severity embrittlement for a strain rate of $1.3.10^{-1}$ s^{-1}: (a) fracture energy as a function of testing temperature, (b) relative reduction of fracture energies

It appears that LME occurs within a finite temperature range between 700°C and 950°C. The ductility is progressively reduced until 850°C where the embrittlement is maximal. Then, the ductility is progressively recovered until 1000°C where no embrittlement occurs. This ductility trough is clearly seen when plotting the relative reduction of fracture energy against temperature.

IV. Influence of strain rate

The effect of strain rate on embrittlement has been investigated for different testing temperatures.

Tensile curves obtained at 800°C for different strain rates are shown in figure III.19. The mechanical response of the EG specimen tested at $1.3.10^{-3}$ s^{-1} does not differ from the bare one i.e. liquid zinc has no detrimental effect for these testing conditions. However, embrittlement of EG specimens for higher strain rates is clearly demonstrated.

No clear effect of strain rate is observed on the elongation to fracture of EG specimens. However, it has an apparent effect on the critical stress as detailed below and also on the time to rupture. The latter logically decreases with increasing strain rate. This effect is detailed in the following chapter.

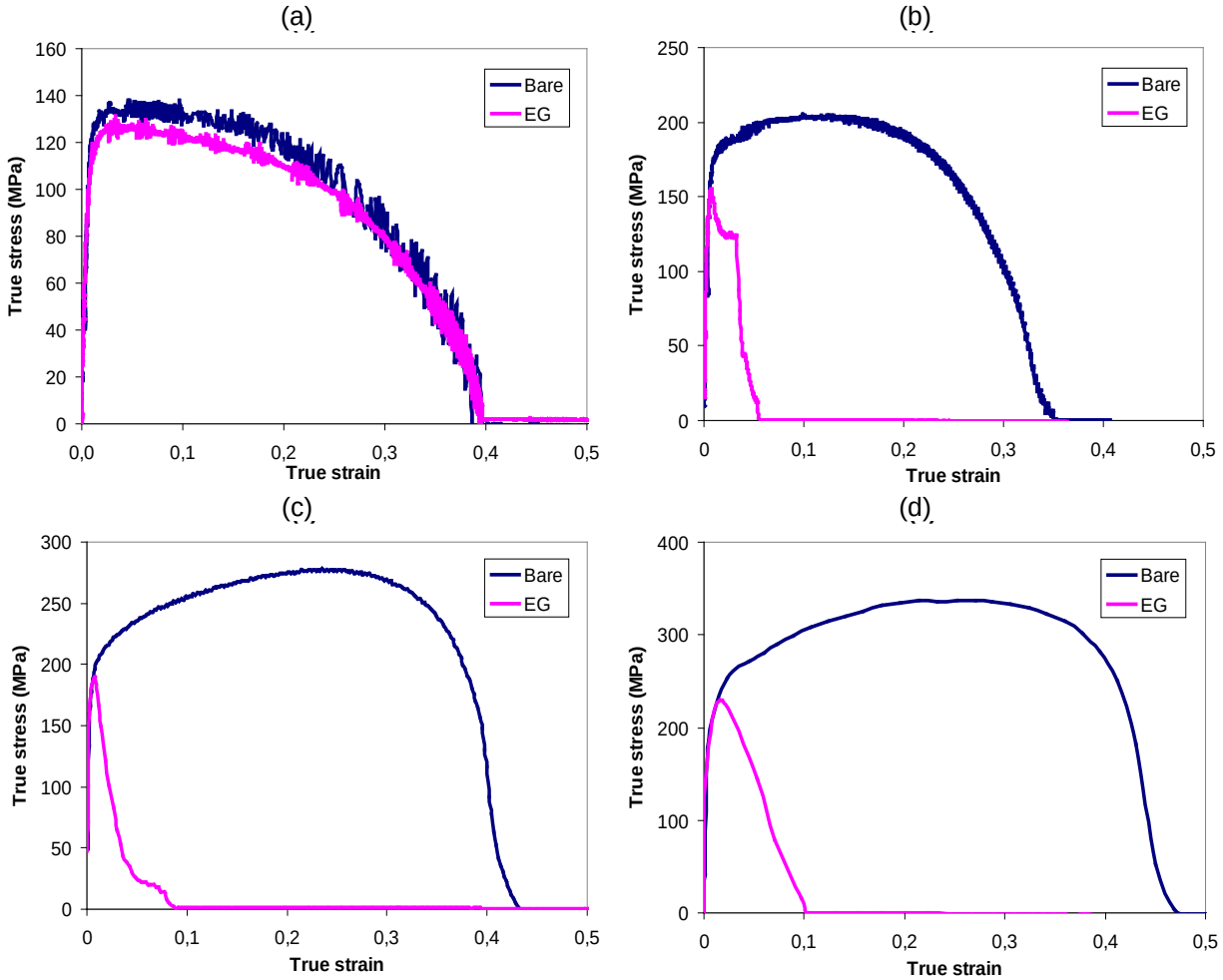

Figure III.19. Influence of strain rate on LME at 800°C: (a) $1.3.10^{-3}$ s^{-1}, (b) $1.3.10^{-2}$ s^{-1}, (c) $1.3.10^{-1}$ s^{-1}, (d) 1.3 s^{-1}

Figure III.20 presents the relative reduction of fracture energies as a function of the testing temperature for the four strain rates.

For a strain rate of $1.3.10^{-3}$ s^{-1} and for all tested temperatures, no significant difference is noticeable between mechanical behaviour of EG and bare specimens resulting in the same fracture energies (the relative reduction of energy is within the measurement scattering of 10%). Increasing strain rate to $1.3.10^{-2}$ s^{-1} results in the occurrence of LME between 760°C and 975°C. Embrittlement is the most severe between 800°C and 850°C where the relative reduction of energy is upper than 90%.

It can be observed that increasing strain rate tends to widen the domain of embrittlement: for a strain rate of 1.3 s^{-1}, embrittlement is already observed at 600°C. Besides, when testing temperature is above 950°C, failure does not occur in the center of gauge length but as far as 15mm from it, where temperature is much lower than the testing temperature. As a consequence, values obtained at T≥950°C and $\dot{\varepsilon}$=1.3 s^{-1} have not been reported on graphs and no conclusions can be drawn concerning LME in those conditions.

The severity of embrittlement is similar at $1.3.10^{-2}$ s^{-1} and $1.3.10^{-1}$ s^{-1}, whereas it is slightly lower at higher strain rates.

The widening of the temperature range of brittleness with increasing strain rate is often reported in literature (see Chapter I, §III.3.6). This is generally explained by an easier plastic flow at low strain rate resulting in a better strain accommodation.

The absence of LME at lower strain rate indicates that the studied steel is sensitive to liquid zinc embrittlement only when appropriate testing conditions are gathered and confirms that the occurrence of LME strongly depends on testing conditions and experimental procedures as reported by Fernandes and Jones [FER 96a]. Moreover, decreasing strain rate results in increasing the time of contact between the substrate and liquid zinc. This is of great importance as described in the next chapter (Chapter IV - §II).

One can imagine that embrittlement tends to disappear for higher strain rates due to a too slow liquid zinc penetration and embrittlement kinetics compared to the tensile load duration.

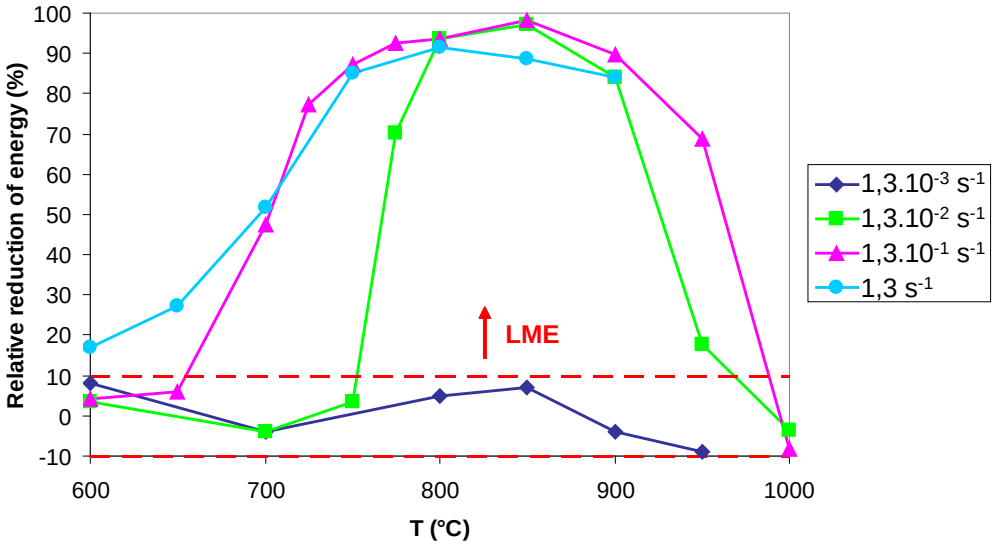

Figure III.20. Effect of strain rate on embrittlement

No LME is observed at the lowest strain rate of $1.3.10^{-3}$ s^{-1}. Increasing strain rate tends to widen the ductility trough to low temperatures.

V. Criterion of occurrence of LME

Conditions of temperature and strain rate leading to LME have been determined. However, in order to predict the cracking during welding simulation in a finite element model for example, it must be precisely determined when cracking occurs. Thus, a stress criterion is proposed.

For each temperature, a critical stress corresponding to the maximal stress achieved during the tensile testing of EG specimens in embrittlement conditions has been determined as described in chapter II. This stress can be considered as the stress required for cracking to occur.

The choice of stress instead of elongation at rupture is motivated by the fact that as soon as cracking initiates, the temperature distribution in the specimen is modified and not necessarily homogeneous due to the Joule effect. Consequently, the end of the tensile curve can be modified.

Firstly, the reproducibility of this parameter has been checked. Figure III.21 displays tensile curves obtained with EG specimens tested in the same conditions. For each condition, it is clearly seen that the critical stress is very similar for all specimens. Hence, the choice of the critical stress is relevant.

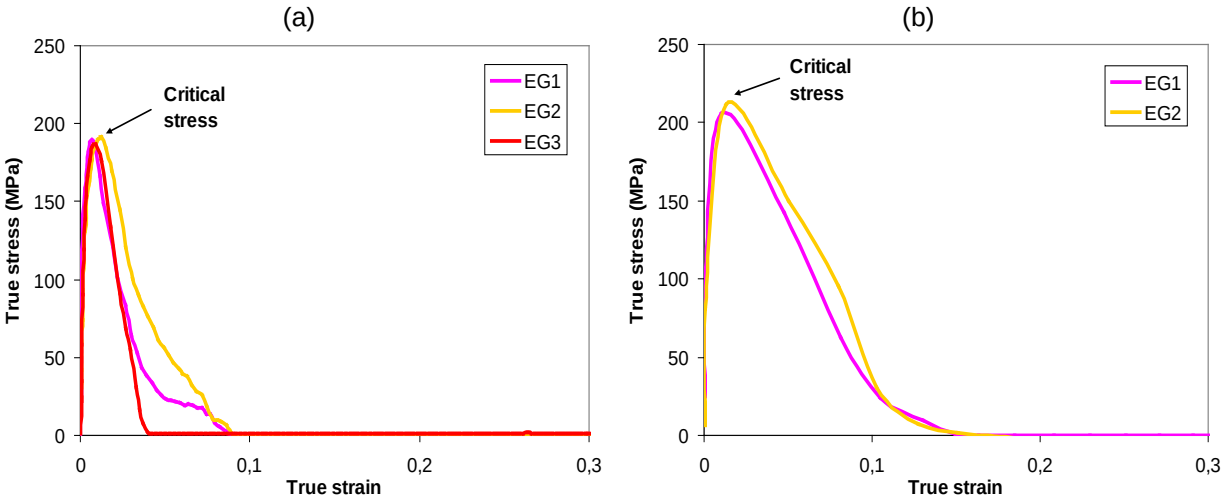

Figure IV.21. Tensile curves obtained on EG specimens in embrittlement conditions: (a) 800°C and $1.3.10^{-1}$ s^{-1} and (b) 850°C and 1.3 s^{-1}

Figure III.22 reports the evolution of the critical stress as a function of testing temperature for a strain rate of $1.3.10^{-1}$ s^{-1}. Globally, the critical stress tends to increase with decreasing temperature.

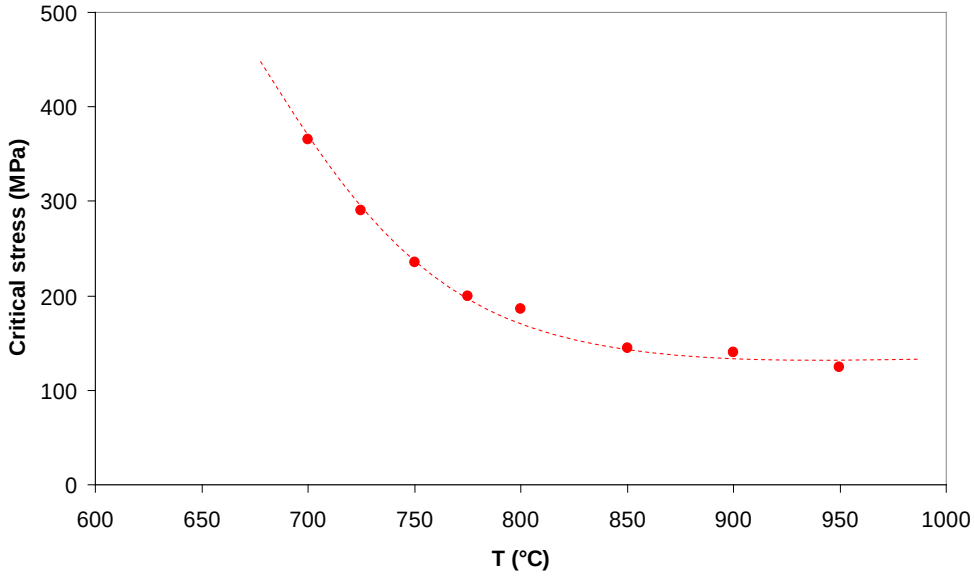

Figure IV.22. Evolution of the critical stress with temperature for a strain rate of $1.3.10^{-1}$ s^{-1}

The critical stress can be compared to the mechanical properties (the flow stresses at 1% and 5% of plastic deformation as well as the ultimate tensile strength (UTS)) of bare material in figure III.23.

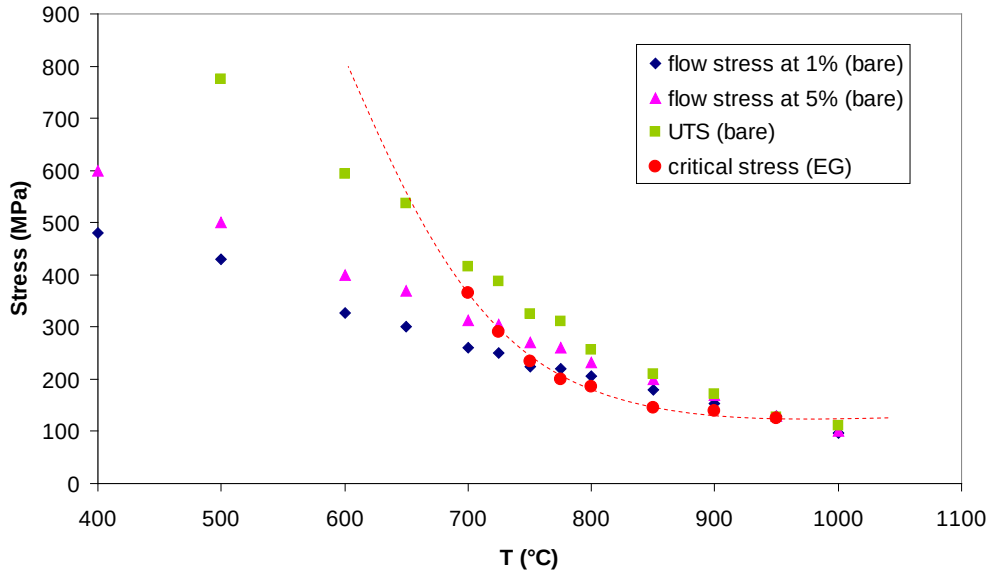

Figure III.23. Evolution of the critical stress and mechanical properties with temperature for a strain rate of $1.3.10^{-1}$ s^{-1}

For T>950°C, the trend curve indicates that critical stress could be higher than the UTS. This can explain the absence of LME for high temperatures. It is also important to point out, as mentioned above, that the zinc boiling point is 907°C. One can reasonably imagine that for higher temperatures, the quantity of liquid zinc is not sufficient for embrittlement.

For temperatures between 775°C and 900°C, cracking occurs before 1% of plastic strain. This is the domain where zinc has the most detrimental effect because the critical stress is quite low as compared to the mechanical strength of the material. For lower temperatures until 700°C, critical stress increases more rapidly than the mechanical strength so that cracking occurs after a varying amount of plastic deformation depending on testing temperature.

For temperature below 700°C, the critical stress seems to sharply increase. Indeed, the trend curve indicates that for T<650°C, the critical stress should be higher than the UTS. This means that the critical stress will never be achieved during a tensile test in these conditions of temperature and strain rate. Hence, LME can not be evidenced for T<650°C in these testing conditions. This does not imply that the studied steel will never undergo liquid zinc embrittlement for T<650°C. Indeed, as previously described, the level of tensile stress can be increased by increasing strain rate, thus, modifying testing conditions and particularly the strain rate leads to changes in LME occurrence.

The critical stress has been determined for different strain rates. Figure III.24 presents the evolution of mechanical properties and critical stress with temperature for different strain rates.

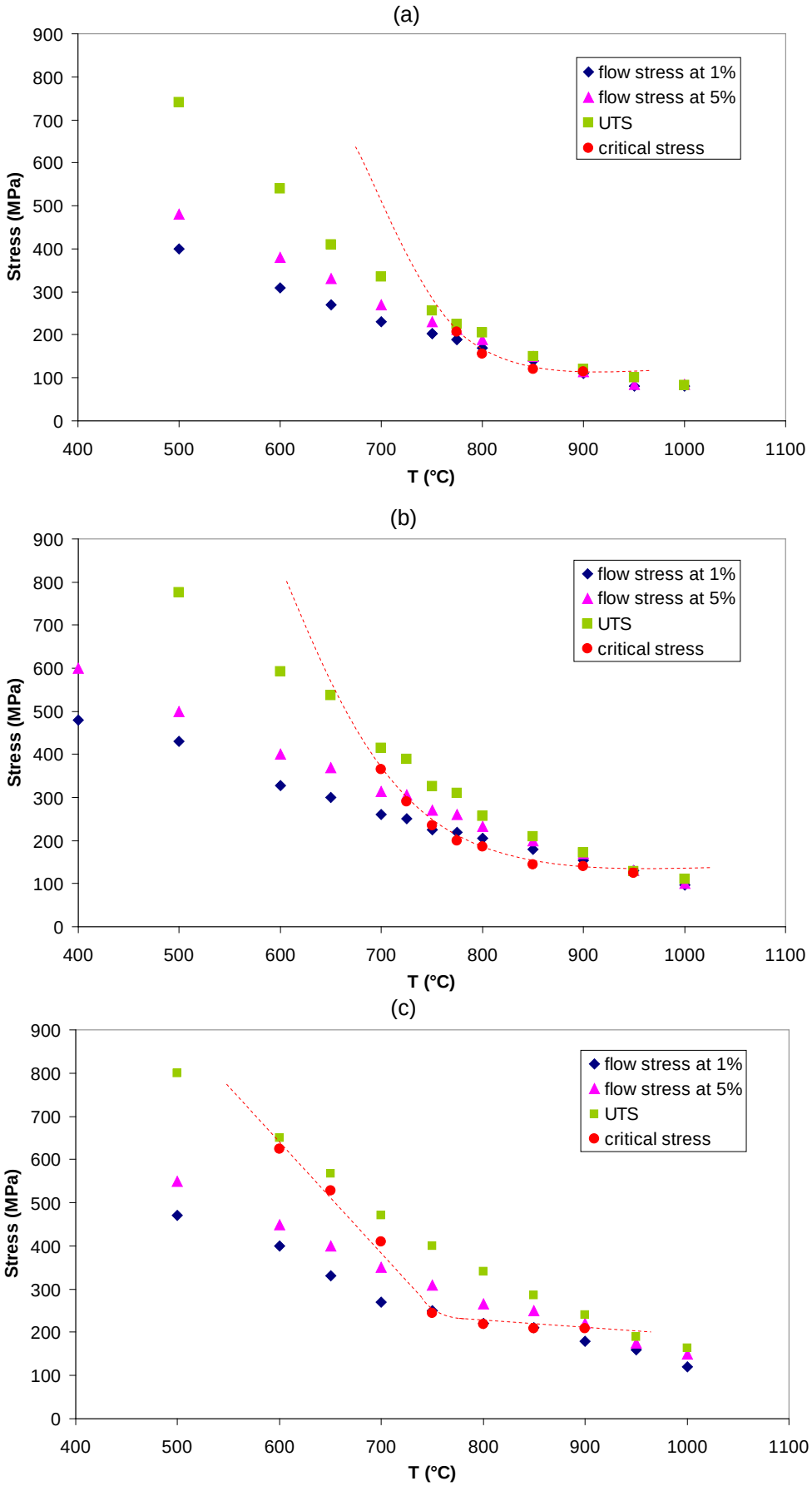

Figure III.24. Evolution of the critical stress and mechanical properties with temperature for different strain rates: (a) $1.3.10^{-2}$ s^{-1}, (b) $1.3.10^{-1}$ s^{-1}, (c) 1.3 s^{-1}

It can be observed that the critical stress increases with decreasing temperatures for the three strain rates considered. However, increasing strain rate permits to increase the level of tensile stress, consequently, tends to increase the risk of reaching the critical stress. Thus, the widening of the ductility trough can be explained by the increase of mechanical strength with strain rate. It is worth reminding that the hardest materials are generally more severely embrittled (see Chapter I, §III.3.4).

Critical stresses corresponding to different experimental conditions are summarized in table III.1. For a given temperature, the critical stress tends to increase with strain rate. For instance, at 800°C, the critical stress is about 160MPa at a strain rate of $1.3.10^{-2}$ s^{-1}, 190MPa at $1.3.10^{-1}$ s^{-1} and 220MPa at 1.3 s^{-1}.
However, for a strain rate of 1.3 s^{-1}, the critical stress is always higher than the flow stress at 1% of plastic strain. The severity of embrittlement is less important than for lower strain rates. Besides, decreasing strain rate results in increasing the time of contact between the solid steel and the liquid zinc. This is of great importance, as explained in next chapter.

σ* (MPa)	$1,3.10^{-2}$ s^{-1}	$1,3.10^{-1}$ s^{-1}	1,3 s^{-1}
600°C	No LME	No LME	600
650°C	No LME	No LME	530
700°C	No LME	365	415
750°C	No LME	235	245
800°C	160	190	220
850°C	120	145	210
900°C	115	140	205
950°C	No LME	125	Fracture outside

Table III.1. Critical stress for different testing conditions

The critical stress is a relevant parameter for predicting the cracking phenomenon in a finite element model. It has been determined for different experimental conditions of temperature and strain rate. From these results, it can be extrapolated for other conditions (intermediate temperatures and strain rates).

VI. Influence of the microstructure

As previously mentioned, as rolled specimens exhibit a microstructure different from the recrystallized ones: defects density is much higher and grains are stretched along the rolling direction. As rolled specimens exhibit higher strength properties to the detriment of ductility (see figure III.8). Hence, testing EG cold rolled specimens should permit to highlight embrittlement at lower temperature in the strain rate range available with the experimental set up.

As grains are stretched along the rolling direction, two types of specimens have been studied: normal to the rolling direction (Transverse Direction TD) and along the rolling direction (Longitudinal Direction LD).

Since for temperature higher than 800°C, cold rolled specimens exhibit the same behaviour as standard specimens due to recrystallization (see figure III.9), embrittlement was investigated for temperatures ranging from 460°C to 700°C.

VI.1. TD specimens

At 460°C, no noticeable difference is seen between mechanical behaviour of bare and EG specimens. For higher temperature, embrittlement is observed. It is worth noticing that cracking occurs for higher strains than in the case of recrystallized specimens. Indeed, as illustrated in figure III.25 (a), cracking occurs within the macroscopic plastic deformation after UTS has been reached. It is important to notice that the microstructure probably evolves during hot tensile test.

As previously mentioned in §I.1.2, cold rolled specimens and particularly EG ones break slantwise as shown in figure III.25 (b). The extensometer does not always manage to correctly measure the end of deformation just before rupture. When this happens, tensile curves are extrapolated in order to measure the fracture energy.

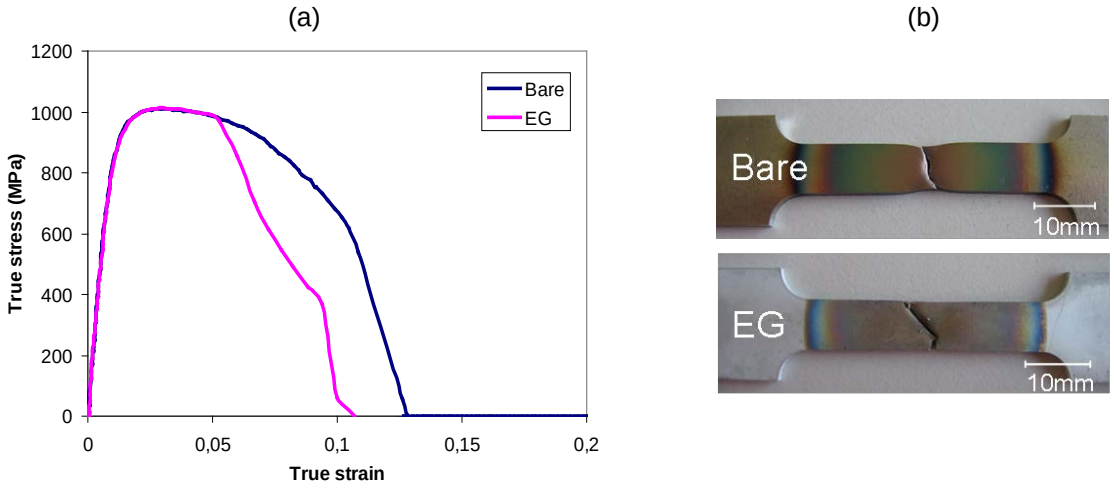

Figure III.25. (a) True tensile curve at 550°C for a strain rate of $1.3.10^{-1}$ s^{-1}: bare and EG as rolled specimens, (b) specimens after tensile test

The ductility trough obtained with cold rolled specimens can be compared to the one obtained with recrystallized specimens in figure III.26. The width of the ductility trough obtained with cold rolled specimens is larger. Indeed, embrittlement is observed from 550°C for cold rolled specimens instead of 700°C for recrystallized ones. Moreover, at 700°C, energy loss is more important in cold rolled specimens (~65%) than in standard ones (~45%). At 800°C, the embrittlement is similar, which is logical since at this temperature, recrystallization occurs in cold rolled specimens.

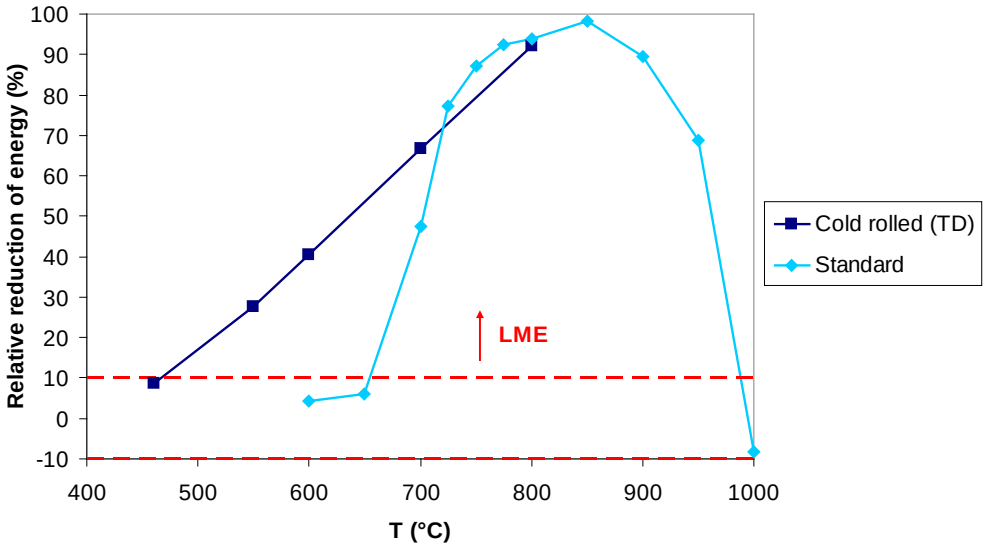

Figure III.26. Comparison of embrittlement between cold rolled and recrystallized specimens at a strain rate of $1.3.10^{-1}$ s^{-1}

Critical stresses have been determined for as rolled TD specimens. From figure III.27, it is seen that for lower temperatures, critical stresses obtained with as rolled specimens are much higher than the UTS of recrystallized specimens. For instance, at 600°C, the critical stress of as rolled specimen is 900MPa while the UTS of recrystallized specimen is about 600MPa. However, at 700°C, both as rolled and recrystallized specimens are embrittled but the critical stresses are quite different. At 800°C, cold rolled specimens exhibit the same behaviour as standard specimens due to recrystallization and as a consequence, the critical stress is identical to the one obtained on standard specimens. This shows that the microstructure is a key parameter in the embrittlement phenomenon.

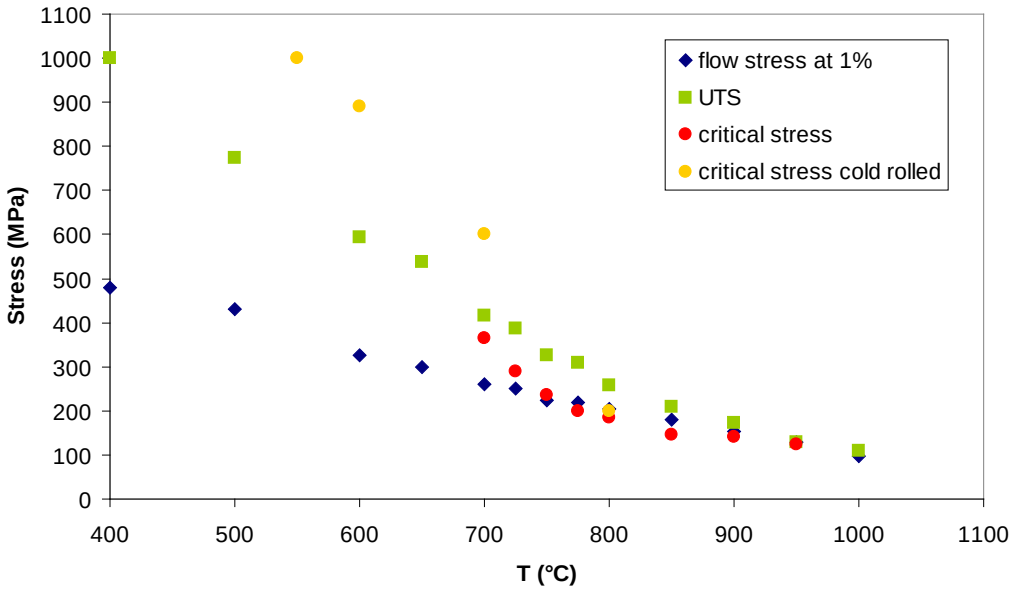

Figure III.27. Comparison of the critical stress of cold rolled and recrystallized specimens with temperature for a strain rate of $1.3.10^{-1}$ s^{-1}

VI.2. Comparison between TD and LD specimens

In order to investigate the influence of grains shape on LME phenomenon, hot tensile tests have been performed on longitudinal direction (LD) specimens.

For T<700°C, no embrittlement is observed on LD specimens meanwhile TD specimens are embrittled from 550°C. Figure III.28 displays the tensile curves obtained at 600°C with (a) LD and (b) TD specimens. It is clearly seen that in those conditions, the LD specimens do not undergo embrittlement by liquid zinc. These results emphasize the influence of microstructure on the LME phenomenon.

However, it must be noticed that stresses reached during tensile tests are different according to the direction of specimens. Indeed, stresses achieved in LD specimens are lower than in TD

specimens (800MPa for LD instead of 930MPa for TD at 600°C). Hence, one can imagine that stresses achieved during tensile tests in LD specimens are not sufficient to initiate cracking.

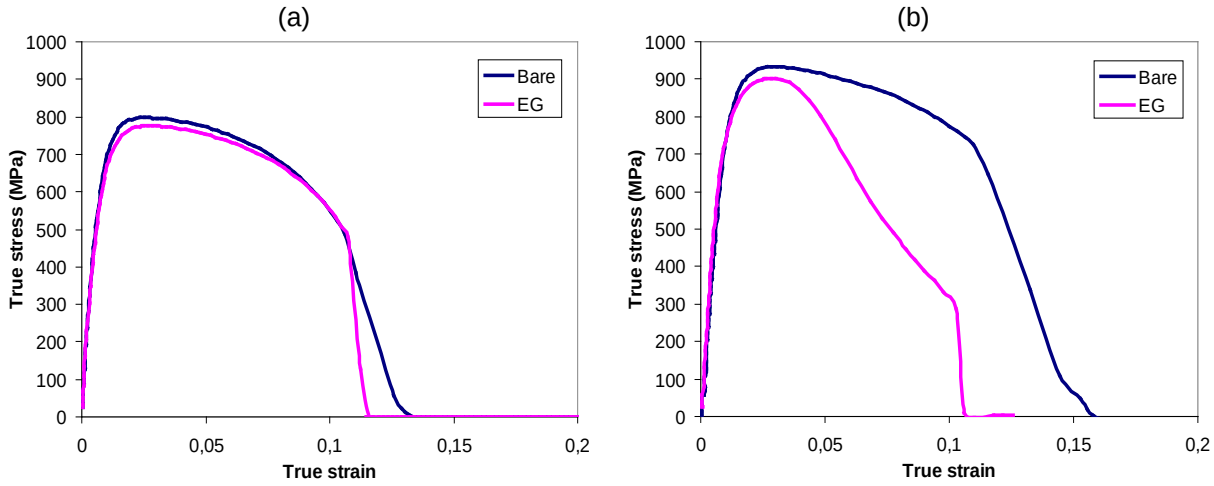

Figure III.28. True tensile curves at 600°C for a strain rate of $1.3.10^{-1}$ s^{-1}: (a) LD and (b) TD specimens

The embrittlement obtained with the different specimens is shown in figure III.29. The cold rolled TD specimens are the most severely embrittled while the LD specimens are less embrittled. The standard specimens exhibit an intermediate behaviour.

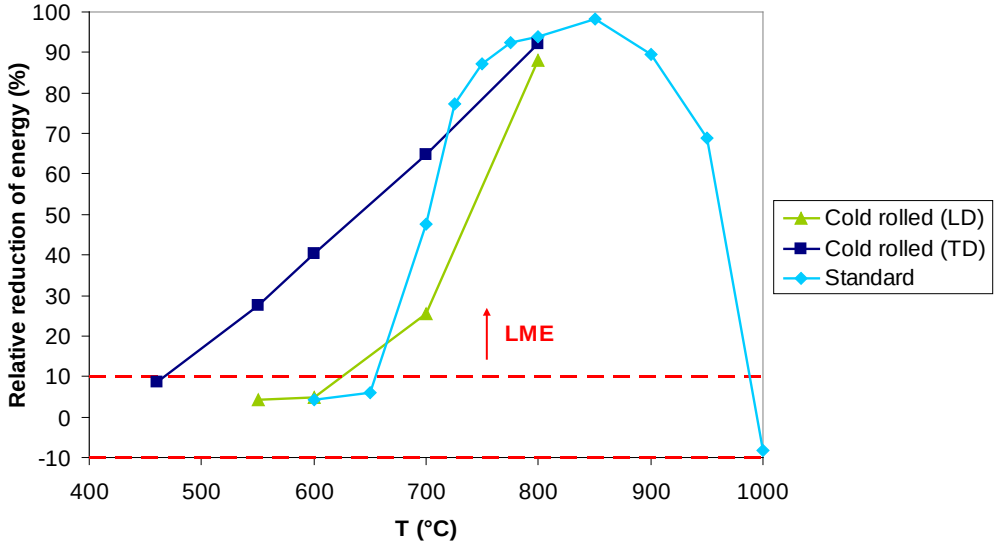

Figure III.29. Comparison of embrittlement between cold rolled longitudinal (LD) and transverse (TD) directions and recrystallized specimens at a strain rate of $1,3.10^{-1}$ s^{-1}

The behaviour of cold rolled (LD and TD) and standard specimens at 700°C can be compared in figure III.30. It can be seen that the three specimens are embrittled but in a different way. In cold rolled specimens (figure III.30 (a) and (b)), cracking occurs after the UTS has been reached while in recrystallized ones (figure III.30 (c)), it takes place during strain hardening. Moreover, it can be noticed that the critical stress is different in each case: 440MPa for the LD cold rolled specimen, 520MPa for the TD cold rolled specimen and 360MPa for the standard one.

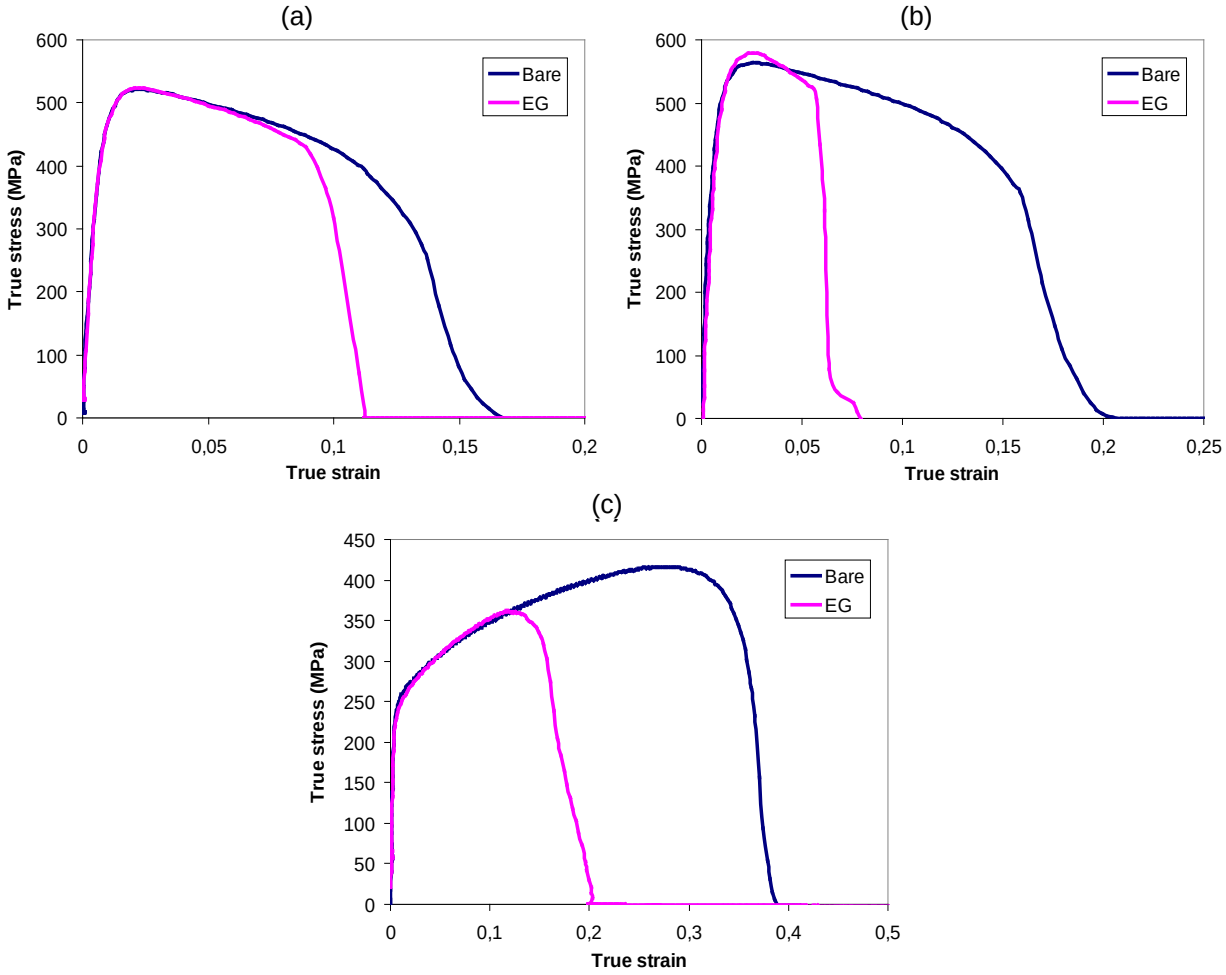

Figure III.30. True tensile curves at 700°C for a strain rate of $1.3.10^{-1}$ s^{-1}: (a) cold rolled LD, (b) cold rolled TD and (c) recrystallized specimens

VI.3. Conclusions

Even if comparison must be done with caution because microstructure is different, results obtained on cold rolled specimens taken perpendicularly to rolling direction prove that embrittlement can be observed at lower temperatures (between 550 and 700°C) provided very

high stresses are reached. Indeed, cold rolled specimens exhibit very high strength. This confirms the hypothesis of a threshold stress necessary for initiating cracking. Nevertheless, the critical stress depends on microstructure (see figure III.30 at 700°C).

The hot tensile tests show that the Fe22Mn0.6C steel is sensitive to the liquid zinc embrittlement. But, the embrittlement actually occurs only when appropriate conditions are gathered. It has been shown that temperature, strain rate and stress are key parameters in the embrittlement phenomenon. Results obtained with cold rolled specimens show that the microstructure is also an important parameter.

VII. Residual stresses

As said above, embrittlement by liquid zinc can occur at low temperature provided sufficient stresses are reached in the specimen. Hot tensile tests were not conclusive for evidencing LME at temperature below 550°C. From the evolution of the critical stress with decreasing temperature, one can think that at lower temperatures, stress level necessary for initiating cracking is very high and is not reached during tensile tests. Cups containing very high residual stresses (upper than 1000MPa) were then considered. The contact with liquid zinc arises from the immersion of the cup in the liquid zinc bath. Before immersion, specimen's surface is prepared according to the protocol detailed in chapter II, §II.2.

VII.1. Description of cracking

When a cup is immersed in the liquid zinc bath, cracking occurs quasi instantaneously. Sounds characteristic of crack initiation and propagation can be heard during the first seconds in liquid zinc. After immersion, many cracks are visible on the cup as illustrated in figure III.31. Immersion time does not seem to have any influence on cracking phenomenon since cracks appear very fast. Indeed, a cup immersed only 10 seconds at 460°C presents as many cracks as a cup immersed 10 minutes at the same temperature. Moreover, cracks lengths are similar for the two cups.

Cracking was observed for temperatures between 440°C and 720°C. No tests at higher temperatures have been performed. Bath temperature does not have any effect on cracks length but might have an influence on number of cracks (number of cracks tends to decrease and cracks are larger with increasing bath temperature).

It is worth noticing that the bath composition (pure zinc or Zn+0,2%Al+0,02%Fe) has no influence on cracking since no difference in terms of number of cracks, cracks length and cracking kinetics has been noticed.

Figure III.31. Cup after immersion in the liquid zinc bath at 470°C during 7 minutes

In order to check that cracking is not caused by thermal shock but by the presence of liquid zinc, a cup has been immersed in a molten salts bath at 515°C during 1 minute. No crack has been observed in the cup. Hence, the presence of liquid zinc is essential to initiate cracks.
Not only is liquid zinc necessary for cracking to occur, but wettability is also a very important parameter in cracking initiation. Indeed, a non fluxed cup immersed at 470°C during 7 minutes in the zinc bath, is not coated and does not exhibit any crack.

VII.2. Determination of critical stress

By immersing cups in liquid zinc bath, it has been proven that cracking can occur for temperature as low as 440°C. The point is now to evaluate the critical stress at this temperature.
Firstly, a cup, heat treated in the molten salts bath at 515°C during 1 minute has been then fluxed and immersed in the zinc bath at 480°C during 7 minutes. No crack can be detected in the cup. A heat treatment of 1 minute at 515°C seems to be sufficient to relieve stresses at a level lower than the one necessary for cracking. The cracking phenomenon appears to be a competition between stress relieving caused by elevated temperature of bath and liquid zinc penetration.
The previous result shows that a threshold stress must be achieved to initiate cracking phenomenon. As residual stresses vary along the cup's wall, the critical stress can be estimated.

According to the FEM calculation in 75mm diameter cup [DIE 09], hoop stresses are maximal at the rim and at approximately 20mm from it, while axial stresses are maximal at approximately 20mm from the rim. The idea is to immerse cups until this limit (from the bottom and from the top) in order to determine if cracks initiate in this zone and to observe the way they propagate. Immersing the cup slantwise permits to determine the minimal immersion height necessary to create cracks.
Two fluxed cups have been partially immersed in the zinc bath at 480°C during 2 minutes.

- For the first one, only the outer surface is immersed from the bottom to a varying height as shown in figure III.32.

Figure III.32. Cups partially immersed from the bottom in the liquid zinc bath at 480°C during 2 minutes

Two large cracks are observed on the almost entirely coated zone as shown in figure III.33 (a). They propagate until the cup rim. The two cracks are covered by zinc even in the not immersed part which reveals that zinc has propagated by capillarity. Numerous cracks are observed in the zone where zinc height is upper than 2 cm as shown in figure III.33 (b). These cracks have not propagated until the cup rim. However, zinc has been detected in the inner surface so that it went through the whole cup's thickness. The absence of cracks in zones hardly immersed (zones where stresses are very low) confirm that high stresses are necessary to initiate cracks. Moreover, cracks seem to initiate in the zone experiencing a biaxial stress state.

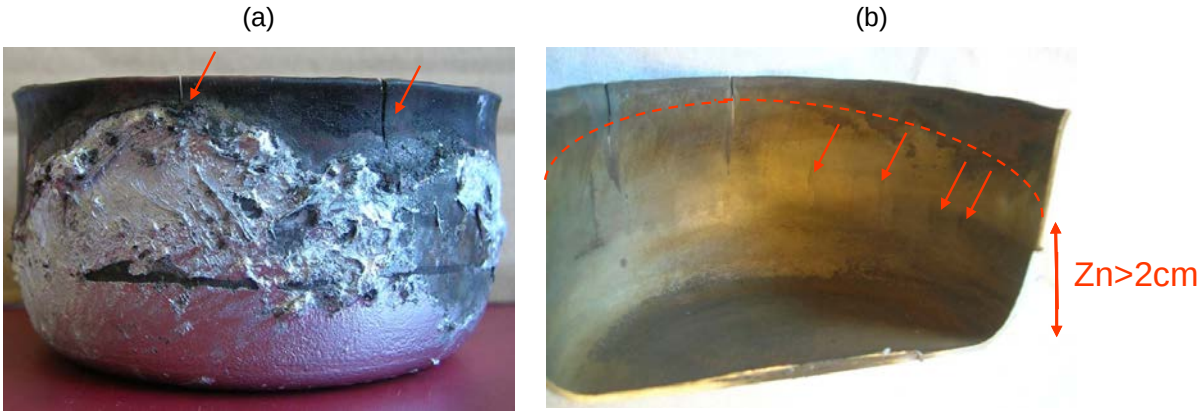

Figure III.33. Cracks observed in a cup partially immersed at 480°C during 2 minutes

- The second one is immersed from the rim to a varying height as shown in figure III.34. Numerous cracks are observed in the immersed part even in the least coated zone. Crack length varies with the zinc height. It appears that cracks propagate where zinc is present in the surface and they stop as soon as surface is not in contact with zinc. However, in some cups, cracks propagate in the zone not immersed, zinc propagating in the crack by capillarity.
As illustrated in figure III.35 (a), at the cup rim, hoop stresses are maximum (upper than 1000MPa), while radial stresses are very low. One can conclude that a biaxial stress state is not necessarily required for cracking. But in that case, hoop stresses upper than 800MPa seem essential to initiate cracks.

Figure III.34. Cups partially immersed from the rim in the liquid zinc bath at 480°C during 2 minutes

Same tests have been performed with 33mm diameter, β 1,6 cups. The stress distribution is different in these cups as illustrated figure 35 (b). At approximately 10mm from the rim, hoop stresses are very low compared to axial stresses. And at the rim, axial stresses are nil while hoop ones are maximum.
When the cup is immersed during 4 minutes at 460°C from bottom, no crack is observed.

However, when it is immersed from the top during 4 minutes at 460°C, numerous cracks are present on the whole circumference. One can deduce that circumferential stress of 800MPa is sufficient to create cracks and axial stresses are not involved in the cracking phenomenon.

These results show that the steel is sensitive to liquid zinc embrittlement provided a threshold stress is reached. The latter, estimated from numerical simulations, is about 800MPa at 480°C. This is coherent with hot tensile tests results. The UTS of the material is around 800 MPa at this temperature (depending on strain rate). One can think that this stress is not reached during tensile test which explains the absence of LME at this temperature.

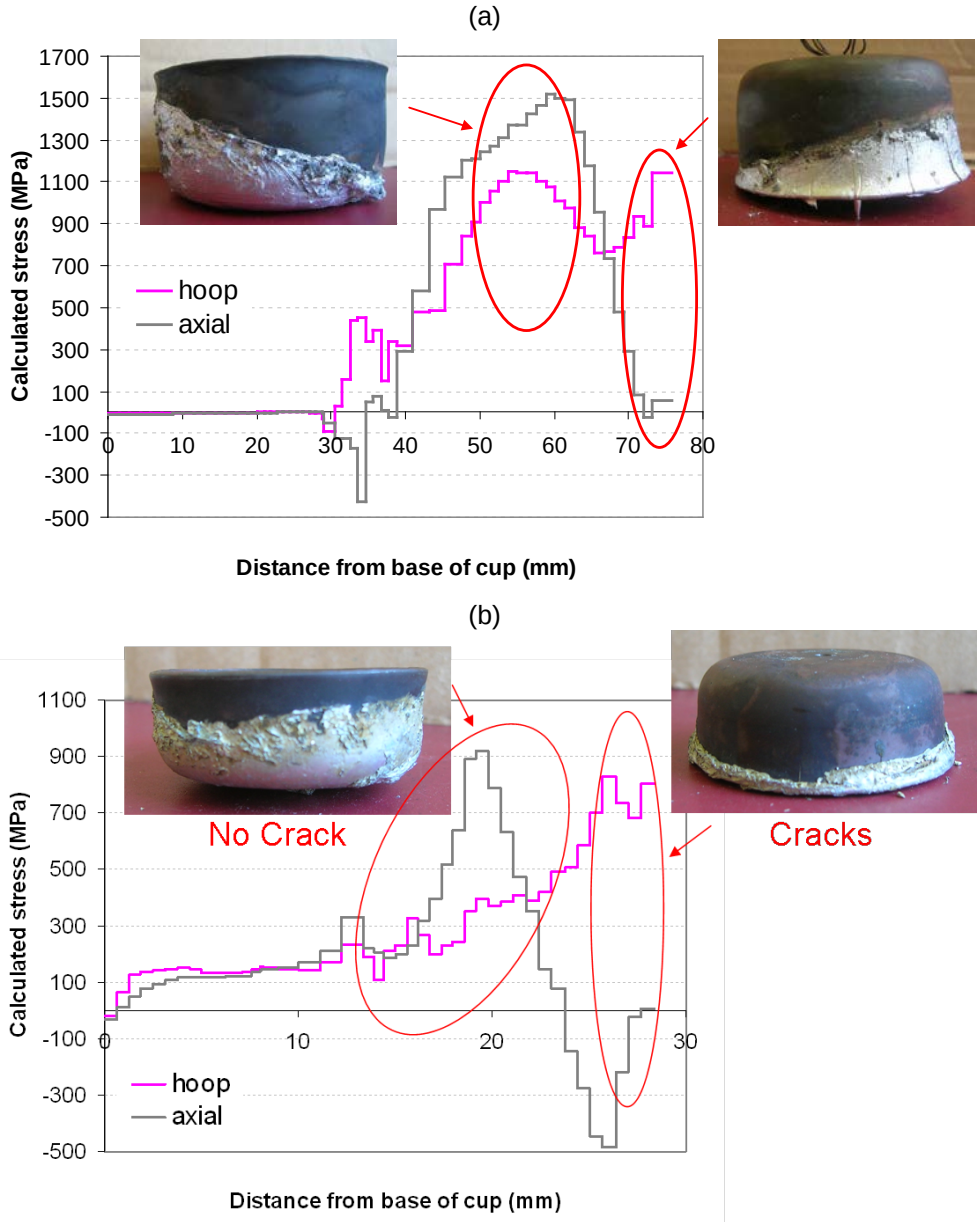

Figure III.35. Comparison of cracking behaviour for (a) 75mm diameter β 1,8 and (b) 33mm diameter β 1,6 depending on immersion conditions

In order to precisely determine the location of crack initiation, a cup was cut by spark machining into twelve parts: 8 rings of 2mm height near the rim (rings 1a, 1b, 2a, 2b … 4b), 3 rings of 5mm height (rings 5, 6 and 7) and the bottom as illustrated in figure III.36 (a). Each ring was fluxed and immersed in liquid zinc at 460°C during 7 minutes. Only rings 1b 2a 2b 3a and 3b opened (figure III.36 (b)).

(a)

(b)

Figure III.36. Cup cut in 12 parts (a) before and (b) after immersion at 460°C

Optical microscopy observations and penetrant inspection do not reveal any other cracks. The existence of only one crack could be explained by the important stress relieving caused by ring opening and temperature in a piece with small dimensions.
One can conclude that critical stress is located at 2-15mm from cup's rim corresponding to hoop stresses higher than 800MPa from numerical simulations.

The circumferential residual stress at the outer surface can be estimated from the ring opening based on Siebel and Mühlhäuser technique [RAG 00], [BER 06].

The circumferential stress is given by the following relation:

$$\sigma_{cir} \cong \frac{E.t}{4\pi}\left(\frac{\delta}{\rho_0^2}\right) \qquad \text{(eq. III.1)}$$

where E is the Young modulus of the metal (174800 MPa at 400°C)

t is the wall thickness (1.5 mm)

δ is the ring opening chord (approximated to a circular arc) given by $\delta = 2\pi.(\rho_1 - \rho_0)$

ρ_0 is the cup mean radius (40.5 mm)

ρ_1 is the ring radius after opening as illustrated in figure III.37 (between 45.7 and 49.5 mm)

The calculated circumferential stresses range from 500 to 700MPa which is a little lower than stresses obtained by numerical simulations (800MPa). Anyway, stress relieving arising from the machining could explain to some extent the difference.

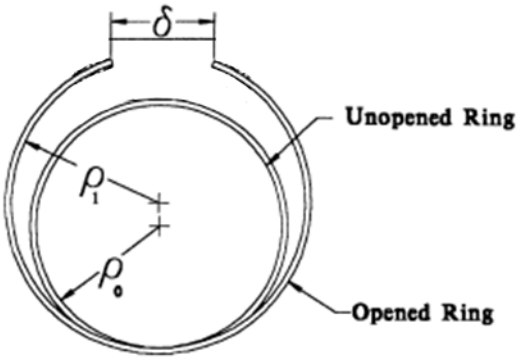

Figure III.37. Change in the ring curvature after opening [RAG 00]

According to the hot tensile tests results, increasing temperature tends to decrease the critical stress. Hence, performing the same test at higher temperature should lead to more cracked rings.

A cup has been cut into 8 parts: 7 rings of 5mm height and the bottom. Each part has been fluxed and immersed in the liquid zinc bath at 820°C during 1 minute. No crack has been observed on any ring. This is probably due to a thermal stress relieving faster than crack initiation.

It is important to point out that stress values have been evaluated by numerical simulations in the initial state. It is clear that immersing the piece in the liquid zinc bath or cutting the cup in rings modify the stress state and causes thermal or mechanical stress relieving. That is why

critical stresses determined from these tests must be considered with caution. They only give a rough approximation of the required stress level.

When a fluxed cup containing high residual stresses is immersed in the liquid zinc bath, cracking occurs quasi instantaneously. Sounds characteristic of crack initiation and propagation can be heard during the first seconds in liquid zinc. In this case, all conditions are gathered for cracking to occur: the presence of high stresses (critical stress of about 800MPa), liquid zinc and a good wettability.

VII.3. Cracks observations

Whatever cup geometry and immersion conditions, periodicity is always observed in cracks distribution. This can be related to stress relieving in the vicinity of a propagating crack.
Crack's lengths never exceed 30mm in a 75mm diameter, β 1.8 cup. It is certainly linked to the stress distribution in cup. At 30mm from rim, circumferential stresses are lower than 500MPa, not sufficient for crack to propagate.

Observation of the section indicates that cracks initiate in the outer surface as shown in figure III.38. This is quite logical since stresses are entirely tensile in the outer surface.

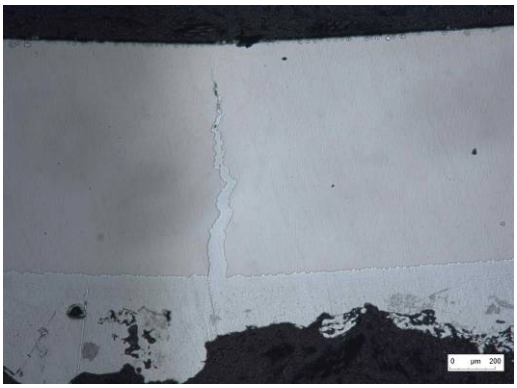

Figure III.38. Optical micrograph of section of cup immersed 7 minutes at 460°C

Figure III.39 shows SEM observations of a crack obtained in a cup immersed 7 minutes at 460°C. Zinc appears lighter than steel. It is clearly seen that zinc fills in the crack in the larger part; however it is more difficult to conclude about the presence of zinc in the crack tip. Indeed, if only a thin Zn film is present in crack, it is not easily observable. Complementary

EDX analyses performed in cracks obtained in different conditions of bath temperature and time immersion reveal the systematic presence of zinc in crack even in the crack tip. Figure III.40 presents the evolution of Fe, Mn and Zn concentrations across crack at the crack tip. Inside the crack, the zinc content is about 30% at.. This means that austenite has been dissolved and Fe-Mn-Zn intermetallic compounds have formed. Microprobe and EDX analyses have been performed along crack for cups immersed in different conditions. Corresponding phases have been determined from the ternary phase diagram (see chapter I, figure I.42). Results show that elements contents (and corresponding phases) vary along crack length. Indeed in crack tip, only Γ and Γ_1 phases (presented in chapter I, § IV.1) are detected while in the middle of crack, δ and ζ phases are identified. It is possible that in the last case, Γ and Γ_1 phases are so thin that can not be detected. However, it appears that in the middle of crack, formed phases are the same as phases formed at the surface of specimen, where zinc quantity is important. This corresponds to what observed by Reumont et al. [REU 95]: when 20-25% Mn alloys are immersed in a pure Zn bath, δ, ζ and η phases are observed. In the case of diffusion heat treatment or phase vapour deposition, namely when less zinc is available, phases formed at the surface of the steel are Γ, Γ_1 and δ phases.

Nevertheless, phases were only identified from chemical analysis and phase diagram. No complementary analyses have been carried out to confirm the exact nature of these phases.

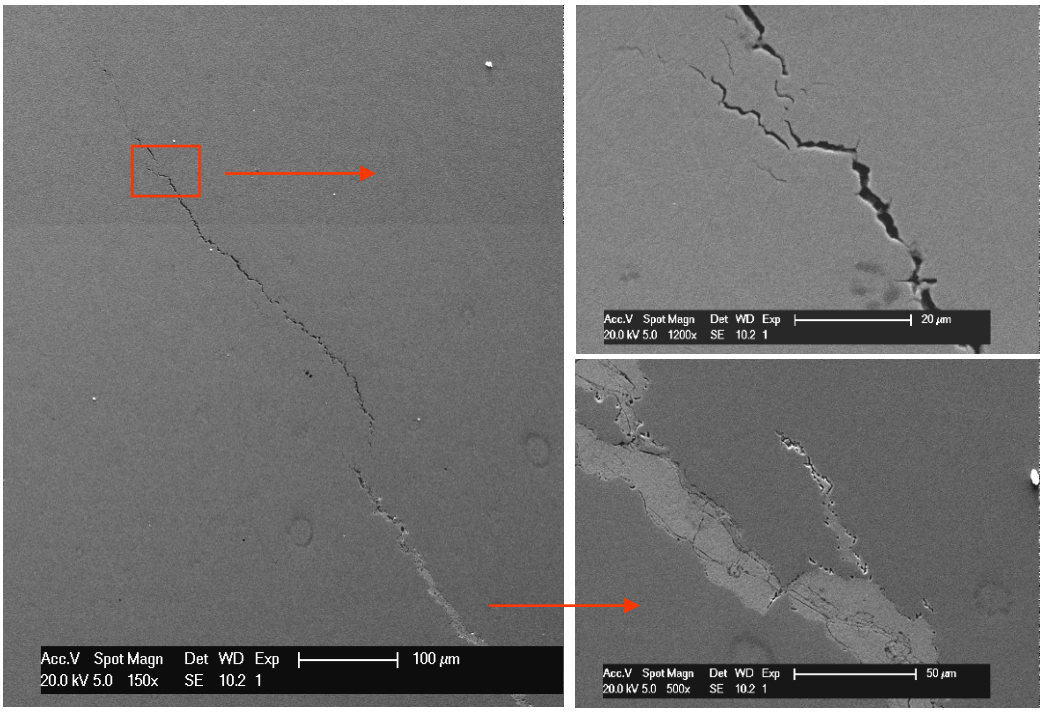

Figure III.39. SEM observations of crack obtained on a cup immersed 7 minutes at 460°C

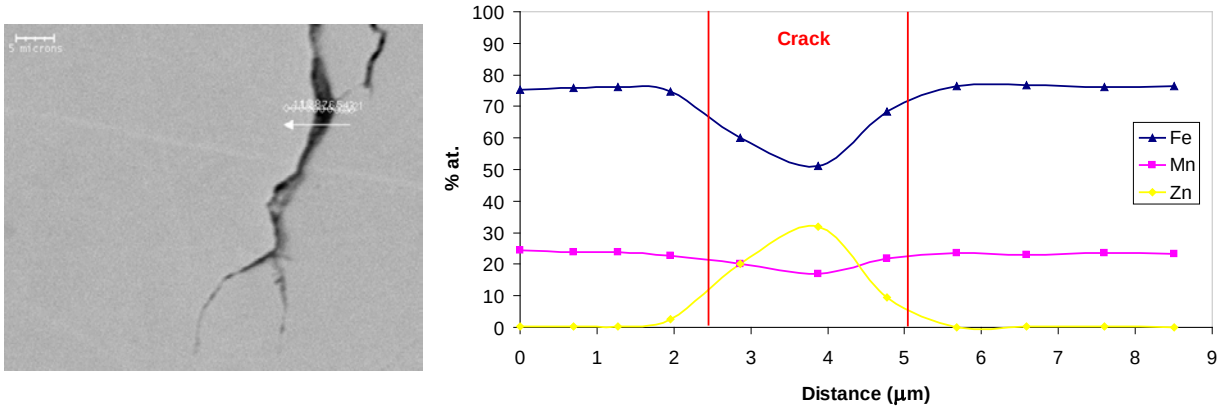

Figure III.40. EDX profile across crack obtained on a cup immersed 18 minutes at 490°C

Figure III.41 displays SEM micrographs of the fracture surfaces corresponding to the cup of figure III.33. A solidified liquid film is seen in the whole fracture surface (figure III.41 (a)), and different layers can be observed in figure III.41 (b). No analyses have been performed to identify the different compounds due to experimental difficulties. Similarly to hot tensile specimens, the original morphology of fracture surface has not been observed because dissolution of the zinc layers leads to a wear of the fracture surface.

(a) (b)

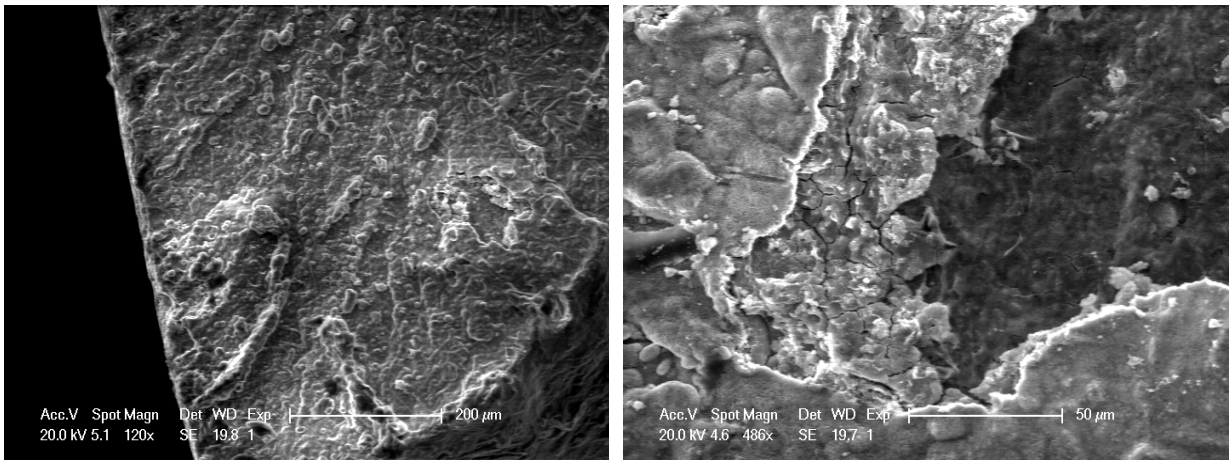

Figure III.41. SEM micrographs of the fracture surface after immersion in the liquid zinc bath at 480°C during 2 minutes

A hypothesis explaining the crack initiation concerns the grains orientation (see Chapter I, § III.3.4): some particular grain boundaries could be more sensitive from an energetic point of view to liquid zinc penetration. EBSD analyses can be performed to determine grains orientation. However, the difficulty lies on finding the initiation site since many grains are present in the thickness.

EBSD analyses have been performed along crack in order to determine if it propagates between grains having particular orientation [LED 09]. Cracks obtained in cups subjected to different treatments (time immersion and bath temperature) were examined.

Figure III.42 presents results for cracks obtained on cup having been immersed (a) 7 minutes at 460°C, (b) 18 minutes at 490°C and (c) 5 minutes at 740°C.

The results show that grains in the vicinity of crack do not possess a preferential orientation, excluding the hypothesis of an orientation more likely to propagate crack. No conclusions can be drawn concerning the crack initiation.

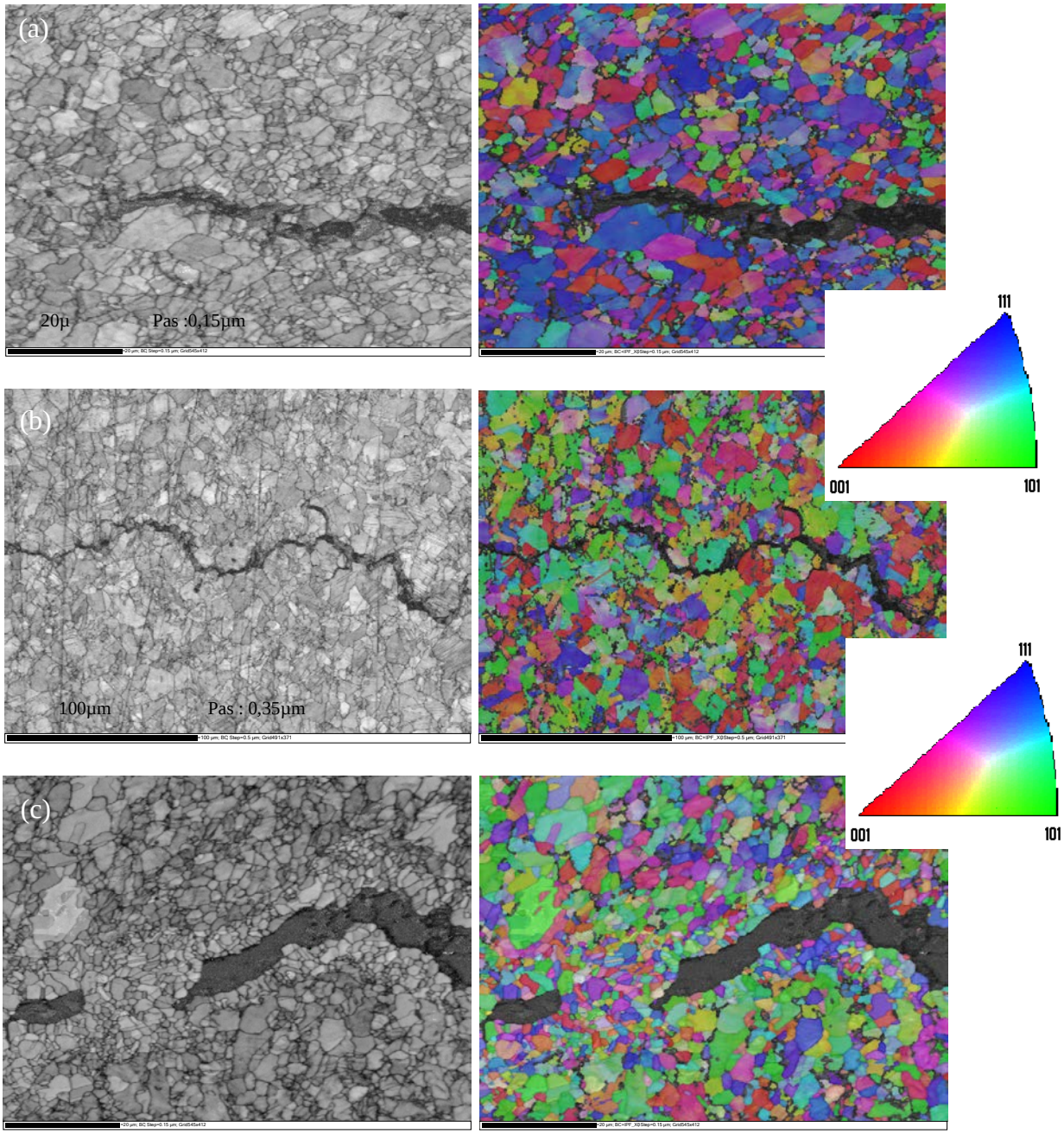

Figure III.42. Band contrast and orientation cartography for cracks obtained on cups immersed (a) 7 minutes at 460°C, (b) 18 minutes at 490°C and (c) 5 minutes at 740°C

For cracks obtained in cups immersed 5 minutes at 740°C, a zone with fine grains is observed along crack and in the crack tip as shown in figure III.43. These fine grains certainly come from nucleation of intermetallic compounds (EDX analyses indicate 10% to 20% at. Zn) once crack has propagated. However, theses compounds must exhibit crystallographic parameters similar to austenite because they have been indexed as face centered cubic. It is worth noticing that this zone does not appear so clearly in the vicinity of cracks formed in cup immersed only 10 seconds at 720°C or immersed 7 minutes at 460°C. This leads to the conclusion that these fine grains are not involved in cracking mechanism.

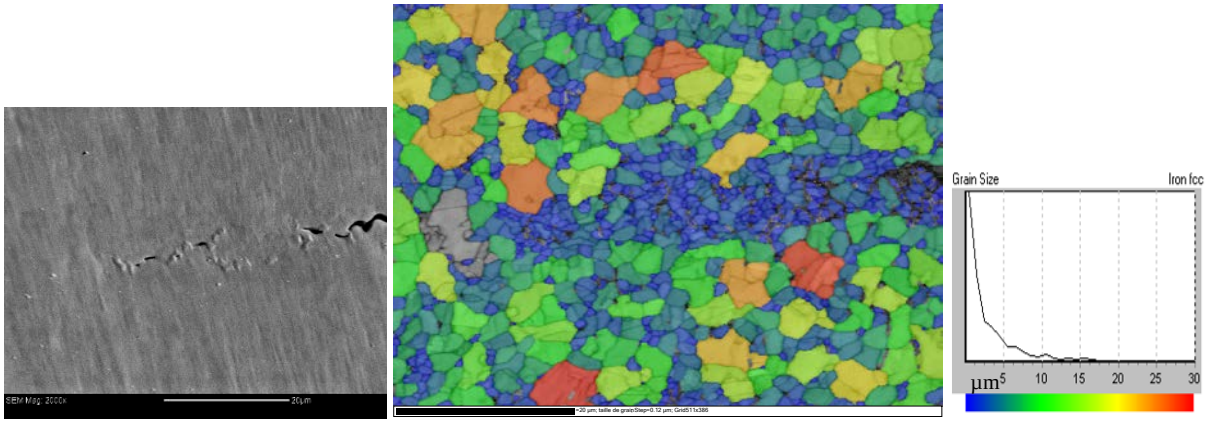

Figure III.43. Grain size cartography of crack tip in a cup immersed 5 minutes at 740°C

Conclusions

Hot tensile tests performed on bare and EG specimens at different temperatures with a constant strain rate of $1{,}3.10^{-3}$ s^{-1} indicate that the 22Mn-0.6C TWIP steel seems to be immune to LME by liquid zinc. However, increasing strain rate of one decade to $1{,}3.10^{-2}$ s^{-1} reveals that the studied steel can be sensitive to liquid zinc embrittlement.

LME was observed over a finite temperature range depending on strain rate as summarized in table III.2. Increasing strain rate tends to widen this temperature range by a decrease of the lower limit: 775°C for $1{,}3.10^{-2}$ s^{-1} instead of 700°C for higher strain rate. The ductility recovery temperature is close to the boiling point of zinc whatever the strain rate.

Strain rate	$1{,}3.10^{-3}$ s^{-1}	$1{,}3.10^{-2}$ s^{-1}	$1{,}3.10^{-1}$ s^{-1}	1,3 s^{-1}
Ductility trough	No LME	[775°C-950°C]	[700°C-950°C]	[600°C-900°C]

Table III.2. Summary of embrittlement conditions

It appears that cracking occurs only when stress exceeds a critical stress and this stress can be used as a LME criterion for predicting this phenomenon in a finite element model for instance. This stress can be applied during hot tensile tests or can be residual stresses resulting from deep drawing of cups.

Hot tensile tests reveal that the critical stress strongly increases with decreasing temperature. This could explain the ductility trough: for lower temperatures, the critical stress is so high that it can not be reached during tensile test. Besides, increasing strain rate increases the stress level which can then exceed the critical stress. Thus, with increasing strain rate, the lower temperature of the ductility trough decreases so that the temperature range of embrittlement widens. Hot tensile tests performed on cold rolled specimens show that the steel can be embrittled at lower temperature: as cold rolled specimens exhibit higher strength, the critical stress is more easily achieved when testing such specimens.

Immersing cup containing high residual stresses permitted to evidence the embrittlement at temperatures as low as 420°C. However, these tests only give trends and do not provide quantitative results. Indeed, during these tests, many parameters can not be precisely known. In particular, residual stresses are estimated from numerical simulations in the initial state that do not take into account the thermal relieving related to the immersion in the liquid zinc bath. Furthermore, it is difficult to estimate the strain rate during these tests to compare with Gleeble tests.

Conditions leading to embrittlement of the Fe22Mn0.6C TWIP steels have been precisely determined. In the next chapter, the influence of additional parameters is investigated in order to propose possible mechanism of the cracking phenomenon.

Chapter IV. Towards an explanation of cracking mechanisms

The studied steel appears to be sensitive to liquid zinc embrittlement. Hot tensile test is well appropriate to study the embrittlement by liquid zinc of steels and permits to investigate the influence of many experimental parameters. It has been shown that embrittlement occurs for particular combinations of temperature and strain rate.

In this chapter, the effects of additional parameters on LME occurrence are studied with the aim of understanding cracking mechanisms.

In the first part, the influence of zinc coating is described. Besides, multiphase steels have been studied in order to determine the influence of constituent phases on the LME. Then, the effect of time of contact between steel and liquid zinc is detailed. This has been investigated by performing holding at high temperature before tensile testing. Finally, a summary of experimental results is presented and cracking mechanisms are proposed.

I. Influence of coating and steel

I.1. Influence of coating

I.1.1. Galvanized specimens

In order to study the influence of the coating on LME, bare specimens have been fluxed and immersed in the pure liquid zinc bath at 485°C during 1 minute. The resulting coating is presented in figure IV.1. It consists of a succession of intermetallic Fe-Mn-Zn phases as described in the chapter I, §IV.1.2.

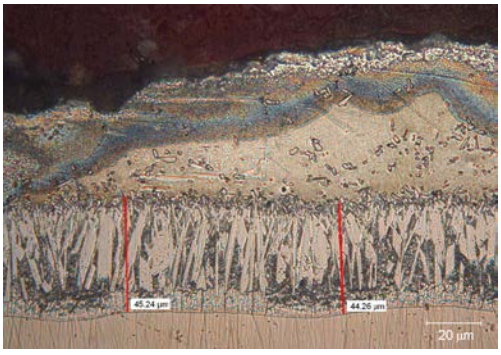

Figure IV.1. Micrograph of coating obtained after 1 minute in the liquid zinc bath at 485°C (Nital etching)

Galvanized specimens were then tested at 800°C at a strain rate of $1{,}3.10^{-1}$ s^{-1}. Results are presented in figure IV.2 where tensile curves of bare and EG specimens obtained in the same tensile conditions are also displayed. Galvanized and EG specimens exhibit a similar behaviour since the critical stress is identical and the fracture energy is almost the same in the two cases.

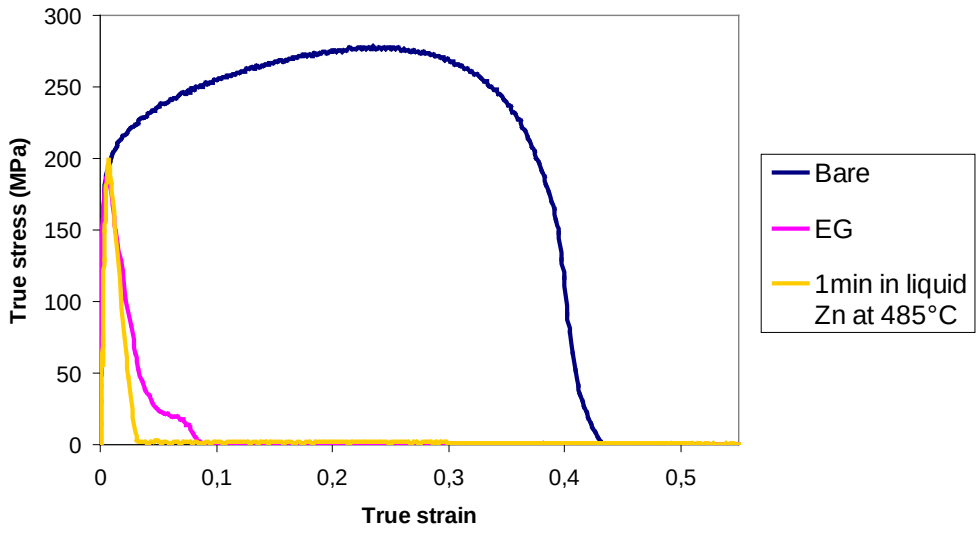

Figure IV.2. Influence of coating process on embrittlement at 800°C

This clearly shows that whatever the process used to obtain the Zn coating, the occurrence of LME is unchanged and the presence of an intermetallic layer does not prevent LME phenomenon.

I.1.2. Annealed EG specimens

The influence of the coating microstructure on the cracking behaviour has been studied by carrying out hot tensile tests on annealed EG specimens.

It has been shown that the resistance to delayed fracture induced by electrogalvanizing process can be improved by performing adequate heat treatments on coated steel leading to a fully alloyed coating [CUG 08]. Such heat treatments depend on material's strength and in the case of the studied steel, it consists in annealing at 280°C during 24h under N_2. During the heat treatment, intermetallic Fe-Mn-C phases form at the interface between steel and the pure zinc layer and the hydrogen content decreases. The resulting coating consists of a 1µm thick layer of (Γ+Γ_1) phases, a 7-8µm thick layer of δ phase. A very thin layer of ζ phase may be present at the extreme surface.

Tensile tests have been performed at 700°C, 800°C and 900°C at different strain rates of $1{,}3.10^{-2}$ s^{-1} and $1{,}3.10^{-1}$ s^{-1}. Figure IV.3 presents the tensile curves obtained with bare, EG and annealed EG specimens at 800°C for two different strain rates. Results show that the annealing treatment performed on EG coated steel has no influence on the embrittlement of the TWIP steel. Indeed, tensile curves are very similar to those obtained with normal EG specimens.

Similar results have been obtained for other testing conditions (strain rate, temperature). Under no circumstances the heat treatment performed on EG specimens implies improvement in cracking resistance.

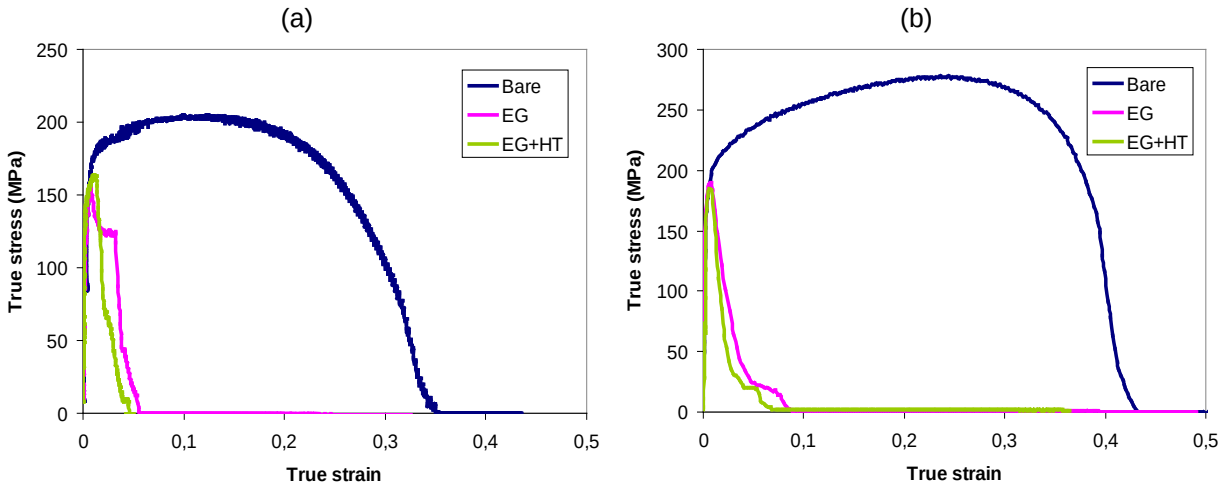

Figure IV.3. Influence of coating on tensile behaviour at 800°C for different strain rates: (a) $1.3.10^{-2}$ s^{-1} and (b) $1.3.10^{-1}$ s^{-1}

If steel is covered by a pure zinc layer or by a succession of intermetallic phases (galvanized or annealed EG), the embrittlement observed during hot tensile tests is the same: identical temperature range and critical stresses.

I.2. Influence of steel

I.2.1. TWIP steel having different chemical composition

The embrittlement by liquid zinc of a FeMnC TWIP steel having a different chemical composition has been investigated: the Mn content has been lowered while the C content has been increased. At temperature higher than 650°C, this steel (TWIP2) exhibits higher yield strength but lower strain hardening and ductility than the Fe22Mn0.6C steel (TWIP1) as illustrated in figure IV.4.

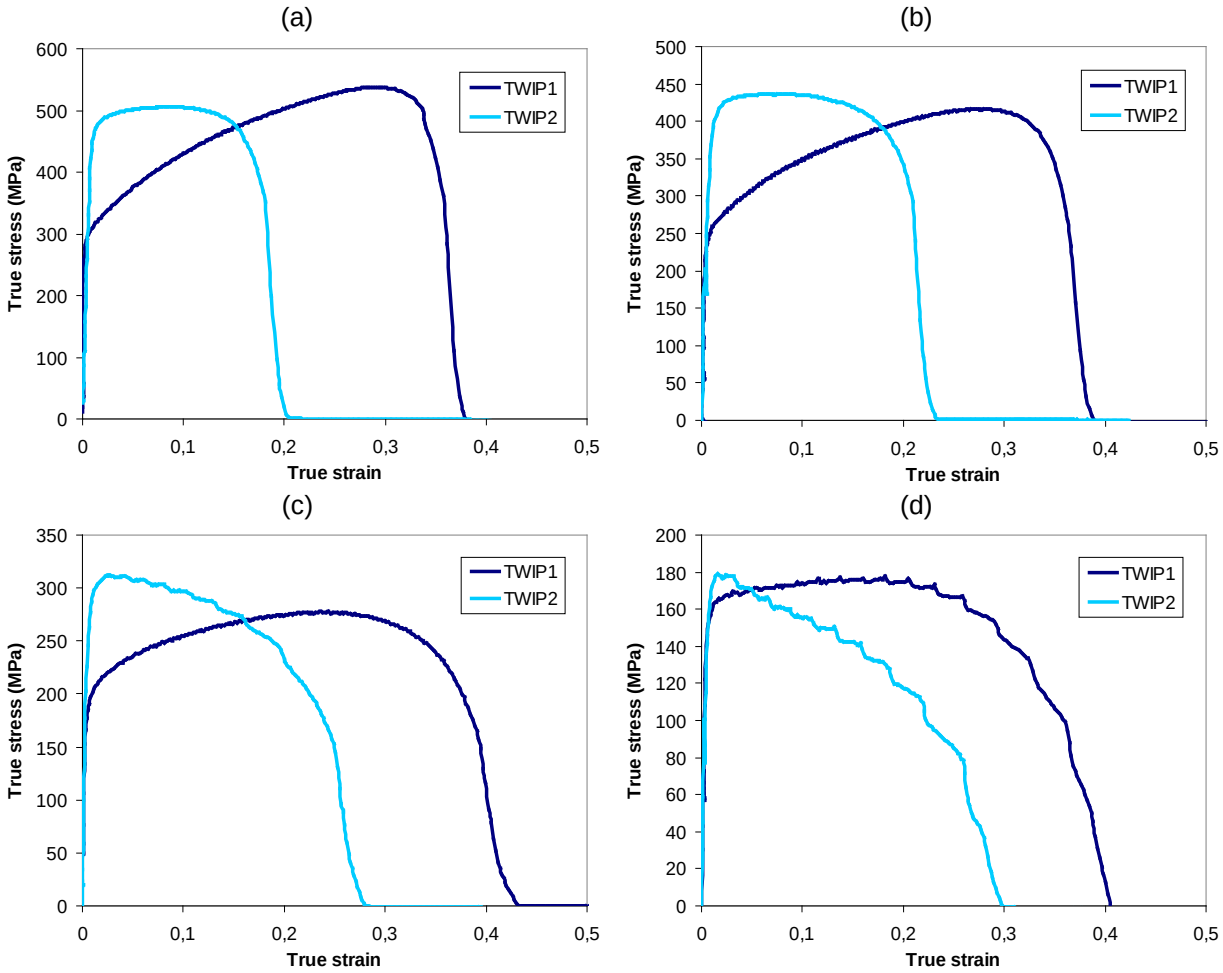

Figure IV.4. Comparison of mechanical behaviour of TWIP1 (Fe22Mn0.6C) and TWIP2 steels at a strain rate of $1.3.10^{-1}$ s^{-1} at different temperatures: (a) 650°C, (b) 700°C, (c) 800°C and (d) 900°C

Hot tensile tests have been conducted on EG specimens at a strain rate of $1.3.10^{-1}$ s^{-1} for temperatures ranging from 650°C to 900°C. The tensile curves are presented in figure IV.5. It is seen that fracture strain is drastically reduced at 800°C and 900°C.

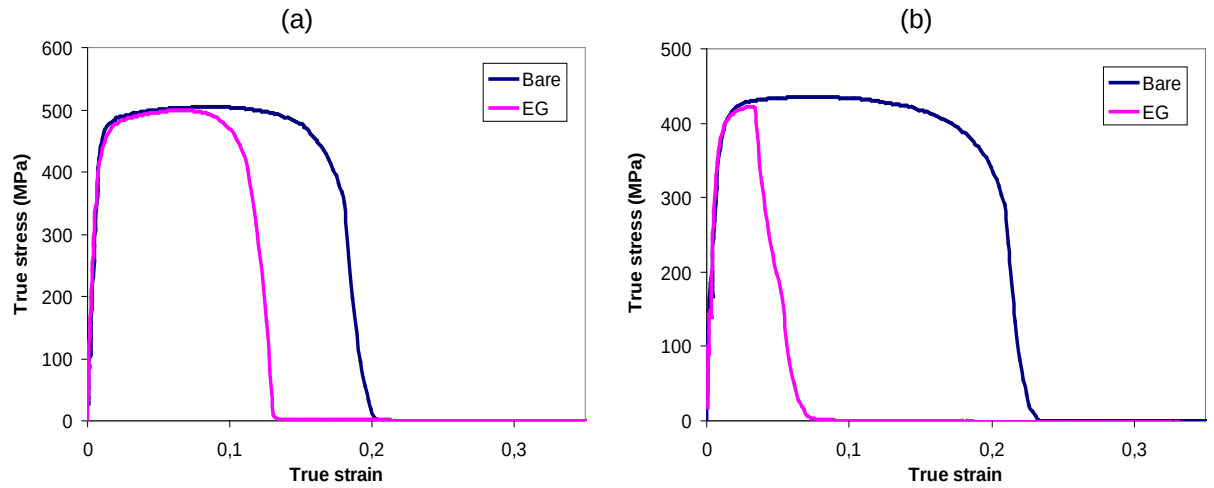

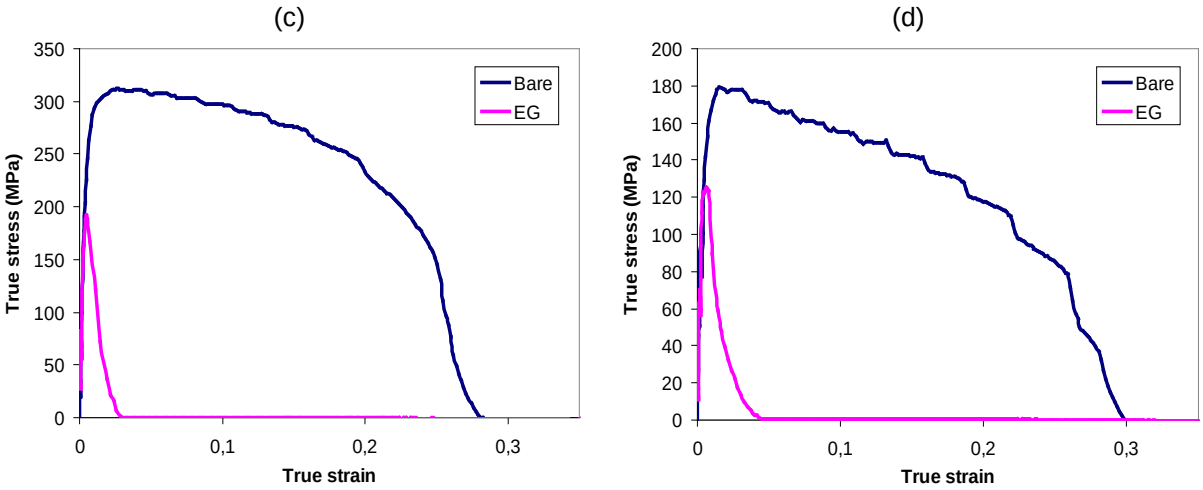

Figure IV.5. Influence of temperature on LME of TWIP2 steel for a strain rate of $1.3.10^{-1}$ s^{-1}: (a) 650°C, (b) 700°C, (c) 800°C and (d) 900°C

The severity of the embrittlement of this steel can be compared to that of the Fe22Mn0.6C (TWIP1) steel in figure IV.6 where the relative reductions of fracture energies are plotted as a function of temperature. It can be seen that the hardest steel (TWIP2) is more severely embrittled in so far as the ductility trough is wider. Indeed, LME is clearly evidenced at 650°C contrary to the TWIP1 (Fe22Mn0.6C) steel. Moreover, at 700°C, the embrittlement is more important (the relative reduction of energy is about 80% against 45% for the Fe22Mn0.6C steel).

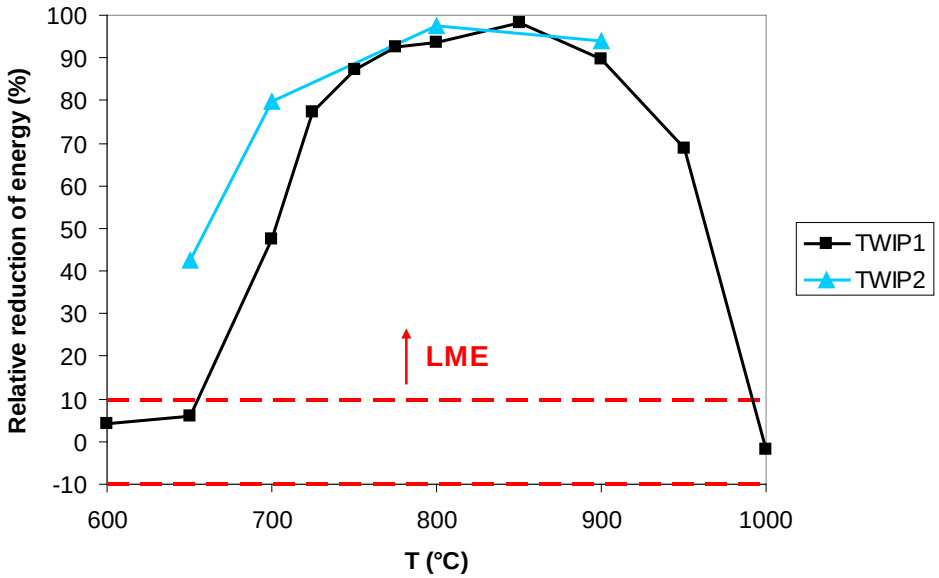

Figure IV.6. Severity of embrittlement for two FeMnC TWIP steels at $1.3.10^{-1}$ s^{-1}

The critical stress has been determined for each temperature. The evolution of the latter with temperature is shown in figure IV.7 (a). It can be compared to that of Fe22Mn0.6C steel in figure IV.7 (b). It can be seen that critical stresses are not so different.

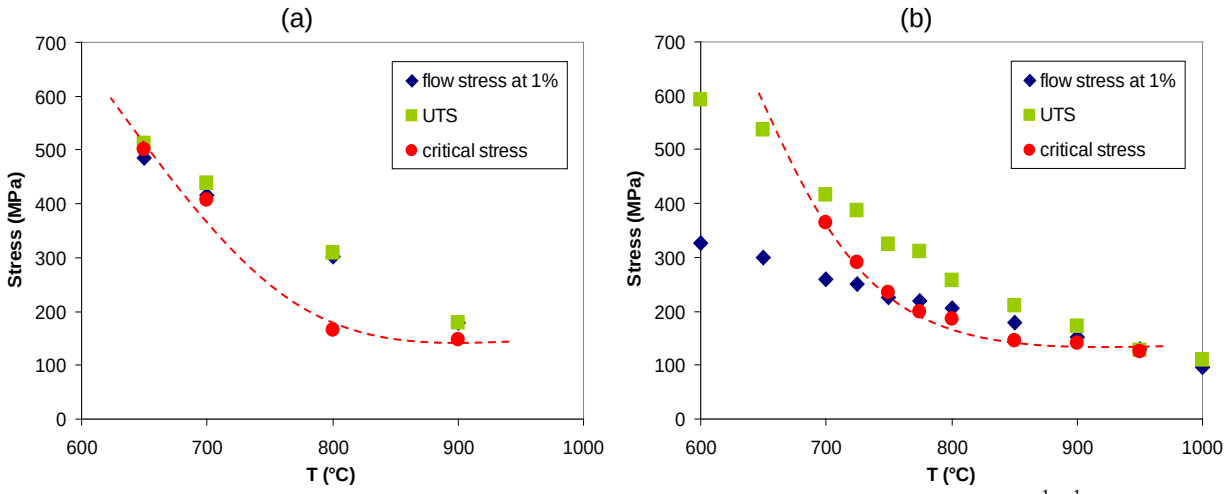

Figure IV.7. Evolution of the critical stress and mechanical properties with temperature at $1.3.10^{-1}$ s^{-1}: (a) TWIP2 and (b) TWIP1

The influence of strain rate has been studied at 800°C: tests have been performed at $1.3.10^{-3}$ s^{-1} and $1.3.10^{-2}$ s^{-1}. Similarly to the Fe22Mn0.6C steel, the steel is not embrittled by liquid zinc at $1.3.10^{-3}$ s^{-1} and when tested with a strain rate of $1.3.10^{-2}$ s^{-1}, EG specimen cracks with a very low fracture strain.

Embrittlement observed with this steel exhibiting higher strength than the Fe22Mn0.6C steel is more important than Fe22Mn0.6C steel in so far as the ductility trough is wider. These results confirm that harder steels are more severely embrittled, as already reported for other metals (see Chapter I, §III.3.4) and corroborates the hypothesis of the critical stress: in harder steels, the risk of achieving the critical stress is higher and this results in a more important embrittlement.

I.2.2. AHSS steels

In order to investigate the influence of phase constituents on LME, hot tensile tests have been performed on two multiphase Advanced High Strength Steels (AHSS): a Dual Phase (DP1180) steel and a Transformation Induced Plasticity (TRIP800) steel. DP steel's

microstructure consists of soft ferritic matrix and islands of hard martensite while TRIP steel contains ferrite, martensite, bainite and retained austenite.

The influence of temperature has been investigated between 700°C and 900°C at a strain rate of $1.3.10^{-1}$ s^{-1}. The influence of strain rate has been studied at 800°C. Three strain rates have been used: $1.3.10^{-3}$ s^{-1}, $1.3.10^{-2}$ s^{-1} and $1.3.10^{-1}$ s^{-1}.

Tensile curves obtained with DP1180 specimens at a strain rate of $1.3.10^{-1}$ s^{-1} are shown in figure IV.8. For T≤750°C, no embrittlement is observed. For higher temperatures, at 800°C and 900°C, fracture strain and fracture strength are significantly reduced.

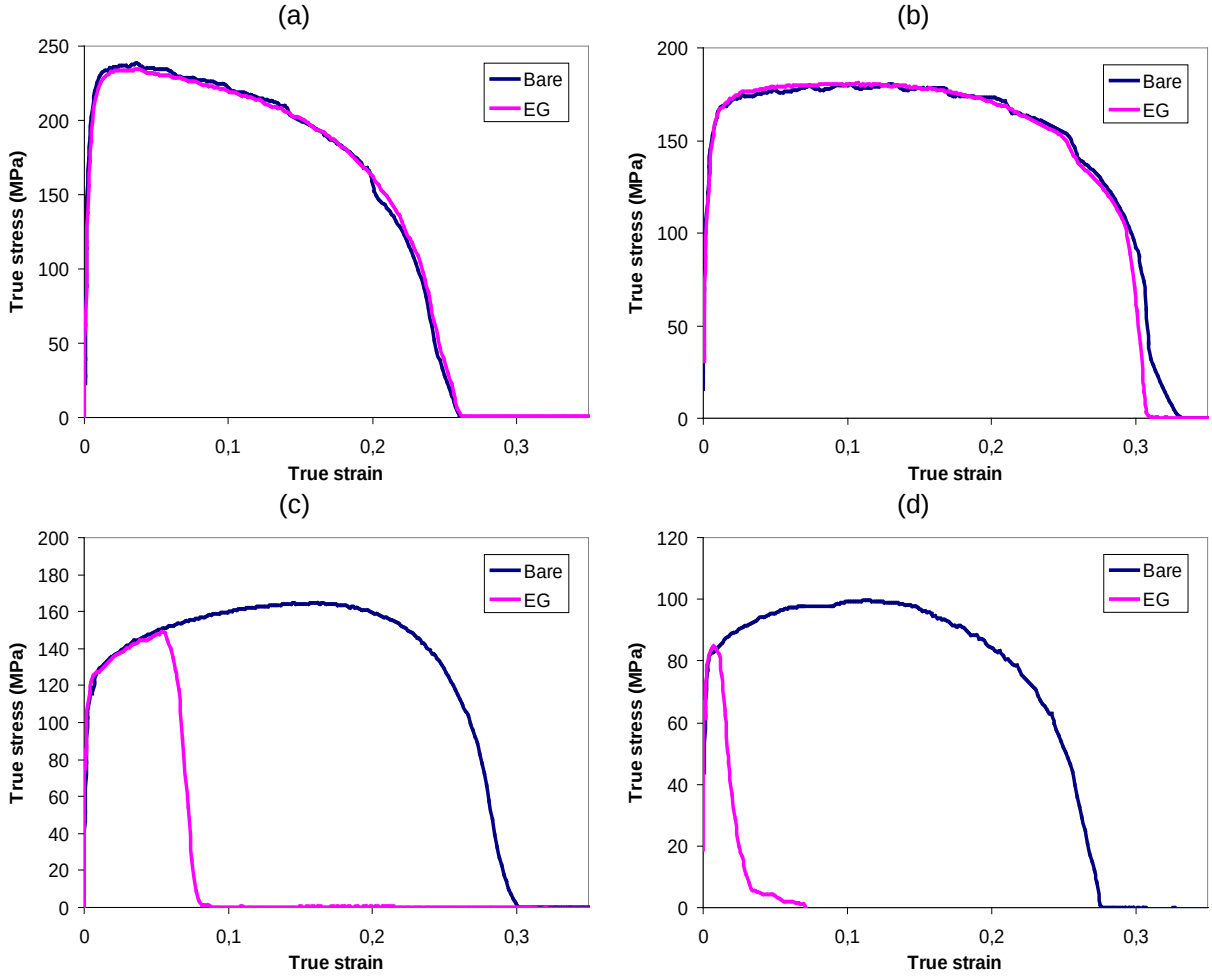

Figure IV.8. Influence of temperature on LME of DP1180 for a strain rate of $1.3.10^{-1}$ s^{-1}: (a) 700°C, (b) 750°C, (c) 800°C and (d) 900°C

The influence of strain rate at 800°C is illustrated in figure IV.9. At this temperature, embrittlement occurs only at the highest strain rate of $1.3.10^{-1}$ s^{-1}. For lower strain rates, tensile curves obtained for bare and EG specimens are identical. It is worth reminding that the Fe22Mn0.6C steel is significantly embrittled at $1.3.10^{-2}$ s^{-1}.

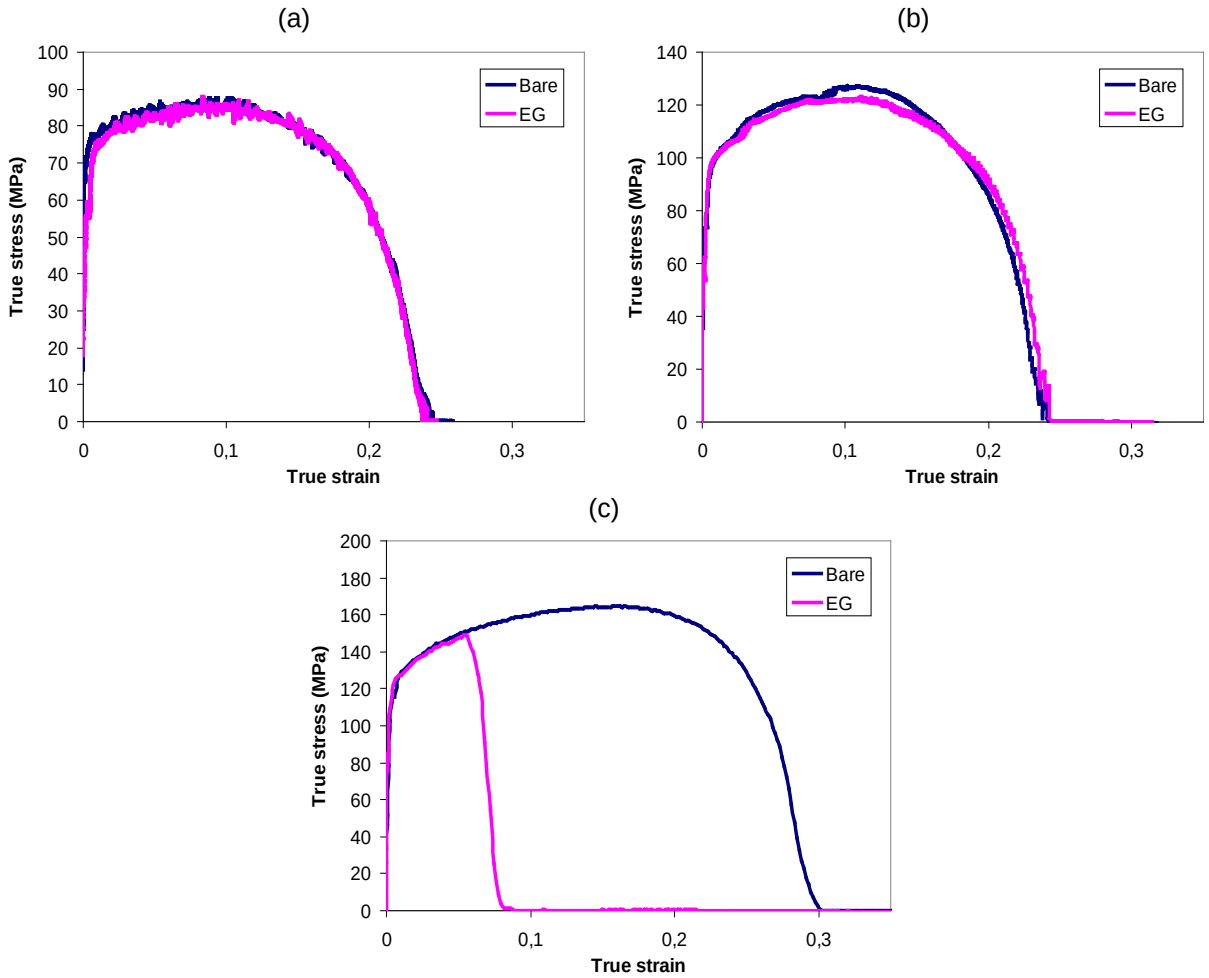

Figure IV.9. Influence of strain rate on LME of DP1180 steel at 800°C: (a) $1.3.10^{-3}$ s^{-1}, (b) $1.3.10^{-2}$ s^{-1} and (c) $1.3.10^{-1}$ s^{-1}

Tests in the same conditions have been performed on the TRIP800 steel.

The severity of embrittlement for the different steels can be compared in figure IV.10. The ductility trough observed on the DP and TRIP steels is narrower than that of the TWIP steel. Indeed, at 700°C, no embrittlement is observed for AHSS steels. Embrittlement appears between 700°C and 750°C for the TRIP steel and between 750°C and 800°C for the DP steel. At 800°C, embrittlement of AHSS steels is less important than that of the FeMnC steel. At 900°C, the DP steel and the FeMnC steel are similarly embrittled while the TRIP steel seems to be more severely embrittled.

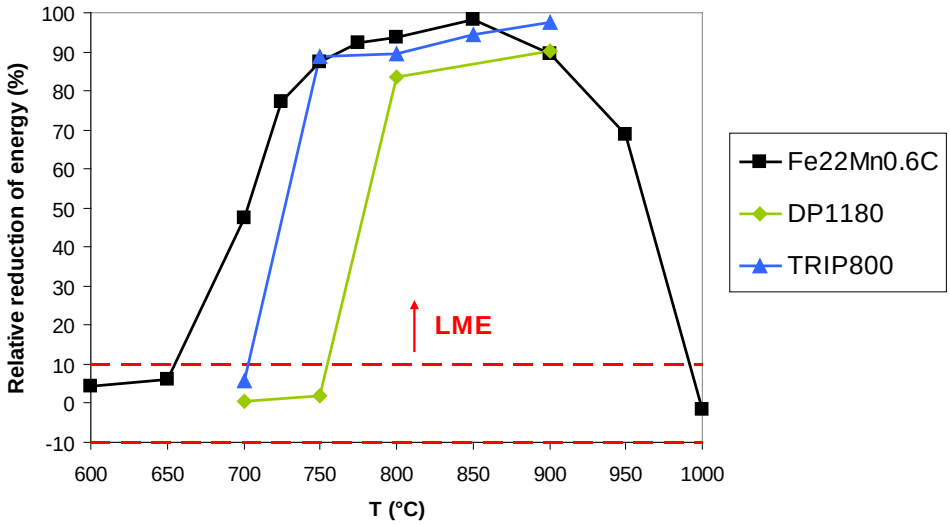

Figure IV.10. Severity of embrittlement for different steels at $1.3.10^{-1}$ s^{-1}

It can be concluded that globally, the DP steel is less sensitive to liquid zinc embrittlement than the TWIP steel. The TRIP steel exhibits an intermediate behaviour.

These differences in embrittlement behaviour can be related to phase transformations. Indeed, AHSS steels can undergo austenite transformation during high temperature tests. It is known that austenitic microstructures are more sensitive to liquid metal embrittlement and particularly to liquid zinc embrittlement (see Chapter I, §III.4). One can imagine that a minimum amount of austenite is required for LME to occur.

In order to determine the transformations temperatures, thermal expansion measurements have been performed for each steel with a heating rate of 80°C/s. The dilatation curves are shown in figure IV.11.

For the DP and for the TRIP steel, temperature at which austenite starts to form is about 720°C and 730°C respectively, and the microstructure is fully transformed at about 810°C and 920°C respectively.

The two steels are embrittled when austenite formation has started. The DP steel is embrittled from 800°C, that is to say when an important amount of austenite phase is formed. The lower limit of the embrittlement temperature range of the TRIP steel is 750°C. At this temperature, one could imagine that sufficient austenite has been formed to make the steel sensitive to liquid zinc embrittlement. Moreover, it is worth noticing that the steel already contains retained austenite in its initial state. If this retained austenite is maintained during heating, it could contribute to the occurrence of embrittlement at lower temperatures.

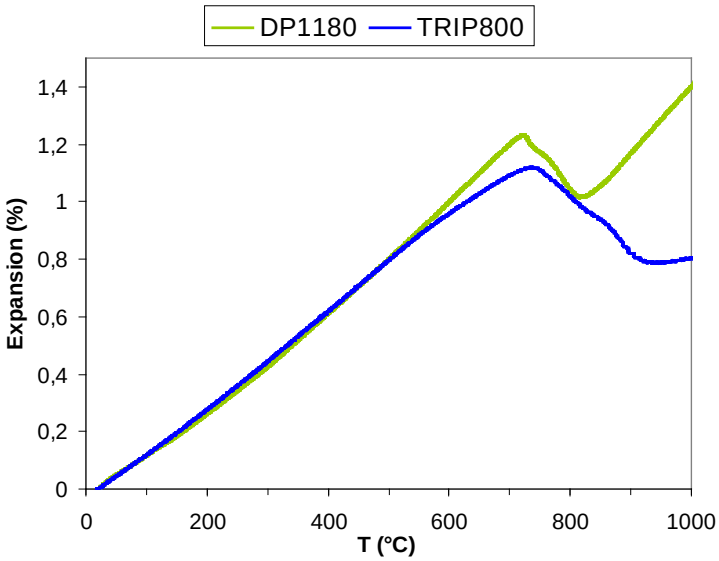

Figure IV.11. Thermal expansion curves of DP1180 and TRIP800 steels during heating with a heating rate of 80°C/s

Hot tensile tests performed on two AHSS steels show that these steels are less sensitive to liquid zinc embrittlement in that the ductility trough obtained with these steels is narrower than that obtained with the TWIP steel. This difference in embrittlement behaviour could be related to the presence of austenite. Indeed, for the AHSS steels, embrittlement occurs only for temperatures for which austenite has started to form. Hence, a minimum amount of austenite seems to be necessary for the occurrence of LME.

II. Influence of time of contact between the substrate and the liquid metal: isothermal holding

As described in the chapter III - § IV, when tensile tests are performed with a strain rate of $1.3.10^{-3}$ s^{-1}, embrittlement is never observed in the testing temperature range while an increase of strain rate leads to the occurrence of LME. If the absence of embrittlement at lower strain rate can be explained by a critical stress higher than the UTS, it must be emphasized that strain rate has a direct effect on the time of contact between the steel and the liquid zinc. Indeed, decreasing strain rate results in rising the time of contact between the solid steel and the liquid zinc.

From the literature review, the influence of the time of contact between the solid and the liquid metals is not clear. For some authors, it has no effect while for others a pre wetting is necessary for LME to occur.

The effect of time of contact between the solid steel and the liquid zinc has been investigated by holding the specimen at high temperature (above zinc melting point) before tensile testing. Two different tests (holding A and holding B) have been performed as detailed in the chapter II; the difference lying in the holding temperature compared to the tensile testing one.

II.1. Holding and tensile testing at the same temperature (Holding A)

Holding and tensile test have been performed at the same temperature ranging from 700°C to 900°C. The holding time was varied from 10s to 5min. The strain rate used for tensile testing is $1.3.10^{-1}$ s^{-1} which permits to correctly observe the embrittlement in the chosen temperature range.

It has been checked that holding the specimen at high temperature before tensile testing has no effect on the mechanical behaviour of the bare material, at least for the range of time used as shown in figure IV.12. Hence, in the following figures, only one curve has been reported for bare specimens.

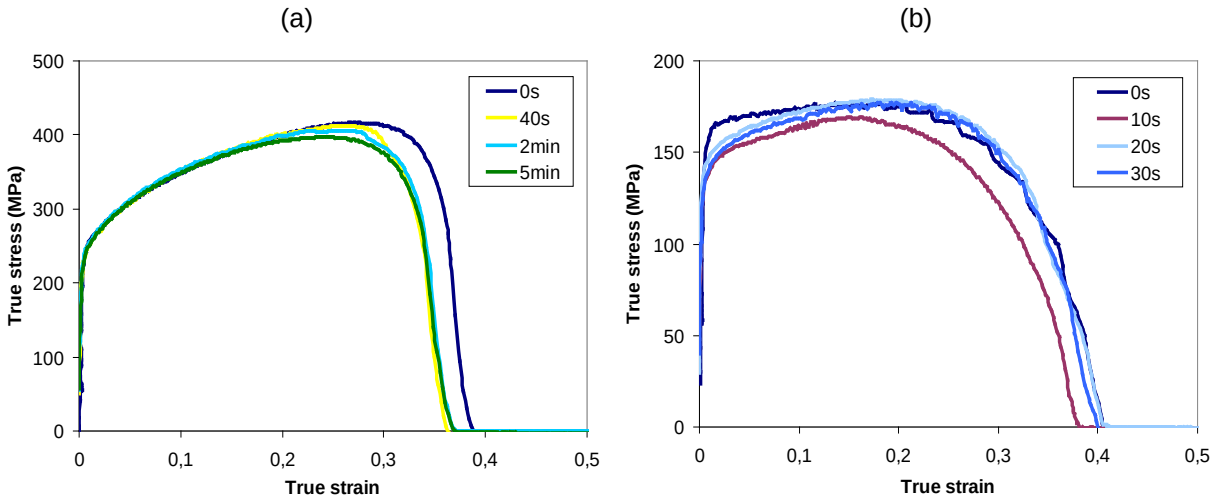

Figure IV.12. Influence of holding time on tensile behaviour of bare steel at (a) 700°C and (b) 900°C

The true strain/true stress curves obtained at 700°C and 900°C with different holding times are shown in figure IV.13.

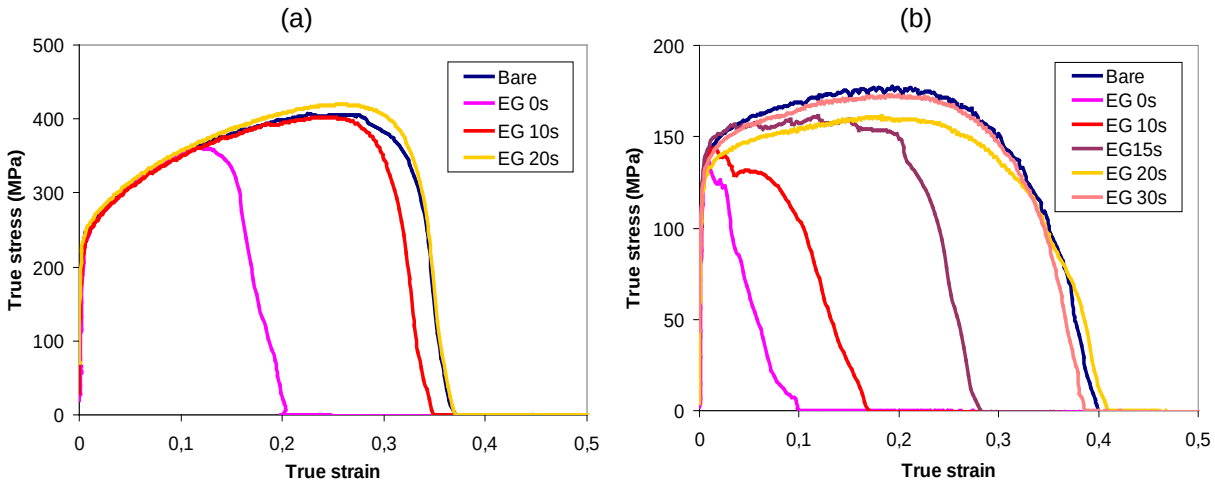

Figure IV.13. Influence of holding time before tensile test at a strain rate of $1.3.10^{-1}$ s^{-1} and different temperatures: (a) 700°C and (b) 900°C

From curves, it is seen that holding the specimen few seconds at temperature is sufficient to inhibit embrittlement during the subsequent tensile test. A progressive ductility recovery is observed with increasing holding time. As mechanical properties of the steel are not modified by holding at high temperature, the evolution of embrittlement observed on EG specimens during tensile test after holding is not related to the critical stress: with or without holding, the critical stress is still likely to be reached during the subsequent tensile test.

The effect on holding time on embrittlement is clearly seen in figure IV.14. Holding of 30s at 900°C is sufficient to recover the whole ductility during tensile test.

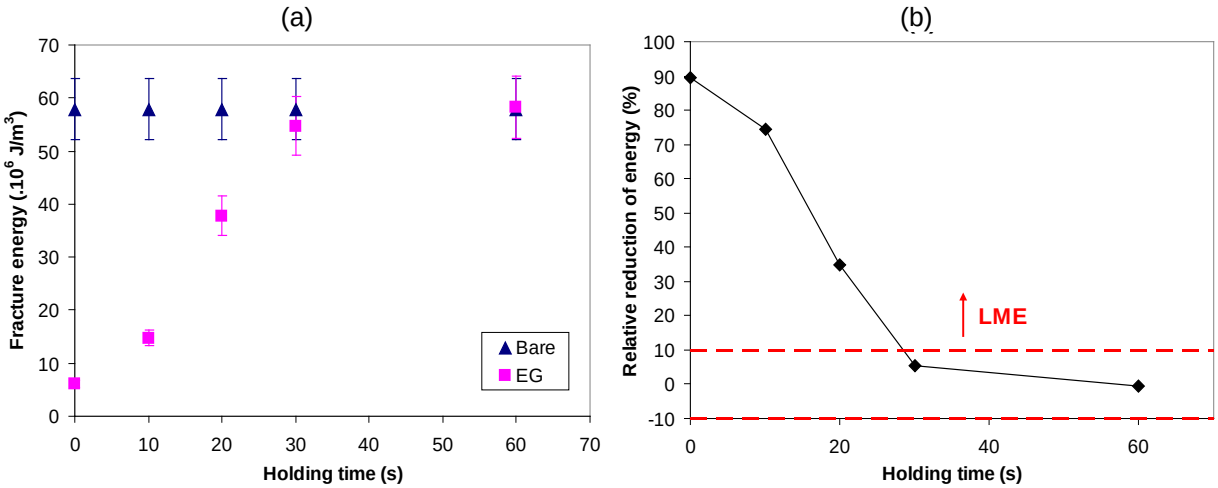

Figure IV.14. Effect of holding time on embrittlement at 900°C: (a) fracture energy as a function of testing temperature, (b) relative reduction of fracture energies

Figure IV.15 presents the evolution of the relative reduction of energy with holding time for different temperatures. For all temperatures, after 30s holding, embrittlement is not observed anymore. At 700°C, 10s holding is sufficient. But at this temperature, the initial embrittlement is not as important as for higher temperatures.

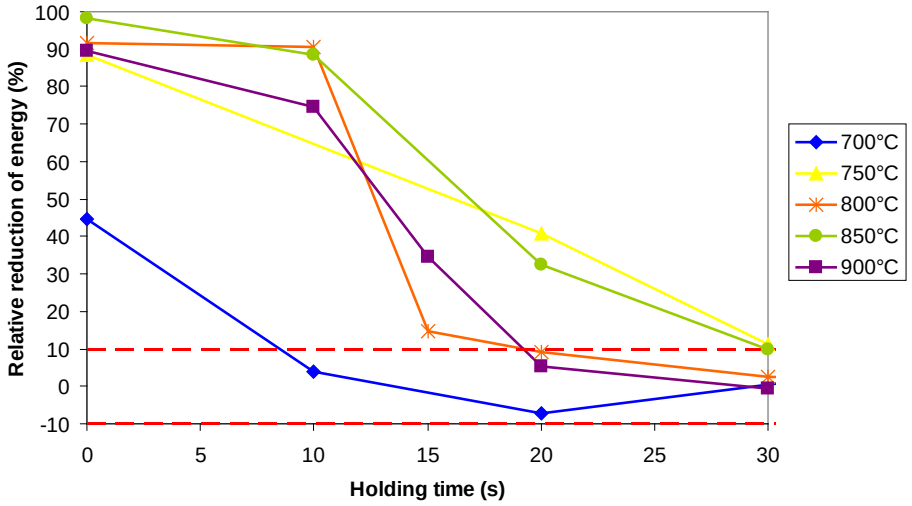

Figure IV.15. Effect of holding time on embrittlement at different temperatures

Table IV.1 summarizes the holding times necessary at each temperature. No clear trend emerges: holding times necessary to inhibit embrittlement are very similar whatever the temperature.

T°C	Time required to inhibit embrittlement
700°C	10s
750°C	30s
775°C	20s
800°C	20s
850°C	30s
900°C	20s

Table IV.1. Holding times required to inhibit embrittlement during the subsequent tensile test

It is important to notice that specimens immersed in the liquid zinc bath at about 800°C during 30s do not exhibit the same behaviour. Some bare specimens have been fluxed and immersed in the liquid zinc bath at 840°C during 30s and at 805°C during 10s. Then, tensile test at 800°C has been performed on the galvanized specimens. Tensile curves are presented in figure IV.16 where results obtained with bare and EG specimens maintained at 800°C

before tensile testing are also displayed for comparison. It is seen that specimens immersed in liquid zinc bath are still embrittled during tensile test and immersion time does not have a significant effect on tensile behaviour. Specimen immersed in the liquid zinc bath at 840°C during 30s is still embrittled during tensile test at 800°C meanwhile after holding of 30s at 800°C in Gleeble, EG specimen behaviour at 800°C is identical to the bare one.

It can be concluded that for the same conditions of temperature (800°C) and time (30s), the contact between the steel and liquid zinc in the Gleeble does not lead to the same results that contact in the zinc bath. The phases formed during galvanizing have no influence on the LME occurrence during hot tensile test. It can be supposed that during the holding of EG specimen in Gleeble, other reactions occur preventing LME.

Besides, it is worth noticing that holding an EG specimen (pure Zn layer at the specimen surface) or an annealed EG specimen (different FeMnZn intermetallic compounds at the specimen surface) during 30s at 800°C in Gleeble leads to the same results: the ductility recovery occurs indifferently according to the phases initially present at the interface between steel and zinc.

It can be pointed out that holding in Gleeble is performed in air and the amount of zinc is limited (initial layer < 10µm) whereas when immersed in the liquid zinc bath, the steel is in contact with a huge quantity of zinc and not with ambient atmosphere.

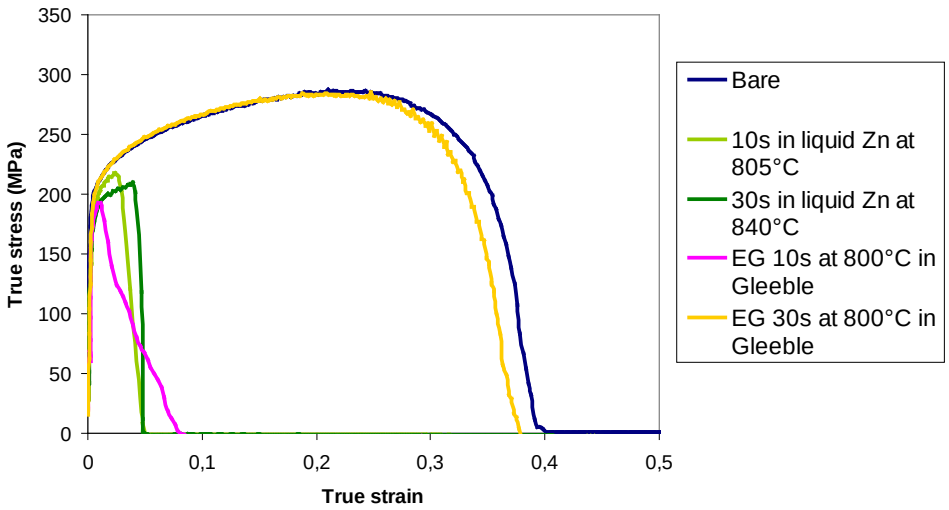

Figure IV.16. Tensile curves at 800°C obtained with bare specimens, specimens immersed in liquid zinc bath and EG specimens

In order to investigate the role of the atmosphere in the suppression of embrittlement after holding, tests have been performed under argon (99.995% purity). First, vacuum is performed in the chamber until $3.5x10^{0}$ Torr, then, the chamber is filled with Ar until -50 kPa.

Results obtained under Ar without and with holding do not differ from those obtained in air as shown in figure IV.17 (a) and (b) respectively: without holding, ductility of EG specimens is drastically reduced whereas holding of 30s is sufficient to recover the whole ductility.

These results are in contradiction with the hypothesis of oxidation.

Specimens tested under Ar have not been analysed to identify the different phases formed during the holding.

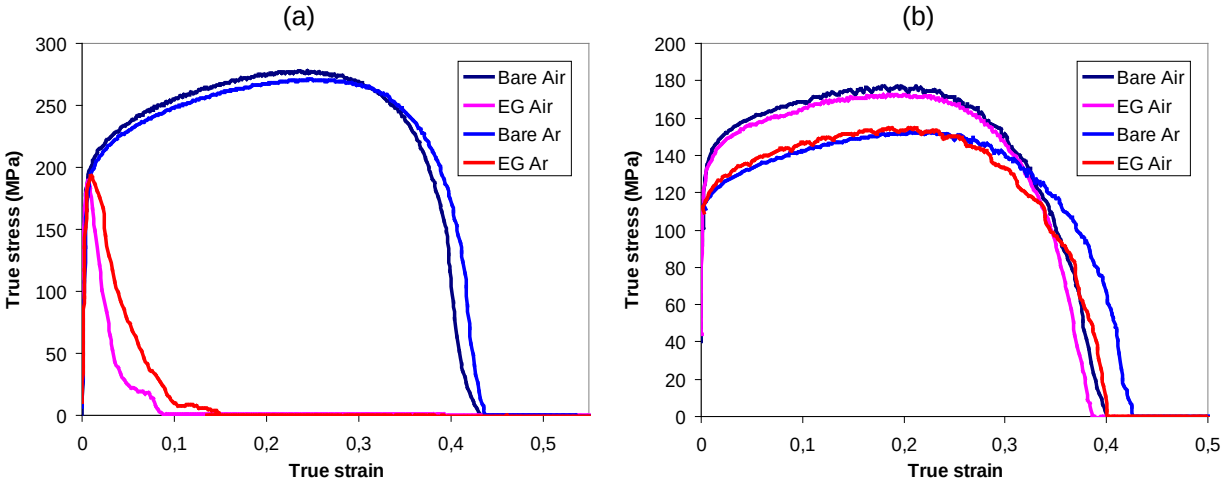

Figure IV.17. Tensile curves obtained at $1.3.10^{-1}$ s^{-1} (a) at 800°C and (b) at 900°C after holding of 30s at 900°C: influence of the atmosphere

In order to explain the effect of holding, the thermo-mechanical cycle illustrated in figure IV.18 (a) has been performed: bare specimens are heated at 800°C during 30s and air cooled in Gleeble. One specimen is fluxed and galvanized in the liquid zinc bath at 630°C during 1min and the other specimen is kept bare as control specimen. Then, hot tensile test at 800°C is carried out on the two (bare and galvanized) specimens. Tensile curves are presented in figure IV.18 (b). It is seen that for the galvanized specimen, fracture strain as well as fracture strength are drastically reduced. It can be concluded that the holding performed on bare specimen before galvanizing does not improve the embrittlement resistance. So, the suppression of embrittlement after holding of EG specimens is due to reactions occurring between the steel and liquid zinc and not due to microstructural evolutions in the steel.

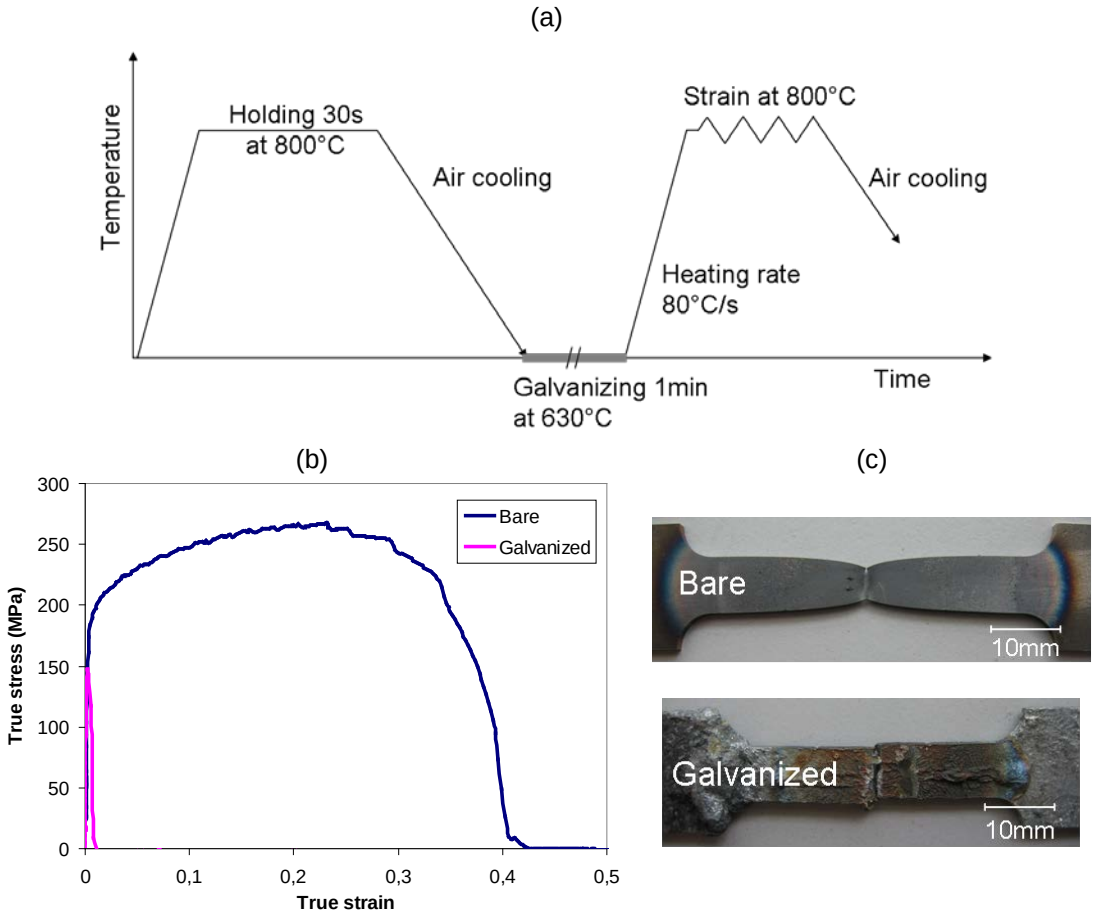

Figure IV.18. Effect of holding in bare specimen: (a) thermo-mechanical cycle, (b) tensile curves and (c) specimens after tensile test

Holding the specimen few seconds at high temperature before tensile testing prevents embrittlement provided holding is performed in Gleeble on EG (or annealed EG) specimens. Holding the specimen in the liquid zinc bath or holding bare specimen at high temperature before galvanizing does not improve the resistance to liquid zinc embrittlement during subsequent hot tensile tests. Besides, tensile tests performed under Ar lead to the same results as tests carried out in air. It can be supposed that the improved ductility after holding is related to reactions occurring between the steel and liquid zinc during holding at high temperature.

II.2. Holding at T and tensile testing at 800°C (Holding B)

The second cycle consists in performing a holding at a temperature lower than 800°C, heating the specimen at 800°C very rapidly (less than 1s) and tensile testing at 800°C. The holding time was varied from 10s to 5min and holding temperatures ranged from 500°C to 775°C. The strain rate used for tensile testing is $1.3.10^{-1}$ s^{-1}.

As mentioned previously, holding at high temperature does not modify the behaviour of the bare steel, thus only one curve is reported for bare specimens and the fracture energy for bare specimens corresponds to the mean value.

II.2.1. Influence of holding time

Figure IV.19 shows the true stress/true strain curves obtained at 800°C and $1,3.10^{-1}$ s^{-1} after holding at 775°C for different times. It can be seen that ductility is progressively recovered with increasing holding time so that after 20s holding, the mechanical behaviour of EG specimen does not differ from the bare one anymore.

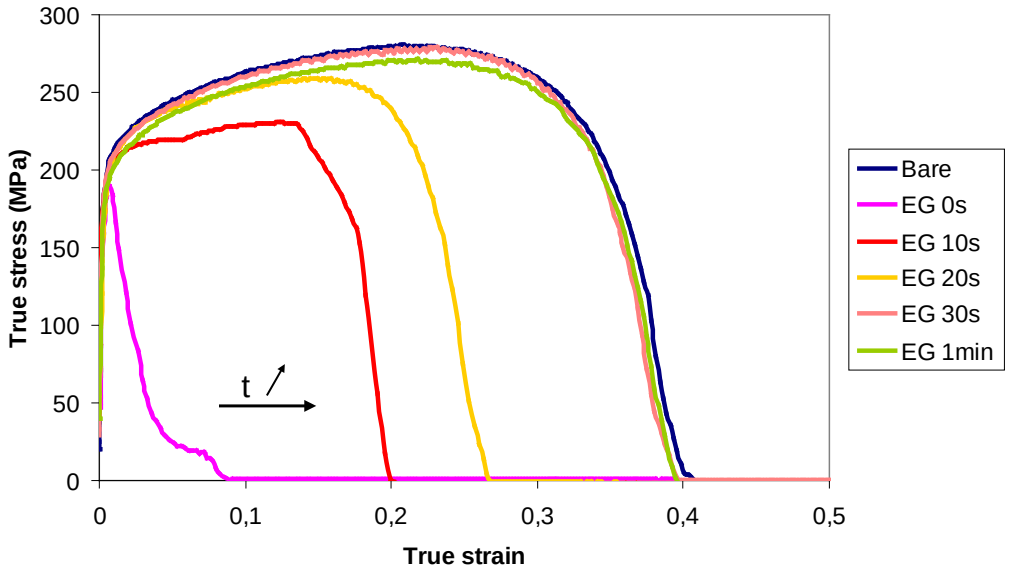

Figure IV.19. True tensile curves at 800°C and $1.3.10^{-1}$ s^{-1} after holding at 775°C for different times

This evolution clearly appears on figure IV.20 (a) where the fracture energy of bare and EG specimens is plotted as a function of the holding time. Figure IV.20 (b) displays the relative reduction of fracture energy vs holding time. It clearly shows that after 30s at 775°C, no embrittlement occurs during tensile testing at 800°C.

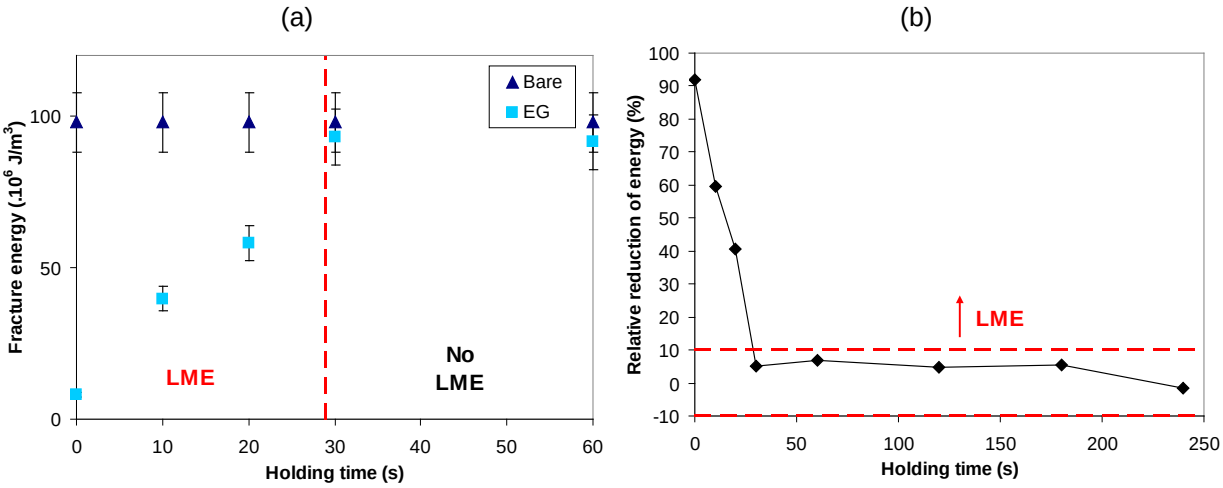

Figure IV.20. Ductility recovery during tensile test at 800°C after holding at 775°C: (a) fracture energy and (b) relative reduction of fracture energies as a function of holding time

II.2.2. Influence of holding temperature

Holdings of 1min, 3min and 5min at different temperatures have been performed before tensile testing at 800°C.

Figure IV.21 presents the tensile curves at 800°C after holding 1min at different temperatures. Heat treatment of 1min at 500°C before tensile testing at 800°C has no effect on embrittlement behaviour. However, for higher temperatures, improvement can be observed. Indeed, increasing holding temperature results in gradually increasing ductility. As described above, holding 1min at 775°C is sufficient to totally prevent embrittlement. It is worth noticing that there is a huge gap in mechanical behaviour between holding at 760°C and 775°C since after 1min at 775°C ductility is more than twice higher that after 1min at 760°C.

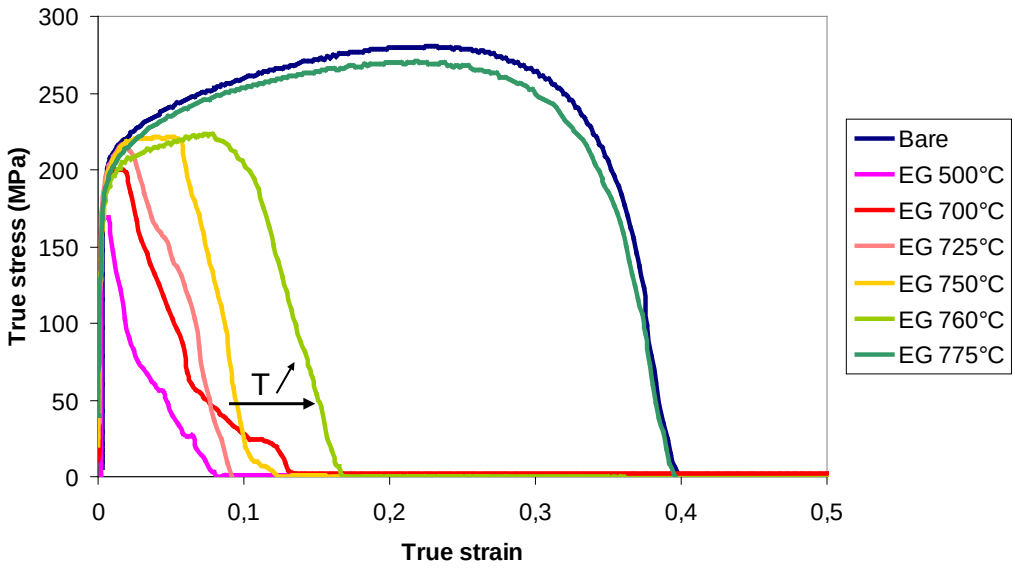

Figure IV.21. True tensile curves at 800°C and $1.3.10^{-1}$ s^{-1} after holding 1min at different temperatures

The influence of holding before tensile test at 800°C is presented in figure IV.22: figure IV.22 (a) underlines the influence of holding time at different temperatures, while figure IV.22 (b) points out the influence of holding temperature for different holding times. The lower the holding temperature is, the longer the required holding time is. For holding temperatures lower than 700°C, even 5 minutes is not sufficient to observe any effect on embrittlement. Actually, holding specimen at 700°C during 5 minutes does not affect the tensile behaviour as shown in figure IV.22 (a), the relative reduction of fracture energy being constant whatever the holding time.

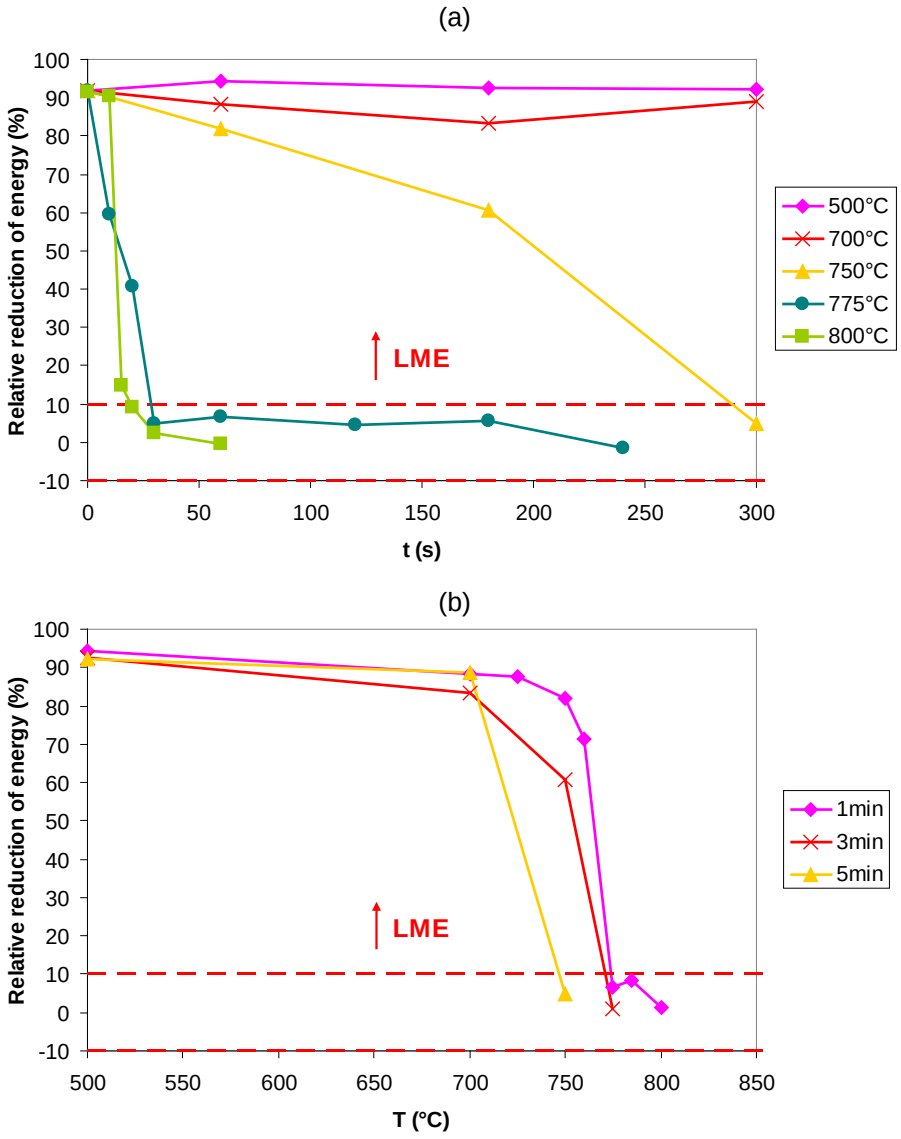

Figure IV.22. Influence of (a) holding time and (b) holding temperature on the liquid zinc embrittlement at 800°C

It has been shown that holding EG specimens at high temperature before tensile testing has a positive effect on embrittlement severity. Indeed, few seconds at high temperature are sufficient to inhibit embrittlement when tensile test is carried out at the same temperature as holding. When holding is performed at a temperature lower than 800°C (temperature of the tensile test), longer holding times are necessary for improving ductility.

Several hypotheses concerning the sensitivity to the time of exposure before testing can be put forward:

- **(i) Zn vaporization during holding decreasing the quantity of liquid zinc available for embrittlement. This hypothesis is possible for temperatures close to 900°C (Zn boiling point = 907°C) but not for lower temperatures**
- **(ii) zinc oxidation during the holding since tests are performed in air environment**
- (iii) **formation of Fe-Mn-Zn intermetallic compound layers at the interface of the bulk steel and the liquid zinc, preventing zinc grain boundary penetration during subsequent stress application.**

II.3. Observations

In order to determine the cause of the beneficial effect of holding, specimens sections have been observed.

The sections of EG specimens subjected to tensile test at 800°C and subjected to holding of 30s at 800°C + tensile test at 800°C are shown in figure IV.23 (a) and (b) respectively.

The fracture strain of the first specimen is drastically reduced (see figure III.11). The premature fracture is evidenced in the SEM micrograph (a)-1 since no sign of plastic deformation is observed and the fracture surface is quite straight and perpendicular to the tensile direction. Moreover, many large cracks are present. On the contrary, necking is clearly visible on specimen subjected to holding before tensile testing (figure IV.23 (b)-1).

Figure IV.23 -2 and -3 also displays micrographs of surfaces taken at higher magnification. Different layers are present at the surfaces. In order to characterize those different layers, EDX analyses have been performed to determine the chemical compositions and XRD analyses have been carried out on the coated surface to identify the different phases.

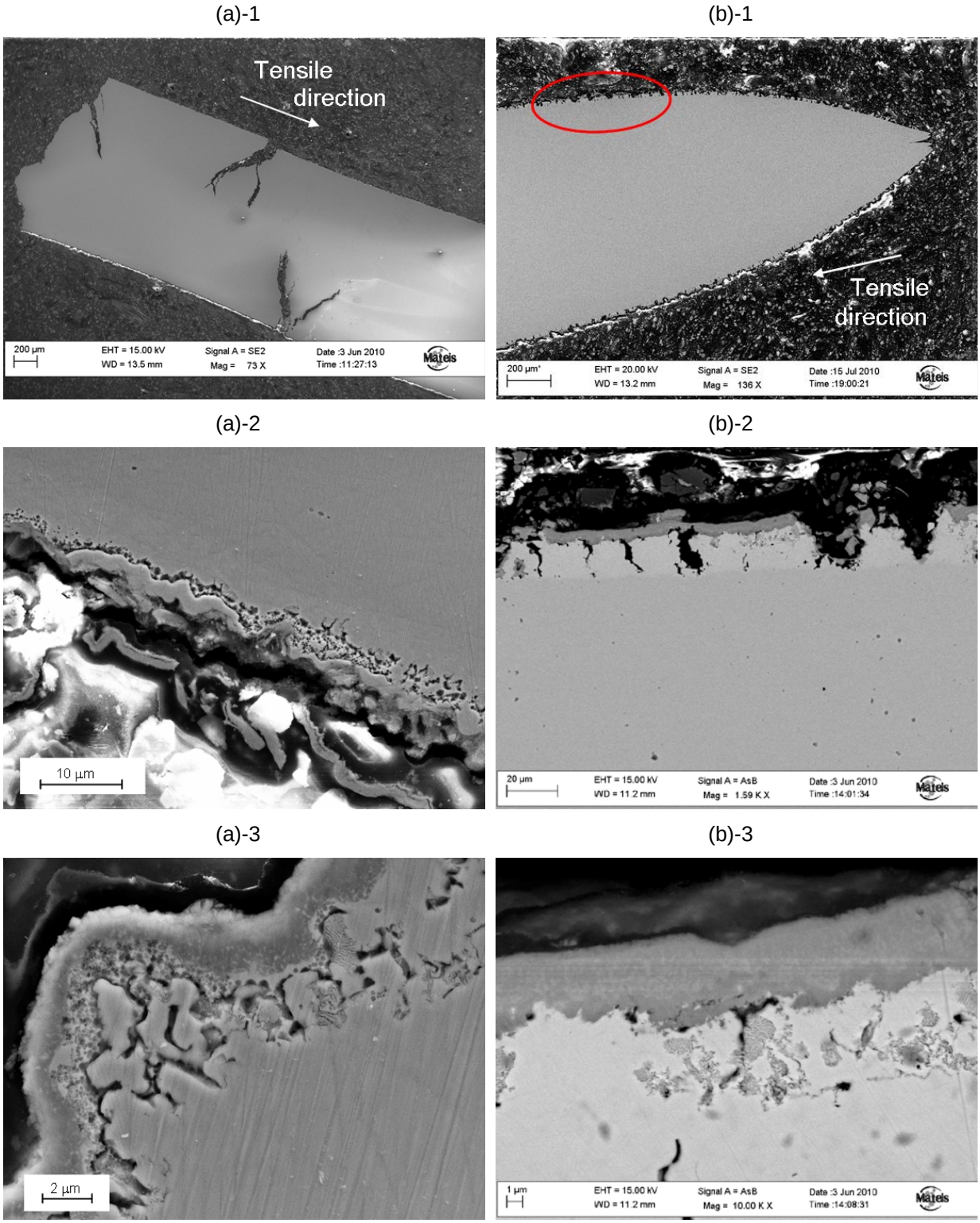

Figure IV.23. SEM micrographs of longitudinal section of EG specimens after (a) tensile test at 800°C and (b) holding 30s at 800°C + tensile test at 800°C

EDX analyses of the embrittled specimens are shown in figure IV.24. At the specimen surface (figure IV.24 (b)), different layers can be distinguished: zinc oxide at the extreme surface, a Mn and Zn rich layer underneath, then, a Zn rich layer, a Fe rich layer and finally the

substrate. It is important to notice the presence of a narrow (~1µm) Mn rich zone and a large (more than 6µm) Mn depleted zone. This means that Mn has diffused from the substrate, through the zinc layer, to the surface very fast.

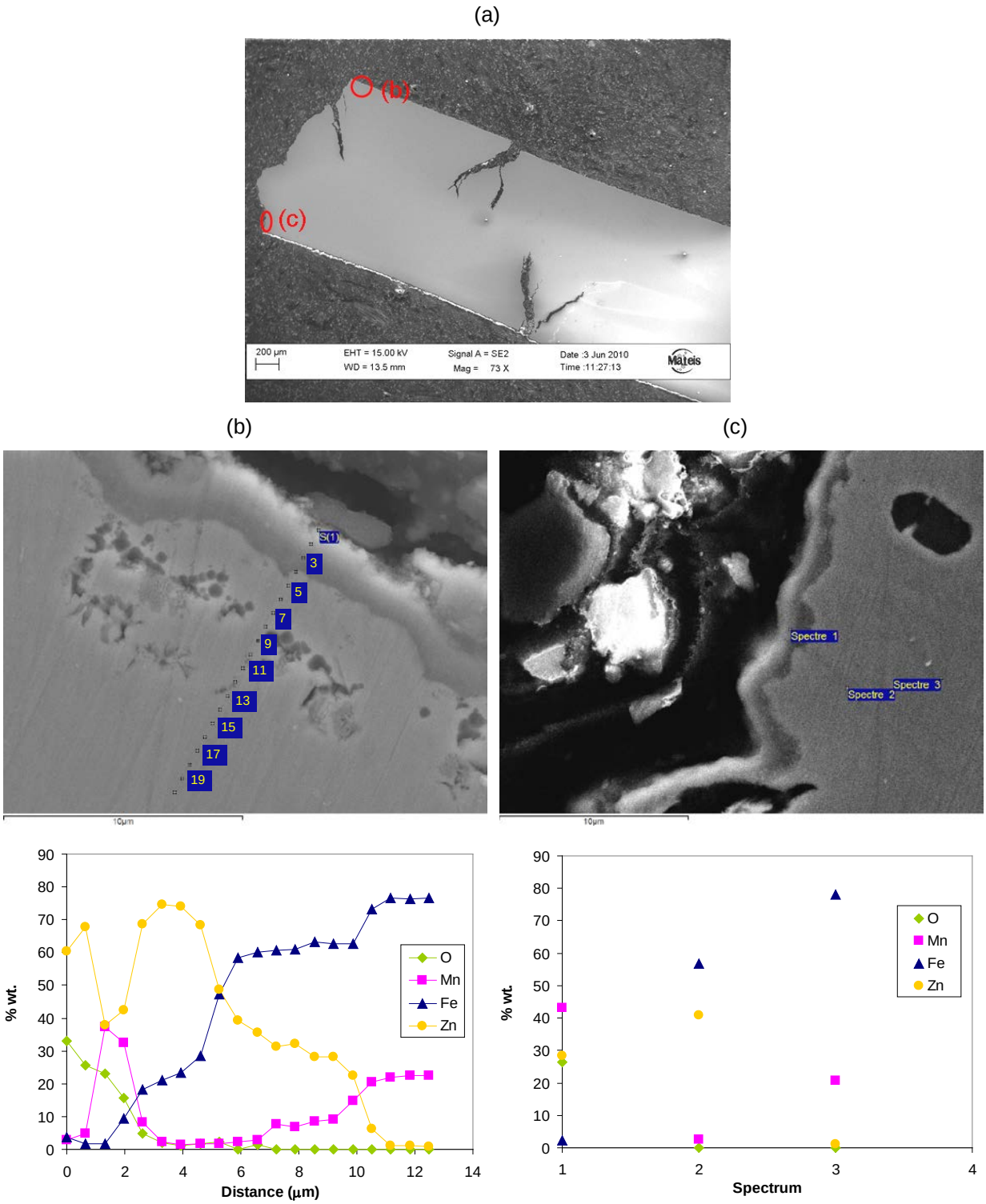

Figure IV.24. EDX analyses of longitudinal section of EG specimen after tensile test at 800°C in different zones shown in (a): (b) at the specimen surface near the fracture zone (c) in the fracture zone

In the fracture zone (figure IV.24 (c)), even if analyses are less numerous and frequent, it can be concluded that the evolution is similar with a Mn rich zone, a Mn depleted zone and the substrate.

Figure IV.25 reports EDX analyses performed on specimen subjected to holding before tensile testing. It is important to remind that this specimen is not sensitive to liquid zinc embrittlement during tensile test at 800°C. Figure IV.25 (b) presents results obtained at the specimen surface at about 1.5mm from the fracture zone. As in the previous case, different layers are present: a Mn-Zn rich zone at the surface and a Mn depleted-Fe rich zone. However, the Mn-Zn layer (~5µm) is larger than the one observed on the embrittled specimen (~1µm) and the Zn rich layer observed on the embrittled specimen is not present in the ductile specimen.
In the fracture zone, no zinc has been detected. Only an oxide layer covers the substrate, as in the case of bare material (see Figure III.5 (d)). This is explained by the fact that this surface is created during tensile straining and hence, is not in contact with zinc.

(a)

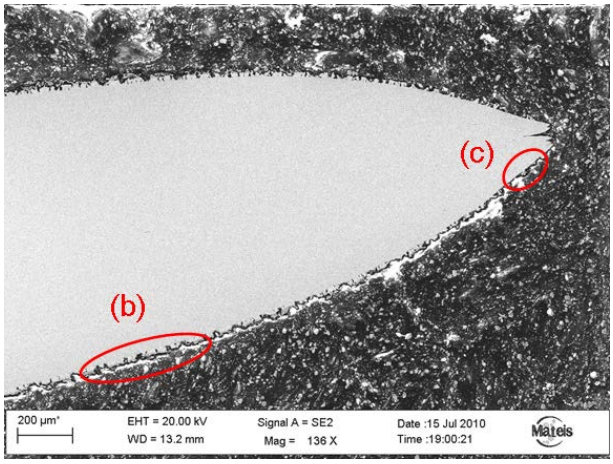

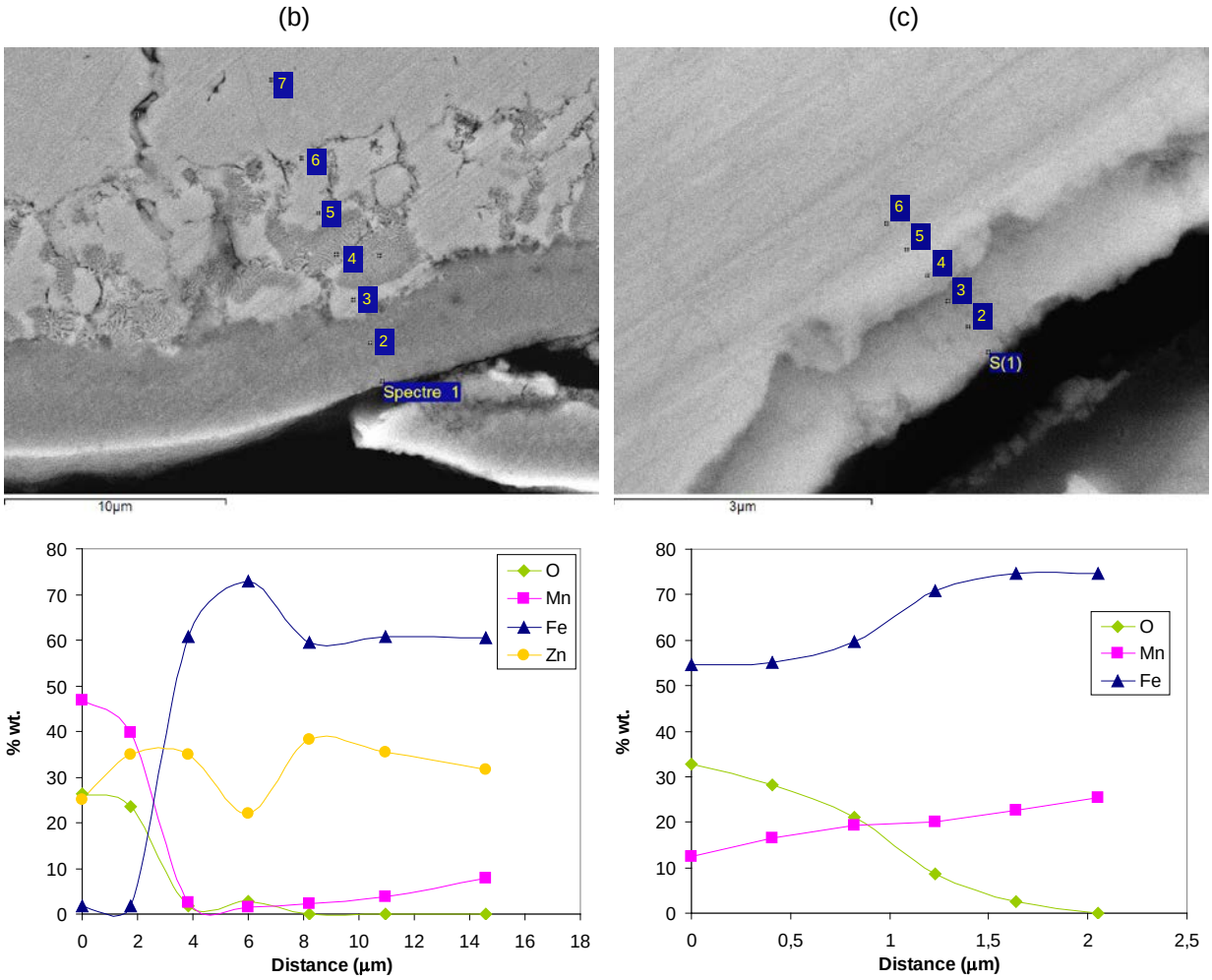

Figure IV.25. EDX analyses of longitudinal section of EG specimen subjected to holding 30s at 800°C + tensile test at 800°C in different zones shown in (a): (b) at the specimen surface at about 1.5mm from the fracture zone (c) at ~100µm from the fracture zone

Differences are also observed on XRD patterns presented in figure IV.26. While XRD on the embrittled specimen mainly reveals the presence of Γ/Γ_1 and δ FeZn (or FeMnZn) intermetallic compounds (figure IV.26 (a)), results obtained on the specimens subjected to holding before tensile testing reveals the presence of Mn and Zn oxides as well as Γ and α FeZn phases. These results are in good agreement with EDX analyses. The succession of different layers in each case is schematically depicted in figure IV.27.

It is important to notice that some phases can form during cooling as no quenching treatment has been performed.

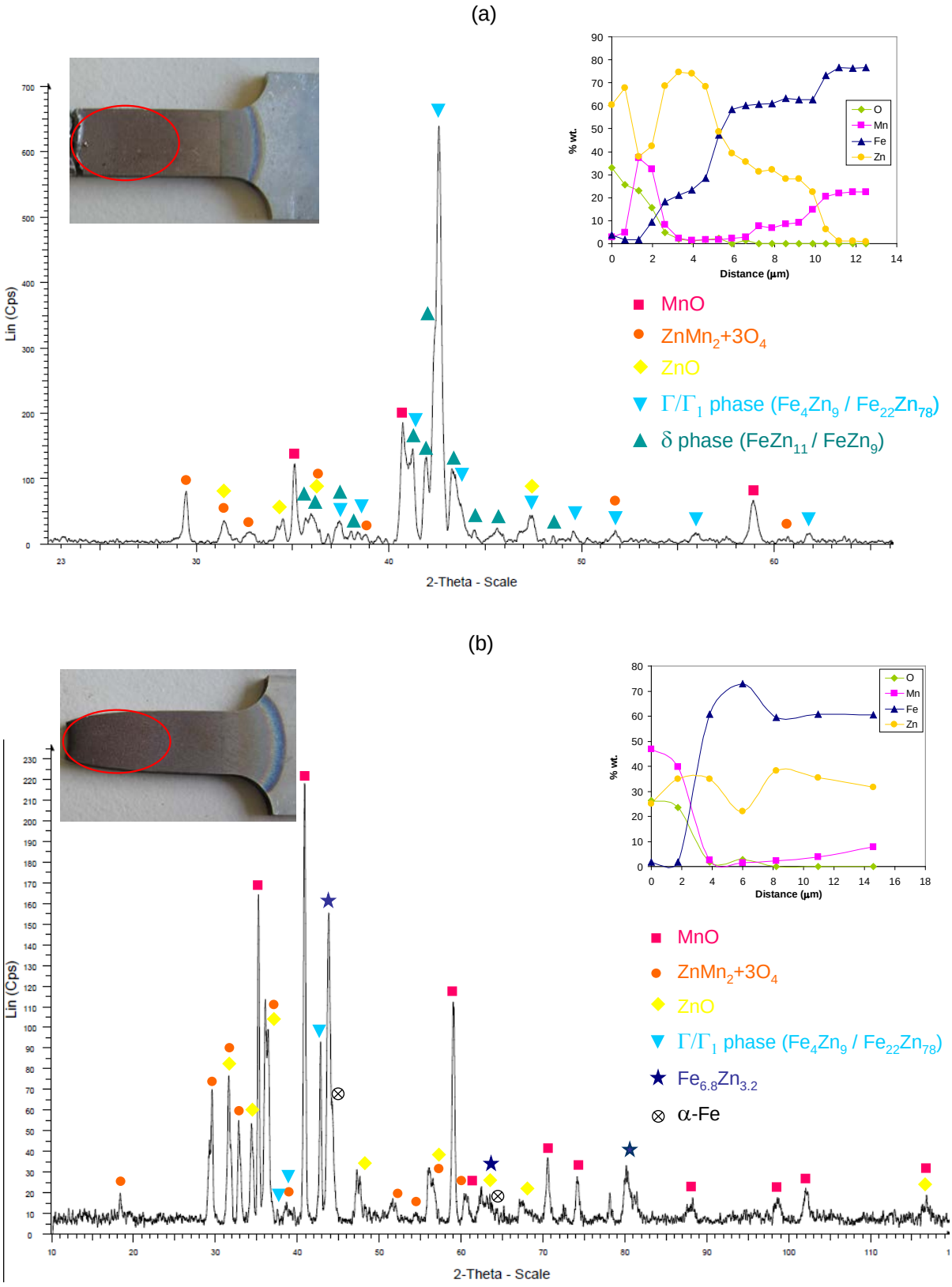

Figure IV.26. XRD patterns of specimens subjected to different thermo-mechanical treatments: (a) tensile test at 800°C and (b) holding 30s at 800°C + tensile test at 800°C

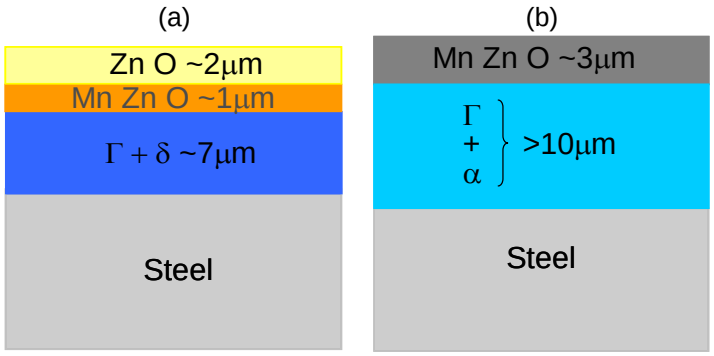

Figure IV.27. Schematic representation of the different layers formed at the interface between steel and zinc during different thermo-mechanical treatments: (a) tensile test at 800°C, (b) holding 30s at 800°C + tensile test at 800°C

These results tend to indicate that the formation of FeMnZn intermetallic compounds during holding would be involved in the ductility improvement during subsequent tensile test. A possible scenario explaining the ductility recovery after holding is described hereafter. Holding the specimen at high temperature allows the formation of large intermetallic compounds layers at the interface between steel and liquid zinc inhibiting the embrittlement during stress application. The gradual growing of intermetallic phases (and the simultaneous liquid zinc consumption) during holding may explain the progressive ductility recovery observed during subsequent tensile test (as observed in figure IV.13 (b)). If the holding is long enough, the whole liquid zinc is consumed by the growing of the intermetallic phases and no liquid zinc is available for embrittlement during tensile test anymore as illustrated in figure IV.28 (a).

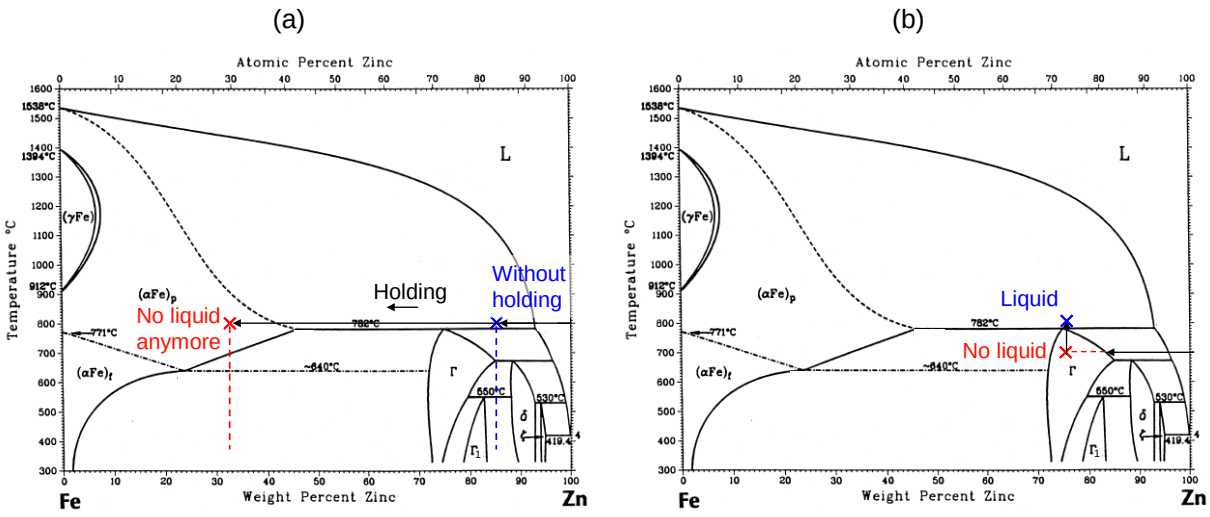

Figure IV.28. Evolution of intermetallic phases during holdings

When holding is performed at temperature lower than the tensile one, one can imagine that some less Fe rich intermetallic compounds form at the interface between the bulk steel and liquid zinc (slower kinetics at lower temperature), however, when temperature is risen up to 800°C (for tensile testing), these compounds are melted and a zinc rich liquid is available for embrittlement as illustrated in figure IV.28 (b). With increasing holding temperature, phase formation kinetics is increased, Fe-richer phases are formed and consequently, the quantity of liquid zinc at 800°C is decreased, which explain the progressive ductility recovery (as illustrated in figure IV.21). Unfortunately, no observations of specimens subjected to holding at lower temperature have been performed to determine the different phases formed during holding.

Even though manganese seems to diffuse very rapidly toward the surface, the presence of manganese may modify the phase diagram and considering the binary FeZn phase diagram is not correct. Ternary diagrams have been calculated at different temperatures and it appears that phases and transformation temperatures are not so different in the presence of manganese. Hence, the explication seems to remain valid. Nevertheless, manganese certainly modifies the phases formation kinetics (see §II.4).

II.4. DP1180 and TRIP800 steels

Holdings at temperature before tensile test have been performed on AHSS steels: DP1180 and TRIP800. Specimens are held 30s at 800°C before tensile testing at the same temperature. These holding conditions have been chosen because they are sufficient to prevent embrittlement in the case of the Fe22Mn0.6C steel. Obtained tensile curves are displayed in figure IV.29.

It must be noticed that, in both cases, ductility of bare specimens is slightly decreased after holding.

Holding EG specimens 30s at 800°C before tensile test is not beneficial for LME resistance: both steels are embrittled after holding. Actually, EG specimens, exhibit a similar mechanical behaviour with and without holding.

From these results, the hypothesis of Zn vaporization during holding at 800°C can be excluded.

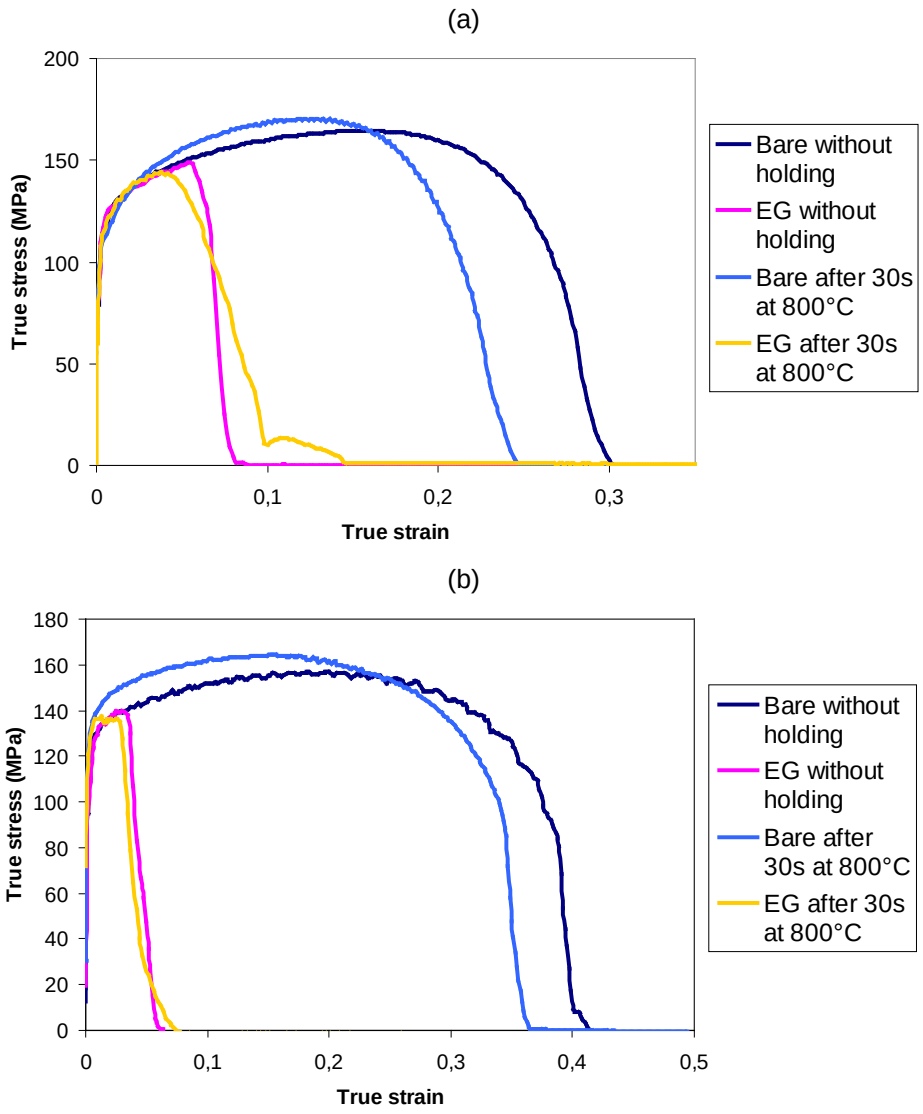

Figure IV.29. Effect of holding of 30s at 800°C on embrittlement at 800°C of two AHSS steels: (a) DP1180 steel and (b) TRIP800 steel

It appears that the ductility of the TRIP800 steel is improved for longer holding times, as illustrated in figure IV.30 where the tensile curves obtained after holdings of 30s, 1min, 2min and 5min are shown. However, holding 5min at 800°C is not sufficient to recover the whole ductility.

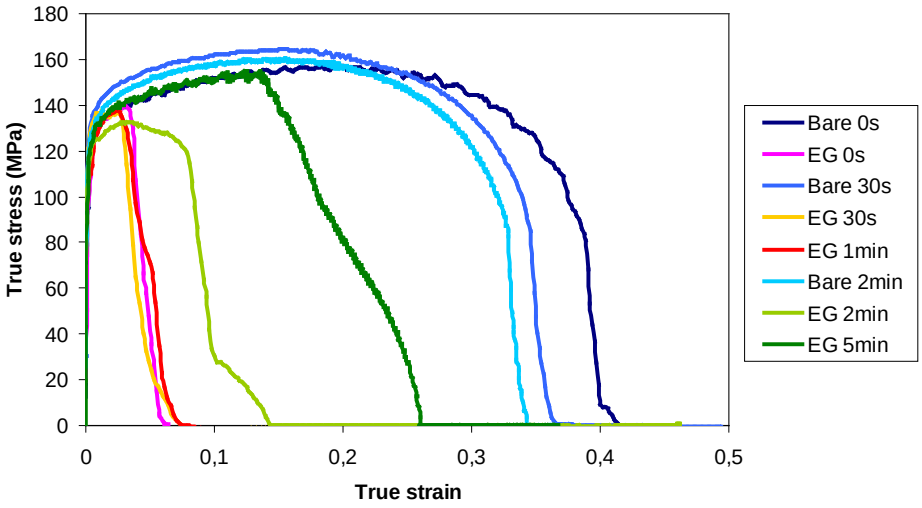

Figure IV.30. Effect of holding time on tensile behaviour of TRIP800 steel at 800°C

For the TRIP800 steel, the time required for improving ductility is much longer than for the FeMnC steel. This can be related to the differences in terms of chemical compositions (the Mn content of these steels is about ten times lower than that of the TWIP steel) as well as in terms of microstructures (at 800°C, the TRIP steel is not fully austenitic).

II.5. Conclusions

It has been shown that holding specimen at high temperature during few seconds can inhibit embrittlement by liquid zinc. Results are summarized in table IV.2. When holding and tensile test are performed at the same temperature, the time required for preventing embrittlement is between 20 and 30s whatever the temperature. At 700°C, this time is lower because at this temperature, embrittlement is less important than at higher temperature. Nevertheless, when holding is performed at a temperature lower than the subsequent tensile test, huge differences are notices in necessary times: holding 5min at 700°C is not sufficient while 30s at 775°C are enough. Furthermore, for the same holding temperature, required times are radically different according to the tensile temperature: for instance, at 700°C, 10s are enough to preclude embrittlement during tensile test at 700°C while 5min are not sufficient to reduce embrittlement during tensile test at 800°C.

EDX and XRD analyses have shown that different compounds are formed at the specimens' surfaces. On the specimen subjected to holding before tensile testing, a large Mn oxide layer and a Fe-rich FeZn compounds underneath are present. These layers are present to a lesser extent on specimens without holding. Consequently, it can be concluded that the formation of

these layers during holding would be responsible for the embrittlement suppression by consuming the liquid zinc necessary for embrittlement.

Time required to prevent embrittlement	Holding and tensile at the same T°	Holding at T + tensile at 800°C
700°C	10s	5min not sufficient
750°C	30s	5min
775°C	20s	30s
800°C	20s	-
850°C	30s	-
900°C	20s	-

Table IV.2. Holding times required to prevent embrittlement during subsequent tensile test

Tests performed under argon lead to the same results as tests performed under air. This permits to exclude the hypothesis of the formation of oxide layers during holding preventing LME.

Holding DP and TRIP steels specimens 30s at 800°C (efficient to prevent embrittlement in the case of TWIP steel) does not have any effect on embrittlement occurrence. For the TRIP steel, longer holding times (5min) are required for preventing embrittlement. These differences can be related to the different chemical compositions and microstructures between TRIP and TWIP steels.

Finally, it is worth noticing that during tensile test at low strain rate ($1.3.10^{-3}$ s^{-1}), the time of contact between the steel and the liquid zinc before achieving high stresses is very long. In addition to the critical stress, the absence of LME at lower strain rate may be related to the extended time of contact between the steel and the liquid zinc equivalent to a holding heat treatment.

It must be emphasized that the embrittlement of steel by liquid zinc is an exception to the empirical rule of LME according to which embrittled systems do not form intermetallic compounds. In the case of hot tensile test (in embrittlement conditions), the formation of intermetallic compounds is not the most spontaneous reaction. The embrittlement phenomenon occurs more rapidly. However, if time is given to the solid steel in contact with liquid zinc before stress application, the formation of intermetallic compounds, consuming the liquid, prevents embrittlement during subsequent tensile test.

III. Cracking mechanisms

It has been shown that the Fe22Mn0.6C steel is sensitive to liquid zinc embrittlement. However, the detrimental effect of liquid zinc actually occurs given the appropriate experimental conditions. It has been shown that many parameters have an influence on the embrittlement occurrence: temperature, strain rate, microstructure, wettability, stress…, and it is difficult to study the influence of a given parameter independently from the others. For example, decreasing strain rate leads to decrease mechanical properties of the steel (and particularly the mechanical strength), but it also increases the time of contact between the steel and liquid zinc. The fact that the studied steel is fully austenitic in the whole temperature range and does not exhibit any phase transformation permits to eliminate the additional parameter 'nature of phase', which is not the case when studying DP and TRIP steels.

Conditions necessary for cracking to occur have been established through two main tests: cups containing high residual stresses immersed in a liquid zinc bath and hot tensile tests performed on EG specimens.
The different tests performed with cups as well as conclusions drawn from these tests are summarized in table IV.3. It can be concluded that not only is liquid zinc necessary but a good wettability (resulting from a good surface preparation) is also required. Moreover, these results permit to outline the existence of a threshold stress (residual stress in this case). It is important to remind that cracking occurs within the 10 first seconds of immersion.

Experimental Conditions	**Observations**	**Conclusions**
Fluxed cup immersed in liquid zinc bath at 460°C	Numerous cracks are observed	All **cracking conditions are gathered**
Not fluxed cup immersed in liquid zinc bath at 460°C	Not coated No crack	A **good wettability** is necessary
Cup, previously immersed in molten salts bath, fluxed and immersed in liquid Zn bath at 480°C	No crack	**Critical stress** is necessary
Cup cut in rings of 2 and 5mm height immersed in the liquid zinc bath	Only rings at 2-15mm from the rim crack	**Critical stresses > 800MPa**

Table IV.3. Summary of tests performed on cups

However, these tests provide only qualitative results. Indeed, different parameters can not easily be measured: the measured temperature (thermocouple immersed in the bath) is not

necessarily the temperature of cup when cracking occurs and stresses are estimated by numerical simulations that do not take into account the thermal stress relieving. On the other hand, Gleeble tests provide quantitative information since all experimental parameters are recorded during the test.

The influence of many parameters has been investigated by Gleeble tests. Different points are discussed below.

Temperature is one of the most important parameter since it affects many others such as mechanical properties (and so stress level reached during tensile test or stress relieving during immersion in liquid zinc bath), microstructure (phase transformation, grains recrystallization in as rolled specimens), diffusion kinetics… Embrittlement has been observed between 420°C (cracking on cups during immersion in liquid Zn bath at 420°C) and 950°C (Gleeble tests), that is to say in the whole temperature range of liquid zinc. However, embrittlement occurs within a limited temperature range defined for a set of experimental conditions (strain rate, microstructure…) as illustrated in figure IV.31.

It is difficult to conclude if the ductility trough is directly related to the effect of temperature or to the indirect effect of temperature on an other parameter.

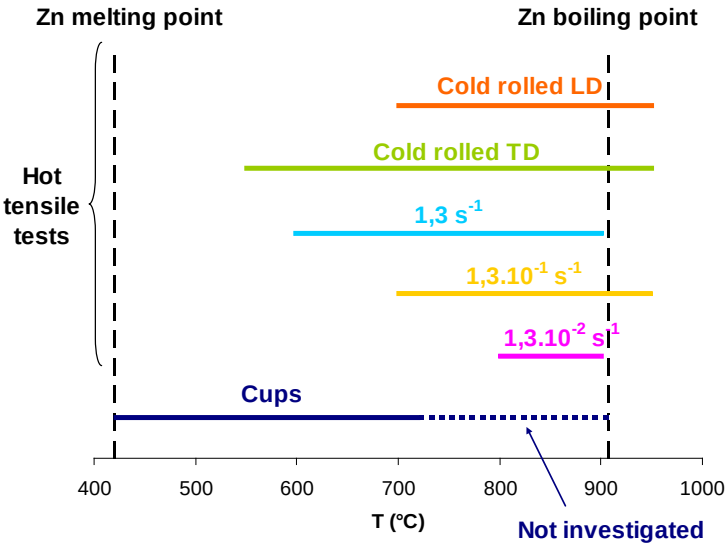

Figure IV.31. Temperature range of brittleness for different experimental conditions

As shown by immersions in liquid zinc, a minimal stress is needed to initiate cracking. Indeed, if steel free of stress (without residual or applied stresses) is in contact with liquid zinc, no detrimental effect of liquid zinc is observed. It can be supposed that without tensile stresses, liquid zinc does not penetrate steel's grain boundaries. Specimens immersed as long

as one hour in liquid zinc bath exhibit normal behaviour during tensile test at room temperature.

Tests performed on cups permit to estimate the threshold stress at about 800MPa. The evolution of this stress with temperature is difficult because of thermal relieving. Gleeble tests permit to precisely determine the critical stress. The latter strongly depends on temperature: it sharply increases with decreasing temperature so that at lower temperatures (<600°C), it is probably higher than the UTS and cannot be reached during tensile test. But if this stress is present in cup as residual stress, as soon as the steel is in contact with liquid zinc, cracking occurs. The critical stress also depends on strain rate and on microstructure (in the same experimental conditions, as rolled specimens are embrittled for higher critical stress than recrystallized ones). The evolution of critical stresses obtained in each case with temperature is displayed in figure IV.32.

The threshold stress is necessary for crack initiation but also for its propagation. Indeed, if tensile test is stopped once critical stress has been reached, cracks initiate on surface specimen but do not propagate through the whole specimen's thickness (see figure III.14).

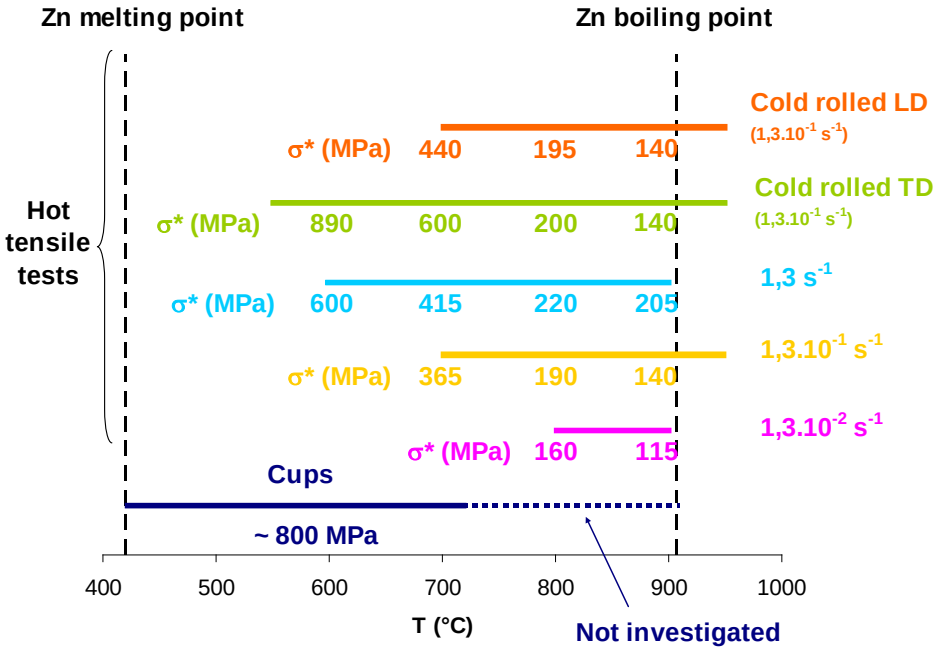

Figure IV.32. Critical stress for different experimental conditions

It appears that austenite is sensitive to embrittlement by liquid zinc. The TWIP steel is fully austenitic in the whole studied temperature range. Consequently, the influence of this parameter can not be determined. However, hot tensile tests performed on DP and TRIP steels reveal that they become sensitive when a sufficient amount of austenite is present. This is of

great interest since during welding processes many steels undergo austenite transformation which strongly increases the risk of liquid zinc embrittlement.

Microstructure, and particularly grains size and shape, has a significant influence on LME occurrence as demonstrated by tests performed on cold rolled specimens in transverse and longitudinal directions: TD specimens are more sensitive to embrittlement than LD ones. This could be explained as follows: in TD specimens, grains are elongated along direction normal to tensile axis contrary to LD specimens, where they are elongated in the tensile along tensile axis. As a consequence, the grain boundary path to cross the specimen is shorter in TD specimen than in LD ones as illustrated in figure IV.33. So, less liquid zinc is required to go through the whole thickness in TD specimens than in LD specimens. This could explain why TD specimens are more sensitive than LD specimens. Moreover, the average stress on the grain boundary is higher in the TD case than in the LD one.

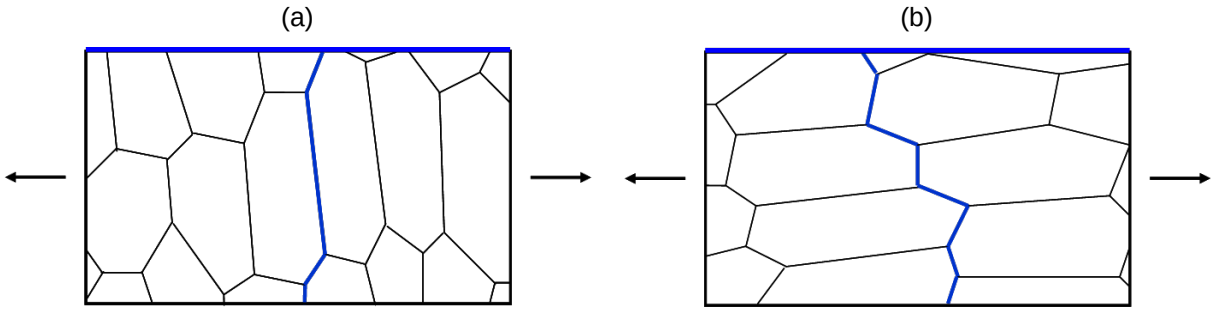

Figure IV.33. Cracks propagation at grains boundaries in cold rolled specimens: (a) TD and (b) LD specimens

Time is also an important factor. The time of contact between steel and liquid zinc has been modified by varying strain rate or by performing holding before tensile testing. When this time is long (low strain rate or holding), reactions occur between steel and liquid zinc inhibiting embrittlement. EDX and XRD analyses have shown that during holding, Mn diffuses from the substrate towards the surface and FeZn intermetallic compounds form at the interface between the bulk steel and liquid zinc consuming the latter. It is important to remind that tensile tests are performed in air environment. Tensile tests performed under argon lead to the same results: holding EG specimens 30s at temperature permits to inhibit embrittlement during the subsequent tensile test. Even if phases formed during holding under argon have not been identified and the diffusion of Mn toward the surface has not been checked in this case, this result seems to indicate that oxidation is not responsible for embrittlement suppression after holding. The ductility recovery observed after holding would be caused by the formation

of intermetallic compounds consuming the liquid zinc and so, preventing embrittlement during subsequent tensile test.
However, when the time of exposure before reaching critical stress is short (very high strain rate), embrittlement severity seems to decrease. This means that phenomenon involved in embrittlement require a minimum time to occur.

From these conclusions, a scenario of embrittlement and resulting cracking can be proposed:

- Grain boundary penetration of zinc because of high tensile stresses and good wettability

- Opening of crack along zinc penetration path because of tensile stresses as illustrated in figure IV.34 (a).

If tensile stresses are not sufficient enough (thermal stress relieving in cup or tensile test at low strain rate), liquid zinc does not penetrate grain boundaries and no embrittlement occurs as shown in figure IV.34 (b).
If an oxide layer is present between steel and liquid zinc (not fluxed cup), neither grain boundary penetration nor embrittlement is possible (figure IV.34 (c)). Depositing a layer between steel and zinc coating could be a solution to avoid cracking during hot temperature processes by inhibiting contact between steel and the embrittling metal.
Finally, if austenite amount is not sufficient (multiphase steel), embrittlement does not occur (figure IV.34 (d)).

(a)

Critical stress + liquid zinc + good wettability

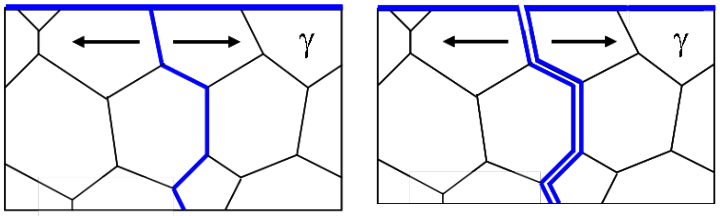

(b)

Liquid zinc + good wettability BUT no critical stress

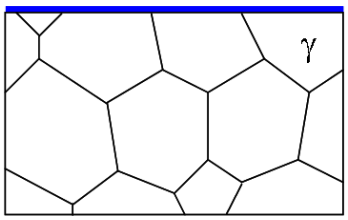

(c)

Liquid zinc + critical stress
BUT not good wettability

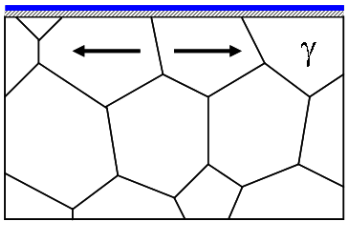

(d)

Liquid zinc + good wettability + critical stress
BUT no austenite

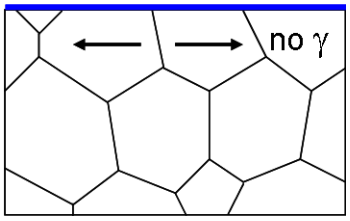

Figure IV.34. Summary of different experimental conditions

However, we can wonder whether the penetration and resulting cracking occurs sharply or progressively. Does crack initiate along zinc penetration path and propagate further (figure IV.35 (a))? Or is the presence of liquid zinc at the crack tip necessary for crack propagation? This scenario is illustrated in figure IV.35 (b):

(i) liquid zinc penetrates at grain boundaries along a certain distance

(ii) crack opens along this distance and is filled in with liquid zinc

(iii) liquid zinc penetrates further than crack tip

(iv) crack opens along zinc penetration path and so on.

The fact that cracks do not propagate through the whole specimen's thickness when tensile stress application is stopped during tensile test lets think that crack propagation is progressive.

(a)

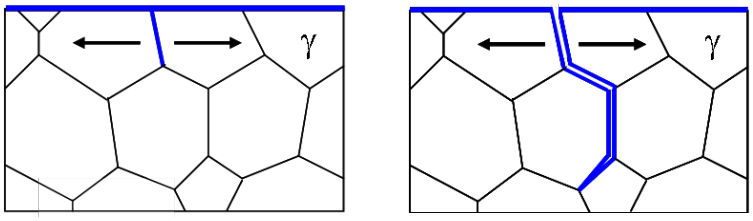

(b)

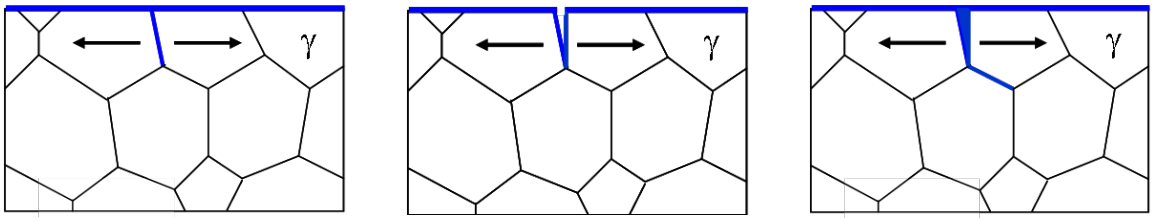

Figure IV.35. Possible scenarios of liquid zinc penetration and crack propagation

Conclusions

Hot tensile tests carried out on galvanized or annealed EG specimens show that the observed embrittlement is identical whatever coating. Testing multiphase steels permits to investigate the influence of constituent phases and particularly austenite. Austenite appears to be more sensitive to liquid zinc embrittlement. This is of great interest since many steels undergo austenite transformation during high temperature processes such as welding.

The effect of time of exposure before testing has been investigated by performing holding at high temperature. Results have shown that holding specimen few seconds at high temperature permits to inhibit embrittlement during subsequent tensile test. The necessary holding time depends on holding temperature and tensile temperature. Mechanisms involved in this ductility recovery are still unclear.

Finally, the necessary conditions for embrittlement to occur have been detailed and a scenario of cracking is proposed.

Chapter V. Links with spot weld cracking

Conditions leading to embrittlement of the steel by liquid zinc have been established from hot tensile tests. Several parameters have an influence on LME occurrence. Among them, temperature, strain rate and stress can be cited. The natural following question is to wonder whether these conditions can be experienced during spot welding of the studied steel.
As direct measures of relevant parameters during welding cycle are arduous due to high temperatures and small size of HAZ, numerical simulation permits to obtain good approximations. The first part of this chapter presents the results of such simulations.
Then, different welding experiments aiming at verifying simulation results and defining the critical welding conditions are described.
Finally, possible solutions permitting to avoid cracking during welding are proposed.

I. Simulations

In order to determine the thermal cycle experienced during spot welding of the studied steel, simulations have been computed with the software Sorpas which is dedicated to simulations of resistance spot welding processes [SWA 08]. The model used is illustrated in figure V.1 (a). The configuration geometry allows an axisymmetric representation. Design (geometry and combinations of materials to be welded, electrodes geometry and material) and welding (process parameters settings and water cooling of electrodes) parameters are directly input using an interface. Three virtual materials are added in order to represent the interfaces electrode-sheet and sheet-sheet. Tools 1 and 2 shown in figure V.1 (a) permit current intensity and pressure applications and tools 3 and 4 model the thermal transfer between electrode and water. Mesh is automatically generated.
Different boundary conditions such as thermal and electrical resistances at sheet-sheet and sheet-electrode interfaces or heat transfer through water cooled electrodes are included in the model.

The thermo-physical and mechanical properties (thermal conductivity, specific heat, density, coefficient of thermal expansion, electrical resistivity, Young's modulus, Poisson's ratio and

mechanical behaviour) of the studied steel have been supplied by ArcelorMittal. The database of the software contains also these properties for the electrodes alloys (CuCrZr).

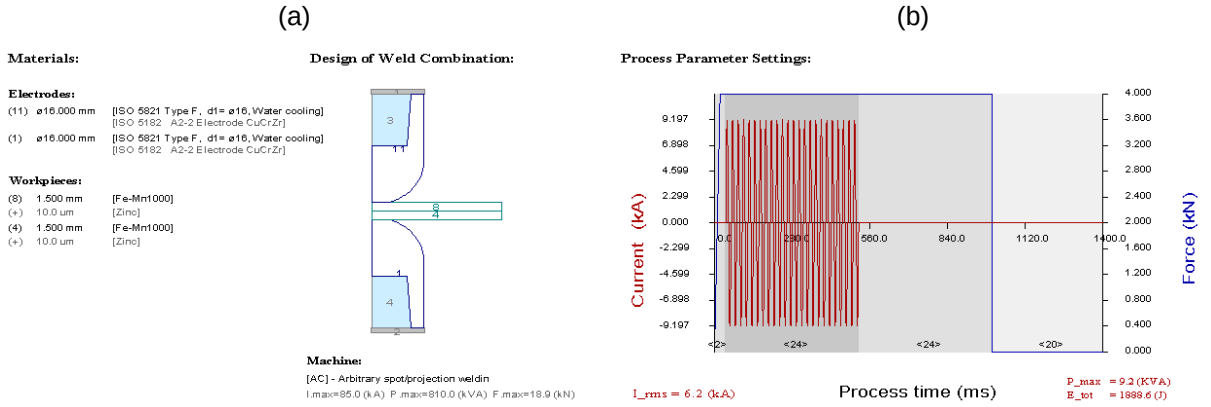

Figure V.1. (a) Materials and (b) process parameters used for Sorpas simulations

Simulations have been performed for homogenous assembly of 1.5mm Fe22Mn0.6C steel sheets. The welding conditions are detailed in table V.1 and displayed in figure V.1.

Electrode	Welding time [cycles][1]	Holding time [cycles][1]	Force [daN]	Welding current [kA]
F16	24	24	400	6.2

Table V.1. Welding parameters used for Sorpas simulations

The thermal cycle experienced during spot welding can be determined at each node. As liquid zinc can be found at the sheet's surface and so, cracking is likely to initiate in this zone, temperatures reached in this zone have been particularly studied. Figure V.2 reports results of simulation. The evolution of temperature at the electrode indentation edge with time is shown. This node has been chosen because it corresponds to the preferential site of observed cracking [BOU 07]. For this set of parameters, the temperature is much higher than Zn melting temperature (420°C), which confirms that liquid zinc is present at the sheet's surface. The peak temperature is about 700°C which is in the range of Gleeble tests and embrittlement conditions. Moreover, the heating rate is higher than 1000°C/s.

It is important to note that these thermal simulations have been experimentally checked by measuring the diameter of the fusion zone (by optical microscopy) in [DAN 09].

[1] 1cycle=1/frequency (50Hz)

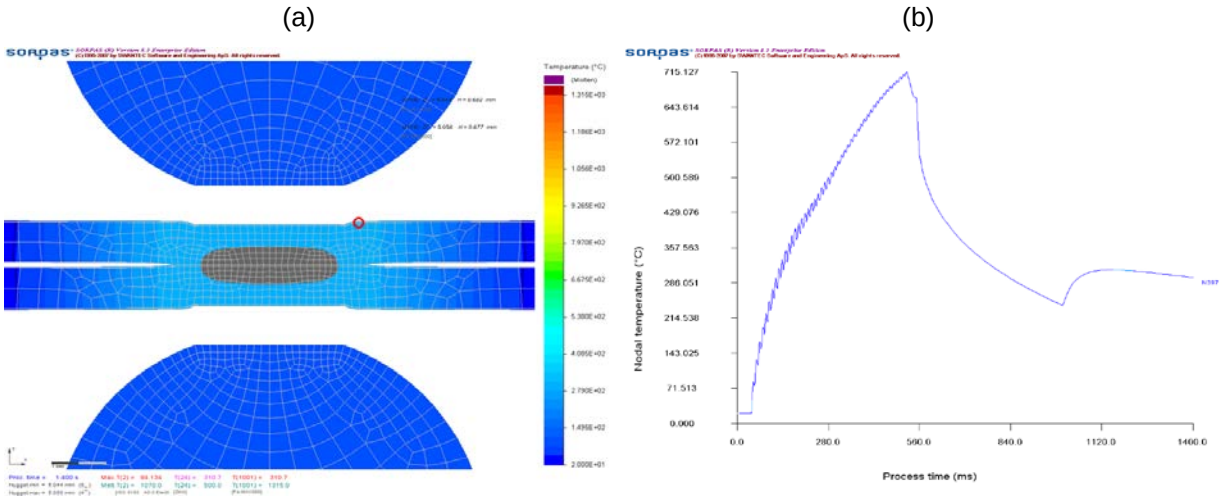

Figure V.2. Results of numerical simulations using Sorpas: (b) evolution of temperature with time during process at the node shown in (a)

Gleeble tests results demonstrate that for cracking to occur the presence of liquid zinc must be associated with particular temperature, strain rate and stress. This thermal simulation reveals that temperature reached at crack initiation site is close enough to the one experienced during Gleeble experiment. However, the calculated heating rate is much higher than the one used for Gleeble experiment as discussed in the next part. Now, the mechanical conditions ($\sigma, \dot{\varepsilon}$) during welding must also be compared to validate our approach of LME by hot tensile test.
For doing so, thermo mechanical simulations have been computed with the software Sysweld permitting to calculate at each node the stress state generated during spot welding process.

Similarly to Sorpas, the geometry of the model is defined by entering electrode and sheets parameters as illustrated in figure V.3 (a). Mesh is automatically generated. Boundary conditions are included in the model: group 1 for current intensity and pressure application, group 2 for thermal transfer between electrode and water, group 3 for thermal transfer between electrode and air, group 4 for thermal transfer between electrode and sheet and group 5 for electrical, thermal, metallurgical and mechanical properties of electrodes. Electro thermal contact resistances between electrode and sheets (E-S), and sheet 1 and sheet 2 (S-S) with respect to temperature are defined in the function file available in Sysweld database. Process parameters settings (intensity frequency, intensity and number of periods, squeezing force and number of periods) are directly input using interfaces as shown in figure V.3. (b). The material database file has been built from electro-thermo-mechanical properties supplied by ArcelorMittal.

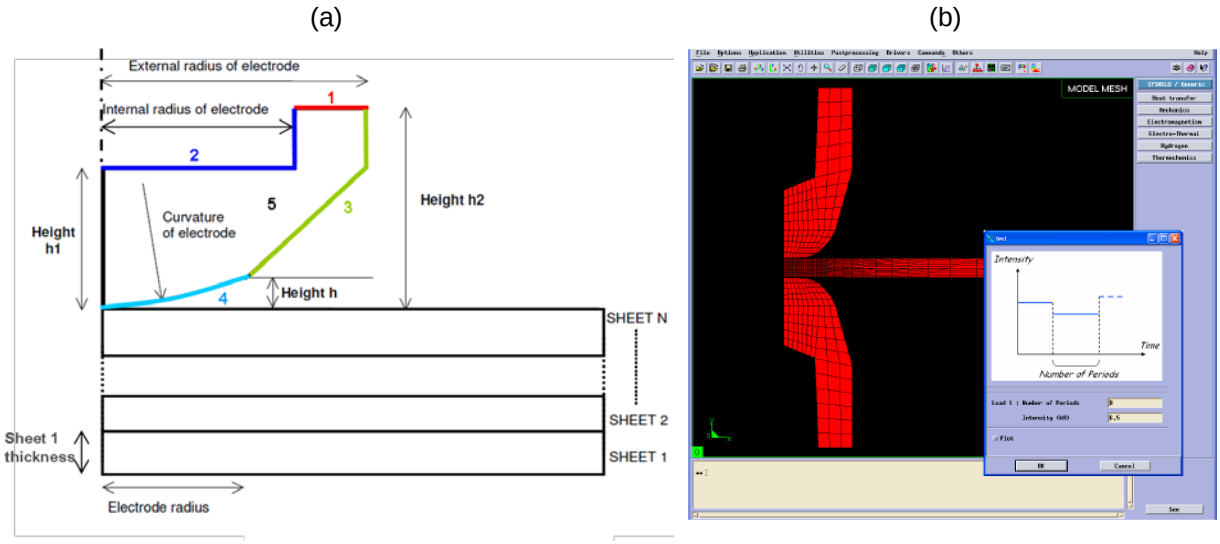

Figure V.3. (a) Schematic representation of model geometry. (b) Resulting meshing and input of electrical settings [ESI 08]

Spot welding simulations of two 1.5mm thickness sheets have been performed in the up welding range [MAR 10]. The welding parameters are detailed in the table V.2. The zinc coating has not been taken into account in simulations since its influence on the mechanical response can be considered as negligible (when LME is not considered).

Electrode diameter [mm]	Welding time [cycles]	Holding time [cycles]	Force [daN]	Welding current [kA]
8	3(7+2)	15	450	6.5

Table V.2. Welding parameters used for Sysweld simulations

The thermal cycle calculated with Sysweld is similar to the one obtained with Sorpas. As Sorpas thermal simulations have been experimentally validated in [DAN 09], one can conclude that Sysweld correctly describes the welding cycle.

The evolution of strain and stress at the sheet's surface in the HAZ (zone 3 in the figure V.4 (c)) during the welding cycle are illustrated in figure V.4 (a) and (b) respectively. Results confirm that temperature and strain rate experienced during spot welding cycles in the HAZ are coherent to what obtained during Gleeble tests. Indeed, temperature (~800°C) and strain rate (~0,044s^{-1}) obtained from simulations correspond to conditions found as necessary for LME to occur during Gleeble tests ([800-900°C] at 0,013 s^{-1} and [700-950°C] at 0,13 s^{-1}).

The magnitude of stresses obtained from simulations (100MPa) is not that different from the critical stresses determined from Gleeble tests (≥120MPa). However, numerical simulations indicate that stresses generated at the electrode indentation edge are compressive (-100MPa). LME is generally investigated during tensile tests and very few data can be found in literature concerning LME in the presence of compressive stresses. Nevertheless, in cups, cracks propagate in the inner surface where stresses are entirely compressive according to FE simulations (figure II.4). Therefore, LME under compressive stresses may be considered.

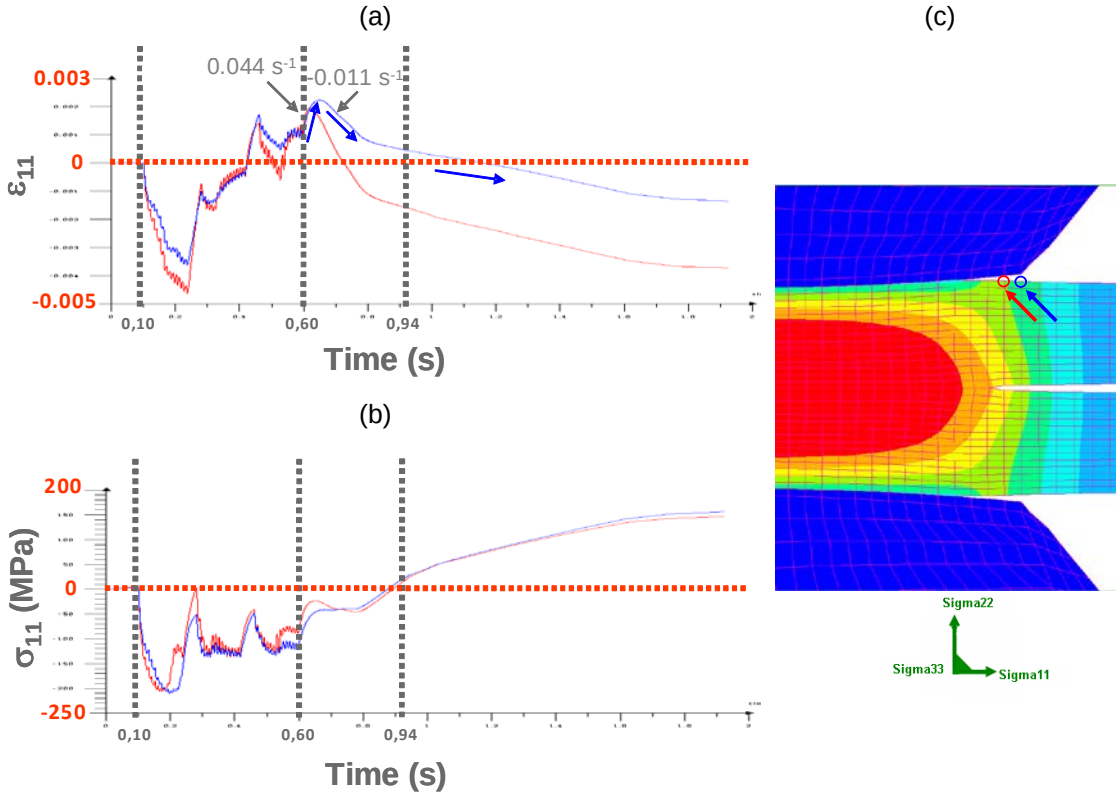

Figure V.4. Evolution of (a) strain and (b) stress during spot welding of two FeMnC 1.5mm sheets at two nodes shown in (c) after Sysweld simulations [MAR 10]

Numerical simulations of homogeneous assembly show that liquid zinc is present at the sheet's surface during spot welding process and reached temperatures and strain rates are in the range of embrittlement conditions. It is more difficult to conclude about critical stress since compressive stresses are generated by the thermo-mechanical cycle according to the FE simulation and no investigation of liquid zinc embrittlement during compressive solicitation have been carried out.

Moreover, thermo-mechanical cycle modifies the steel's microstructure. Even if the studied steel does not exhibit any phase transformation, the microstructure and particularly the grain size can be modified by the thermo-mechanical cycle underwent during spot welding. As shown in chapter III, the microstructure is an important parameter in LME occurrence. This parameter is not taken into account in simulations. Besides, if the studied steel is welded to different steels, one can reasonably imagine that stresses generated in steel are much higher due to differences in physical properties (coefficient of thermal expansion for instance). No simulations have been made to check this point.

II. Influence of heating rate

In the previous paragraph, it has been shown that heating rates experienced during spot welding are around 1000°C/s. Hot tensile tests have been performed at a heating rate of 80°C/s. Consequently, the influence of heating rate on embrittlement must be investigated in so far as embrittlement observed during tensile tests could have been underestimated compared to welding conditions.

The influence of heating rate has been studied at three testing temperatures for which embrittlement is observed with a heating rate of 80°C/s: 700°C, 800°C and 900°C. Tensile tests have been performed at a strain rate of $1{,}3.10^{-1}$ s^{-1} and three heating rates have been compared: 10°C/s, 80°C/s and 1000°C/s. Tensile curves are shown in figure V.5.

For the lower heating rate (10°C/s), it can be observed that:

- at 700°C, embrittlement is not observed since curves obtained for bare and EG specimens are identical

- at 800°C and 900°C, the embrittlement obtained with this heating rate is similar to the one obtained with higher heating rates.

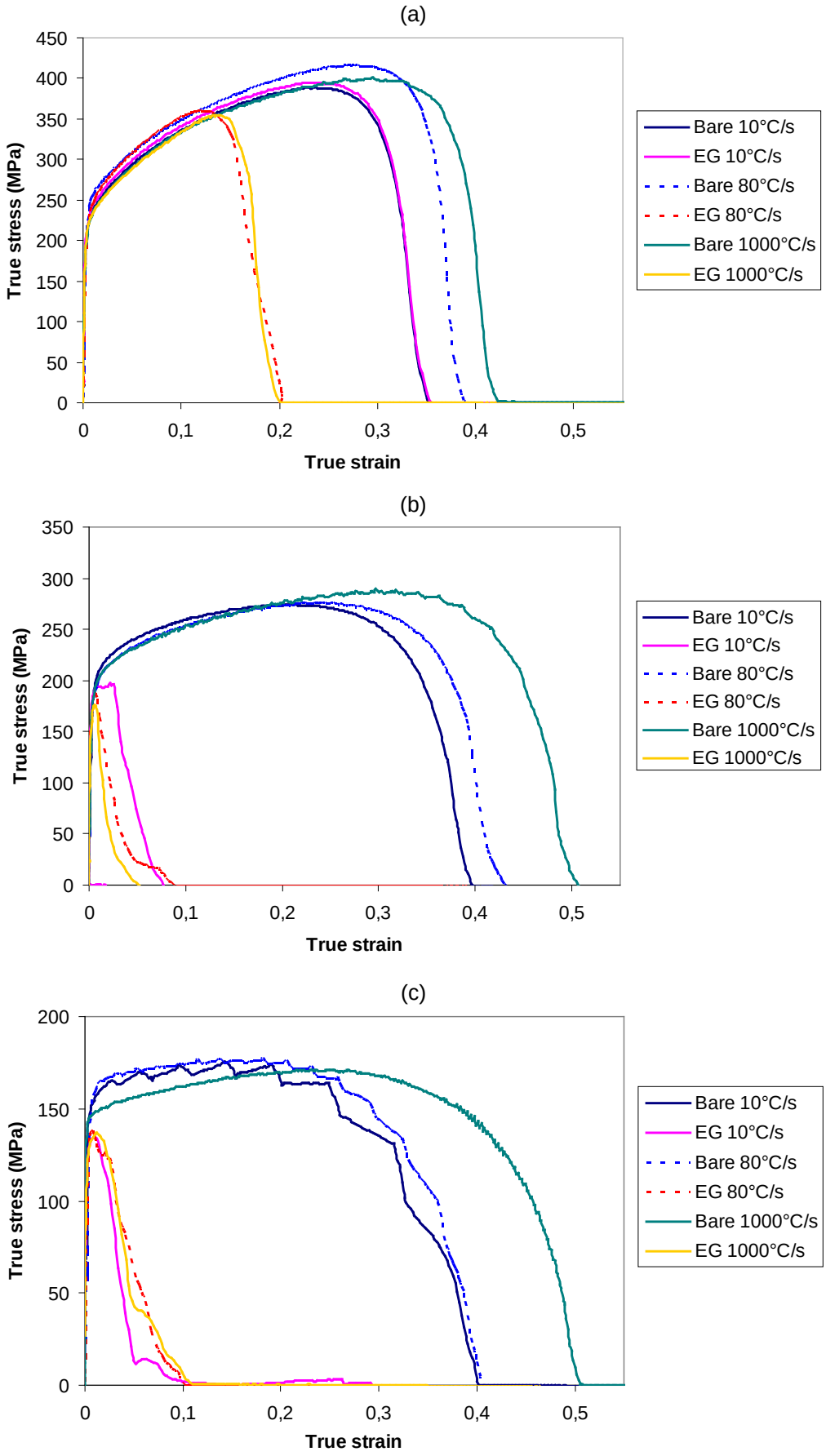

Figure V.5. Influence of heating rate on tensile behaviour at (a) 700°C, (b) 800°C and (c) 900°C

The effect of heating rate is linked to the time where contact between the steel and the liquid zinc is effective before stress application: it increases with decreasing the heating rate. As previously described in chapter III, holding the specimen a few seconds at 700°C before tensile test at the same temperature prevents embrittlement. At 800°C and 900°C, the necessary holding time is higher and so, 10°C/s is not slow enough to reduce embrittlement.
This heating rate is not appropriate to investigate LME since results obtained at 700°C could have led to the wrong conclusion that the steel is not sensitive to LME a this temperature; higher heating rates are required.

For the three testing temperatures, embrittlement observed with a heating rate of 1000°C/s is similar to that obtained with a heating rate of 80°C/s. Hence, embrittlement has been correctly described by tests carried out with heating rate of 80°C/s, and the obtained results can be correlated to welding conditions.

III. Welding experiments

With standard welding conditions, no crack has been observed on homogeneous (Fe22Mn0.6C EG 1.5mm /Fe22Mn0.6C EG 1.5mm) spot welds. This absence of cracking confirms the results of simulations: embrittlement conditions are not experienced during standard homogeneous spot welding.
In order to find the critical welding conditions, different experiments were performed with the aim of creating additional tensile stresses in sheets.

III.1 Welding with spacers

In order to create additional tensile stresses in sheets, two sheets of 1,5mm thickness were welded with spacers between sheets (figure V.6 (a)). To investigate the influence of zinc, two configurations have been welded: bare/bare and EG/EG. The height of gaps was varied from 1 to 3 mm and different process parameters such as current intensity and electrodes alignment were also modified. Detailed welding parameters are listed in table V.3. Moreover, to create additional stresses, 10 spots per sheet were performed in a specific order: the firsts were made at each tip, and the following spot was made in the middle of the two previous ones so that last points are clamped as illustrated in figure V.6 (c). Length between spots is about 38mm. Numerous combinations of gap height, current and electrode alignment have been tested, in

particular the ones providing the most severe conditions for steel specimen. Then, spots were analysed by X-Ray imaging and optical microscopy observations.

Even with very severe conditions, no crack has been detected (figure V.7).

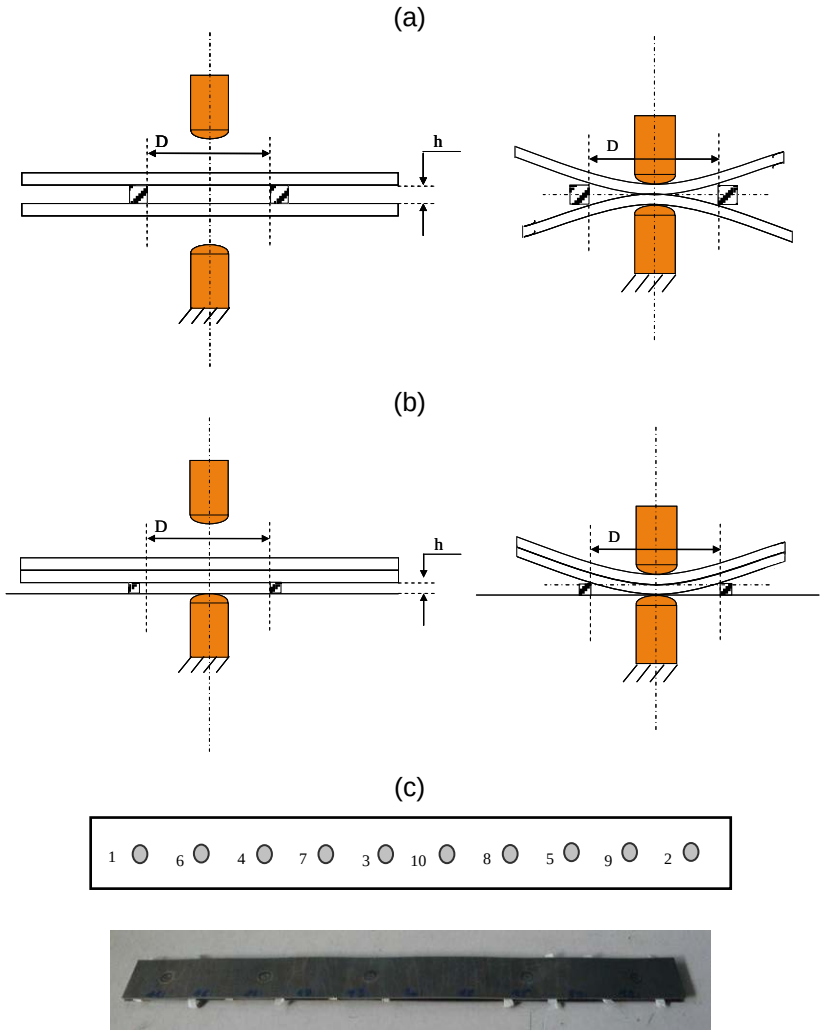

Figure V.6. Configurations for welding with (a) gaps between sheets, (b) gaps under sheets (c) in a specific order

Gaps	Electrode	Welding time [ms]	Holding time [ms]	Force [daN]	Welding current [kA]	Gap height [mm]	Electrode misalignment [mm]
Between sheets	F16 ϕ6mm	480	480	400	5.4 - at splashing	1 - 2 - 3	0 - 1
Under sheets	F16 ϕ6mm	480	480	400	6.2 - 6.6	3 - 5 - 6	0

Table V.3. Welding parameters

Figure V.7. Cross section observation of spot weld with 3mm gaps between sheets

The second experiment is based on the same principle, but spacers are placed under sheets so that tensile stresses are created at the lower surface of each sheet as illustrated in figure V.6 (b). The height of gaps was varied from 3 to 6 mm. Current intensity was varied and pre heating (120ms, 4kA) was performed in some specimens. Detailed welding parameters are listed in table V.3. Spots were then, analysed by optical microscopy observations.

Small surface cracks of about 50µm depth are present on some specimens but the presence of crack is not systematic. As shown in figure V.8, cracking can occur under the electrodes or in the electrode indentation edge on the lower surface where gaps were placed.

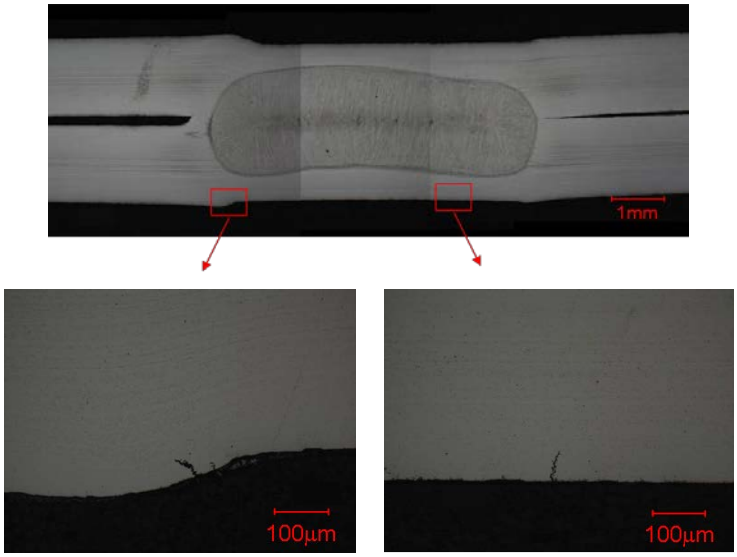

Figure V.8. Cross section observations of spot weld with 3mm gaps under sheets

These observations lead to the conclusion that the combination of thermal/mechanical/microstructural conditions for occurrence of LME is encountered only in very specific cases. Moreover, it does not seem to be that reproducible in welding conditions. It highlights the fact that the methodology of the Gleeble test developed during this PhD is worth since it provides a reproducible index of sensitivity to LME.

III.2 Welding of scratched sheets

Spot welds have been preformed on scratched EG sheets of 1,5mm thickness, with the idea that cracks may initiate from those defects. Two configurations were tested: one with the scratched surface outside and one with the scratched surface at the interface of the two sheets as illustrated in figure V.9. The critical combination FeMnC EG 1.2mm/Usibor 2.5mm/Usibor 1.75mm was also spot welded with scratches in FeMnC sheet surface.

Welding parameters are listed in table V.4.

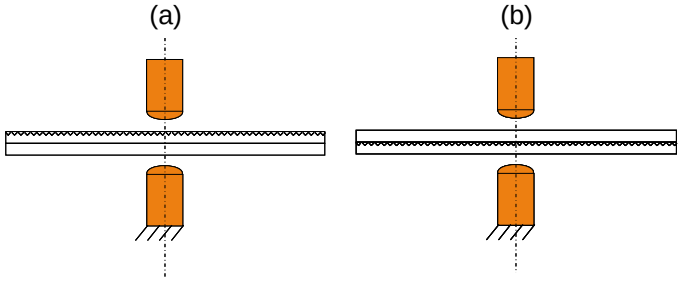

Figure V.9. Two configurations with (a) the scratched surface outside and (b) the scratched surface at the interface of the two sheets

Electrode	Welding time [cycles]	Holding time [cycles]	Force [daN]	Welding current [kA]
TH8	3(9+2)	20	450	6 for FeMnC/FeMnC 7 for FeMnC /Usibor/Usibor

Table V.4. Welding parameters

Cross sections of the spot welds were examined by optical microscopy. Figure V.10 shows optical micrographs of cross sections of FeMnC/FeMnC and FeMnC/Usibor/Usibor spots welds with external scratches for both. No crack can be observed and more generally, crack has never been observed.

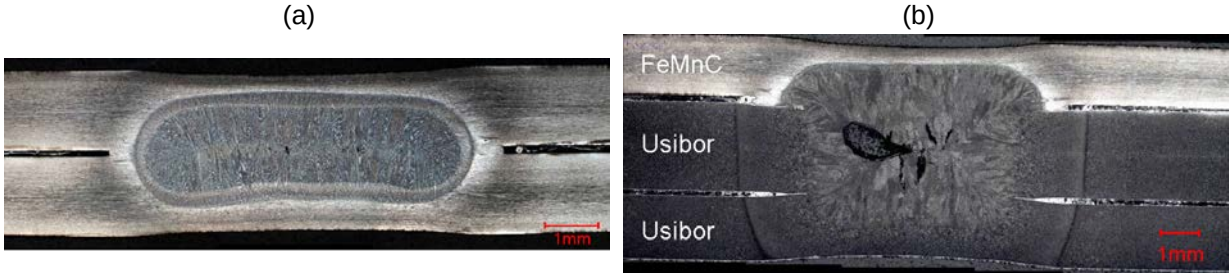

Figure V.10. Optical micrographs of cross sections of (a) FeMnC/FeMnC and (b) FeMnC/Usibor/Usibor spots welds with external scratches for both

These results highlight the difficulty in producing cracks during spot welding of the studied steel. Surface cracking has been observed in very severe conditions (high spacers under the sheets and in the up welding range creating higher stresses) and the observed cracks are not deeper than 50μm.

This difficulty in obtaining cracking tends to confirm that embrittlement conditions are not experienced during standard homogeneous spot welding.

During heterogeneous welding, higher stresses can be generated in steels due to differences in thermal-mechanical characteristics (coefficient of thermal expansion for instance) which can increase the risk of embrittlement. However, this case has not been widely investigated in this study. Moreover, in industrial processes, spot welding guns are widely used. This process is likely to generate higher stress levels.

III.3 Influence of expulsion on cracking

It has been noticed that surface cracking is very often observed on welds with expulsion as illustrated in figure V.11.

Besides, by recording the evolution of the force during the spot welding cycle, it can be observed that the force sharply increases (>10kN) during expulsion as shown in figure V.12 which could induce an increase of stress and/or strain rate. In this case, one can think that stresses achieve critical stress and so, all embrittlement conditions are present.

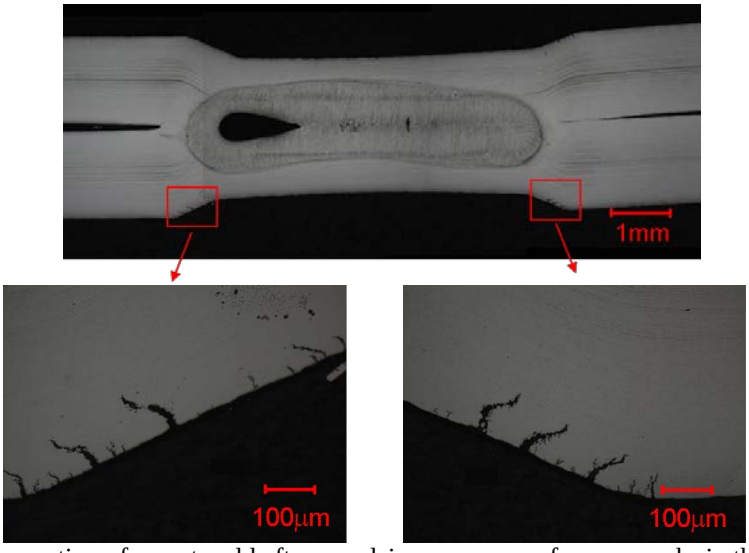

Figure V.11. Cross section of a spot weld after expulsion: presence of many cracks in the indentation edge

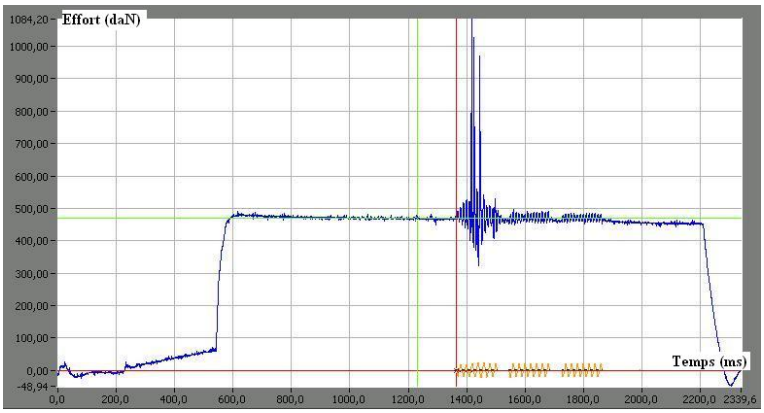

Figure V.12. Evolution of the force during spot welding and particularly during expulsion

IV. Solutions to avoid cracking during spot welding

In previous parts, it has been shown that cracking is quite rare during spot welding of the studied steel in standard conditions (although heterogeneous assemblies have not been widely investigated). Nevertheless, cracking has been observed during other welding processes used in the automotive industry, particularly during arc welding (MIG brazing).

Conclusions drawn from Gleeble tests and solutions proposed hereafter can just as well be applied to other welding processes.

In the light of Gleeble tests results and spot welds experiments, different solutions can be proposed to reduce the risk of embrittlement by liquid zinc:

- **Increasing the time of contact between the steel and liquid zinc before stress application**

  It has been shown that holding specimens few seconds at high temperature before tensile test is sufficient to prevent embrittlement. Hence, a preheating can be performed (figure V.13 (a)).

  Moreover, decreasing the heating rate to 10°C/s is sufficient to prevent embrittlement during subsequent tensile test at 700°C. Consequently, applying the current progressively (up slope), as illustrated in figure V.13 (b), can be a solution for decreasing the heating rate.

- Decreasing stresses generated during welding process

The first point is to avoid welding in the up welding range to limit the risk of expulsion and decrease stress level.

Secondly, in order to decrease the cooling rate and the resulting stresses, a down slope can be performed (figure V.13 (c)).

- Preventing contact between the substrate and the liquid zinc

As described in chapter I, § III.3.1, an intimate contact between the solid metal and the liquid one is necessary for LME to occur. Depositing a buffer layer at the solid metal surface (see figure V.13 (d)) acting as a barrier between the solid metal and the embrittling liquid metal precludes contact between them and could inhibit embrittlement. However, the buffer layer must be impermeable to liquid zinc, must be ductile enough to withstand large deformations and must offer a good adhesion to the steel and zinc as well.

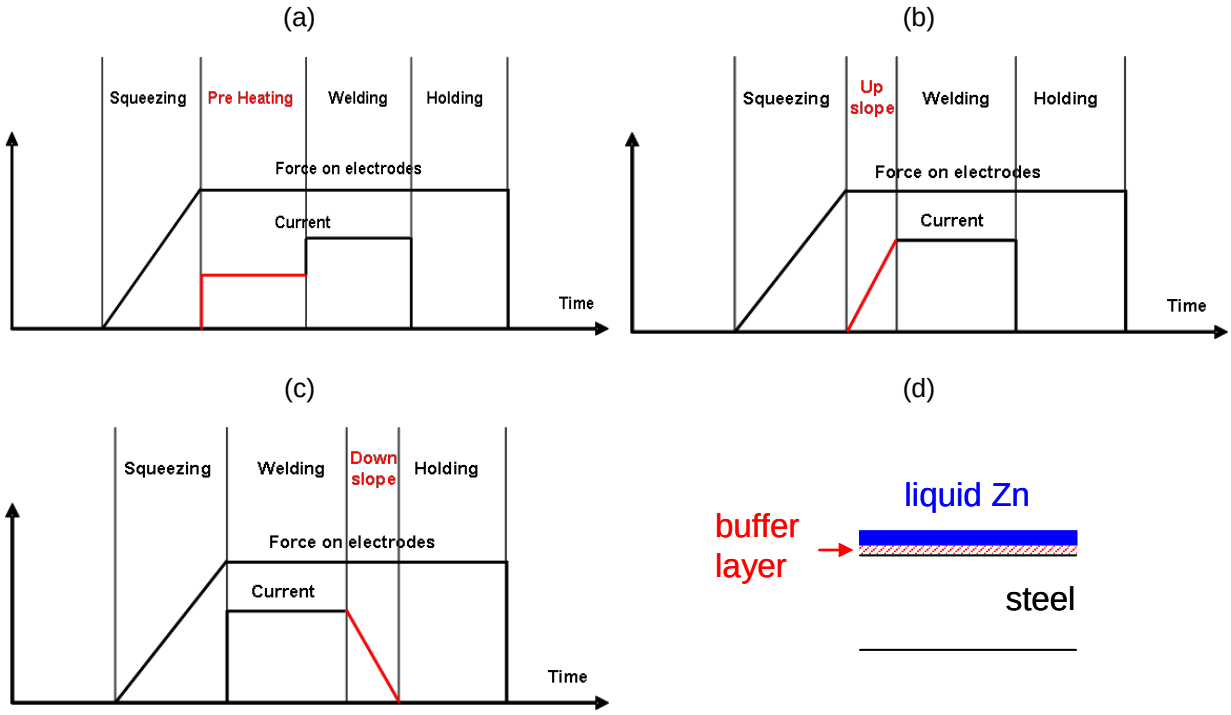

Figure V.13. Different suggestions for reducing the risk of embrittlement by liquid zinc: (a) preheating, (b) up slope and (c) down slope during welding cycle and (d) depositing of a buffer layer between the steel and zinc coating

Conclusions

Numerical simulations provide good approximations of thermo-mechanical cycles experienced during spot welding process. Spot welding simulations of Fe22Mn0.6C steel in homogeneous configuration and standard conditions permit to determine the evolution of temperature, strain and stresses during process.

Temperature and strain rate are in good agreement with critical values determined from Gleeble tests. Heating rate during welding (>1000°C/s) is much higher than the one used during Gleeble tests (80°C/s), but it has been shown that embrittlement conditions do not differ with higher heating rate.

However, stress level estimated from simulations is compressive whereas Gleeble tests provide tensile critical stresses. This can explain why cracking has never been observed in spots welded in standard conditions. Hence, different spot welding tests have been carried out in order to generate tensile stresses. Few cracks are observed in assemblies welded with spacers placed under sheets. Many cracks are present in welds with expulsion. The sharp increase of force during expulsion could explain the presence of these cracks.

Even if cracking of the studied steel seems to be very rare in standard welding conditions, solutions can be proposed for reducing the risk of embrittlement. Three points are given to consider: increasing the time of contact between the steel and liquid zinc before welding, decreasing stress generated during cooling and preventing contact between the steel and liquid zinc by depositing a buffer layer.

Conclusions

The objective of this PhD was to understand the cracking occurring during spot welding of electrogalvanized austenitic TWIP steel with the aim of preventing this phenomenon. It appears that spot weld cracking of the studied steel is related to the liquid metal embrittlement phenomenon. The presence of liquid zinc and high stresses are necessary conditions for cracking to occur. As direct measures of relevant parameters such as temperature or stress are arduous and the variation of these parameters is limited during welding process, different tests gathering liquid zinc and high stresses have been performed: immersion of cups containing high residual stresses in a liquid zinc bath and Gleeble hot tensile tests.

Tests with cups immersed in the liquid zinc bath have shown that for cracking to occur the following conditions must be gathered: a good wettability and stresses higher than a threshold stress. These tests permitted to evidence the embrittlement at temperatures as low as 420°C, however, they provide only qualitative results since the main parameters (stress, strain rate…) can not precisely be measured.
A methodology has been developed for studying the sensitivity of the steel to liquid zinc embrittlement. It consists in performing hot tensile tests in the thermo-mechanical simulator Gleeble. Tests performed at temperature higher than the zinc melting point on bare specimens provide the reference behaviour while tests on EG specimens permit to obtain the behaviour of the steel in presence of liquid zinc. Analysis of tensile curves provides a reproducible and relevant index of sensitivity to LME. The influence of many parameters such as temperature, strain rate, time of contact between steel and liquid zinc, microstructure…, has been investigated.

Results have revealed that the Fe22Mn0.6C steel is sensitive to liquid zinc embrittlement but the detrimental effect of liquid zinc is actually observed provided appropriate experimental conditions are present. Hot tensile tests performed at different temperatures with a constant strain rate of $1.3.10^{-3}$ s^{-1} indicate that the steel is immune to embrittlement by liquid zinc in these conditions. However, increasing the strain rate to $1.3.10^{-2}$ s^{-1} permits to evidence the embrittlement within a limited temperature range depending on strain rate: increasing strain rate tends to widen this temperature range by a decrease of the lower temperature of the ductility trough. Contrary to what has been reported in literature, the lower limit of the

embrittlement temperature range is much higher than the melting point of the embrittling metal. This could be linked to the experimental procedure: the specimen is not immersed in the liquid zinc and its contact with the latter is due to the melting of the zinc coating during heating. The ductility recovery temperature is close to the zinc boiling point whatever the strain rate.

Conditions (temperature and strain rate) leading to cracking have been widely determined. It appears that, in the latter conditions, cracking occurs when stress reaches a threshold stress. The existence of a critical stress has already been pointed out during immersion of cups in liquid zinc bath. The critical stress strongly increases with decreasing temperature so that for lower temperatures, the critical stress is higher than the UTS and can not be reached during tensile test. Increasing the stress level by increasing strain rate or modifying the microstructure (as rolled specimens) has permitted to evidence embrittlement at lower temperature and led to the following conclusion: harder steels are embrittled in a wider temperature range. This critical stress can be used as a criterion for predicting cracking during welding in finite element model for instance.

In addition to temperature and strain rate which appear as key parameters in the phenomenon, the influence of different parameters has been investigated. It is worth noticing that the complexity of the phenomenon leads to difficulties for studying parameters independently from each other and for interpreting obtained results.
The influence of coating has been investigated by performing tests on galvanized, electrogalvanized and annealed electrogalvanized (280°C during 24h under N_2) specimens. The differences in the initial coating do not lead to differences in the cracking behaviour. However, a preliminary contact between steel and liquid zinc at high temperature before testing has a great effect on embrittlement: holding EG specimen few seconds at high temperature is sufficient to prevent embrittlement during subsequent tensile test. Tests performed under Ar atmosphere have led to the same results that those obtained in air environment. Consequently, the hypothesis of zinc oxidation during holding is excluded but no further analyses of specimens tested under Ar have been carried out.
The suppression of embrittlement after holding at high temperature may be related to the formation of FeMnZn intermetallic compounds consuming the liquid zinc necessary for embrittlement. The growing of intermetallic phases (and the simultaneous liquid zinc

consumption) during holding may explain the progressive ductility recovery observed during subsequent tensile test.

Hot tensile tests performed on DP and TRIP steels have shown that a sufficient amount of austenite is required for cracking to occur. This is of great importance since during welding processes many steels undergo austenite transformation which strongly increases the risk of liquid zinc embrittlement.

In order to check that cracking conditions determined from Gleeble tests are in good agreement with conditions experienced during spot welding, numerical simulations have been performed. Temperature and strain rate obtained from simulations are in the range of embrittlement conditions. It is more difficult to conclude about critical stress since the stress level generated during spot welding cycle is compressive according to FE simulations, and no investigation of liquid zinc embrittlement of the studied steel during compressive solicitation has been carried out. This may explain why cracking has been rarely observed during homogeneous spot welding in standard conditions. Cracking is much more frequent when expulsion occurs.

Mechanisms involved in the cracking phenomenon are still unclear. However, some elements for understanding cracking mechanisms have been reported and practical solutions for reducing the risk of embrittlement by liquid zinc during welding have been proposed: increasing the time of contact between the steel and liquid zinc before stress application, decreasing stresses generated during welding process or preventing contact between the substrate and the liquid zinc by depositing a buffer layer between steel and coating.

Outlooks

In order to better understand cracking mechanisms, advanced microstructural investigations must be undertaken. From a microstructural point of view, the liquid zinc grain boundary penetration and the resulting grains decohesion must be investigated. The reactions occurring during holding and leading to embrittlement suppression have to be precisely determined.

The study of the influence of microstructure and particularly the nature of phase and the grain size on LME phenomenon would bring understanding elements in cracking mechanisms. As austenite appears to be more sensitive to LME and many steels undergo austenite transformation during welding processes, it appears necessary to investigate the LME phenomenon in other steels and particularly to study the influence of alloying elements with the purpose of proposing solutions to inhibit embrittlement. The construction of a database would permit to compare the cracking behaviour of different steels (embrittlement temperature range, critical stress).

The influence of additional parameters on liquid zinc embrittlement of steels must be investigated. It would be particularly interesting to change the stress state by introducing stress triaxiality (notch effect). This is a known way of enhancing LME effects. Also, it would be of great interest to study the LME phenomenon during compressive solicitation.

Finally, extensive numerical simulations must be performed to correlate results of Gleeble tests with the applied case of spot welding. As cracking appears rarely during spot welding and it takes much time to analyse spot welds and detect cracks, numerical simulations would permit to determine quickly and precisely the critical cases (critical assemblies, critical welding parameters…). Moreover, cracking could be predicted in simulations by introducing the stress criterion in the finite element model.

References

[ALA 10] ALAM S. N., POLOJU M., Zinc Oxide Nanostructures in the Zinc Electrode of a Zinc-Carbon Dry Cell, Microscopy and Analysis 24(6), 2010, pp. 9-12

[ALL 03] ALLEY D.W., BARKER D.J., MUCEK M.W., BRADLEY S.A., Liquid Metal Embrittlement of Alloy 800 Hydrogen Unit Preheat Tubes, Corrosion 2003, Paper No. 03659

[ALL 04] ALLAIN S., Caractérisation et modélisation thermomécaniques multi-échelles des mécanismes de déformation et d'écrouissage d'aciers austénitiques à haute teneur en manganèse – Application à l'effet TWIP, PhD Thesis, INPL, 2004

[ALL 04a] ALLAIN S., CHATEAU J.-P., BOUAZIZ O., A physical model of the twinning-induced plasticity effect in a high manganese austenitic steel, Materials Science and Engineering A 387-389, 2004, pp. 143-147

[ALL 04b] ALLAIN S., CHATEAU J.-P., BOUAZIZ O., MIGOT S., GUELTON N., Correlations between the calculated stacking fault energy and the plasticity mechanisms in Fe–Mn–C alloys, Materials Science and Engineering A 387-389, 2004, pp. 158-162

[ALL 04c] ALLAIN S., CHATEAU J.-P., DAHMOUN D., BOUAZIZ O., Modeling of mechanical twinning in a high manganese content austenitic steel, Materials Science and Engineering A 387–389, 2004, pp. 272-276

[ARA 97] ARAI M., ADACHI Y., NAKAMORI T., USUKI N., Formation and growth of iron-zinc compound phases in galvannealed coatings on phosphorous-containing steel, Tetsu-to-Hagane 83(11), 1997, pp. 713-718

[AUG 05] AUGER T., LORANG G., Liquid metal embrittlement susceptibility of T91 steel by lead–bismuth, Scripta Materialia 52, 2005, pp. 1323-1328

[BAR 09a] BARBIER D., Etude du comportement mécanique et des évolutions microstructurales de l'acier austénitique Fe-22Mn-0.6C à effet TWIP sous sollicitations complexes. Approche expérimentale et modélisation, PhD Thesis, Université Paul Verlaine de Metz, 2009

[BAR 09b] BARBIER D., GEY N., ALLAIN S., BOZZOLO N., HUMBERT M., Analysis of the tensile behavior of a TWIP steel based on the texture and microstructure evolutions, Materials Science and Engineering A 500, 2009, pp. 196-206

[BAY 04] BAYRAKTAR E., KHALID F. A., LEVAILLANT C., Deformation and fracture behaviour of high manganese austenitic steel, Journal of Materials Processing Technology 147, 2004, pp. 145-154

[BEU 06] BEURROT S., Modélisation de la cinétique de recristallisation et du grossissement des grains d'un acier FeMnCV, Internship report, 2006

[BER 06] BERRAHMOUNE M. R., Transformation martensitique et rupture différée dans l'acier austénitique instable 301LN, PhD Thesis, École Nationale Supérieure d'Arts et Métiers, 2006

[BHA 91] BHAN S., LAL A., SINGH S., The Fe-Mn-Zn System, Journal of Phase Equilibria, Vol. 12, N° 6, 1991, pp. 667-672

[BLO 01] BLONDEAU R., Procédés et applications industrielles du soudage, Hermes Science Publications, Lavoisier, 2001

[BOS 07] BOSCH R.W., VAN DYCK S., AL MAZOUZI A., Investigation of the susceptibility of EUROFER97 in lead–lithium to liquid metal embrittlement (LME), Fusion Engineering and Design 82, 2007, pp. 2615-2620

[BOU 01] BOUAZIZ O., GUELTON N., Modelling of TWIP effect on work-hardening, Materials Science and Engineering A319–321, 2001, pp. 246-249

[BOU 07] BOUZEKRI M., ArcelorMittal internal presentation, 2007

[BOU 08] BOUAZIZ O., ALLAIN S., SCOTT C., Effect of grain and twin boundaries on the hardening mechanisms of twinning-induced plasticity steels, Scripta Materialia 58, 2008, pp. 484-487

[BOU 09] BOUZEKRI M., Capitalization report on X-IP® 1000 welding, ArcelorMittal Internal Report, N° 2009 11885 RDMA, 2009

[BRA 07] BRACKE L., KESTENS L., PENNING J., Transformation mechanism of α'-martensite in an austenitic Fe–Mn–C–N alloy, Scripta Materialia 57, 2007, pp. 385-388

[BRA 09] BRACKE L., VERBEKEN K., KESTENS L., PENNING J., Microstructure and texture evolution during cold rolling and annealing of a high Mn TWIP steel, Acta Materialia 57, 2009, pp. 1512-1524

[CAR 10] CARPIO J., CASADO J.A., ÁLVAREZ J.A., MENDEZ D., GUTIERREZ-SOLANA F., Stress corrosion cracking of structural steels immersed in hot-dip galvanizing baths, Engineering Failure Analysis 17, 2010, pp. 19-27

[CAZ 93] CAZES R., Techniques de l'ingénieur, Soudage par résistance, B 7 720, 1993

[CHO 99] CHOI H. C., HA T. K., SHIN H. C., CHANG Y. W., The formation kinetics of deformation twin and deformation induced ε-martensite in an austenitic Fe-C-Mn steel, Scripta Materialia, Vol. 40, N° 10, 1999, pp. 1171-1177

[CLE 01] CLEGG R. E., A fluid flow based model to predict liquid metal induced embrittlement crack propagation rates, Engineering Fracture Mechanics, 68, 2001, pp. 1777-1790

[CLE 03] CLEGG R.E., JONES D.R.H., Liquid metal embrittlement of tensile specimens of En19 steel by tin, Engineering Failure Analysis 10, 2003, pp. 119-130

[COLL 03] COLLINS M. G., LIPPOLD J. C, An Investigation of Ductility Dip Cracking in Nickel-Based Filler Materials - Part I, Welding Journal, 82(10), 2003, pp. 288s-295s

[CUG 05] CUGY P., HILDENBRAND A., BOUZEKRI M., CORNETTE D., GÖKLU S., H. HOFMANN, First International Conference Super-High Strength Steels, Rome, 2005

[CUG 08] CUGY P., PETITGAND G., REMY B., MOREL I., ALLELY C., SCOTT C., THEYSSIER M.-C., Capitalization report on the development of an alloyed coating on X-IP steel by batch annealing, ArcelorMittal Internal Report

[CUR 10] CURTZE S., KUOKKALA V.-T., Dependence of tensile deformation behavior of TWIP steels on stacking fault energy, temperature and strain rate, Acta Materialia 58, 2010, pp. 5129-5141

[DAI 99] DAI Q., YANG R., CHEN K., Deformation Behavior of Fe-Mn-Cr-N Austenitic Steel, Materials Characterization 42, 1999, pp. 21-26

[DAI 10] DAI Y.-J., TANG D., MI Z.-L., Lü J.-C., Microstructure Characteristics of an Fe-Mn-C TWIP Steel After Deformation, Journal of iron and steel research, International, Vol. 17, Issue 9, 2010, pp. 53-59

[DAN 09] DANCETTE S., Comportement mécanique des soudures par points : mécanismes et stratégies de prédiction dans le cas des tôles en acier pour automobile, PhD Thesis, Institut National des Sciences Appliquées de Lyon, 2009

[DEL 04] DELOFFRE P., BALBAUD-CELERIER F., TERLAIN A., Corrosion behaviour of aluminized martensitic and austenitic steels in liquid Pb–Bi, Journal of Nuclear Materials 335, 2004, pp. 180-184

[DEP 07] DEPETRIS-WERY M., AYEDI H. F., Electrozingage, In : Techniques de l'ingénieur, Ref M1600

[DIE 09] DIETSCH P., ArcelorMittal Internal Report, 2009

[DIL 90] DILLON C. P., Liquid Metal Cracking of Stainless Steels in Chemical Plants, Materials Performance, Vol. 29, No. 11, 1990, pp.54-55

[DIN 09] DINI G., NAJAFIZADEH A., MONIR-VAGHEFI S.M., EBNONNASIR A., Predicting of mechanical properties of Fe–Mn–(Al, Si) TRIP/TWIP steels using neural network modelling, Computational Materials Science 45, 2009, pp. 959-965

[DRO 93] DROUART C., Soudage par résistance, Publications du Soudage et de ses Applications, 1993

[DUM 07] DUMAY A., CHATEAU J.-P., ALLAIN S., MIGOT S., BOUAZIZ O., Influence of addition elements on the stacking-fault energy and mechanical properties of an austenitic Fe–Mn–C steel, Materials Science and Engineering A Vol. 483-484, 2008, pp. 184-187

[ESI 08] ESI France, User's guides for SYSWELD spot welding simulation, 2008

[FER 96a] FERNANDES P.J.L., JONES D.R.H., Specificity in liquid metal induced embrittlement, Engineering Failure Analysis, Vol. 3, N° 4, 1996, pp. 299-302

[FER 96b] FERNANDES P.J.L., JONES D.R.H., The effect of temperature on fatigue crack growth in liquid metal environments, Corrosion Science, Vol. 38, No. 5, 1996, pp. 745-754

[FER 97] FERNANDES P.J.L., JONES D.R.H., The effects of microstructure on crack initiation in liquid-metal environments, Engineering Failure Analysis, Vol. 4, No. 3, 1997, pp. 195-204

[GAM 04] GAMAOUN F., DUPEUX M., GHETTA V., GORSE D., Cavity formation and accelerated plastic strain in T91 steel in contact with liquid lead, Scripta Materialia 50, 2004, pp. 619-623

[GEL 74] GELLINGS P.J., Mechanism of the reaction between liquid zinc and steel, Corrosion Science, Vol. 14, 1974, pp. 507-509

[GIO 04a] GIORGI M.-L., GUILLOT J.-B., NICOLLE R., Modélisation des réactions de galvanisation, La Revue de Métallurgie-CIT, 2004, pp. 839-847

[GIO 04b] GIORGI M.-L., DURIGHELLO P., NICOLLE R., GUILLOT J.-B., Dissolution kinetics of iron in liquid zinc, Journal of Materials Science 39, 2004, pp. 5803-5808

[GLA 03] GLASBRENNER H., GRÖSCHEL F., KIRCHNER T., Tensile tests on MANET II steel in circulating Pb–Bi eutectic, Journal of Nuclear Materials 318, 2003, pp. 333-338

[GLA 04] GLASBRENNER H., GRÖSCHEL F., Bending tests on T91 steel in Pb–Bi eutectic, Bi and Pb–Li eutectic, Journal of Nuclear Materials 335, 2004, pp. 239-243

[GRÄ 00] GRÄSSEL O., KRÜGER L., FROMMEYER G., MEYER L.W., High strength Fe-Mn-(Al, Si) TRIP/TWIP steels development-properties-application, International Journal of Plasticity 16,

2000, pp. 1391-1409

[GUT 10] GUTIERREZ-URRUTIA I., ZAEFFERER S., RAABE D., The effect of grain size and grain orientation on deformation twinning in a Fe–22 wt.% Mn–0.6 wt.% C TWIP steel, Materials Science and Engineering A 527, 2010, pp. 3552-3560

[HAM 07a] HAMADA A.S., Manufacturing, mechanical properties and corrosion behavior of high-Mn TWIP steels. Oulun Yliopisto, 2007, 56 p. (Online: <http://herkules.oulu.fi/isbn9789514285844/isbn9789514285844.pdf> (accessed on 17.08.2010))

[HAM 07b] HAMADA A.S., KARJALAINEN L.P., SOMANI M.C., The influence of aluminum on hot deformation behavior and tensile properties of high-Mn TWIP steels, Materials Science and Engineering A 467, 2007, pp. 114-124

[HAN 71] HANCOCK P.C., IVES M.B., The Role of Plastic Deformation in Liquid metal Embrittlement, Canadian Metallurgical Quarterly, Volume 10, Number 3, 1971, pp. 207-211

[HAM 08] HAMOUCHE Z., Etude de la fragilisation des aciers T91 et 316L par l'eutectique Plomb-Bismuth liquide, PhD Thesis, Université Paris XII – Val de Marne, 2008

[HIL 95] HILDITCH J.P., HURLEY J.R., SKELDON P., TICE D.R., The liquid metal embrittlement of iron and ferritic steels in sodium, Corrosion Science, Vol. 37, No. 3, 1995, pp. 445-454

[HON 03] HONG J.-H., OH S.-J., KWON S. J., Mössbauer analysis of the iron-zinc intermetallic phases, Intermetallics 11, 2003, pp. 207-213

[HUG 98] HUGO R.C., HOAGLAND R.G., In situ TEM observation of aluminum embrittlement by liquid gallium, Scripta materialia, Vol. 38, N° 3, 1998, pp. 523-529

[HUG 99] HUGO R.C., HOAGLAND R.G., Gallium penetration of aluminum: in situ TEM observations at the penetration front, Scripta Materialia, Vol. 41, No. 12, 1999, pp. 1341–1346

[HUG 00] HUGO R.C., HOAGLAND R.G., The kinetics of gallium penetration into aluminum grain boundaries in situ TEM observations and atomistic models, Acta mater. 48, 2000, pp. 1949-1957

[IDR 09] IDRISSI H., RYELANDT L., VERON M., SCHRYVERS D., JACQUES P.J., Is there a relationship between the stacking fault character and the activated mode of plasticity of Fe–Mn-based austenitic steels?, Scripta Materialia Vol. 60, Issue 11, 2009, pp. 941-944

[IDR 10] IDRISSI H., RENARD K., RYELANDT L., SCHRYVERS D., JACQUES P.J., On the mechanism of twin formation in Fe–Mn–C TWIP steels, Acta Materialia 58, 2010, pp. 2464-2476

[INA 04] INA K., KOIZUMI H., Penetration of liquid metals into solid metals and liquid metal embrittlement, Materials Science and Engineering A 387–389, 2004, pp. 390-394

[JAM 09] JAMES M. N., Designing against LMAC in galvanised steel structures, Engineering Failure Analysis 16, 2009, pp. 1051-1061

[JOH 74] JOHNSON W.H., Proceedings of the Royal Society of London 23, 1874, pp. 168

[JOS 98] JOSEPH B., BARBIER F., DAGOURY G., AUCOUTURIER M., Rapid penetration of liquid Bi along Cu grain boundaries, Scripta Materialia, Vol. 39, No. 6, 1998, pp. 775-781

[JOS 99a] JOSEPH B, PICAT M., BARBIER F., Liquid metal embrittlement: A state-of-the-art appraisal, The European Physical Journal Applied Physics 5, 1999, pp. 19-31

[JOS 99b] JOSEPH B., BARBIER F., AUCOUTURIER M., Embrittlement of copper by liquid bismuth, Scripta Materialia, Vol. 40, No. 8, 1999, pp. 893-897

[KAM 87] KAMDAR M.H., "Liquid Metal Embrittlement", Metals Handbook, 9th Edition, Vol. 13, Corrosion (Materials Park, OH: ASM International, 1987), pp. 171-184

[KAR 00a] KARAMAN I., SEHITOGLU H., BEAUDOIN A. J., CHUMLYAKOV Y. I., MAIER H. J., C. N. TOME, Modeling the deformation behavior of Hadfield steel single and polycrystals due to twinning and slip, Acta mater. 48, 2000, pp. 2031-2047

[KAR 00b] KARAMAN I., SEHITOGLU H., GALL K., CHUMLYAKOV Y. I., MAIER H. J., Deformation of single crystals Hadfiels steel by twinning and slip, Acta mater. 48, 2000, pp. 1345-1359

[KAR 01] KARAMAN I., SEHITOGLU H., GALL K., CHUMLYAKOV Y. I., MAIER H. J., KIREEVA I.V., Extrinsic stacking faults and twinning in Hadfield manganese steel single crystals, Scripta mater. 44, 2001, pp. 337-343

[KIK 82] KIKUCHI, M., IEZAWA, T., Effect of Stress-Concentration Factor on Liquid Metal Embrittlement Cracking of Steel in Molten Zinc, Journal of the Society of Materials Science, Japan, Vol. 31, No. 352, 1982, pp. 271-276

[KIN 04] KINSTLER T.J., Current knowledge of the cracking of steels during galvanising, GalvaScience LLC for the American Institute of Steel Construction, 2004 <http://www.aisc.org/Content/ContentGroups/Engineering_and_Research/Research1/Final5906.pdf> (accessed on 25/07/2010)

[KOB 06] KOBAYASHI M., TODA H., UESUGI K., OHGAKI T., KOBAYASHI T., TAKATAMA Y., AHN B.-G., Preferential penetration path of gallium into grain boundary in practical aluminium alloy, Philosophical Magazine, Vol. 86, No. 28, 2006, pp. 4351-4366

[KOU 03] KOU S., Solidification and Liquation Cracking Issues in Welding, JOM, Volume 55, Number 6, 2003, pp. 37-42

[LAP 05] LAPORTE V., Pénétration intergranulaire fragilisante du cuivre par le bismuth liquide : identification de la cinétique et du mécanisme de type diffusionnel entre 300 et 600°C, PhD thesis, Ecole Nationale Supérieure des Mines de Saint Etienne, 2005

[LEB 09] LEBEDKINA T.A., LEBYODKIN M.A., CHATEAU J.-Ph., JACQUES A., ALLAIN S., On the mechanism of unstable plastic flow in an austenitic FeMnC TWIP steel, Materials Science and Engineering A 519, 2009, pp. 147-154

[LED 09] LEDAIN N., Internship report, 2009

[LEG 00] LEGRIS A., NICAISE G., VOGT J.-B., FOCT J., GORSE D., VANÇON D., Embrittlement of a martensitic steel by liquid lead, Scripta Materialia, 43, 2000, pp. 997-1001

[LEG 02] LEGRIS A., NICAISE G., VOGT J.-B., FOCT J., Liquid metal embrittlement of the martensitic steel 91: influence of the chemical composition of the liquid metal. Experiments and electronic structure calculations, Journal of Nuclear Materials 301, 2002, pp. 70-76

[LIP 05] LIPPOLD J.C., Recent developments in weldability testing for advanced materials, ASM International, 2005

[LIU 06] LIU R.P., DONG Z.J., PAN Y.M., Solidification crack susceptibility of aluminum alloy weld metals, Trans. Nonferrous Met. SOC. China 16, 2006, pp. 110-116

[LUD 00] LUDWIG W., BELLET D., Penetration of liquid gallium into the grain boundaries of aluminium: a synchrotron radiation microtomographic investigation, Materials Science and Engineering A 281, 2000, pp. 198-203

[LUD 05] LUDWIG W., PEREIRO-LOPEZ E., BELLET D., In situ investigation of liquid Ga penetration in Al bicrystal grain boundaries: grain boundary wetting or liquid metal embrittlement?, Acta Materialia 53, 2005, pp. 151-162

[LV 10] LV B., ZHANG F.C., LI M., HOU R.J., QIAN L.H., WANG T.S., Effects of phosphorus and sulfur on the thermoplasticity of high manganese austenitic steel, Materials Science and Engineering A 527, 2010, pp. 5648-5653

[MAG 96] MAGNIN B., MAENNER L., KATGERMAN L., ENGLER S., Ductility and Rheology of an Al-4.5%Cu alloy from room temperature o coherency temperature, Materials Science Forum, Vol. 217-222, 1996, pp.1209-1214

[MAR 00a] MARIÉ N., WOLSKI K., BISCONDI M., Grain boundary penetration of Nickel by liquid Bismuth as a film of nanometric thickness, Scripta Materialia Vol. 43, N° 10, 2000, pp. 943-949

[MAR 00b] MARDER A.R., The metallurgy of zinc-coated steel, Progress in Materials Science 45, 2000, pp. 191-271

[MAR 01] MARIÉ N., WOLSKI K., BISCONDI M., Intergranular penetration and embrittlement of solid nickel through bismuth vapour condensation at 700°C, Journal of Nuclear Materials 296, 2001, pp. 282-288

[MAR 10] MARCELLIN M.-A., ArcelorMittal internal report, 2010

[MUR 94] MURRY G., Techniques de l'ingénieur, Soudage et soudabilité métallurgique des métaux, M 715, 1994

[NAM 09] NAM H.-S., SROLOVITZ D.J., Effect of material properties on liquid metal embrittlement in the Al–Ga system, Acta Materialia 57, 2009, pp. 1546-1553

[NIC 61] NICHOLS H., ROSTOKER W., Acta Metallurgica, 9(5), 1961, pp. 504

[NIC 01a] NICAISE G., Sensibilité de l'acier martensitique Z10CCNbV9-1 à la fragilisation par les métaux liquides, PhD Thesis, Université des Sciences et Technologies de Lille, 2001

[NIC 01b] NICAISE G., LEGRIS A., VOGT J.B., FOCT J., Embrittlement of the martensitic steel 91 tested in liquid lead, Journal of nuclear materials 296, 2001, pp. 256-264

[NIS 03] NISSLEY N.E., LIPPOLD J.C., Development of the strain-to-fracture test for evaluating ductility-dip cracking in austenitic alloys, Welding Journal, 82(12), 2003, pp. 355s-364s

[PAR 10] PARK K.-T., JIN K. G., HAN S. H., HWANG S. W., CHOI K., LEE C. S., Stacking fault energy and plastic deformation of fully austenitic high manganese steels: Effect of Al addition, Materials Science and Engineering A 527, 2010, pp. 3651-3661

[PER 03] PEREIRO-LOPEZ E., LUDWIG W., BELLET D., BARUCHEL J., Grain boundary liquid metal wetting: A synchrotron micro-radiographic investigation, Nuclear Instruments and Methods in Physics Research B 200, 2003, pp. 333-338

[PER 04] PEREIRO-LOPEZ E., LUDWIG W., BELLET D., Discontinuous penetration of liquid Ga into grain boundaries of Al polycrystals, Acta Materialia 52, 2004, pp. 321-332

[PER 06] PEREIRO-LOPEZ E., LUDWIG W., BELLET D., LEMAIGNAN C., In situ investigation of Al

bicrystal embrittlement by liquid Ga using synchrotron imaging, Acta Materialia 54, 2006, pp. 4307-4316

[PET 08] PETITGAND G., ArcelorMittal internal presentation, 2008

[PRI 86] PRICE, C. E., FREDELL R. S., A comparative study of the embrittlement of monel 400 at room temperature by hydrogen and mercury, Metallurgical transactions A 17, 1986, pp. 889-898

[QUA 04] QUANTIN D., Galvanisation à chaud, In: Techniques de l'ingénieur, Ref. COR1530, 2004, 27 p.

[RAG 00] RAGAB M.S., ORBAN H.Z., Effect of ironing on the residual stresses in deep drawn cups, Journal of Materials Processing Technology 99, 2000, pp. 54-61

[RAG 03] RAGHAVAN V., Fe-Mn-Zn (Iron-Manganese-Zinc), Journal of Phase Equilibria, Vol. 24, N°6, 2003, pp. 556-557

[REU 95] REUMONT G., DUPONT G., PERROT P., The Fe-Zn-Mn System at 450°C, Z. Metallkd., 86(9), 1995, pp. 608-613

[ROQ 75] ROQUES-CARMES C., Comparaison entre les mécanismes de corrosion et de fragilisation intergranulaires des métaux par les métaux liquides, Journal de Physique, Colloque C4, supplément au no 10, Tome 36, Octobre 1975, pp. 403-406

[ROS 60] ROSTOKER W., MCCANGHEY J. M., MARKUSH., Embrittlement by Liquid Metals, Reinhold Publishing Corporation, Van Nostrand-New York, 1960

[ROS 07] ROSSILLON F., Influence des conditions de soudage sur le comportement en fatigue d'un acier THR Dual Phase soudé par point, PhD Thesis, Université Blaise Pascal – Clermont II, 2007

[SAM 96] SAMPLE T., FENICI P., KOLBE H., Liquid metal embrittlement susceptibility of welded MANET II (DIN 1.4914) in liquid Pb-17Li, Journal of Nuclear Materials 233-237, 1996, pp. 244-247

[SAM 00] SAMPLE T., KOLBE H., Liquid metal embrittlement (LME) susceptibility of the 8-9% Cr martensitic steels F82H-mod., OPTIFER IVb and their simulated welded structures in liquid Pb-17Li, Journal of Nuclear Materials, 283-287, 2000, pp. 1336-1340

[SCO 09] SCOTT C., P. DIETSCH, J-L.COLLET, J. GONCALVES, G. PETITGAND, D. BARBIER, P. CUGY, Measuring Residual Stresses In Cold Formed Sheets by Synchrotron X-ray Diffraction, ArcelorMittal Internal Report, N° IRD/AUP/2009/11091, 2009

[SEN 00] SENKARA J., ZHANG H., Cracking in Spot Welding Aluminum Alloy AA5754, Welding Research Supplement, 2000, pp. 194-201s

[SHA 03a] SHANKAR V., GILL T.P.S., MANNAN S.L., SUNDARESAN S., Effect of nitrogen addition on microstructure and fusion zone cracking in type 316L stainless steel weld metals, Materials Science and Engineering A343, 2003, pp. 170-181

[SHA 03b] SHANKAR V., GILL T.P.S., MANNAN S.L., SUNDARESAN S., Solidification cracking in austenitic stainless steel welds, Sadhana Vol. 28, Parts 3 & 4, 2003, pp. 359-382

[SHI 08] SHIEKHELSOUK M.N., FAVIER V., INAL K., CHERKAOUI M., Modelling the behaviour of polycrystalline austenitic steel with twinning-induced plasticity effect, International Journal of Plasticity Vol. 25, Issue 1, 2009, pp. 105-133

[SIG 08] SIGLER D.R., SCHROTH J.G., YANG W., GAYDEN X.Q., JIANG C., SANG Y., MORIN P.J., Observations of Liquid Metal-Assisted Cracking in Resistance Spot Welds of Zinc-Coated Advanced High-Strength Steels, Sheet Metal Welding Conference XIII, Livonia, MI, May 2008

[SWA 08] SWANTEC Software and Engineering ApS. Sorpas Version 9.0 – User manual. Kgs. Lyngby, Denmark, 2008

[TZI 01] TZIMAS E., PAPADIMITRIOU G., Cracking mechanisms in high temperature hot-dip galvanized coatings, Surface and Coatings Technology 145, 2001, pp. 176-185

[UEJ 08] UEJI R., TSUCHIDA N., TERADA D., TSUJI N., TANAKA Y., TAKUMERA A., KUNISHIGE K., Tensile properties and twinning behavior of high manganese austenitic steel with fine-grained structure, Scripta Materialia 59, 2008, pp. 963-966

[VEB 08] VEBERT C., T-07077 : Résultats supplémentaires obtenus suite aux essais réalisés sur les godets FeMn (LAF et LAC), ArcelorMittal Internal Report, N° 2008 9290 AUP, 2008

[VER 04] VERCAMMEN S., BLANPAIN B., DE COOMAN B.C., WOLLANTS P., Cold rolling behaviour of an austenitic Fe–30Mn–3Al–3Si TWIP-steel: the importance of deformation twinning, Acta Materialia 52, 2004, pp. 2005-2012

[VER 05] VERLEENE A., Comportement en fatigue de l'acier martensitique T91 à 300°C dans l'eutectique plomb-bismuth liquide, PhD thesis, Université des sciences et technologies de Lille, 2005

[WES 79] WESTWOOD A. R. C., LATANISION R. M. (1979), Adsorption-induced embrittlement by liquid metals. Corrosion of liquid metal of the 1969 fall meeting of the metallurgical society of AIME, Philadelphia, Pennsylvania, Plenum Press

[WOL 02] WOLSKI K., RENAUDOT N., HARABASZ A., MARIÉ N., AGNIN T., BISCONDI M., The Use of Ultra-High-Puritty Metals and Alloys to Study Environment-Sensitive Damage Mechanisms in Nuclear Power Plants, Phys. Stat. Sol., (a) 189, N°1, 2002, pp. 59-62

[WOU 03] WOUTERS O., DE HOSSON J. Th. M., Lead induced intergranular fracture in aluminum alloy AA6262, Materials Science and Engineering A 361, 2003, pp. 331-337

[XIO 09] XIONG R.-G., FU R.-Y., SU Y., LI Q., WEI X.-C., LI L., Tensile Properties of TWIP Steel at High Strain Rate, Journal of Iron and Steel Research International 16(1), 2009, pp. 81-86

[YAN 01] YANG J.-G., OU B.-L., Hot ductility behavior and HAZ hot cracking susceptibility of 7475-T7351 aluminum alloy, Scandinavian Journal of Metallurgy, Vol. 30, N° 3, 2001, pp. 146-157

[YAN 06] YANG P., XIE Q., MENG L., DING H., TANG Z., Dependence of deformation twinning on grain orientation in a high manganese steel, Scripta Materialia 55, 2006, pp. 629-631

[YOU 08] YOUNG G. A., CAPOBIANCO T. E., PENIK M. A., MORRIS B. W., MCGEE J. J., The Mechanism of Ductility Dip Cracking in Nickel-Chromium Alloys, Welding Journal Supplement, February 2008, pp. 31s-43s

[ZHA 06] ZHANG H., SENKARA J., Resistance Welding, Fundamentals and Applications, Taylor & Francis Group, 2006

[ZIN 10] Zinc coatings, American Galvanizers association, (On line) http://www.galvanizeit.org/images/uploads/publicationPDFs/Z-ZC-06.pdf, accessed on 04/08/10

FOLIO ADMINISTRATIF

THESE SOUTENUE DEVANT L'INSTITUT NATIONAL DES SCIENCES APPLIQUEES DE LYON

NOM : BEAL DATE de SOUTENANCE : 25/03/2011

Prénoms : Coline

TITRE : Mechanical behaviour of a new automotive high manganese TWIP steel in the presence of liquid zinc

NATURE : Doctorat Numéro d'ordre : 2011-ISAL-0029

Ecole doctorale : Matériaux de Lyon

Spécialité : Matériaux

Cote B.I.U. - Lyon : T 50/210/19 / et bis CLASSE :

RESUME :
High manganese TWIP (TWinning Induced Plasticity) steels are particularly attractive for automotive applications because of their exceptional properties of strength combined with an excellent ductility. However, as austenitic steels, they appear to be sensitive to liquid zinc embrittlement during welding, the liquid zinc arising from the melted coating due to the high temperatures reached during the welding process. In this framework, the cracking behaviour of a high manganese austenitic steel has been investigated in relation to the liquid metal embrittlement (LME) phenomenon by hot tensile tests carried out on electro-galvanized specimens using a Gleeble 3500 thermomechanical simulator. The influence of different parameters such as temperature and strain rate on cracking behaviour has been studied.
Embrittlement appears within a limited range of temperature depending on experimental conditions. Conditions for which cracking occurs could be experienced during welding processes. The existence of a critical stress above which cracking appears has been evidenced and this critical stress can be used as a cracking criterion.
Finally, the study of the influence of different parameters such as time of contact between steel and liquid zinc before stress application, coating and steel on LME occurrence provides understanding elements of LME mechanism and permits to suggest solutions for preventing cracking during spot welding of such steels.

MOTS-CLES :
TWIP steels - High manganese austenitic steels - Liquid Metal Embrittlement - Cracking - Hot tensile tests - Gleeble - Zinc - Resistance Spot welding

Laboratoire (s) de recherche : MATEIS

Directeurs de thèse: Xavier KLEBER, Damien FABREGUE

Président de jury : Michel SUERY

Composition du jury : Mohamed BOUZEKRI, Damien FABREGUE, Pascal JACQUES, Xavier KLEBER, Pascal PAILLARD, Colin SCOTT, Michel SUERY